Micael Simões Silva

Licenciado em Bioquímica

Design of bio-inspired ionic liquids for protein stabilisation

Dissertação para obtenção do Grau de Mestre em
Química Bioorgânica

Orientador: Prof. Doutor Eurico José da Silva Cabrita,
Professor auxiliar, FCT-UNL
Co-orientador: Doutor Ângelo Miguel Mendes Pinto de
Figueiredo, Investigador de pós-doutoramento, FCT-UNL

Júri:

Presidente: Prof. Doutora Paula Cristina de Sério Branco,
Professora auxiliar, FCT-UNL
Arguente: Doutor Luís Alexandre Almeida Fernandes Cobra Branco,
Investigador principal, FCT-UNL
Vogal: Prof. Doutor Eurico José da Silva Cabrita,
Professor auxiliar, FCT-UNL

FACULDADE DE CIÊNCIAS E TECNOLOGIA
UNIVERSIDADE NOVA DE LISBOA

Setembro de 2015

Micael Simões Silva

Licenciado em Bioquímica

Design of bio-inspired ionic liquids for protein stabilisation

Dissertação para obtenção do Grau de Mestre em
Química Bioorgânica

Orientador: Prof. Doutor Eurico José da Silva Cabrita,
Professor auxiliar, FCT-UNL
Co-orientador: Doutor Ângelo Miguel Mendes Pinto de
Figueiredo, Investigador de pós-doutoramento, FCT-UNL

Júri:

Presidente: Prof. Doutora Paula Cristina de Sério Branco,
Professora auxiliar, FCT-UNL
Arguente: Doutor Luís Alexandre Almeida Fernandes Cobra Branco,
Investigador principal, FCT-UNL
Vogal: Prof. Doutor Eurico José da Silva Cabrita,
Professor auxiliar, FCT-UNL

FACULDADE DE CIÊNCIAS E TECNOLOGIA
UNIVERSIDADE NOVA DE LISBOA

Setembro de 2015

Design of bio-inspired ionic liquids for protein stabilisation

"In the winter of our first experiments… looking on snow with new eyes. There the snow lay around my doorstep - great heaps of protons quietly precessing in the Earth's magnetic field. To see the world for a moment as something rich and strange is the private reward of many a discovery"

(E. M. Purcell, Nobel Lecture, 1952).

Agradecimentos

Em primeiro lugar e antes de tudo, quero agradecer aos meus orientadores: Ao Professor Eurico Cabrita, por sempre ter acreditado em mim, não apenas neste "projeto ambicioso", mas desde tempos remotos em que nem eu acreditava em mim. Obrigado por todo o empenho e esforço. Ao Doutor Ângelo Figueiredo, por todo o apoio e esforço. O início da tese foi algo complicada, demorada e desmotivante mas tudo melhorou com esta nova combinação de diferentes temáticas que abordo nesta tese. Grande parte da minha cultura científica que tenho devo-a a vocês. Um abraço.

Estes agradecimentos estendem-se aos seniores do grupo, Dra. Ana Sofia, Dra. Marta Corvo, Dra. Filipa Marcelo, obrigado por todas as discussões construtivas, ah um obrigado especial à Dra. Ana Sofia pela ajuda do fitting no DOSY!

Um agradecimento também para o Doutor Jorge Dias pelos vários esclarecimentos na produção de proteínas recombinantes.

Um agradecimento "carinhoso" aos meus colegas de laboratório, cuja companhia foi insuportável… mas não os podemos escolher! (cof cof) Um abraço para Tiago Paiva, Ricardo Martinho, Wagner e um grande beijinho às "alcoviteiras" Ana Diniz, Inês Rosete e Helena Coelho. Obrigado por toda a companhia e ajuda em severas horas de trabalho. Vá também mando cumprimentos à Carmen e ao Leo.

Um enorme abraço para Tiago Páscoa, João Cascão, PP (Bibó o Porto, ganhámos hoje ao Chelsea!), Sandro Casaleiro por me ter aturado na Costa da Caparica e ao Miguel aka Ressacas por todas as distrações! E por falar em ti, um beijinho para a Daniela!

Um abraço especial (assim ~ assim para não se acostumarem) ao Açores (João Silva) e Poeira (Diogo), autênticos amigos, de trabalho… e alguns copos (pequenos).

E aqueles que também me apoiaram diretamente nesta longa e cansativa jornada, amigos, sem vocês isto era tudo muito mais difícil, de nome Maria Carlos, Ana Gonçalves, Rafaela Santos, Tiago Pereira e André Rocha. Intitulamo-nos de "bananas" mas sem razão aparente, e que continue assim ☺ Obrigado por tudo, às vezes, 2 palavras vossas num dia mau, valem tudo. Um beijinho para as xu's Susana Oliveira, Talia Meireles e Sónia Alves (vá um abraço para o Loiro), obrigado por momentos fantásticos. A quem esqueci… diga-me qualquer coisa que podemos retomar a conversa para um café.

E por último e de tudo o mais importante, a família, obrigado por todo o esforço e trabalho para que esta tese fosse desta maneira conseguida. Nomeadamente, os meus pais, Manuel R., e Maria Rosa e claro ao meu irmão, Nelson, obrigado por todo o apoio e boa disposição. Dizem que somos parecidos.

Ah e obrigado a si, por começar a ler esta tese, não desista agora, vai valer a pena. Um abraço se for um ele, um beijinho se for uma ela.

Resumo

Líquidos Iónicos (LIs) consistem em sais orgânicos que são líquidos à temperatura ambiente ou próxima. Uma vez que os LIs são compostos inteiramente por iões, a formação de pares iónicos deverá ser uma característica essencial para a descrição de solvatação em LIs.

Nos últimos anos, as interações proteína – líquido iónico (P-LI) têm sido objeto de estudos intensivos, principalmente devido à sua capacidade de promover estabilização ou vice-versa em proteínas. No entanto, os pares iónicos e os seus tempos de vida na temática P-LI é esquecida, uma vez que a ação dos LIs é o resultado de um equilíbrio subtil entre interações catião-anião, ião-solvente e ião-proteína.

O trabalho desenvolvido nesta tese inova nesta temática, uma vez que o *design* de LIs para a estabilização de proteínas foi bio-inspirado nas altas concentrações de metabolitos orgânicos e carregados, encontrados no interior de uma célula. Embora esta perceção seja esquecida, as suas concentrações combinadas foram estimadas em cerca de ~300 mM, isto entre as macromoléculas em concentrações superiores a 300 g/L (condições de aglomeração macromolecular) e, claro, um par iónico transiente pode ocorrer naturalmente e ter um papel biológico especifico.

Por isso, o objetivo principal deste trabalho é desenvolver novos bio-LIs com um par iónico detetável e compreender os seus efeitos sobre a estrutura e estabilidade de proteínas, isto num ambiente aglomerado, utilizando técnicas avançadas de RMN e de calorimetria.

O LI glutamato de colina ([Ch][Glu]) foi sintetizado e caracterizado. O seu par iónico foi detetado (menos de 5.7 Å de distancia catião-anião) em água, utilizando principalmente a técnica de NOE – RMN. Através da mesma técnica, foi possível detetar uma promoção do par iónico semelhante tanto em ambientes naturais como sintéticos de aglomeração. Usando a espectroscopia de RMN (difusão de proteínas, experiencias de HSQC, e permuta deutério-protão) e calorimetria, a proteína modelo GB1 (produção e purificação em meio isotópico rico) foi estudada com [Ch][Glu] em condições de aglomeração macromolecular/ condições celulares mimetizadas.

Sob condição diluída, é possível afirmar que o [Ch][Glu] induziu uma hidratação preferencial através de interações fracas e não especificas, o que levou a uma estabilização significativa. Por outro lado, sobre ambiente de aglomeração, em que o par iónico é promovido, a proteína é destabilizada por fracas mas favoráveis interações hidrofóbicas que interrompem a hidratação na superfície. No entanto, tal capacidade pode anular o efeito dos agentes de aglomeração.

No geral, este trabalho explorou a existência de um par iónico e as suas consequências sobre as proteínas em condições similares às do meio celular. Desta forma, os metabolitos carregados encontrados na célula podem ser entendidos como um papel altamente relevante na estabilização de proteínas e a indústria farmacêutica pode ser revolucionada.

Palavras-chave: Líquidos Iónicos; Pares iónicos; estabilização de proteínas; aglomeração macromolecular; meio celular.

Abstract

Ionic Liquids (ILs) consist in organic salts that are liquid at/or near room temperature. Since ILs are entirely composed of ions, the formation of ion pairs is expected to be one essential feature for describing solvation in ILs.

In recent years, protein - ionic liquid (P-IL) interactions have been the subject of intensive studies mainly because of their capability to promote folding/unfolding of proteins. However, the ion pairs and their lifetimes in ILs in P-IL thematic is dismissed, since the action of ILs is therefore the result of a subtle equilibrium between anion-cation interaction, ion-solvent and ion-protein interaction.

The work developed in this thesis innovates in this thematic, once the design of ILs for protein stabilisation was bio-inspired in the high concentration of organic charged metabolites found in cell milieu. Although this perception is overlooked, those combined concentrations have been estimated to be ~300 mM among the macromolecules at concentrations exceeding 300 g/L (macromolecular crowding) and transient ion-pair can naturally occur with a potential specific biological role.

Hence the main objective of this work is to develop new bio-ILs with a detectable ion-pair and understand its effects on protein structure and stability, under crowding environment, using advanced NMR techniques and calorimetric techniques.

The choline-glutamate ([Ch][Glu]) IL was synthesized and characterized. The ion-pair was detected in water solutions using mainly the selective NOE NMR technique. Through the same technique, it was possible to detect a similar ion-pair promotion under synthetic and natural crowding environments.

Using NMR spectroscopy (protein diffusion, HSQC experiments, and hydrogen-deuterium exchange) and differential scanning calorimetry (DSC), the model protein GB1 (production and purification in isotopic enrichment media) it was studied in the presence of [Ch][Glu] under macromolecular crowding conditions (PEG, BSA, lysozyme).

Under dilute condition, it is possible to assert that the [Ch][Glu] induces a preferential hydration by weak and non-specific interactions, which leads to a significant stabilisation. On the other hand, under crowding environment, the [Ch][Glu] ion pair is promoted, destabilising the protein by favourable weak hydrophobic interactions , which disrupt the hydration layer of the protein. However, this capability can mitigates the effect of protein crowders.

Overall, this work explored the ion-pair existence and its consequences on proteins in conditions similar to cell milieu. In this way, the charged metabolites found in cell can be understood as key for protein stabilisation.

Keywords: Ionic liquids; ion-pairs; protein stabilisation; macromolecular crowding; cell milieu

Table of contents

List of Figures

List of Schemes

List of Tables

Nomenclature

[1,3 Dp][Glu]	1,3 Diaminopropane-glutamate ionic liquid
[Arg][Glu]	Arginine-glutamate ionic liquid
[Ch][Glu]	Choline-glutamate ionic liquid
AAIL	Amino acids ionic liquid
Bio-IL	Bio - ionic liquid
BSA	Bovine serum albumin
Ch	Choline cation
D_2O	Deuterium oxide
Dhp	Dihydrogen phosphate anion
DOSY	Diffusion Ordered Spectroscopy
E. Coli	*Escherichia Coli*
GB1	Immunoglobulin-binding domain B1 of *streptococcal* protein G
HSA	Human serum albumin
HSQC	Heteronuclear Single Quantum Coherence
IL	Ionic Liquid
IPTG	Isopropyl 1-thio-β-D-galactopyranoside
LMW	Low molecular weight
M9	Minimal medium
MW	Molecular weight
NMR	Nuclear Magnetic Resonance
NOE	Nuclear Overhauser effect
OAc	Acetate anion
PEG	Polyethylene glycol
PFGSE	Pulsed Field Gradient Spin Echo
pI	Isoelectric point
P-IL	Protein - ionic liquid
SDS-PAGE	Sodium dodecyl sulfate-polyacrilamide gel electrophoresis
T1	Longitudinal relaxation

Amino acids list

A/Ala	Alanine
C/Cys	Cysteine
D/Asp	Aspartic acid
E/Glu	Glutamate
F/Phe	Phenylalanine
G/Gly	Glycine
H/His	Histidine
K/Lys	Lysine
L/Leu	Leucine
M/Met	Methionine
N/Asn	Asparagine
P/Pro	Proline
Q/Gln	Glutamine
R/Arg	Arginine
S/Ser	Serine
T/Thr	Threonine
U/Sec	Selenocysteine
V/Val	Valine
W/Trp	Tryptophan
Y/Tyr	Tyrosine

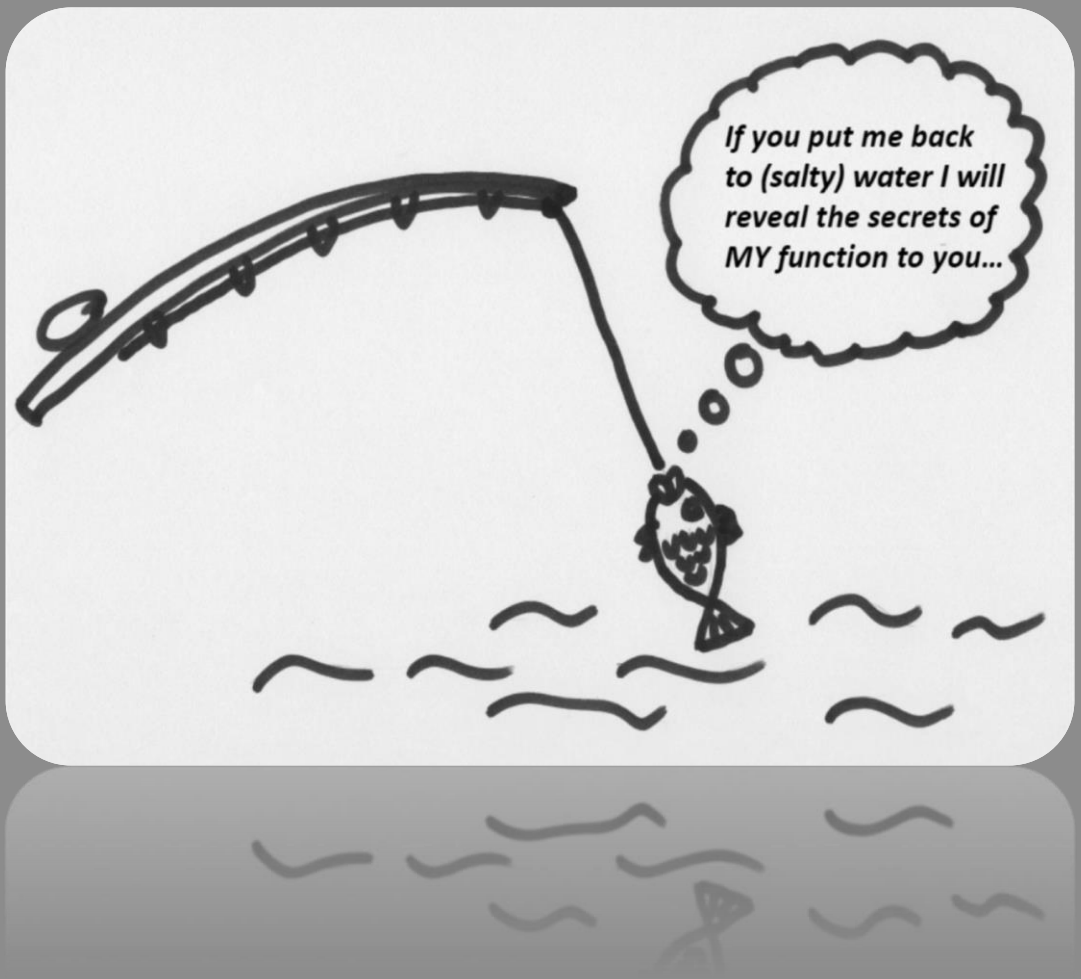

Cartoon representing that water (with salt ions and osmolytes) is essential for proper functioning of biological molecules (represented as a fish in the drawing).

Biological Water or Rather Water in Biology?
Pavel Jungwirth
The Journal of Physical Chemistry Letters **2015** *6* (13), 2449-2451

Chapter I: Introduction

In this chapter, the bio – ionic liquids (ion-pair), protein - ionic liquid interaction and macromolecular crowding themes were approached, likewise was created the hypothesis that ILs exists in vivo from the combination of charged metabolites to play specific biological roles in the cell. I will show some specific examples and biotechnological applications that can result from understanding how the interaction protein-ionic liquid works at molecular level under crowding conditions.

Table of contents

I. Introduction

I. 1. Ionic liquids

Simple inorganic salts, such as NaCl, melt at very high temperatures, which provide their routine use as solvents for chemical processing impossible. Salts with organic cations open a window for the liquid state in ionic environments near or even below room temperature. Adopting such ideas, the past decade has seen the advent of a new class of solvents, referred to as "ionic liquids" (ILs).[1,2] This term describes organic salts that are liquid at or near room temperature, taking 100 ºC as an arbitrary upper limit.

The birth of ionic liquids goes back to 1914, first research efforts dealt with the synthesis of ethylammonium nitrate ($[EtNH_3][NO_3]$; mp. 13-14 ºC), which was formed by neutralisation of ethylamine with concentrated nitric acid.[3,4] However, it was not recognized that chemistry in such solvents could become of broad interest.

The first ionic liquids with chloroaluminate ions were developed in 1948 by Hurley and Wler[5] at the Rice Institute in Texas as bath solutions for electroplating aluminum. However, these systems were not studied further until the late 1970s when the Osteryoung and Wilkes groups[6] replaced them. For the first time, they succeeded in preparing room temperature liquid chloroaluminate melts (they are now considered to form the first generation of ILs). Research and development concentrated mainly on electrochemical applications at this time. However, owing to rapid hydrolysis, such salts require an inert-gas atmosphere. These early developments are discussed in depth in an extremely interesting review by Plechkova and Seddon,[7] the paper discusses the history of the academic research and industrial application of ionic liquids with a few prospects for future developments.

As early as 1967, a publication by Swain *et al*.[8] described the use of tetra-n-hexylammonium benzoate as a solvent for kinetics and electrochemistry, this investigation had a revolutionary significance because it already contained a quantitative determination of the ionization strength of the ionic medium. In the 1980s initial, the groups of Seddon and Hussey[9] began to use chloroaluminate melts in polar solvents for the investigation of transition metal complexes focusing on the electrochemical aspects, Wilkes and Hussey[10] were fully realised in the studies when the $[C_2mim]Cl–AlCl_3$ ionic liquid archetypal system showed less viscous and much wider electrochemical range than the $[C_4py]Cl–AlCl_3$ system, this combination was the first example of an system that was liquid at room-temperature (inside an inert atmosphere box), followed by spectroscopic and chemistry experiments.[9]

In the 1990s it became increasingly clear that many cation-anion combinations form water-stable room temperature ILs. In 1992, the report "Air and water stable 1-ethyl-3-methylimidazolium

based ionic liquids" by Wilkes and Zaworotko[11] demonstrated the preparation and characterisation of a new range of ILs with the previous 1-ethyl-3-methylimidazolium $[C_2mim]^+$ cation, but now also contained a new variety of anions as $[CH_3CO_2]^-$, $[NO_3]^-$ and $[BF_4]^-$. Since this year, a wide range of ILs has been developed incorporating many different anions as $[PF_6]^-$, $[N(CN)_2]^-$, $[CF_3SO_3]^-$, *etc*. With this references, we should not forget that the first $[EtNH_3][NO_3]$ IL was a nitrate and other report in the same year when the Wilkes and Zaworotko paper appeared, "New, stable, ambient-temperature molten salts" by Cooper and O' Sullivan[12] in a conference proceedings (therefore less familiar in ILs science), reported the synthesis of $[C_2mim][CF_3SO_3]$ and $[C_2mim][CH_3SO_3]$. Therefore, ILs based on more hydrophobic anions were synthetized by Grätzel group.[13,14]

After the beginning of water stable ILs, chloro-aluminates have only subsisted in some places of electrochemistry (due to their moisture sensitivity), their use in organic and catalytic experiments was well reported in 1999 by Seddon and Holbrey[15] and Tom Welton.[1]

In 1995, for the first time, the NOE NMR technique was employed for ILs in the study by Osteryoung and co-workers[16], the pioneering research work demonstrated the existence of intermolecular NOE interactions between ring protons (cation-cation) in $[C_2mim][Cl]$ - $AlCl_3$ suggesting a local/ short range on the structure.

Over the years that followed, a new class of ILs based on phosphonium, pyrrolidinium and imidazolium were explored. Specially, the 1-alkyl-3-methylimidazolium salts were focused in an overwhelming number of publications, the imidazolium based cation can be combined with a large range of anions, from simple inorganic ions as $[Cl]^-$ or $[BF_4]^-$ to novel such as $[dca]^-$ or perfluorated anions ($[Tf_2N]^-$).[17] **Scheme I.1** presents some important ions studied in this new class of ILs.[18] Apart from the explored 1-alkyl-3-methylimidazolium ions (**I**), the most preferred salts are those with pyrrolidium (**II**), pyridinium (**III**), tetraalkylammonium (**IV**), or tetraalkylphosphonium ions (**V**). Around the year 2008, existed an increasing interest in cations functionalized, such as polar, fluorinated, or chiral side chains which are often optimized for given applications. These ILs were denoted as "build on purpose" [task-specific ILs].[19]

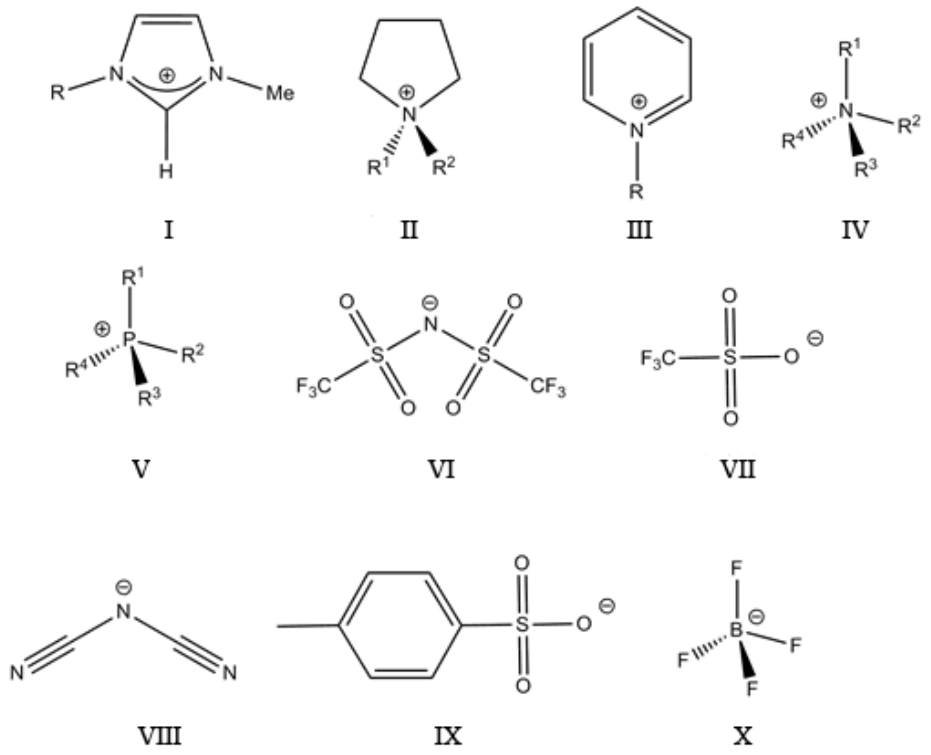

Scheme I.1. Important ions with their abreviations.
I: 1-alkyl-3-methylimidazolium ($[C_nmim]^+$); **II**: 1,1-dialkylpyrrolidinium ($[C_mC_npyr]^+$); **III**: 1-alkylpyridinium ($[C_npy]^+$); **IV**: tetraalkylammonium ($[N_{ijkl}]+$); **V**: tetraalkylphosphonium ($[P_{ijkl}]+$); **VI**: bis(trifluoromethanesulfonyl)amide ($[Tf_2N]^-$); **VII**: trifluoromethanesulfonate ($[TfO]^-$); **VIII**: dicyanamide ($[(CN)_2N]^-$ or $[dca]^-$); **IX**: tosylate ($[OTos]^-$); **X**: Tetrafluoroborate ($[BF_4]^-$). Adapted from Weingärtner.[18]

Among the anions, halides give rise to unfavourable properties and are strongly hygroscopic. Considerable work has focused on salts based on $[BF_4]^-$ (**X**) or $[PF_6]^-$ ions, but in moisture condition, these anions hydrolyse, release HF for example.[20] Since these reports, the more complex perfluorated anions are preferred: $[Tf_2N]^-$ (**VI**) or $[TfO]^-$ (**VII**), or halogen-free ions, such as dicyanamide (**VIII**) or tosylate (**IX**).

Accordingly with Weingärtner,[18] the combination of long-range Coulombic forces between the net charges cation-anion and extremely directional short range forces found in their molecular and electronic structures results in unique physico-chemical properties and solvent properties,[21] such as polarity,[22] melting point,[13] ionic conductivity[23] and viscosity.[24] Thus and using the term described by Freemantle in 1998,[25] the ILs are denoted as "designer solvents".

In analogy to the familiar classification of molecular solvents one can distinguish between aprotic and protic ILs. Despite the huge number of ILs is aprotic, the protic ILs are important due the high ionic conductivity, they resulted by proton transfer from a Brönsted acid to a Brönsted base, thus the cation provides a vehicle for exchangeable protons. The properties and application of these ILs was well reviewed by Greaves and Drummond.[26]

Another type of solvent with similar physical properties and phase behaviour to ILs with great interest are "deep eutectic solvents" (DES),[27] recently alleged by Dai *et al.* as new potential media for green technology. [28]

ILs have emerged as a novel class of compounds to be used in many fields,[29] namely electrochemistry, organic synthesis, (bio) catalysis,[30,31] electrochemistry, and carbon dioxide capture.[32] ILs have also been applied in the field of self-assembling amphiphilic systems, in aqueous solutions ILs can form surfactants with their amphiphilic nature found in the cation or anion, or in both.[33] In this thesis, I consider applications of ILs in protein (bio) chemistry, in detail later.

Recently, apprehensions have risen over the potential toxicity as well as the low biodegradability and poor biocompatibility of most of the currently employed ILs aforementioned.[17,34] To overcome this problem, ionic liquids from non-toxic and renewable biosources and natural products (amino-acids, vitamins, *etc*.) thus meeting environmentally nonthreatening (green chemistry) have been highly conceived and proposed. [35–38] The natural ions with an interesting molecular diversity have the potential to be converted into ILs by means of green procedures, such as simple ion exchange and/or acid–base reactions.[39]

Natural amino acids were first used in 2005 by Fukumoto *et al.* for the synthesis of different twenty amino acid 1-ethyl-3-methylimidazolium-based ILs (AAILs).[40] An aqueous solution of [C_2mim][Cl] was passed down a column of ion exchange resin to generate a dilute aqueous solution of [C_2mim][OH], which was then neutralized with an aqueous solution of the amino acid. This procedure was confirmed successfully for when the hydroxide salt is unavailable and for ILs with more basic anions, since the typical metathesis step and subsequent washings/separations cannot be performed for some cation-anion combinations. Amino acids besides being one of the most abundant sources and chiral pools in nature, reported as non-toxic, biodegradable and biocompatible products, are candidates to ideal functional ILs. They can act as cation or anion due to the fact that they contain an amino and a carboxylic acid group in a single molecule.[41,42] Such ILs proclaimed a new research field, "Bio-ILs", being able to find application in all of the biological and pharmaceutical sciences (some structure ions used in AAILs are represented in **Scheme I.2**).

Also Ohno's group synthetized tetraalkylphosphonium-based amino acid ILs (**III**), besides such ILs had halogen-free and relatively high decomposition temperatures, their importance reflects only in CO_2 capture.[43]

In addition, another important green natural ion is choline (**II**), a quaternary ammonium cation, $[NMe_3(CH_2CH_2OH)]^+$, which is an essential micronutrient for normal functioning of all cells.[44,45] Less attention has been paid to ILs with cholinium as the cation and amino acids as the anions ([Ch][AA]) and reported applications of such ILs have focused solely on their activities as catalysts.[38]

However, in 2012 Qiu-Ping Liu et al.[35] synthetize eighteen [Ch][AA] ILs and gave us a new viewpoint about this pioneering and natural combination, nonetheless such ILs have never been studied in biological systems.

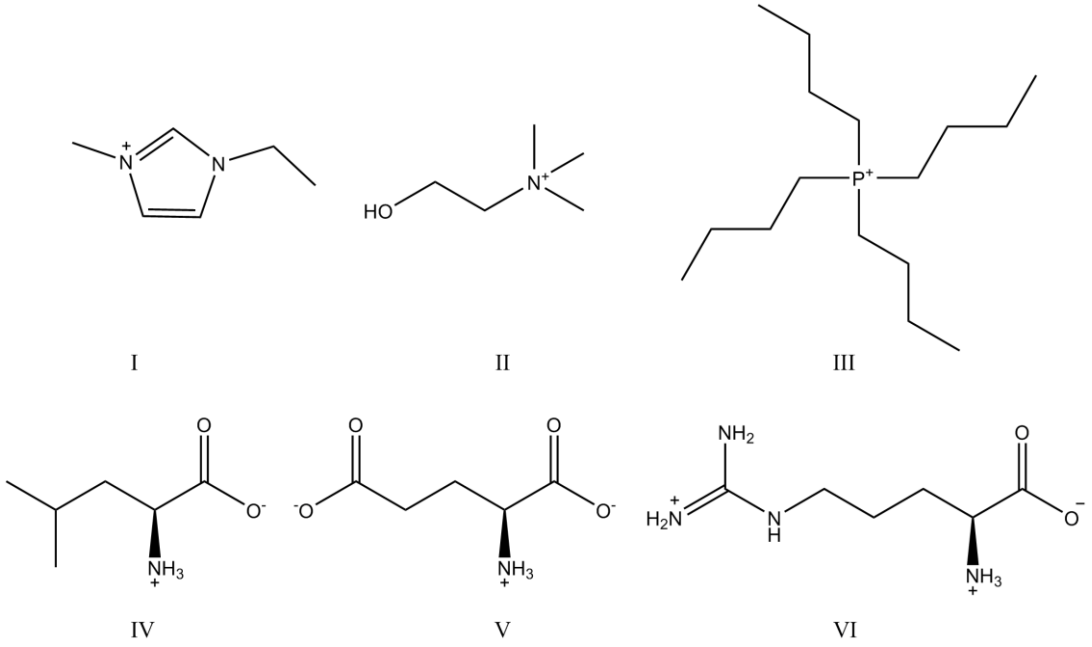

Scheme I.2. Structures of the cations (I-III) and few amino acids (IV-VI) at physiological pH, generally used in AAILs.
I: 1-ethyl-3-methylimidazolium ($[C_2mim]^+$); **II**: Choline ($[Ch]^+$); **III**: Tetrabutylphosphonium ($[TBP]^+$); **IV**: Amino acid Isoleucine ([Ile]); **V**: Amino acid Glutamate ($[Glu]^-$); **VI**: Amino acid Arginine ($[Arg]^+$).

Since the study of Pernak *et al.* about the eco-toxicity of ILs,[46] it became important to evaluate this class of green solvents in their toxicity and biodegradability. Arning *et al.*[47] showed that head groups of the cations of ILs play a major role in toxicity. Specifically the ILs containing quaternary ammonium cation (like choline incorporating a polar hydroxyl group) generally display much lower toxicity and environmental impact than those with aromatic cations such as imidazolium and pyridinium.[36,48–50]

Furthermore, a variety of cholinium-based ILs has been reported to have low toxicity and to be highly biodegradable. [51–54]

I. 1. 1. Ion-pairing in ILs

Since ILs are entirely composed of ions, the formation of ion pairs is expected to be one essential feature for describing both solvation in ILs and solvation of ILs in other media.[22] The commonly accepted fundamental equilibrium species are the fully solvated ions, $C^+ + A^-$, solvent-separated ion pairs, $C^+||A^-$, and contact ion-pairs, (CA), *i.e.* fully associated ions.[55] Typically, large ion concentrations, low dielectric media, and small ion radii all shift the equilibrium toward ion-pairing in general and the contact ion-pair species in particular. Lower temperatures also shift the

equilibrium toward ion-pair formation but in most cases lower temperatures favour the solvent-separated ion-pair species over the contact ion-pair species.[55,56]

The apparent deficiency of strong cation–anion interactions not only results in low melting points (ionic bonds are more stronger than non-covalent forces such as Van der Waals or hydrophobic bonds), but also presumably gives significant structural changes and short-lived ion pairs.[23]

Among the features of cation-anion interactions, the alleged formation of ion-pairs has attracted much attention recently, because the intense attractive interaction between ions is expected to yield long-lived association of ions. There are, still, questions remaining about the nature and the detailed source of this possible association. It has been suggested by some authors that cations and anions are bonded to ion-pairs through hydrogen bonds for some ionic liquids such as $[C_2mim][Tf_2N]$[57] and $[C_4mim][Cl]$[58,59] in which the existence of hydrogen bonds of high binding energy between cation and anion has been shown in the gas phase.

Following Welton *et al.*[60], Tubbs *et al.*[56] and Kodderman *et al.*,[57] it is presumed that the $[C_2mim]^+$ cation progressively forms ion pairs with the anion with decreasing concentration in organic dilute solution. Yet Tubbs[56] found two resonance sets by ^1H NMR, indicate ion-pair species with long life times in low dielectric media (main solvent was $CDCl_3$).

In a simulation study, Del Popólo and Voth[61] have suggested that the reduction in conductivity on $[C_2mim][NO_3]$ might result from the short relationship in the motion of neighbouring cations and anions at a sub-picosecond time scale (200 ps), that indicate the presence of short-lived anion-cation pairs. The principal contribution to the configurational energy comes from the long-range Coulombic interactions, and this results in charge-ordering effects. A screening length of 7 Å indicates a fast decaying effective interaction between the ions. In addition, three-dimensional charge distributions around cations show the localization of $[NO_3]^-$ in different regions of the first coordination shell.

In other molecular dynamics simulation work, Zhao *et al.*[62] studied $[C_4mim][PF_6]$ and reported hydrogen bond lifetimes with less than 1 ps, whereas the lifetime of cation-anion contacts is in the range of nanoseconds mainly mediated by Coulombic forces. In addition, some authors have confirmed the hydrogen bonding with the C2-H of imidazolium is not essential for the attraction in the ion pair.[63–66] Also, Fraser *et al.*[67] have revealed that phosphonium-based ILs appear to be of relatively low degree of ionicity due to strong ion pairing.

By multinuclear pulsed field gradient spin-echo (PFGSE) NMR techniques it is possible to accurate measure the ions self-diffusion coefficients (cation and anion) and that has enabled many successful studies along this thematic of ion pairing, once the diffusion of each ion is critically affected by extension of ion-pair. In particular, the early studies by Watanabe's group have a great impact on the current interpretation about ion pairing.[68–70]

Experimental results on C-H vibrations coming from FT-IR spectroscopy indicates that ion-pair interactions may be observed at sub-picosecond time-scale.[57] Other experimental results that come from dielectric relaxation spectroscopy indicates that no such interactions are detected above the nanosecond time-scale.[71]

The lifetime of the ion pair is also pertinent for the interpretation of the intermolecular NOE by NOESY/ROESY NMR methods,[72,73] the existence of a measurable intermolecular NOE in cation-anion interaction has been exploited in several studies.[21,74] The ion pair has to survive long enough to be detect, typically on nanosecond time-scale (0.5 ns in ^{1}H NMR) with minimum average inter-nuclear cation-anion distance of 5 Å for intermolecular NOE.[75] Pochapsky and Stone determined the ^{1}H,^{1}H and ^{11}B,^{1}H NOEs in the $[(C_4H_9)_4N][BH_4]$ ion pair using HOESY NMR.[76] But the first investigations in neat ILs were performed by Mele *et al.*[77] for $[C_4mim][BF_4]$ and $[C_4dmim][BF_4]$ using the rotating frame NOE experiment (ROESY). The influence of IL as co-solvent was studied by Nama *et al.*[78] for ion pairs in neat, methanol and dichloromethane solvents. They have observed that the addition of methanol separates the ions, but in dichloromethane solution the anions and cations show strong HOESY contacts (strong ion pairing). However, the first to apply homonuclear ^{1}H,^{1}H HOESY NMR spectroscopy on ionic liquids in organic solvents to study ion pairing was Dupont,[79] they found ^{1}H,^{1}H NOEs as a proof for ion pairs in dilute [1-*n*-butyl-3-methyl-imidazolium] $[BPh_4]$ IL in $CDCl_3$ with hydrogen bonding distances to the phenyl ring centroid around 2.3 Å.

An interesting study were the results of the intermolecular ^{1}H,^{19}F NOE in $[C_4mim][BF_4]$ at dichloromethane solvent media by Giernoth's research group,[80] which seems to indicate the existence of cation-anion pairs with life times on the nanoseconds time. Their measurements of dilute samples demonstrated the increase of ion pairing based on Coulombic forces in less polar unlike to highly polar (dimethyl sulfoxide) in the expected way.[81]

Nevertheless the long-time NOE factors can been attributed to the existence of long-lived hydration shells as reported by Halle's group.[82] Accordingly with Weingärtner,[21] the lifetime of these cation–anion correlations is limited to the sub-picosecond-to-picosecond regime, which contradicts the intuitive representation of long-lived pairs.

Lately, some groups used molecular dynamics simulation for the study of new and important imidazolium-based AAILs class where the anion is a natural amino acid, such ILs emerged due to the classic work of Fukumoto *et al.* cited above.[40] Initially, Woo and co-workers[83] simulated certain equilibrium and transport properties of AAILs. They revealed that all $[C_2mim][AA]$ ionic liquids were in the strongly coupled regime. The amino acids with acidic and amide functional groups had strong anion side chain-cation and anion-anion hydrogen bonding, which lowers the ionic conductivities in these ILs. This indicates that strong ion-pair formation is an important contributor to the small ionic conductivity of some of these ionic liquids. Stronger ion pairs form when the functional group R on the amino acid side chain includes polar groups that can interact electrostatically with the cation from

two polar functional groups on the molecule, strengthening the interaction between positive and negative ions.

Following this study, Dagade *et al.*[84] reported thermodynamics of ionic hydration and discussed solvent–solute interactions of AAILs in water at room conditions. In detail, the hydrophobic interaction exists in aqueous AAIL solutions along with strong cooperative anionic hydration. The anion−anion hydrophobic interactions are more prominent in aqueous solutions of [C_2mim][Leu] IL and [C_2mim][Ile] IL, whereas interactions between unlike charges (cation−anion) are more significant in aqueous solutions of [C_2mim][Gly], once glycine has non hydrophobic character.

Overall, these studies and their extension for other amino acid ionic liquids with different cations will reveal more information about ionic and non-covalent interactions which can help to comprehend the potential use of these AAILs toward a better understanding of more complicated biological processes.

To date, ion pairs and their lifetimes of ILs in water are not well understood and their relevance in cation-anion interactions and ion-solvent interactions makes them unpredictable.

I. 2. Biomolecules and ionic liquids

The first example of using an enzyme in an IL was reported in 1984 when Magnuson and co-workers[85] demonstrated the activity and stability of alkaline phosphatase in aqueous mixtures of [$EtNH_3$][NO_3] exposed by Walden in 1914.[3] Unfortunately, this discovery did not attract significant attention due to the absence of knowledge of ILs at that time.

The stabilization of proteins is a priority for several important fields, most notably the pharmaceutical industry. Due to widespread application, it is necessary to maintain the three-dimensional structure of proteins through some weak interactions including hydrogen bonds, hydrophobic and ionic interactions. A change in microenvironment of proteins disrupts these interactions, causing denaturation of proteins which leads to protein unfolding and inactivation.[86,87]

Although there are many factors that cause denaturation of proteins, thermal denaturation is a major problem in storage of proteins and similarly during its reaction process. To stabilize proteins outside their native conditions, several strategies like chemical modification, immobilization, genetic modification, and addition of stabilizing agents have been developed but without great success. The long shelf-lives of many proteins, including therapeutic proteins can be achieved by lyophilisation (freeze-drying). In order to increase the solubility and to prevent denaturation and aggregation of protein therapeutics, some excipients like sugars, salts and amino acids have been used.[88,89]

Over the last decade, the manipulation of ILs as co-solvents for water in protein stability[90–92], activity[93,94], refolding[95–99] and aggregation[100,101] has been subject of intensive studies.[102–105]

Notably, the encounter of proteins with ILs can alter the thermodynamically stable conformation leading to unfolding/misfolding/refolding depending upon the IL type and physiological conditions, which have generate the protein–IL studies highlighted. [93,100,106–108]

I. 2. 1. Effect of cations and anions

The effect of salts on water structure at surfaces has been explored,[109] these ions have long been classified as being either kosmotropes (structure makers) which tend to precipitate proteins from solution and prevent protein unfolding or chaotropes (structure breakers) which increase solubility and promote the denaturation of proteins, according to their relative abilities to induce the structuring of water. Small ions (kosmotropes) due to their high charge densities cause strong electrostatic ordering of nearby waters, breaking hydrogen bonds (strongly hydrated). But the overall entropy is lower because the water molecules are highly organized near the cation.[110] In contrast, large ions (chaotropes) have low charge densities and singly-charged ions such as $[SCN]^-$ (thiocyanate), $[H_2PO_4]^-$ ($[dhp]^-$, dihydrogen phosphate), $[HSO_4]^-$, $[HCO_3]^-$, $[I]^-$, $[NO_3]^-$, $[BF_4]^-$, $[NH_4]^+$, $[Cs]^+$, $[K]^+$, $[(NH_2)_3C]^+$ (guanidinium), $[(CH_3)_4N]^+$ (tetramethylammonium), *etc*. and therefore surrounding water molecules are largely hydrogen bonded (weakly hydrated).[111] Such effects exhibit a re-occurring trend called the Hofmeister series, shown in **Scheme I.3 (top)**, which is observed to be more pronounced for anions than for the cations, based on nature, size and polarizability.[112–114] Mason and co-workers[115] found two important chaotropes (guanidinium and thiocyanate ions) poorly hydrated, allowing them to preferentially interact with the protein rather than the water.

Galamba *et al.*[116] reported that the interaction of the ions with the hydrophilic/ hydrophobic amino acid group is considerable more significant than ion-induced long range water structure perturbations. Kumar and Venkatesu[102] finished their review admitting the interaction of the Hofmeister series - protein surface is a result of the ability of the ions to disrupt hydrogen bonding, non-polar interactions, and electrostatic effect for protein stability contribution and ions do not necessarily stabilize/destabilize the biomolecules in perfectly the same Hofmeister order. Also stability studies on ribonuclease A (Rnase A),[93] bovine serum albumin (BSA)[117] and human serum albumin (HSA)[108] have indicated that for aqueous ILs the combination cation-anion can be important where the anionic moieties play a main role in the IL-protein interactions following an anion specificity order (almost Hofmeister order) according to their protein stabilising, denoted in **Scheme I.3 (bottom).** That represents the stability and destability of the protein through direct interactions of the ILs with the protein surface based on their specific properties to stabilize the water structure.[102]

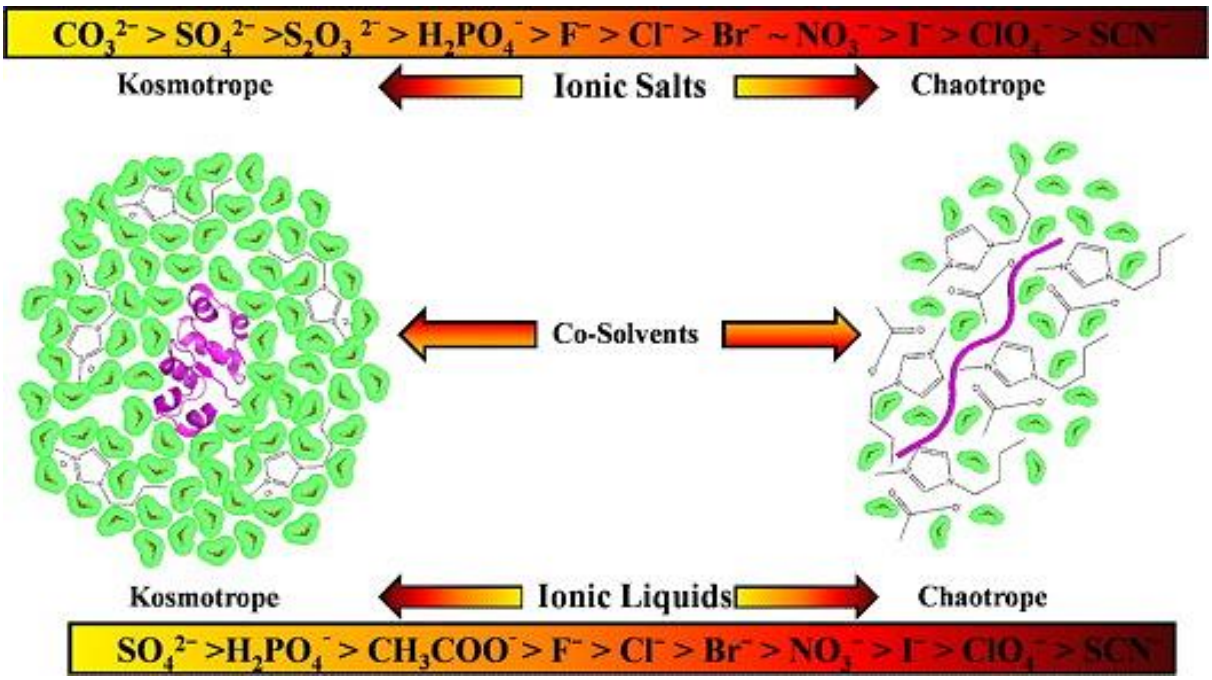

Scheme I.3. The typical order for the anion Hofmeister series (top) and anion specificity order accordingly with protein stability (bottom).
Adapted from Kumar and Venkatesu.[102]

Fujita *et al*.[106] have studied the stability of cytochrome c in different ILs with varying kosmotropicity/ chaotropicity and reported that hydrated choline dihydrogen phosphate [Ch][dhp] IL is an excellent combination of chaotropic cation and kosmotropic anion to stabilize cytochrome c, beyond that the structural activity remained for 18 months at room temperature. Likewise, high enzyme stabilities were achieved for the same combination in the Zhao *et al*.[110] and Weaver *et al*.[118] reports.

In another investigation, the activity and stability of *Penicillium expansum* lipase (PEL) enzyme was observed by Lai *et al*.[119] that in aqueous solution of 14 different ILs follows the Homeister series. In presence of ILs containing same anion, PEL activity decreased in the order of $[C_1mim][MeSO_4]$ > $[C_2mim][MeSO_4]$ > $[C_4mim][MeSO_4]$, $[NMe_4][OAc]$ > $[NBu_4][OAc]$, $[NHMe_3][MeSO_3]$ > $[NBu_4][MeSO_3]$, and $[NHMe_3][dhp]$ > $[NHEt_3][dhp]$ > $[NHBu_3][dhp]$, while for the ILs containing same cation, the order was [Ch][OAc] > $[Ch][MeSO_3]$ > $[Ch][NO_3]$, $[NBu_4][OAc]$ > $[NBu_4][MeSO_3]$.

It has been reported that the anion effect on protein stability is largely dominant.[90,92,93] Explicitly, Sedlák *et al*.[120] reported the interactions between charged groups on surface of acidic *Desulfovibrio desulfuricans* apoflavodoxin and basic horse heart cytochrome c proteins and the ions in solution. These charged groups were found to interact strongly with the chaotropic anions (such as $[SCN]^-$) and weakly with kosmotropic cations (such as Na^+, K^+). Other example, β-glycosidase have very low activity in aqueous solutions of $[C_4mim][BF_4]$, because of chaotropic nature of its anion. [121]

Although ILs unfold/refold/stabilize the protein over a wide range of temperature, the thermal stability of proteins depends on the specificity of ILs: The protic IL, ethylammonium nitrate, induced reversible thermal unfolding/refolding and long period stabilization of lysozyme against aggregation and hydrolysis but refolding was not observed for other proteins like myoglobin or cytochrome c.[100] Atkin's group also observed high thermal stabilization and activity of lysozyme in ethylammonium formate.[122] Constatinescu *et al.*[101] work aforementioned, investigated Rnase A with different ILs and stated that though choline-based IL stabilized and imidazolium-based IL destabilized the protein, however both the ILs suppressed aggregation. In addition to this study, exist other reports that characterized the effect of imidazolium-based ILs as strong denaturants.[93,107,108,117,123–125]

I. 2. 2. Ionic liquids acting as an osmolyte

Like salts, osmolytes have significant effects on protein folding and stability.[88,126,127] Osmolytes are small organic solutes, that can occur in zwitterionic form, that are accumulated at high intracellular concentrations by nature to protect the cell and cellular components against particular denaturing/osmotic stress such as variations in internal stress, temperature, salinity and pH.[128,129] Certain osmolytes, like urea are non-compatible and degrade protein function and disrupt their structures in cell (it is widely used as a denaturant), whereas other compatible osmolytes such as trimethylamine-N-oxide (TMAO) and betaine are powerful stabilizers **(**Scheme I.4).[130–132]

Accordingly with Zang and Cremer,[133] the protein structure at molecular level in the presence of osmolytes can be affected by: direct mechanisms involving hydrogen bonding between osmolyte molecules and peptide backbones and/or polar and charged side chains or indirect effects as influences of osmolytes on the solvation of hydrophobic portions of the protein or changes to bulk water structure. The stabilization of compact native structures typically results of preferential exclusion of osmolytes from the vicinity of the macromolecule surface. Energetically, unfavourable interactions can exist between osmolyte and hydration surfaces of the protein. The exclusion of osmolytes from the proximity of the protein surfaces inevitably means the inclusion of water in the surface of proteins, which is naturally termed preferential hydration (hydration layer).[134–136]

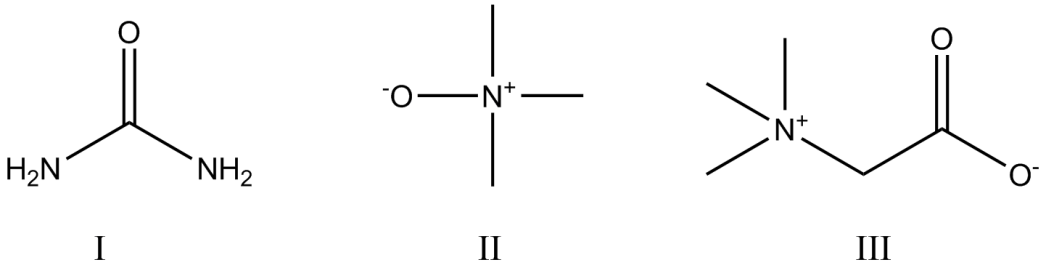

Scheme I.4. Structures of the osmolytes best known.

I: Urea (non-compatible); **II**: Trimethylamine-N-oxide (TMAO) and **III**: Betaine (compatibles).

Being composed of organic ions, ILs can also act as osmolyte but protective action may vary depending on the type of constituent ions and protein type. Generally, the protective or denaturing action of osmolytes depends upon the displacement of the water molecule by added osmolyte from the hydration layer around the protein in aqueous media.[104] For example the compatible osmolytes[129] like polyols, amino acids, methylamine assists in preferential hydration of proteins and hence stabilizes them.[134] Nonetheless, non-compatible osmolytes[129] like urea and guanidinium-hydrochloride (GdnHCl) denature the protein by favourable interaction with the interior of protein leading to solvent-accessible surface area of protein hydrophobic patches leading to protein unfolding.[134]

Attri *et al.* [137,138] have investigated the thermodynamic stability of model peptides and α -chymotrypsin enzyme with ILs containing ammonium cation with varying chain length and anions as an osmolyte. They reported an unfavourable interaction of ILs with the peptides surface for their stability, indicating the non-interacting propensity of ILs ions with protein residues due to their exclusion by water molecules from the proteins hydration layer.

Other osmolyte effect of ILs was presented by Sankaranarayanan *et al.*,[139] $[C_2mim][EtOSO_3]$ on protein β-lactoglobulin induced hierarchical helix-beta conformational transition of protein at pH 4.0 and non-hierarchical conformation at pH 7.5 by changing the microviscosity around the secondary structure of protein with the exothermic enthalpy changes. At low pH the solvation contributes to the enthalpy change with higher enthalpy IL-protein interaction, contrariwise at physiological pH, as an osmolyte, the IL moieties excludes the water molecules from hydration layer around the protein by non-specific interactions and induced conformational changes in the secondary structure of protein.

Furthermore, Bhattacharyya and co-workers[140] reported the decrease of HSA solvation dynamics when adding imidazolium-based ILs (protein unfolding), for that, the protein was covalently labeled by a fluorophore attached via the lone cysteine group and the probe studied by solvation dynamics. Also, Yoshimura's group described structural change in chicken egg white lysozyme in the highly concentrated aqueous $[C_4mim][NO_3]$ solutions (0–24 M). The protein adopted a partially globular state (tertiary structure was disrupted), that was explained by dehydration of the important protein binding sites at high contents of IL.[141]

In our previous studies with imidazolium-based ILs, it has addressed the nature of Protein-IL (P-IL) focusing on protein structural modifications and specific P-IL interactions, discerning the level of cation towards protein stability.[107,108] In Figueiredo *et al.*[107] work, it has shown that protein destabilisation is a consequence of a direct effect of the IL interaction with the small alpha-helical protein Im7 governed by a combination of hydrophobic and electrostatics interactions dictated by the charge at the protein surface. The IL cation and anion have different effects on structure and stability where the denaturing interactions with the anion are dominant and dictate the overall stability, however cation still plays a key role. Specifically, $[C_2mim][dca]$ causes an partial dehydration of

protein leading their denaturation compared to less dehydrating [C_2mim][Cl], thus these ILs can be considered non-compatible osmolytes. In Silva *et al.*[108] work, it has investigated the effect of imidazolium cation on denaturation of human serum albumin (HSA) and reported that increasing hydrophobic chain length increases the denaturation due to increased surface contacts between cation and protein, mediated by weakly hydrophobic and non-specific interactions where the mostly hydrated anion (their nature modulated cation-protein interaction) is accumulated around the protein. Still, was proposed that destabilising anion effect on proteins may have arisen from partial contributions from the cation via cation-anion pair and cation-protein interactions. The importance of the side chain length of imidazolium-based IL in protein stability was also denoted by Akdogan *et al.*[123] Thus, more water-biocompatible ILs should be used in protein studies, such as those containing choline (hydroxylated cation) with a less degree of protein interactions that allow inclusion of water in the protein surface stimulating the hydrogen-bond strength of interfacial water acting as an bio-compatible osmolyte.[133,142] Notwithstanding, the choice of the anion must be careful once the protein stability and their solvation rely on the results of a subtle equilibrium between anion-cation pair strength, ions-solvent and ions-protein interactions.

Nevertheless, most of the reported data in protein stability concerns the effect of imidazolium-, ammonium- and choline-based ILs, little attention has been given to the biocompatible ILs using amino acids as anions (AAILs) on proteins. Recently, Chevrot *et al.*[143] using molecular dynamics simulations have investigated the structure of model mini-protein (20 AA) in the imidazolium-based AAILs aqueous solutions. They report the complete substitution of water by organic cations and anions further results in hindered conformation flexibility of the mini-protein. Also a recent publication[144] has demonstrated that the chemical properties of the protein or the surface also enforce a significant contribution to the resulting preferential binding or preferential exclusion behaviour. Followed by the study of the influence of 1-ethyl-3-methylimidazolium acetate [C_2mim][OAc] IL, on the stability of a small β-hairpin peptide (the C-terminal from the B1 domain of the protein G with residues 41–56, denoted by its PDB identifier 2GB1) by atomistic molecular dynamics simulations.[145] The presence of large cations like $[C_2mim]^+$, which form a first layer around the peptide is compulsory for the accumulation of the acetate ions. Hereby, $[C_2mim]^+$ cations of the first layer attract the oppositely charged OAc^- ions due to electrostatic interactions. The preferential binding of OAc^- at shorter distances is then facilitated by an unfolding of the native structure showing that such IL behaves like a denaturant (chaotropic co-solute). In addition and agreeing with osmolytes action, it was proposed that denaturants directly interact with protein surfaces while protectants are located in the second or the third hydration shell.

According to the protein-AAILs computational analysis[143,145] and isolated computation studies in ion-pair of such ILs,[83,84] AAILs emerge as an exciting candidate co-solvent acting as an compatible osmolyte for a robust protein solvation, conservation, and storage.

I. 2. 3. Charged metabolites and bio–ionic liquids

Lately, ionic liquids synthesis has been directed to the use of natural and bioorganic ions (bio-ILs), such biocompatible ILs hold the water mimicking property, acting as a bio-protective osmolytes helping protein conformational dynamics. Although this perception is overlooked, these type of ions can be part of metabolites found in cell milieu. In reality, the combined concentrations of organic metabolites (mainly charged) have been estimated to be ~300 mM![146] Recent advances in metabolomics technologies have allowed the concentrations of large numbers of metabolites to be measured in cells,[146,147] with that Selenko and co-workers[148] have discussed the composition of the prokaryotic and eukaryotic cytoplasm in terms of average ion and metabolite concentrations, as depicted briefly in **Table I.1**:

Table I.1. *E. Coli* Statistics from CyberCell database and metabolite concentrations in glucose fed. Adapted from Bennett *et al*.[146]

	Small molecule concentrations in *E. Coli* cell	
Regular cell	**Number of water molecules/ cell**	$2.34x10^{10}$ (23.4 billion)
	Number of ions/ cell	120,000,000 (300 mM)
	Number of small organics/ cell	18,000,000 (40-50 mM)
	Number of K^+ ions	90,000,000 (200-250 mM)
	Number of Na^+ ions	2,000,000 (5 mM)
	Number of glucose/ cell	400,000 (1 mM)
	Number of ATP/ cell	3,000,000 (7.0 mM)
	Number of NADP/ cell	240,000 (0.63 mM)
	Number of all free amino acids/ cell	6,000,000 (1.5 mM)
In glucose fed	**Combined concentrations of metabolites**	300 mM
	Glutamate (Glu^-)	96 mM
	Glutathione	17 mM
	ATP	9.6 mM
	Polyamine metabolites: putrescine; spermidine	~20-30 mM; ~6-7 mM (respectively)

In glucose fed, exponentially growing *Escherichia coli (E. coli)* cells the combined concentrations of metabolites have been estimated to be ~300 mM, with glutamate (Glu^-) being the most abundant metabolite by far (96 mM), followed by glutathione, fructose 1,6-bisphophate and adenosine triphosphate (ATP) at 17 mM, 15 mM and 9.6 mM, respectively.[146] However, these concentrations depend on the culture medium. By changing the carbon source from glucose to glycerol or acetate, intracellular metabolites levels differ slightly.[146] However, CyberCell lists the combined *E. coli* concentrations of all small organic molecules as 40−50 mM (undefined growth medium and stage), concentrations of free amino acids total ~15 mM, and ATP is indicated between 1.3 and 7.0 mM, depending on growth conditions and sugar sources.[149] In eukaryotes, metabolite concentrations are issue both to variations between subcellular organelles, and to variations between cell and tissue

types. In human cells, according to the human metabolome database,[147] $[HCO_3]^-$ is the most abundant metabolite at ~11 mM, followed by 2,3 diphosphoglyceric acid at 4.0−5.0 mM, glutathione at ~2−5 mM, L-malic acid at ~3−4 mM, ATP at ~1−2 mM, and Glu^- at ~1−2 mM.

Not measured in the above studies are the significant polyamine metabolites, found in all eukaryotes and most prokaryotes, such as putrescine, spermidine, and spermine.[150] These polycations have roles in cell growth and proliferation, however with reduced levels are related with aging and increased levels are associated with cancer.[151] Studies in *E. coli* reported concentrations of ~20−30 mM for putrescine and ~6−7 mM for spermidine. Levels of putrescine and spermidine in mammalian cells are significantly lower (~1 mM).[152] Polyamines have been found to accelerate the in vitro aggregation and fibrillation of α-synuclein, an intrinsically disorder protein (IDP) implicated in Parkinson's disease (PD), also the extent of these effects increases with polyamine charge, length and concentration, suggesting that they can also occur *in vivo*.[148] Other metabolites such as compatible osmolytes aforementioned: glycerol, trehalose and zwitterions such as ectoine, proline, TMAO and betaine, stabilize proteins at intracellular concentrations between 100 and 300 mM.[127,128] Overall, these data indicate that metabolite concentrations in the range of ~300 mM are sufficient to cation-anion interactions and transient ion-pairs.

This viewpoint can change the selection trial of ions for new ILs. For example, the combination between glutamate anion or other amino acids (at high concentrations in cell) and polyamines already mentioned or choline, an essential micronutrient for normal functioning of all cells (required to make membrane phospholipids, precursor of the neurotransmitter acetylcholine and source of labile methyl groups)[44,45,153] and also a protic cation well known in ILs thematic.[35] Curiously, Pugh *et al.* have reported possible links between choline and glutamate to white matter anomalies and hyper-excitability in human studies of reading disability.[154]

Such natural combinations were strengthened by the recent identification of a naturally occurring protic IL in Chen *et al*.[155] Such IL can be formed during confrontations between the ants *S. invicta* and *N. fulva*. After being sprayed with alkaloid-based *S. invicta* venom, *N. fulva* detoxifies by grooming with its own venom, formic acid, that combination resulting in the mixed-cation ammonium formate milieu. So, given that ionic liquids can and do have biological effects oscillating from the level of individual biomolecules up to entire organisms, the possibility that naturally occurring hydrated ILs (transient ion-pairs) may form from the combination of charged metabolites exist to play specific biological roles (in the cell) cannot be dismissed.

I. 3. Macromolecular crowding

Biophysical characterizations of protein conformational changes and protein-ionic liquids interactions have mostly been carried out under dilute conditions (the concentration of macromolecules rarely exceeds 10 g/L). However, the environments where proteins perform their biological functions, *i.e.* extracellular space, cell membrane, and cytoplasm, are crowded with macromolecules. The cytoplasm of *E. coli* contains a large amount of macromolecules at concentrations exceeding 300 g/L[156] with volume occupancies of 30%, of which 10% are cytoskeletal filaments and 90% are soluble globular proteins, along with substantial amounts of RNA (75-120 g/L), DNA (11-18 g/L), biopolymers such as lipids and glycans, inorganic ions and organic metabolites.[157,158] The **Figure I.1** is a dramatic representation of such conditions.[159]

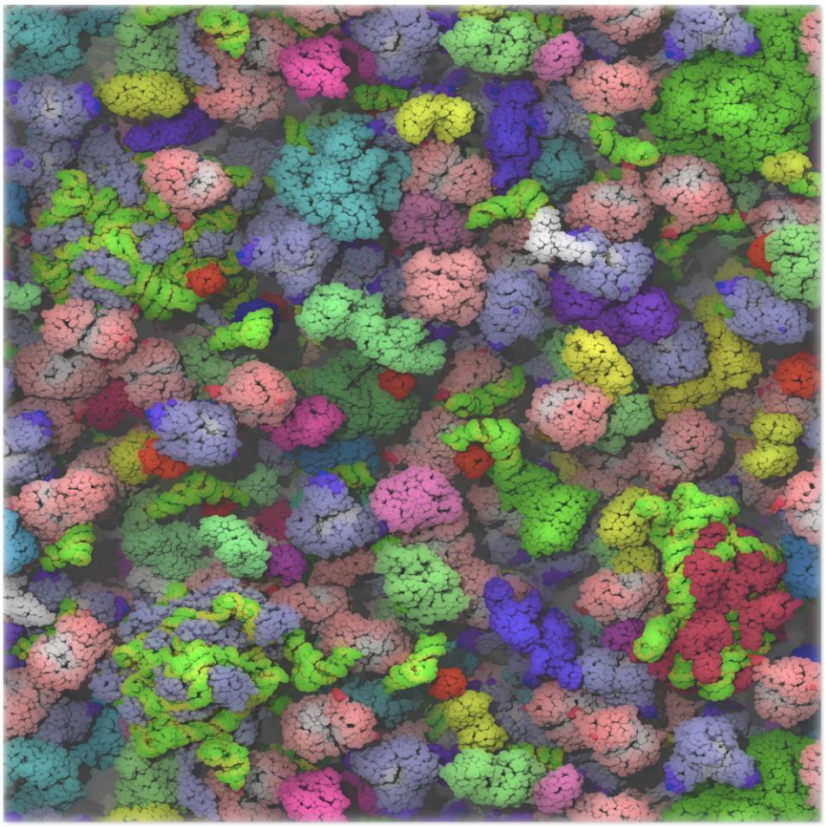

Figure I.1. The *Escherichia coli* cytoplasm, as modeled by McGuffee and Elcock.[159]

Consequently, macromolecules occupy 10−40% of any cell volume and make this space unavailable to other macromolecules. In 1981, Minton and Wilf[160] coined the phrase "macromolecular crowding" to connote the influence of mutual volume exclusion on the thermodynamic, kinetic and structural properties of macromolecules in crowded media. The most recent crowding paper to evoke attention among biochemists is from the groups of Wittung-Stafshede and Cheung, showing that crowding can deform the native state of a distinctly non- spherical globular protein, because a non-native state takes up less space than its native state.[161] Two provoking review's

by Elcock[162] and by Ellis[157] of crowding research showcases the current state of the field. Recently, the effects of crowding on protein stability[148,163–166] had been explored as opposed to crowding and protein function.[167] However, Dhar *et al.*[168] bring function to the forefront again with their study of the enzyme phosphoglycerate kinase, they report the increasing enzyme's activity by bringing together the two halves of the active site under crowding.

Cellular interiors are generally mimicked by using various macromolecules as "crowders". The addition of high concentrations of natural and synthetic macromolecules to such dilute solutions (buffers) enables crowding to be mimicked adding it as a variable to study.[162,169–171] Typically and well reported, the crowding agents used are (artificial) synthetic polymer crowders[156,163,171–176] such as polyvinylpyrrolidone (PVP), polyethylene glycol (PEG)[177] and ficoll (branched carbohydrate derivative)[178] or/ and natural globular proteins crowders (inert but with charge)[164,179–182] such as bovine serum albumin (BSA)[183] and lysozyme.[184]

While the original use of term denoted effects of inert repulsive forces, it has since been updated to also include weak attractive or repulsive interactions.[165] Specifically, recent experimental results indicate that the presence of weak, nonspecific attractive interactions in the heterogeneous cellular environment can modulate or even dominate the effects of hard-core repulsion that are at the basis of molecular crowding.[165,185,186] The role of such "chemical interactions" is a subject of debate also for proteins and PEG.[162,171]

The hard-core repulsive effect is entirely entropic since steric repulsions affect only the arrangement of molecules (decrease the space available), not the chemical interactions between them. Soft, or chemical interactions can be attractive or repulsive and arise from a diversity of sources, including charge−charge interactions, hydrogen bonding, and the hydrophobic effect. Repulsive chemical interactions are stabilizing because they reinforce the hard-core repulsion. On the other hand, attractive interactions are destabilizing for the same cause than urea is destabilizing, mainly nonspecific interactions (favourable) with the protein backbone help exposure of more surface, which leads to unfolding of protein. Attractive interactions are known to have an enthalpic component.[164,181]

For example, Miklos *et al.*[187] assessed chymotrypsin inhibitor 2 (CI2, 7.4 kDa, pI 6.0) stability in solutions crowded by BSA (66 kDa, pI 4.7) and lysozyme (15 kDa, pI 11.0), using the NMR-detected amide proton exchange technique, since such stability can be measured at room temperature in the presence of any non ^{15}N-containing co-solute (test molecule with isotopic enrichment).[188] In contrast to the stabilization observed with synthetic polymers, the protein crowders destabilized CI2 protein. This statement suggests that the proteins interact favourably and non-specifically with the backbone of CI2 so as to overcome the stabilizing effect of hard-core repulsions. These authors also showed that a portion of these weak non-specific interactions originate from charge–charge interactions. Also, Pielak's group discovered that proteins and synthetic polymers have dramatically different effects on CI2 diffusion.[179] Both globular proteins and synthetic polymers as

crowders affect the rotational diffusion of globular proteins less than is expected, though synthetic polymers affect transitional diffusion less than expected, but globular proteins have either a small negative or a positive effect on translational diffusion. The results elucidate the difficulty in obtaining in-cell NMR spectra of globular proteins.[189–191] Studies of protein diffusion in the bacterium *E. coli* give a remarkably different picture, using fluorescence to measure the translational diffusion of GFP, they exposed that the eukaryotic cytoplasm slows diffusion no more than 4-fold and the cytoplasm of *E. coli* slows diffusion 10-30-fold (much slower than *in vitro* studies).[192]

However, as pointed out by Benton *et al*.,[174] some of the complication observed for synthetic polymers may arise from the effect of preferential hydration. In a provoking paper, Kim A. Sharp[193] said "What is missing, however, is the solvent: principally water and small ions."

Further, water as the solvent for both the protein and the crowder could play a critical role in fully describing the macromolecular crowding effect. Senske *et al.* showed that ubiquitin is stabilized by dextran by a similar thermodynamic mechanism as by glucose, indicating a mechanism that is closely related to the enthalpy mediated stabilization observed for different osmolytes.[194,195] A recent review by the Harries group highlights how thermodynamic concepts from osmolyte research, especially the role of the aqueous solvent in crowding.[196]

The macromolecular crowding effect is separate into the different contributions: excluded volume, nonspecific interactions and the mostly important, solvent properties.[197–199] Preferential hydration of the protein is a solvent-mediated enthalpic stabilization by an exclusion of the co-solute from the direct contact with the protein.[197]

Therefore, it is important to study proteins under several conditions to assess the phenomena that give rise to crowding effects. Gaining an understanding of the nature of crowding will not only provide fundamental knowledge about biology but also help solve practical difficulties. For instance, such knowledge will facilitate the design of synthetic polymers or these combination with natural ions that increase the stability of industrially useful enzymes and protein-based pharmaceuticals.

As far as we know, ionic liquids have never been studied under macromolecular crowding, although exists a few studies of protein stability with other osmolytes and the hydration thematic has been approached.[194,200–202]

I. 4. Objectives and outline of the thesis

The main aim of this work is to explore the possibility of ion-pair formation in aqueous solution raised by natural, organic and hydrophilic cation-anion combinations (hydrated bio ionic liquids) under macromolecular crowding conditions and its effects on protein structure and stability, using advanced NMR techniques and calorimetric techniques.

Our concept is based on the possibility that naturally occurring *transient ion-pairs* may form from the combination of charged metabolites to play specific biological roles in the cell.

Scheme I.5 resumes our work hypothesis: formation of transient ion pairs from charged metabolites under macromolecular crowding as sources for hard and soft interactions.

For this purpose two different research subjects have been combined: ionic liquids (with relevance on ion pair studies) and macromolecular crowding.

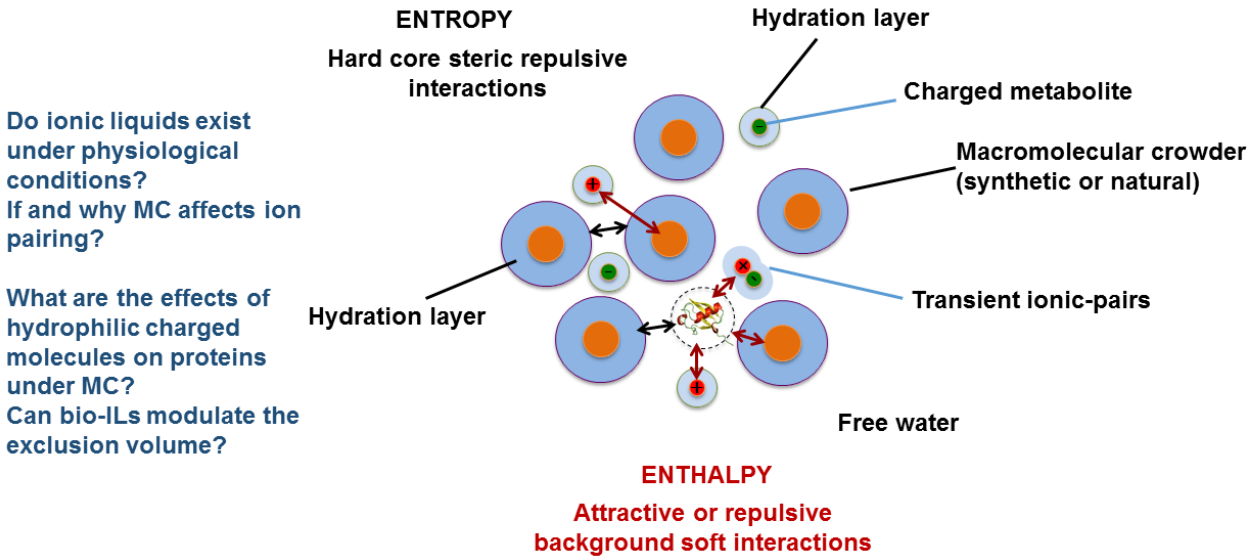

Scheme I.5. Representation of excluded volume effects and background interactions (small organic charged metabolites and transient ionic pairs as sources) under macromolecular crowding.

The study is organized around three main objectives:

- The design, synthesis and characterization of new bio–ILs based on natural organic sources according with charged metabolites statistics found in the cell interior (glutamate, arginine, polyamines and choline). Characterization of ion-pair formation in water solution for the new bio-ILs using NMR techniques: self-diffusion by DOSY NMR and NOE NMR techniques.
- The study of ion-pairing under macromolecular crowding using synthetic and natural crowders in order to evaluate the relevance on of crowding in ion interactions.
- The study of a model protein GB1 [203] (previous production and purification in isotopic enrichment media) with a selected bio-IL under macromolecular crowding. For this purpose, the NMR spectroscopy (protein diffusion, HSQC experiments, and hydrogen-deuterium exchange) and differential scanning calorimetry (DSC) were applied.

Undoubtedly, bio-ILs are excellent candidates for a robust protein solvation, conservation and storage on pharmaceutical industry. Studying these ILs with relevance in ionic pair under crowding environment (mimicking the cell milieu) using NMR and calorimetric tools via high-resolution at atomic detail can help to answer such daunting questions.

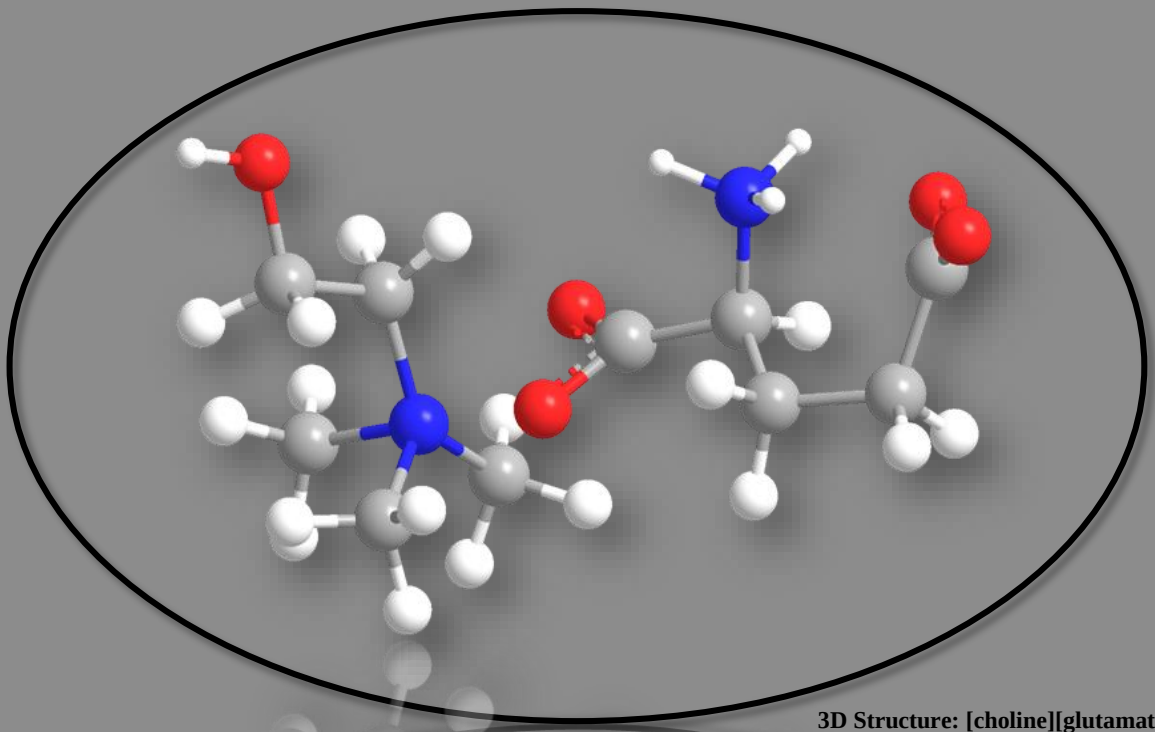

3D Structure: [choline][glutamate]

Chapter II: Preparation and characterization of Bio-ILs

In this chapter, I describe the synthesis of a new bio – ionic liquid based on the combination of biologically relevant organic cation and anion. The possibility of ion pair existence in dilute solution is probed by NMR.

Table of Contents

II. Preparation and characterization of bio-ILs

II. 1. Introduction

Among the large number of ionic liquids (ILs) that have been synthesized and characterized, the traditional imidazolium- and pyridinium- based ILs have demonstrated to be badly biodegradable and poorly biocompatible.[17] In some of these ILs the presence of long alkyl side-chains increased their toxicities considerably.[34] To overcome the matter mentioned, the study of non-toxic and environmentally nonthreatening ILs from renewable materials has been highly explored.[35–37] As explained in chapter I, it is a very attractive proposal that biocompatible (bio) - ILs can be designed and synthetized using glutamate as the source for the anion and arginine, choline or different polyamines for the different cations.

In this work, five assumptions of bio-ILs, arginine-glutamate [Arg][Glu], $[Arg]_2[Glu]$, 1,3 diaminopropane-glutamate $[NH_3C_3NH_3][Glu]$, choline-glutamate [Ch][Glu], and $[Ch]_2[Glu]$ were synthesized from the combination of choline hydroxide with diaminopropane and amino acids, via simple neutralization reactions. Only the choline-based salts obtained were liquid at room temperature. All salts were characterized by NMR spectroscopy, although only those based on choline by differential scanning calorimetry (DSC).

An important pre-requisite is the characterization and understanding of the structure and dynamics of these Bio-ILs.[18] Specifically, if the anion – cation interaction is sufficiently strong, contact ion pairs will be the dominant structures in solution, and if the ion-solvent interaction is stronger solvent-shared and solvent-separated ion-pairs will prevail. This will have implications for the type of interactions that these will ILs establish with proteins[107,108] as I explore in chapter IV.

The lifetime of the ion pair is also relevant for the interpretation of the intermolecular NOE by NOESY methods. The NOE reflects cross-relaxation between two nuclear spins, *I* and *S*, because of magnetization transfer through coupling of their magnetic dipole moments. With increasing inter-nuclear distance *r* the cross-relaxation rate σ_{IS} decays as $1/r^6$. Thus, a NOE is only achieved, if *r* is less than 4–5 Å.[75] While derived for spins in the same molecule, a rule like this is also applied to intermolecular cross-relaxation, implying that the NOE essentially captures molecules in the innermost coordination sphere of the relaxing particle. To generate a notable probability for magnetization transfer the lifetime of these configurations has to be at least of the order of the inverse Larmor frequency $1/\omega_I$ of the relaxing spin *I*. In ^1H - NMR spectroscopy this time is typically of the order of 0.5 ns.[75]

The existence of a measurable intermolecular NOE in ILs has been exploited in several studies.[21,74] An interesting study is the results of the intermolecular ^1H–^{19}F NOE in $[C_4mim]$ $[BF_4]$ by Giernoth's research group,[80] which appears to indicate the existence of cation-anion pairs with life

times on the nanosecond time scale. However the long-time NOE factors can been attributed to the existence of long-lived hydration shells as in studies of protein hydration.[82] The Selective 1D NOE was applied to study local interactions in choline – glutamate.

For understanding the solvent properties of ILs the characterization and understanding of the molecular motions are just as important as the knowledge of their structure. The self-diffusion of the ions in order to estimate the extent of ion pairing[21] was also approached in this chapter.

II. 2. Experimental section

The initial strategy and preparation of new bio-ILs was done with the help of Doutor Luís Branco from Photochemistry and Supramolecular Chemistry FCT/ UNL Group and based on the experimental sections of Ferraz *et al.*,[204] Alcalde *et al.*[39] and Liu *et al*.[35]

II. 2. 1. Materials and general methodologies

L-arginine (Purity ≥ 98%) and the ion exchanger resin Amberlyst A-26 (OH- form) were purchased from *Alfa Aesar*. Sodium hydroxide (NaOH), 1,3–diaminopropane (Purity ≥ 99%) and choline chloride [Ch][Cl] (Purity ≥ 99% and dried for 24 h under vacuum at 60 ºC) were purchased from *Sigma-Aldrich*. L-glutamic acid (Purity ≥ 99%) and hydrochloric acid (HCl) were purchased from *Panreac*. Distilled water and Milli-Q water were obtained from laboratory facility instruments. Deuterium oxide (D_2O) 99.9% [D] was purchased to *Euriso-Top*. The pH was measured with *Docu-pH, Startovarius*.

Melting points were determined by a melting point apparatus (*STUART SMP11*). ^{1}H and ^{13}C NMR spectra were recorded with a *Bruker AVANCE III 400 MHz* instrument operating at 400.15 MHz for protons and 100.6 MHz for ^{13}C, equipped with a 5 mm high-resolution BBO probe with pulsed gradient units, capable of producing magnetic field pulsed gradients in the z-direction of 0.54 T. m^{-1}. Chemical shifts (δ) are expressed in ppm relative to internal TMS as standard. Signals are abbreviated as follows: s, singlet; d, doublet; t, triplet; q, quartet; m, multiplet.

The glass transition temperatures (T_g) were determined with a differential thermal analyser (*DSC 131, Setaram, France*) with a heating rate of 10 °C/min, after cooling samples to -130 °C using liquid nitrogen.

II. 2. 2. Bio – ionic liquids preparation

II. 2. 2. 1. Preparation of arginine-glutamate

L-arginine in 10 mL of water (0.593 g, 3.4 mmoles, 1 equiv.) was added dropwise to a L-glutamic acid in 20 mL of water (0.5 g, 3.4 mmoles, 1 equiv.), as represented in **Scheme II.1**. The mixture was stirred at about 25 °C for 24 h in the dark, and the solvent (water) was subsequently evaporated under reduced pressure. The product was dried *in vacuo* for 24 h at 60 °C.

The same procedure was repeated using 2 equivalents of arginine to 1 equivalent of glutamate: L-arginine in 20 mL of water (1.186 g, 6.8 mmoles, 2 equiv.) was added dropwise to a L-glutamic acid in 20 mL of water (0.5 g, 3.4 mmoles, 1 equiv.), as represented in **Scheme II.2.**

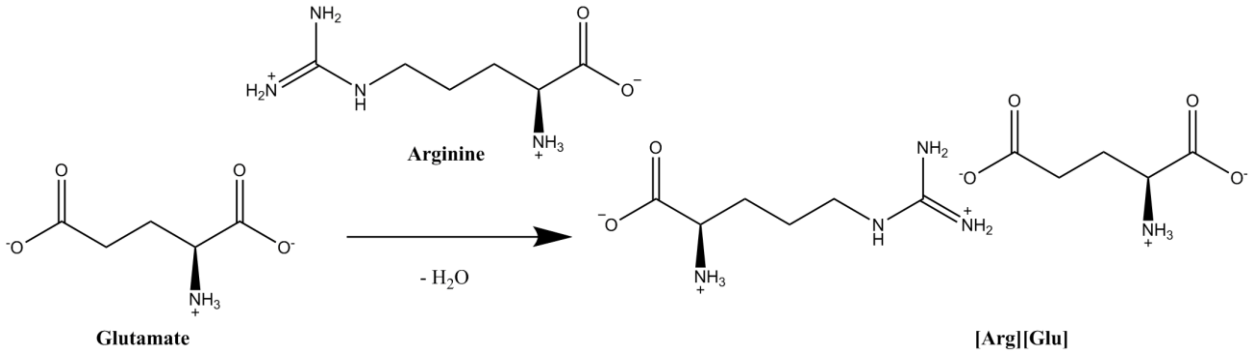

Scheme II.1. Schematic synthetic procedure for the preparation of [Arg][Glu].

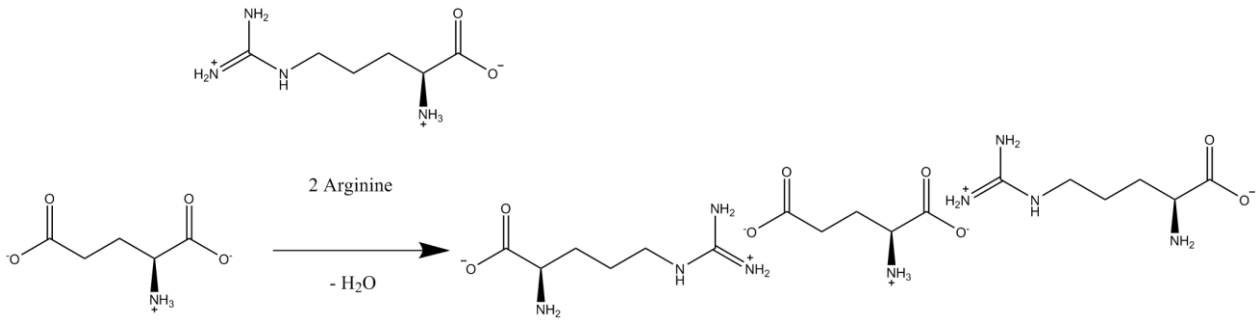

Scheme II.2. Schematic synthetic procedure for the preparation of $\{[Arg]_2[Glu]\}^{2-}$.

The mass obtained of [Arg][Glu] (1 equiv.) was around 1.02 g (white solid and the pH in aqueous solution was 6.26) and to $[2Arg][Glu]^{2-}$ (2 equiv.) was around 1.58 g (white solid, the pH in aqueous solution was 9.12). The yields were more than 95%. Melting points of compounds [Arg][Glu], 201 ºC; $[2Arg][Glu]^{2-}$, 192 ºC.

[Arg][Glu]. ^{1}H NMR (400.15 MHz, D_2O, 25 ºC) δ_H: 1.485 – 1.69 (m, 2H, CH_2, Arg), 1.75 – 1.87 (m, 2H, CH_2, Arg), 1.90 – 2.09 (m, 2H, CH_2, Glu), 2.258 (apparent q, 2H, CH_2, Glu), 3.148 (t, 4H, J = 6.88 Hz, CH_2, CH_2, Glu), 3.64 – 3.70 (apparent t, 2H, CH-N, CH-N, Glu and Arg).

^{13}C NMR (100.6 MHz, D_2O, 25 ºC) δ_C: 23.87 (Arg), 26.92 (Glu), 27.53 (Arg), 33.45 (Glu), 40.5 (Glu), 54.30 (Arg), 54.62 (Glu), 156.79 (Arg), 174.36 (Arg), 174.51 (Glu), 181. 21 (Glu).

{[Arg]$_2$[Glu]}$^{2-}$. ^{1}H NMR (400.15 MHz, D_2O, 25 ºC) δ_H: 1.44 – 1.60 (m, 4H, CH_2, CH_2, Arg), 1.60 – 1.76 (m, 4H, CH_2, CH_2, Arg), 1.815 – 2.017 (m, 2H, CH_2, Glu), 2.198 (apparent q, 2H, CH_2, Glu), 3.10 (t, 4H, J = 5.36 Hz, CH_2, CH_2, Glu), 3.448 (t, 2H, J = 6.10Hz, CH-N, CH-N, Arg), 3.534 (apparent q, 1H, J= 4.91, 7.05 Hz, CH-N, Glu).

^{13}C NMR (100.6 MHz, D_2O, 25 ºC) δ_C: 23.89 (Arg), 26.94 (Glu), 27.59 (Arg), 33.46 (Glu), 40.7 (Glu), 54.38 (Arg), 54.68 (Glu), 156.82 (Arg), 174.4 (Arg), 174.54 (Glu), 181. 28 (Glu).

II. 2. 2. 2. Preparation of 1,3–diaminopropane-glutamate

A first attempt was tried by mixing 1,3-diaminopropane ($[NH_3C_3NH_3]^{2+}$) (previously distilled) with hydrochloric acid (0.5 M in water) to obtain 1,3-diaminopropane dihydrochloride and dissolving L-glutamic acid in a moderately basic sodium hydroxide solution (1 M) to get disodium glutamate. The combination of the two products with a slight excess of disodium glutamate by dropwise addition of 0.758 mL of 1,3-diaminopropane (4.64 mmoles, 1 equiv.) in 18.56 mL of 0.5 M HCl to 1.04 g of [2Na][Glu] (dry, 5.34 mmoles, 1.15 equiv.) in 10 mL of water to promote the acid-base reaction resulted in $[NH_3C_3NH_3]$[glutamate] with a considerable amount of NaCl, this method failed due to poor solubility and similar to NaCl in most common organic solvents for extraction of product from NaCl (only resulted the small extraction of product with dichloromethane).

Despite the poor reactivity of reagents, the initial procedure was modified by simple dropwise addition of 1,3-diaminopropane (1.135 mL, 13.6 mmoles, 1 equiv.) to L-glutamic acid (2 g, 13.6 mmoles, 1 equiv.) an equimolar ratio in 40 mL of water, as represented in **Scheme II.3**. The mixture was stirred at about 25 °C for 24 h in the dark, after which the solvent was evaporated under reduced pressure. The product was dried *in vacuo* for 24 h at 60 °C.

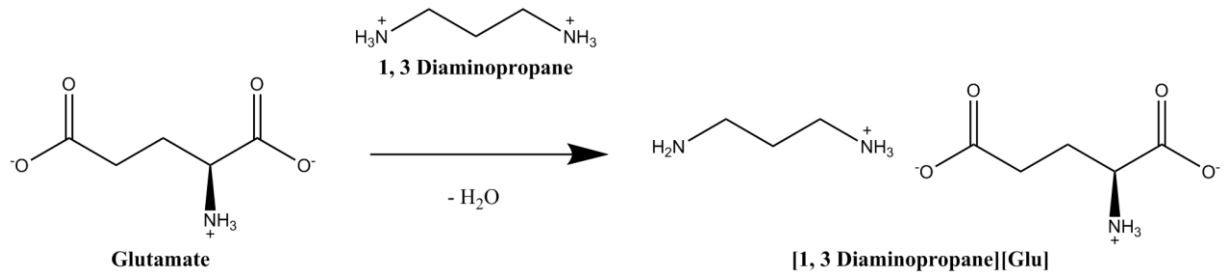

Scheme II.3. Schematic synthetic procedure for the preparation of $[NH_3C_3NH_3]$[glutamate].

The mass of $[NH_3C_3NH_3]$[Glu] obtained was 2. 152 g (the yield was 92%) as a white solid with a melting point of 221 ºC. The pH in aqueous solution of the product was 9.15.

[$NH_3C_3NH_3$][Glu]. ^{1}H NMR (400.15 MHz, D_2O, 25 ºC) δ_H: 1.736 – 1.965 (apparent m, 4H, CH_2, CH_2, Glu), 2.16 (apparent q, 2H, CH_2, Glu), 2.84 (apparent t, 4H, J = 7.63 Hz, CH_2, CH_2, 1,3-diaminopropane), 3.48 (q, J = 5.01, 7.19 Hz, 1H, CH-N, Glu).

^{13}C NMR (100.6 MHz, D_2O, 25 ºC) δ_C: 27.21 (Glu), 28.03 (Glu), 33.60 (Glu), 37.07 (1,3-diaminopropane), 54.88 (Glu), 176.40 (Glu), 181. 57 (Glu).

II. 2. 2. 3. Preparation of choline-glutamate

Choline hydroxide [Ch][OH] aqueous solution was prepared from choline chloride [Ch][Cl] (4.75 g, 34 mmoles) in 50 mL of water that was passed slowly through a column packed with ~ 43 mL of anion exchange Amberlyst A-26 resin (in order to exchange chloride to the hydroxide form) and then washed with 150 mL of water. The presence of chloride content was determined by a silver nitrate qualitative test, a small sample was acidified by adding dilute nitric acid. The nitric acid reacts with, and removes, other ions that might also form precipitates with silver nitrate. Silver nitrate solution is then added, and the chloride can be identified from the presence of white and insoluble precipitate (silver chloride). The final solution not revealed chloride traces (≤ 10 ppm of Cl^- in solution).

A [Ch][OH] aqueous solution from exchange in Amberlyst A-26 resin (31 mmoles, 175 mL, 0.194 M) was added dropwise an equimolar ratio to L-glutamic acid (4.5 g, 31 mmoles, 0.3 M) in 100 mL of water (as represented in **Scheme II.4**). The reaction was monitored by reading the solution pH until it reached a value of 7.09 and the [Ch]/ [Glu] ratio was checked by ^{1}H NMR (it was necessary 143 mL of [Ch][OH] solution). The mixture was stirred at about 25 °C for 24 h in the dark and subsequently the solvent was evaporated under reduced pressure. The product was dried *in vacuo* for 24 h at 60 °C.

The same procedure was repeated lesser amounts for 2 equivalents of choline to glutamate: A [Ch][OH] aqueous solution from 3.8 g of [Ch][Cl] (27.2 mmoles) exchange in Amberlyst A-26 resin (24.6 mmoles, 147 mL, 0.185 M) was added dropwise in a 2 equiv. of excess to L-glutamic acid (1.8 g, 12.3 mmoles, 0.25 M) in 50 mL of water (as represented in **Scheme II.5**). The reaction was monitored by reading the solution pH until it reached a value of 10.7 and the $[Ch]_2$/ [Glu] ratio was checked by ^{1}H NMR (it was necessary 135 mL of [Ch][OH] solution).

The mass obtained of [Ch][Glu] (1:1) was 8.48 g (99.4%) and to $[Ch]_2$[Glu] (2:1) was 4.73 g (97.9%). The [Ch] [Glu] and $[Ch]_2$[Glu] glass transition temperatures (T_g) were -39.59 ºC and -78.28 ºC, respectively. Both [Ch][Glu] and $[Ch]_2$[Glu] are yellow oily compounds at room temperature.

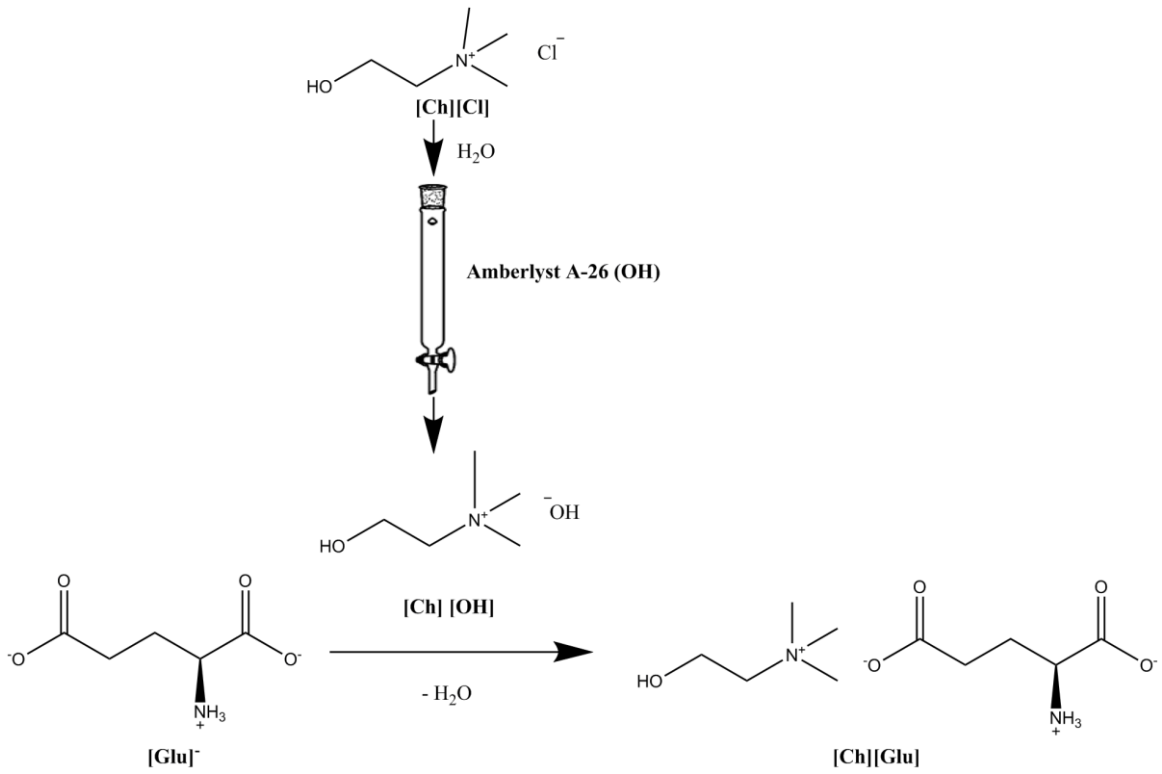

Scheme II.4. Schematic synthetic procedure for the preparation of [Ch][Glu].

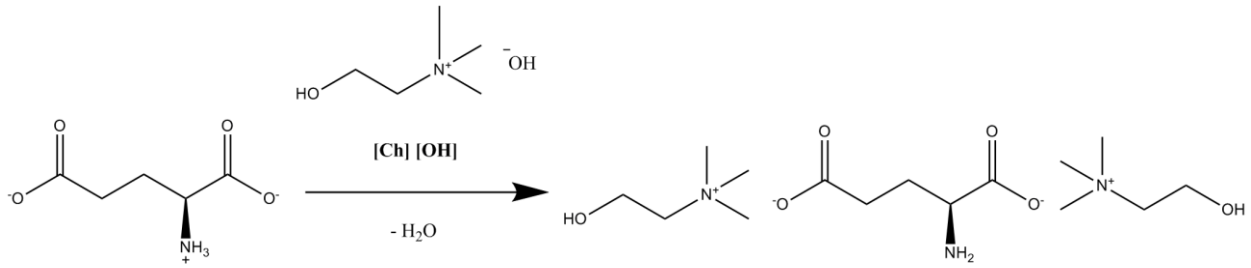

Scheme II.5. Schematic synthetic procedure for the preparation of $[Ch]_2[Glu]$.

[Ch][Glu]. ^{1}H NMR (400.15 MHz, D_2O, 25 ºC) δ_H: 1.84 – 2.02 (m, 2H, CH_2, Glu), 2.20 (apparent q, 2H, CH_2, Glu), 3.05 (s, 9H, CH_3, CH_3, CH_3, Ch), 3.365 (apparent t, 2H, CH_2, Ch), 3.60 (q, J = 4.87, 7.12 Hz, 1H, CH-N, Ch), 3.88 – 3.93 (m, 2H, CH_2, Glu).

^{13}C NMR (100.6 MHz, D_2O, 25 ºC) δ_C: 27.34 (Glu), 33.6 (Glu), 53.90 (Ch), 54.8 (Glu), 55.61 (Ch), 67.45 (Ch), 175.1 (Ch), 181.36 (Ch).

$[Ch]_2[Glu]$. ^{1}H NMR (400.15 MHz, D_2O, 25 ºC) δ: 1.705 – 1.92 (m, 2H, CH_2, Glu), 2.16 (apparent t, 2H, CH_2, Glu), 3.118 (s, 18H, CH_3, CH_3, CH_3, CH_3, CH_3, CH_3, Ch), 3.292 (q, J = 5.36, 7.25 Hz, 1H, CH-N, Glu), 3.435 (apparent t, 4H, CH_2, CH_2, Ch), 3.956 – 4.00 (m, 4H, CH_2, CH_2, Ch).

^{13}C NMR (100.6 MHz, D_2O, 25 ºC) δ_C: 30.5 (Glu), 34.05 (Glu), 53.93 (Ch), 55.61 (Glu/ Ch), 67.47 (Ch), 180.53 (Ch), 182.34 (Ch).

II. 2. 3. Diffusion studies (DOSY)

Diffusion measurements were conducted at 298 K using a 500 µL solution of [Ch][Glu] 0.5 M in 99.9% D_2O (pH meter reading pH 7.71 (uncorrected for deuterium isotope effect) in a 5 mm NMR tube.

The pulse sequence from the Bruker library (ledbpgp2s pulse sequence)[205] that uses a stimulated echo and a longitudinal eddy current delay (LED) with bipolar gradient pulses for diffusion encoding (without convection compensation) and 2 spoil gradients was used. This is usually preferred to the standard pulsed gradient spin echo or PGSE sequence, resulting in a better signal-to-noise ratio. The spectrum was recorded with 16 scans in a matrix with 32 K points in t2 in a spectral window of 6002.401 Hz centred at 1878.57 Hz. 32 gradients steps were acquired with the gradient strengths augmented linearly from 5% to 95% of the maximum gradient strength using a sine shaped gradient sine form: the smoothed square (SMQ10.100) with shape factor of 0.9.

Self-diffusion coefficients were obtained by varying the gradient strength (g) while keeping the gradient pulse length (δ) and the gradient pulse intervals constant within each experimental run. The duration of the encoding/ decoding gradient (little delta, δ) was calibrated to 2.0 ms, the duration of diffusion time (big delta, Δ) was calibrated to 100 ms. The duration of the spoil gradient was set to 800 µs, the eddy current delay was 5 ms and the gradient recovery set to 200 µs. The data was analysed using the variable gradient fitting routines in Bruker's TopSpin™ 3.5 software. All peaks intensities were fitted using a mono-exponential decay based in Stejskal-Tanner equation:[206]

$$\boldsymbol{I = I_0 e^{\left[-D(\gamma g \delta)^2\left(\Delta - \frac{\delta}{3} - \frac{\tau}{2}\right)\right]}}$$

(Equation II.1)

Where I_0 is the signal intensity at zero gradient strength, γ the magnetogyric ratio of the observed nucleus (proton in this case, 2.675×10^8 rad. $T^{-1}.s^{-1}$), g and δ are the strength and duration of the gradient, respectively, Δ is the diffusion time, τ is the gradient pulse recovery time and D is the self-diffusion coefficient to be extracted.

II. 2. 4. Selective 1D – NOE experiments

All experiments were performed at 298 K using the same sample used in diffusion measurements.

Spin-lattice (T_1) relaxation times becomes critically important for quantitative, exchange, or cross-relaxation types of experiments such as NOESY. They were obtained by the pulse sequence from the Bruker library (t1ir1d pulse sequence): the standard inversion recovery (180 – τ – 90 – acquisition) sequence.

The T_1 relaxation data of all protons was determined through the time at which the magnetization becomes a null (τ_n):

$$\boldsymbol{I_t = I_0\left(1 - e^{-\frac{\tau}{T_1}}\right) \; and \; T_1 = \frac{\tau_{1/2}}{\ln(2)} \approx \tau_{\frac{1}{2}} \times 1.4}$$

(Equation II.2)

Where I_t is the intensity at time τ, I_0 is the intensity at equilibrium and $\tau_{\frac{1}{2}}$ is the null intensity at time 1/2 (null time, τ_n).

The spectra was recorded with 1 scan in a matrix with 32 K points in a spectral window of 4000 Hz centred at 1219.95 at 298 K. A quick null time (d7) estimation was performed for each proton in order to set the appropriate relaxation time T_1 that varied between 0.812 s (T_1 fastest of interest - *foi*) to 2.66 s (T_1 longest of interest - *loi*).

Once the T_1 was determined the value was used to adjust the relaxation delay for the selective 1D-NOESY experiments. Typically for a Selective 1D – NOESY, the relaxation delay (d1) was 3 x T_1 *loi* and the mixing time (d8) was 0.1 – 1.5 x T_1 *foi*.

NOE measurements were recorded using the pulse sequence from the Bruker library (selnogpz pulse sequence) that uses a selective inversion scheme with a shaped pulse and adiabatic pulse. The selective inversions were performed using a Gaussian shaped 180º pulses with a length of 80 ms (calibrated by a previous pulse sequence with a selective excitation – selzg). In the pulse sequence presented was incorporated a new method developed by Thrippleton and Keeler[207] for supressing zero-quantum coherence, this method involves applying simultaneously a swept-frequency pulses and a gradient. The selection of the parameters of the swept-pulse/ gradient pair was based on the procedure of supporting information of Thrippleton and Keeler.[207] The swept-frequency pulses used were adiabatic 180º CHIRP pulses, the frequency swept was 20 kHz in τ_f = 50 ms and the Gradient strength G_f (GPZ0) was calibrated to 4% of the maximum.

The spectra were recorded with 32 scans repeated 4 times in a matrix with 16 K points in a spectral window of 4000 Hz centred at 1563.15 Hz, 1219.28 Hz and 876.20 Hz, each corresponding to a frequency of a proton of interest and to one NOE *build-up*. The relaxation delay was set to 8 s and in each experiment 10 spectra were recorded corresponding to different NOE mixing times. For selective irradiation in the choline (H3-Ch, centred at 1563.15 Hz with receiver gain of 181 and H1-Ch, 1219.28 Hz with receiver gain of 144) the mixing times were: 0.110 s, 0.16 s, 0.325 s, 0.49 s, 0.65 s, 0.812 s, 1.0 s, 1.2 s, 1.5 s, and 2.0 s; for selective irradiation in glutamate (H1'-Glu, centred at 876.20 Hz with receiver gain of 128, in this case the T_1 *foi* observed in Glu was 2.0 s), the mixing times were: 0.110 s, 0.2 s, 0.4 s, 0.8 s, 1.2 s, 1.6 s, 2.0 s, 2.2 s, 2.5 s, 3.0 s).

NMR data were processed and analysed in Bruker's TopSpin™ 3.5 software. The same phase correction was used for each NOE - build up experiment. The NOE intensities were normalized with

respect to that the highest response, *i.e.* the relative NOE with the highest intensity was set to 1.0 as a reference and all other NOE signals were calculated accordingly.

II. 3. Results and discussion

II. 3. 1. Synthesis and physicochemical analysis of bio-ILs

The most conventional synthetic preparation of ILs involves a metathesis reaction of an anion halide with an adequate alkaline salt and this was also used in the preparation of some bulky imidazolium and pyridinium ILs. The pure IL can be obtained by eliminating undesirable inorganic salts (mainly sodium and potassium) using precipitation followed by filtration.[208] The need to obtain pure ILs, especially halide-free ones, has been one of the central concerns within the IL community. In the case of a large number of organic anions, ion exchange resin methods were considered, and the methods recently developed by Ohno *et al*.[40] are being successfully used as alternative anion exchange processes. Amberlite resin (in the OH form) has been used in order to exchange halides (chloride in my case) to the hydroxide form and then this basic solution is neutralized by the addition of an adequate acid solution. The resin was used only to exchange [Ch][Cl] to [Ch][OH], and in all reactions the reagents were added dropwise from base to acid via simple neutralization reactions carefully monitored by ^{1}H NMR and pH, in order to get a right cation/ anion ratio with right charge neutralization.

The acid–base reaction gives the desired salt or IL with yields around 90-98% with 99% purity. In dry conditions, just the Choline-based ILs obtained were liquid at room temperature, then [Arg][Glu], [2Arg][Glu] and [1,3–diaminopropane][Glu] were considered as salts since they were solids at room temperature with melting points above 200 ºC. The set of ^{1}H NMR spectra are available as **Appendix A, Fig. A1 – A5**. Based on differential scanning calorimetry (DSC), no melting points were observed in the temperature range scanned for the [Ch][AA] ILs. The [Ch] [Glu] and [2Ch][Glu] glass transition temperatures (T_g) were -39.59 ºC and -78.28 ºC, respectively.

Less attention has been paid to ILs with cholinium as the cation and amino acids as the anions ([Ch][AA]) and reported applications of such ILs have focused solely on their activities as catalysts.[38] I have used the same procedure as Qiu-Ping Liu *et al*.[35] used in 2012 to prepare eighteen [Ch][AA] ILs. The physicochemical properties for [Ch][Glu] are shown in **Table II.1.**

Table II.1. Properties of the [Ch][Glu] from reference.[35]

[a]T_g were determined by DSC with a heating rate of 10 ºC/min, after cooling samples to -70 ºC under nitrogen. [b]Decomposition temperatures (T_d) were measured by TGA with a heating rate of 5 ºC/ min under nitrogen. [c]At 25 ºC. [d]Solution in CH_3OH (c = 2).

IL	T_g (ºC)[a]	T_d (ºC)[b]	Viscosity (mPa·s)[c]	$[\alpha]_D^{20}$ [d]
[Ch][Glu]	-18	202	2308	-10.19

Generally, an increase in the number of carbon atoms in the side chain of amino acid resulted in an increase of T_g. Moreover, the introduction of an additional hydroxyl or carboxylic acid group led to increasing T_g values, possibly due to strong hydrogen bond interactions.[41,208] The [Ch][Glu] exhibited relatively high T_g (-18 ºC) comparatively to other [Ch][AA]. The glass transition temperature is the midpoint of a small heat capacity change on heating from the amorphous glass state to a liquid state, useful to determining the lower end of the useful operating range where the fluid is a liquid.

The decomposition temperature (T_d) showed a clear dependence on the anion structures where the combination with glutamate anion is much more stable than with the other [AA] (T_d ~170 ºC). Also, in addition to the molecular size of the anion, the introduction of extra carboxylic acid or amide group substantially increased the viscosity of the ILs possibly owing to strong hydrogen bond interactions. For instance, one of the high viscosities was recorded for [Ch][Glu] and their amide analogs by Qiu-Ping Liu.[35] The larger anion size and stronger intermolecular forces such as van der Waals, hydrogen bond, and π-stacking interactions also might contribute to the high viscosity.[209] The optical rotations of some ILs were different from those of amino acids they contained, the phenomenon was reported by Allen *et al*.[210]

The [Ch][Glu] synthesized in the present work provides higher liquid phase stabilization than that reported by Qiu-Ping Liu (-39.6 ºC vs. -18 ºC).[35] Probably, this difference due to a small amount of water in my sample. When the proportion Ch:Glu goes to 2:1 the T_g decreases to -78 ºC, probably less viscous at room temperature due the extra electrostatic interaction between the other carboxylic group of Glu^- and head group of the second Ch^+ (compared with 1:1 proportion, since one carboxylic group is occupied with head group of Ch^+ via electrostatic interaction), unfortunately this IL in water solution presents a pH very far from physiological (10.7 vs. 7.2).

Recently, a variety of cholinium-based ILs has been reported to have low toxicity (choline saccharinate and choline acesulfamate;[51] choline phosphate ILs;[52] and a range of linear alkanoate anions combined with choline[53]), most examples tested are highly biodegradable and the anion has also proven to contribute to the overall toxicity of ILs.[53] Furthermore, in 2013 Xue-Dan Hou *et al.*[36] demonstrated that the readily biodegradable [Ch][Glu] displayed low toxicity to enzymes and bacteria's. The pH of a 0.5 M aqueous solution of this IL was around 7.0 (physiological pH) and it shows a high water solubility.

II. 3. 2. Detection of ion-pair in choline-glutamate

Only two of the compounds synthetized were revealed as room temperature ILs, the [Ch][Glu] and $[Ch]_2[Glu]$, however just one is relevant in biological conditions: [Ch][Glu] with physiological pH, thus it is the only compound which continues to this study and for next chapters.

One of the main targets of this work is the investigation of ion-pairing formation in solution with NMR. In this context, a specific approach has been outlined consisting first in the determination of self-diffusion coefficients using diffusion-ordered spectroscopy (DOSY), and second in the recording of selective 1D NOE measurements to ascertain cation-anion contact of choline-glutamate by intermolecular interactions in water solution. While in the case of DOSY measurements, translational motion can be directly observed and interpreted via diffusion coefficients, which results from exponential decaying of the NMR signal as it was explained previously in this chapter, in the case of NOE, the build-up during the mixing time can be used to obtain distance information:

The theory of the NOE, in the context of intermolecular interactions was based in the paper of Brand, Cabrita and Berger.[73] For the extraction of spatial information the dependency of the NOE effect (or its buildup rate) on the internuclear distance r_{IS} is used:

$$\boldsymbol{NOE \equiv f_I\{S\}(\tau_m) = e^{-(R-\sigma_{IS})\tau_m}(1 - e^{-2\sigma_{IS}\tau_m})}$$

(Equation II.3)

Where R represents the total longitudinal relaxation rate constants of both the *I* and *S* spins, assumed to be equal, and τ_m is the mixing time. The initial buildup rate of the NOE is proportional to σ_{IS}, as can be seen if we take the first derivative with respect to the mixing time, at time zero:

$$\frac{\boldsymbol{dNOE}}{\boldsymbol{d\tau_m}} \equiv \frac{\boldsymbol{f_I\{S\}(\tau_m))}}{\boldsymbol{d\tau_m}}|_{\boldsymbol{\tau_m=0}} = \boldsymbol{2\sigma_{IS}}$$

(Equation II.4)

The study of the early stage of the NOE buildup of the *I* enhancement for short mixing times ($\tau_m \rightarrow 0$) allows the determination of σ_{IS}. This can also be achieved by measuring the complete kinetics of the NOE buildup and fitting the experimental data to **(Equation II.3)**. Once σ_{IS} is known, r_{IS} can be determined after evaluation of the other variable upon which *s* depends, which is the correlation time τ_c. However, the most used method for internuclear distance determination from NOE data relies not on the direct determination of σ_{IS} and τ_c, but on the use of a reference or calibration distance. By comparing σ_{IS} with σ_{AB}, relative to two nuclei (A and B) whose internuclear distance (r_{AB}) is known, an estimation of r_{IS} can be obtained if the proportionality constant between σ and r^{-6} is the same for the two pairs of nuclei (*IS* and *AB*):

$$\frac{\boldsymbol{\sigma_{IS}}}{\boldsymbol{\sigma_{AB}}} = \left(\frac{\boldsymbol{r_{IS}}}{\boldsymbol{r_{AB}}}\right)^{\boldsymbol{-6}}$$

(Equation II.5)

As the effect decreases with the sixth power of the distance, suitable distances are limited (usually 5 Å).

II. 3. 2. 1. Diffusion studies

The LED-NMR method for the determination of the self-diffusion coefficient allows evaluation of the diffusivity of ions without the use of any additional probe molecules, which might affect the diffusion of the ions. As far as we know, although many diffusional studies have been carried out in IL/water mixtures, none has had the objective of studying the ion-pair dynamics in choline-glutamate IL.

The diffusion ordered spectroscopy spectra obtained for [Ch][Glu] is displayed in **Figure II.1** and the calculated diffusion coefficients are presented in **Table II.2**.

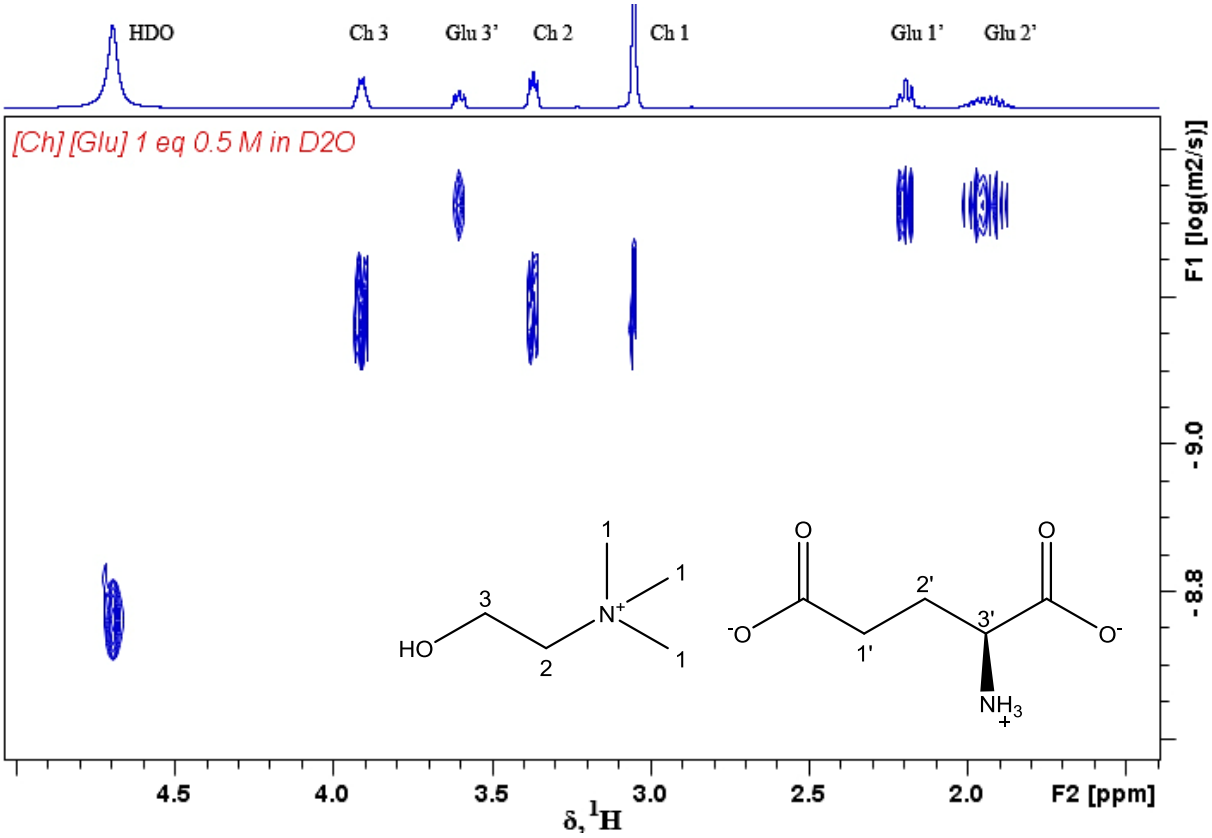

Figure II.1. ^{1}H-DOSY plot of 0.5 M [Ch][Glu] in 99.9% D_2O.

Table II.2. Diffusion coefficients comparisons of 0.5 M [Ch][Glu] in 99.9% D_2O as extracted from ^{1}H- DOSY plots.

		choline glutamate ([Ch][Glu])	
Protons	**HDO**	**Ch^+**	**Glu^-**
Diffusion Coefficients (D) (10^{-10} m^2 s^{-1})	14.4 ± 0.1 [a]	5.71 ± 0.09 [b]	4.20 ± 0.02

[a, b] The standard deviation in HDO and in ions were obtained by fitting and by average of different signals, respectively.

A basic supervision over the ions (cation and anion) diffusion coefficients data (**Figure II.1** and **Table II.2)** in dilute solution (82.2% water content) reveals that the cation diffuses faster than the anion. So it is possible assume that Glu^- is relatively larger than Ch^+ (0.7 larger). However, the extent of the difference reflects the degree of ion pairing (if the cation-anion difference is smaller, the ion pair association is greater).[72]

Inopportunely the neat [Ch][Glu] is highly viscous, not possible to measure with our NMR apparatus.

II. 3. 2. 2. NOE studies

For the first time, the anion-cation contact of cholinium-based ILs was determined by qualitative and quantitative NOE NMR investigations. The 1D selective NOE spectra obtained for [Ch][Glu] is displayed in **Figure II.2** and the calculated NOE intensities are presented in **Table II.3**.

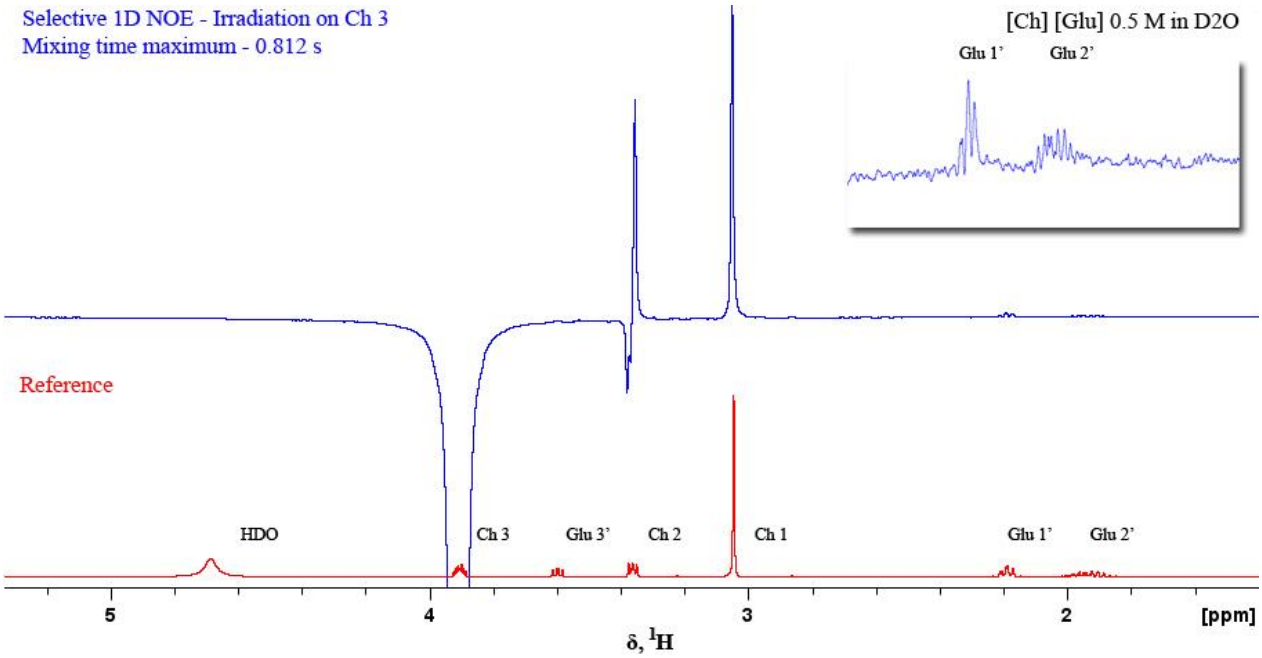

Figure II.2. NOE data for H3 – Ch of [Ch] [Glu] (1564.15 Hz in D2O) from a selective 1D-NOESY with 0.812 s mixing time (Top) and reference spectrum with resonance assignments (bottom).

The choice of intermolecular NOE studies is related with the fact that to observe a measurable intermolecular NOE the ion-pair needs to have a sufficient lifetime to result in a notable probability for cross relaxation, condition that would imply that the process occurs at nanosecond time-scale.[74] Thus, by the obtained intermolecular NOE result in **Figure II.2** (cross correlation response of H1' - Glu and H2' - Glu from irradiation on H3 - Ch) it is proposed that the lifetime of ion-pairs might be long enough to be detected, more than ion-pair lifetime with a few picoseconds related by Weingärtner.[18] Concerning the NOE, because of the limitation of the effect itself, namely its rapid decrease with increasing distance (the maximum distance at which NOE can be observed is

approximately 5 Å).[75] This tight cation-anion distance reinforces the idea that ion pair [Ch][Glu] exists in dilute solution.

As mentioned earlier, the steady state NOE in an ideal two-spin system delivers no information on inter-nuclear distances. However, the buildup rate of the NOE during the mixing time can be used to obtain distance information. For that, each 1D Selective NOESY was obtained for a different mixing time (τ_m) in a series of experiments. Once the irradiation was selectively in Ch 3, the mixing times selection was done according to the relaxation T_1 of the fastest proton of interest in glutamate (0.812 s), the range varied from 0.110 s to 2.0 s (0.13 – 2.5 x T_1 fastest).

The build-up data is available as **Appendix A, Fig. A.7 and A.8** and is summarized in **Table II.3** where the individual signal intensities represents the qualitative and quantitative order of magnitude of the particular cross relaxation and thus the intensity of interaction. Plotting these intensities against the mixing time leads to the NOE build-up curves shown in **Figure II.3** and **Figure II.4.** To obtain the right proportions with respect to each proton, the intensities have to be weighted by the number of the corresponding nuclei and normalized with respect to that of the highest response.

Table II.3. 1D - NOE data for H3 - Ch on [Ch][Glu] on the range 110 s - 2000 s.

[a]Not possible to integrate.

Irradiation on H3 - choline

Mixing time (ms)	Normalized relative NOE intensities (a. u.)		
	H1 - Ch	**H1' - Glu**	**H2' - Glu**
110	0.080	0.008	0.009
160	0.102	0.019	0.020
325	0.259	0.047	0.041
490	0.418	0.057	0.044
650	0.557	0.068	0.056
812	0.643	0.084	0.068
1000	0.748	- [a]	- [a]
1200	0.827	0.112	0.086
1500	0.918	0.098	0.072
2000	1.000	0.095	0.025

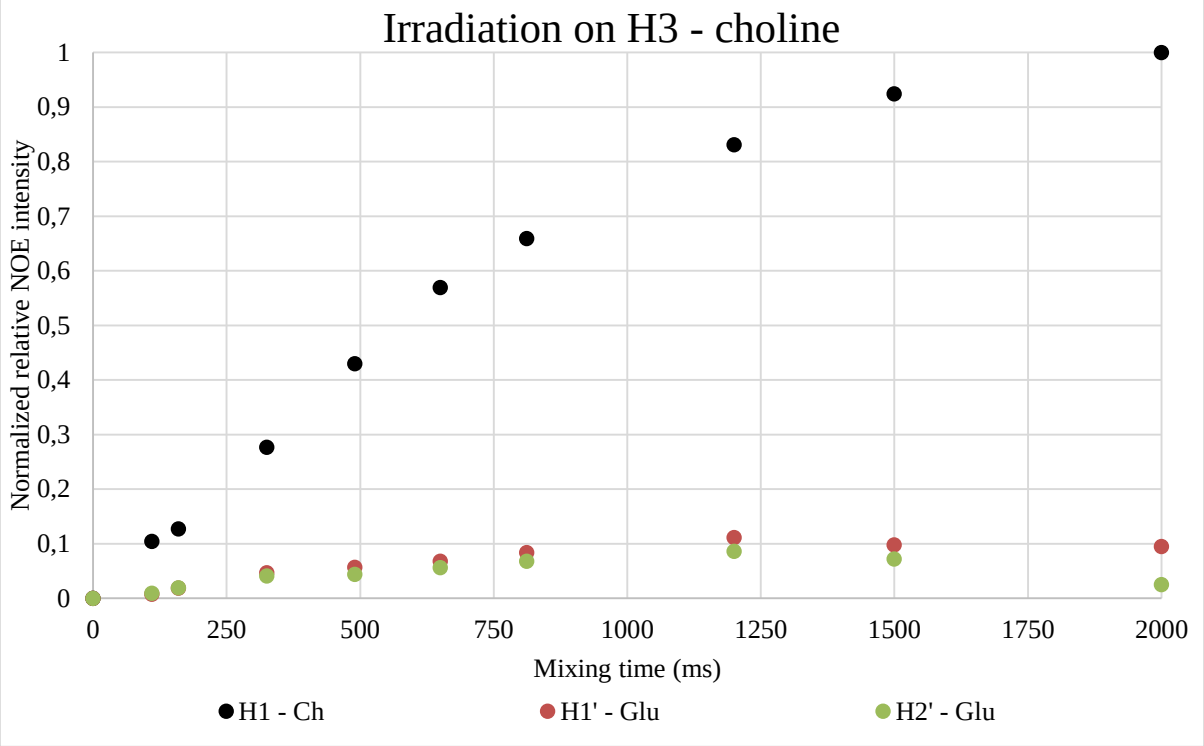

Figure II.3. Calculated normalized relative NOE intensity (1D-NOE build-up curves) for H1 - Ch (intramolecular NOE), H1'- Glu and H2' - Glu (intermolecular NOE) for the time range 110 – 2000 ms.

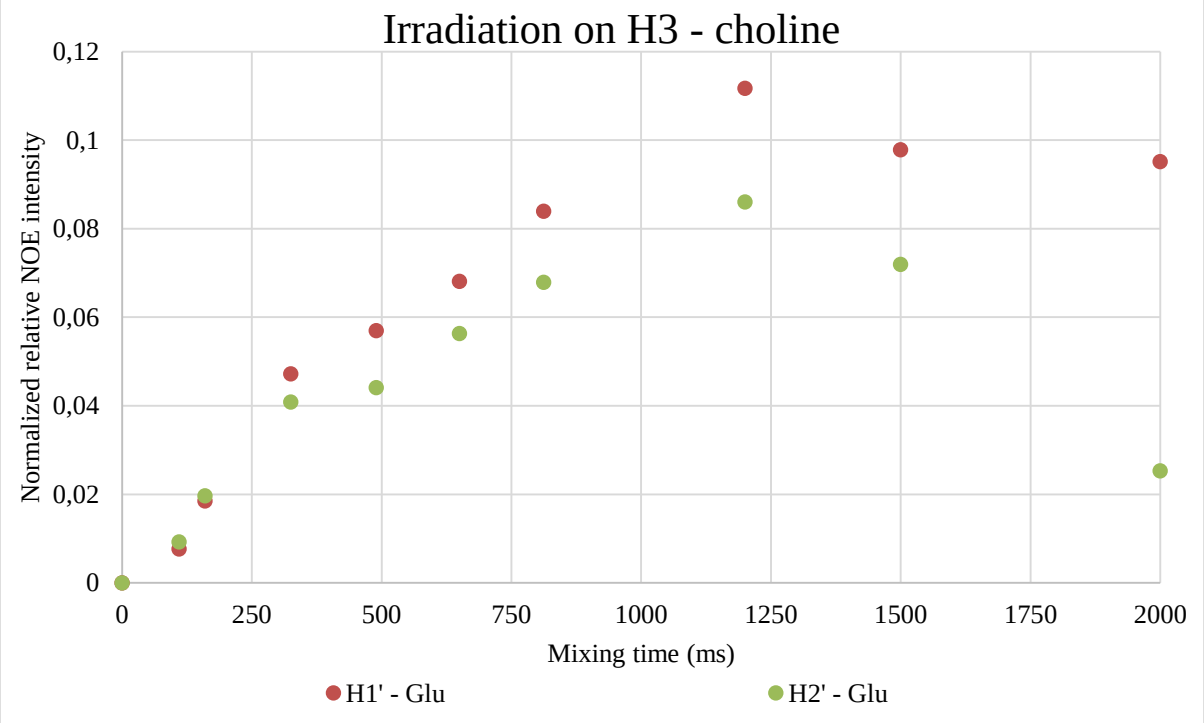

Figure II.4. Calculated normalized relative NOE intensity (1D-NOE build-up curves) for H1'- Glu and H2' - Glu for the time range 110 – 2000 ms.

A direct evidence of NOE contact for intermolecular interaction is shown in **Figure II.4.** by the observation of NOE build-up curves from H1'–Glu and H2'–Glu upon selective irradiation on H3–Ch (H2–Ch and H3'–Glu showed contact but their integration were not possible). The detected

NOEs from irradiation on H3–Ch is represented in **Figure II.5**. However, NOE investigations were also performed by irradiating at H1–Ch and H1'–Glu, the results are available as **Appendix A, Fig. A9 – A14**. On H1–Ch the NOE response by protons of glutamate (H1'–Glu and H2'–Glu) did not increase linearly with mixing time. A NOE between H1–Ch and H1'–Glu/ H2'–Glu likely had contributions from spin diffusion: the magnetization follows a path from H1–Ch to H3–Ch and then from H3–Ch to H1'–Glu/ H2'–Glu but appears to be directly from H1–Ch to H1'–Glu/ H2'–Glu. This phenomena supports the close interaction demonstrated above. On H1'–Glu the NOE response by protons of choline shown us a weak interaction, still difficult to interpret in order to get a build-up curve.

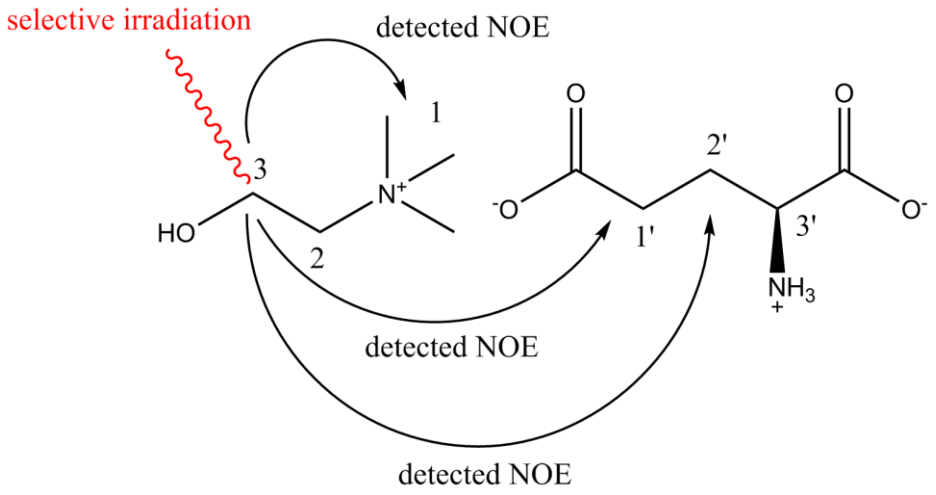

Figure II.5. Representation of detected NOEs from irradiation on H3 – Ch.

Based on theoretical explanation in the beginning of this section, the initial buildup rate of the NOE is proportional to σ_{IS}, accordingly, three initial build-up rates with irradiation on H3 - Ch (one intramolecular and two intermolecular) were fitted as shown in **Figure II.6.**

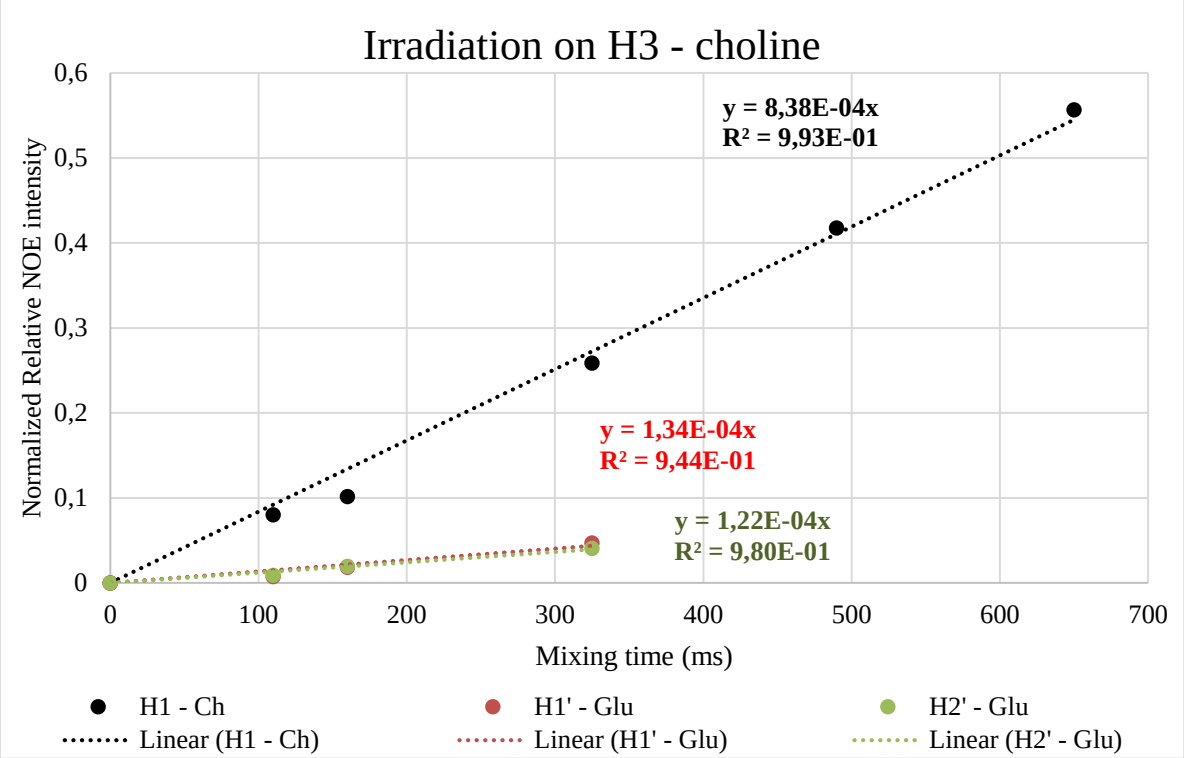

Figure II.6. 1D - NOE Build-up initial stage curves with linear fitting for H1 – Ch, H1'- Glu and H2'- Glu for the time range 110 – 700 ms.

The inter-nuclear distance determination from NOE data relies on the use of calibration distance, specifically the intra-nuclear distance H3–Ch /H1–Ch. Based on the optimized structure of choline cation reported by Alcorn *et al*,[211] and since their computational NMR chemical shifts was shown to lead to reasonable agreement with the experimental NMR chemical shifts and J - coupling obtained in this work (^{1}H NMR and ^{13}C NMR spectra are available as **Appendix A, Fig. A.5 and A.6**), the geometry of choline was calibrated by Chem3D Pro 14.0 with the bond lengths, angles and dihedral angles of related work as represented in **Figure II.7.** Consequently the H3–Ch (2H) /H1–Ch (9H) average spatial distance was determined as 4.144 Å (where the shortest distance was 1.723 Å and the longest was 5.575 Å).

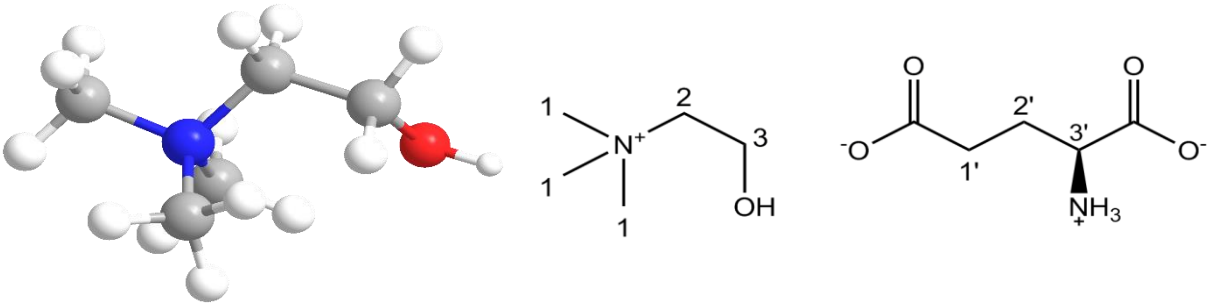

Figure II.7. 3D Structure of choline^{+} generated with Chem3D Pro 14.0 (left) and assignments in [Ch][Glu] structure (right).

Using the **(Equation II.5** aforementioned in the beginning of this section, with the known r_{AB} and the σ_{AB} and σ_{IS} extracted from **Figure II.6**, it was possible to determine the intermolecular average distance (r_{IS}) from H3–Ch protons to H1'–Glu protons and H2'–Glu protons:

$$\frac{\boldsymbol{\sigma_{IS}}}{\boldsymbol{\sigma_{AB}}} = \left(\frac{\boldsymbol{r_{IS}}}{\boldsymbol{r_{AB}}}\right)^{-6} \Leftrightarrow \frac{\boldsymbol{\sigma_{IS}}}{\boldsymbol{\sigma_{AB}}} = \left(\frac{\boldsymbol{r_{AB}}}{\boldsymbol{r_{IS}}}\right)^{6} \Leftrightarrow \sqrt[6]{\frac{\boldsymbol{\sigma_{IS}}}{\boldsymbol{\sigma_{AB}}}} = \frac{\boldsymbol{r_{AB}}}{\boldsymbol{r_{IS}}} \Leftrightarrow \boldsymbol{r_{IS}} = \frac{\boldsymbol{r_{AB}}}{\left(\sqrt[6]{\frac{\boldsymbol{\sigma_{IS}}}{\boldsymbol{\sigma_{AB}}}}\right)}$$

Table II.4. Intermolecular distances Ch-Glu determined with calibration distance.
[a]The intramolecular distance (r_{AB}) and his standard deviation were determined with the geometry of optimized choline cation.

Out H3 - Ch	**Intramolecular**	**Intermolecular**	
Protons	**H1 - Ch**	**H1' - Glu**	**H2' - Glu**
Initial build up NOE rate (10^{-4})	8.38	1.34	1.22
σ_{IS}/σ_{AB}	1.000	0.160	0.146
Average distance, r (Å)	4.1 ± 0.7 [a]	5.6 ± 0.7	5.7 ± 0.7

The strongest NOE (*i.e*. the shortest inter-ionic distance) was observable for the H3–Ch /H1'–Glu protons, the second strongest cross relaxation takes place between H3–Ch /H2'–Glu. Unfortunately, the intermolecular interaction with H3'–Glu was unreadable. However, the determined distances are averages with ± 0.713 of standard deviation since the ion pair is highly dynamic and time dependent. Probably for NOE detection, at a specified time, the H3–Ch /H1'–Glu and H3–Ch /H2'–Glu distances were 4.9 Å and 5.0 Å, respectively.

This detection of intermolecular cross-correlation is a strong indication that the ion pair exists even for dilute [Ch][Glu] aqueous solution. The alcohol group of the choline cation seems to be positioned near the centre of glutamate anion, once the protons of methylene group 3 of Ch^+ are a distance of ~ 5.7 Å from protons of 1'–Glu and 2'–Glu. Likely the head group of Ch^+ was close to the carboxylic group of Glu^- by Coulombic forces.[18] There is still a possibility of hydrogen bond shared between OH group of Ch^+ and NH_3^+ group of Glu^-.

In addition, based on report of Lingscheid *et al*[80] for imidalozium-based ILs by $^{19}F,^{1}H$ HOESY experiments, these interactions are not restricted to the plane of the cation (which would be the case if H-bonding would be the dominant force), furthermore the authors described that the strongest interactions were in a defined radius. Also relevant is the work of Dupont,[79] they found H,H NOEs as an evidence for ion pairs in dilute [1-*n*-butyl-3-methyl-imidazolium] $[BPh_4]$ in $CDCl_3$ with hydrogen bonding distances to the phenyl ring centroid around 2.3 Å.

II. 4. Conclusions

The work presented in this chapter reports an efficient method for the synthesis of choline-based ILs using anion exchange Amberlite resin. With the careful selection of the organic anion as other [AA]/ lactate$^-$/ AMP$^-$ it is possible the new bio-inspired combinations with important physical and thermal properties.

Using selective NOE it was possible detect a contact ion pair of the dilute biocompatible [Ch][Glu] IL in biological solvent (water) and determine the inter-nuclear distance average cation – anion of ~5.65 Å.

Due to their excellent physicochemical properties, [Ch][Glu] IL appears to be a hopeful osmolyte for protein stabilization in crowded environments.

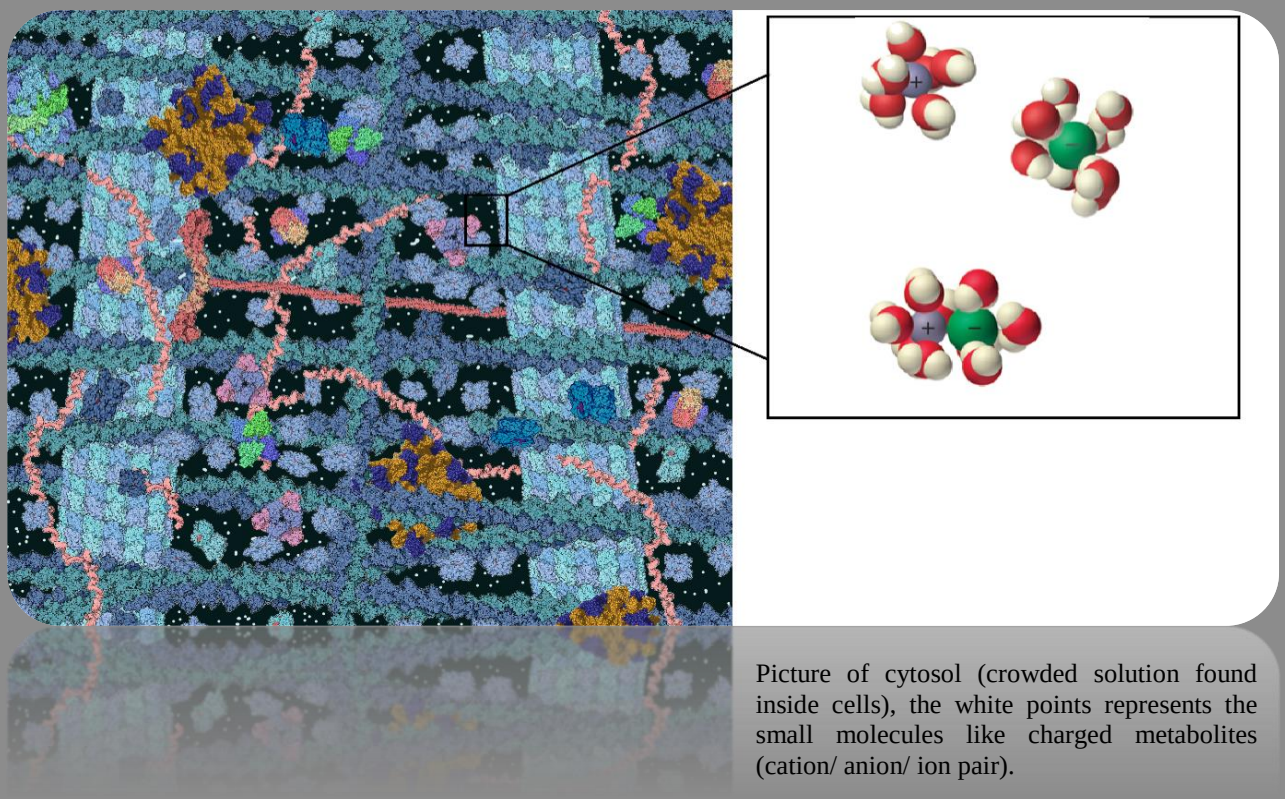

Picture of cytosol (crowded solution found inside cells), the white points represents the small molecules like charged metabolites (cation/ anion/ ion pair).

Chapter III: Bio – ILs under crowding conditions

The focus of this chapter is on the promotion of ion pair association using crowding agents commonly used to mimic the interior of a cell. Using NOE – NMR, I was able to estimate the cation-anion distance under macromolecular crowding.

Table of contents

III. Bio – ILs under crowding conditions

III. 1. Introduction

The environment inside cells is exceptionally complex and contains a large amount of macromolecules at concentrations exceeding 300 g/L[156] with volume occupancies of 30%, vastly different from the dilute, idealized conditions usually used in biophysical studies.[157,158] The addition of high concentrations of natural and synthetic macromolecules (crowder agents) to such dilute solutions (buffers) enables crowding to be mimicked adding it as a variable to study.[162,169–171] Recently, the effects of crowding on protein stability had been explored [148,163–166] and arise from two phenomena: short range (steric) repulsions and longer range interactions, as explained in chapter I (macromolecular crowding section).

However, cells contain more than macromolecules, the high concentrations of charged organic metabolites (small molecules)[147,148] allow many cation-anion combinations and transient ion-pairs have been detected in nature,[155] as was already explored in detail in Chapter I (I. 2. 3. Charged metabolites and bio–ionic liquids section).

This densely packed conditions were used to study choline-glutamate IL for the first time in order to promote ion-pairing, since their high concentrations found in cell.

As far as we know, ILs have never been studied under macromolecular crowding, although exists a few studies of protein stability with the osmolyte Glycine Betaine (in zwitterionic form),[128,130,200,201] Sarkar and Pielak[202] showed that the osmolyte glycine betaine can mitigate the lysate's (model of *E. Coli* proteome prepared by Sarkar *et al.*)[181] destabilizing effect on the test protein CI2, however the interaction osmolyte-CI2 and how osmolyte mitigates the attractive interactions protein lysate-CI2 remains to be determined (probably by increasing weak attractive interactions). Hopeful the studies with [Ch][Glu] IL on proteins under crowding might help to elucidate this effect (Chapter IV).

Typically, in macromolecular crowding studies, the crowding agents are: synthetic polymer crowders[156,163,172–176] such as polyvinylpyrrolidone (PVP) and polyethylene glycol (PEG), both with a random coil polymer,[177] and ficoll, a cross-linked and branched derivative of sucrose (more globular);[178] and natural proteins crowders (globular)[164,179–182] such as bovine serum albumin (BSA)[183] and lysozyme[184].

Despite the fact that BSA–ILs interactions have been shown to be important[117] for BSA stabilization, this was only studied for dilute protein solutions (~50 μM) and not under conditions were BSA acts like a crowding agent. In this work, under high concentrations of globular protein BSA (150 g/L) this was considered to act like a collection of inert spheres. However its global charge (positive) can be relevant when [Ch][Glu] is introduced in the crowding solution.

PEG was reported as a biocompatible polymer that is non-immunogenic, uncharged and highly soluble in water,[212,213] these characteristics make PEG widely used for biomedical applications[214] and for mimicking inert crowding agents, up to physiologically realistic volume fractions of crowder of ~40%.[156] In particular studies, the terminal hydroxyl groups of the PEG molecules provide a ready site for covalent attachment to other molecules and surfaces such as ILs on the cation (reported in an review about PEG-Based ILs by Colacino *et al.*)[215] and proteins.[216] However, specifically the interactions PEG-IL should be minimal due the uncharged crowder and the high concentrations.

Recent experimental results indicate that the presence of weak, nonspecific attractive interactions in the heterogeneous cellular environment can modulate or even dominate the effects of hard-core repulsion that are at the basis of molecular crowding.[165,185,186] The role of such chemical interactions is a subject of debate also for proteins and PEG.[162,171] The existence of ion-pair in Choline-Glutamate IL under dilute condition with intermolecular distance of ~5.7 Å for H3-Ch /H1'-Glu, H2'-Glu, specifically the shortest distance between the positively charged head group of choline and the negatively charged group of glutamate, can be decreased under physiologically relevant crowded conditions and play a biological key role. The approach presented here allows the relative contributions of steric exclusion (excluded volume) effects and soft interactions in ion pair association of Choline-Glutamate in 150 g/L synthetic crowder PEG and natural crowder BSA, the properties of crowders and IL are presented in **Table III.1**.

Table III.1. Properties of [Ch][Glu] and crowders.

Molecule	MW, Da	pI	Charge at pH 7.10 [a]
[Ch][Glu] IL	251.3	NA[b]	Neutral
PEG 3350	3350	NA	Neutral
BSA	66 000	4.7	Anionic

[a] pH of aqueous solution with 0.5 M [Ch][Glu] IL; [b] NA: Not Applicable.

Remarkably, the NOE NMR is a powerful tool for investigating cation-anion interactions because of its abilities to detect spatial distances below 5 Å,[75] to screen the partial existence of ionic pair, and to detect a change in crowding conditions by conformational changes.

Thereby, I use selective 1D NOE NMR spectroscopy (in the same way as the previous chapter) to study choline – glutamate interactions and evaluate the extension of ion pairing under two different crowded conditions of 150 g/L (PEG/ uncharged vs. BSA/ negatively charged).

III. 2. Experimental section

III. 2. 1. Materials

Lyophilised bovine serum albumin (BSA) and poly (ethylene glycol) average M_n 3,350 in powder (PEG 3350) were purchased from *Sigma-Aldrich* with a purity of 99%. Choline-glutamate [Ch][Glu] IL was synthetized as explained in experimental section of previous chapter (II). This IL was at least 99% pure and was dried for 24 h under vacuum at 60 ºC. Deuterium oxide (D_2O) 99.9% [D] was purchased to *Euriso-Top*. pH values are direct meter readings uncorrected for any isotope effect and were measured with *Docu-pH, Startovarius*.

III. 2. 2. Selective 1D - NOE experiments

NMR experiments were performed at 298 K in a Bruker AVANCE III 400 MHz spectrometer operating at a proton Larmor frequency of 400.15 MHz equipped with a 5 mm high-resolution BBO probe. A 5mm NMR tube was used with a [Ch][Glu] concentration of 0.5 M in 99.9% D_2O with a total volume of 500 µL and a crowder concentration of 150 g/L. NOE experiments were performed as explained in experimental section of Chapter II.

PEG 3350. The pH meter reading for [Ch][Glu]-PEG 3350 solution was pH 7.62 (uncorrected for deuterium isotope effects). The spectra were recorded with 160 x 4 scans in a matrix with 16 K points in a spectral window of 4000 Hz centred at 1571.31 Hz, 1229.67 Hz and 884.96 Hz, each corresponds a one *build-up* NOE. The relaxation delay was 6.6 s and 11 mixing time points in each experiment were collected: at irradiation in choline (centred on H3 – Ch at 1571.31 Hz, with receiver gain of 181 and H1 – Ch at 1229.67 Hz with receiver gain of 64): 0.110 s, 0.134 s, 0.27 s, 0.40 s, 0.54 s, 0.67 s, 0.80 s, 1.0 s, 1.2 s, 1.5 s, and 2.0 s; at irradiation in Glutamate (centred on H1' - Glu at 884.96 Hz with receiver gain of 25.4): 0.110 s, 0.17 s, 0.34 s, 0.67 s, 1.0 s, 1.2 s, 1.34 s, 1.5 s, 1.7 s, 2.0 s, 3.0 s).

BSA. The pH meter reading for [Ch][Glu]-BSA solution was pH 7.19 (uncorrected for deuterium isotope effects). The spectra were recorded with 160 scans repeated 4 times in a matrix with 16 K points in a spectral window of 4000 Hz centred at 1561.41 Hz, 1217.91 Hz and 875.69 Hz, each corresponds a one *build-up* NOE. The relaxation delay was 5.3 s, the receiver gain was 90.5 and 11 - 12 mixing time points in each experiment were collected: at irradiation in choline (centred on H3 – Ch at 1561.41 Hz and on H1 – Ch at 1217.91 Hz): 0.110 s, 0.134 s, 0.27 s, 0.42 s, 0.54 s, 0.70 s, 0.80 s, 1.0 s, 1.2 s, 1.5 s, and 2.0 s; at irradiation in glutamate (centred on H1' – Glu at 875.69): 0.110 s, 0.17 s, 0.34 s, 0.67 s, 0.9 s, 1.0 s, 1.2 s, 1.33 s, 1.5 s, 1.7 s, 2.0 s, 3.0 s).

The mixing times selection was done according to the relaxation T_1 of the proton fastest of interest in glutamate: crowded by PEG - 0.72 s; crowded by BSA – 0.70 s, the range varied from 0.110 s to 2.0 s (0.13 – 2.5 x T1 fastest).

III. 3. Results and discussion

III. 3. 1. Ion Pair association in [Ch][Glu] under crowding conditions

The ion-pair association under macromolecular crowding can be promoted and the distance anion-cation calculated by intermolecular interactions. The results of Chapter II were used as reference to comparisons: in aqueous solution (dilute), the distance H3-Ch /H1'-Glu, H2'-Glu was around 5.7 Å, has shown by Selective 1D NOE with selective irradiation on Ch 3. The representative scheme is presented in **Figure III.1.**

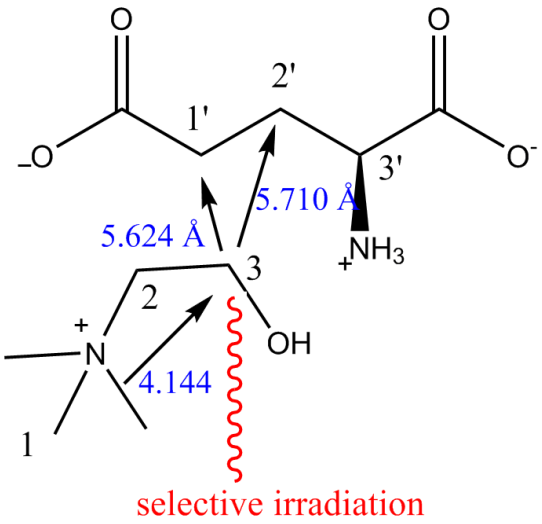

Figure III.1. Structure assignment of [Ch][Glu] and representative NOE effect with selectively irradiation on H3 – Ch, in dilute condition.

As before the buildup rate of the NOE during the mixing time was used to obtain distance information. NOE studies were performed by irradiating at H1-Ch, H3-Ch and H1'-Glu under crowding conditions. All results show a weak intermolecular contact as seen on **Appendix B, Figure B.2 and B.3.**

The data obtained for selective saturation of H3-Ch under crowding was analysed in detail in order to compare with H3-Ch data obtained for dilute conditions. The H3-Ch individual NOE data and their NOE build-up curves under PEG condition are available as **Appendix B, Fig. B.4 and B.5**, and with BSA as **Appendix B, Fig. B.6 and Fig. B.7**.

The H1 - Ch - 1 D NOE data under PEG/ BSA are available as **Appendix B, Table B.1** and their individual NOE data and build-up curves under PEG as **Fig. B.8 and B.9**; with BSA as **Fig. B.10 and B.11**. These results demonstrated the same spin diffusion from H1-Ch to H3-Ch and from this to H1'-Glu, H2'-Glu, as happens in dilute condition.

Furthermore, when selectively irradiating H1'-Glu under crowding using PEG, it was not possible to observe a NOE build-up curve for H3'-Glu because it is necessary intramolecular interaction for distance calibration, not possible due to overlap of PEG signals with H3'-Glu

(observable in **Figure B.2. in Appendix B**); And crowded by BSA, it was not possible plotting these intensities against the mixing time leads to the NOE build-up curves due to weak intensities of signals (observable in **Figure B.12, in Appendix B**).

Selective 1D-^{1}H-NOE spectra for H3-Ch corresponding to the maximum NOE build-up are presented in **Figure III.2** and **Figure III.3** for PEG and BSA, respectively. The normalized relative NOEs for the mixing time range are resumed in the **Table III.2**, where the relative NOE with the highest intensity was set to 1.0 as a reference and all other NOE signals were calculated accordingly.

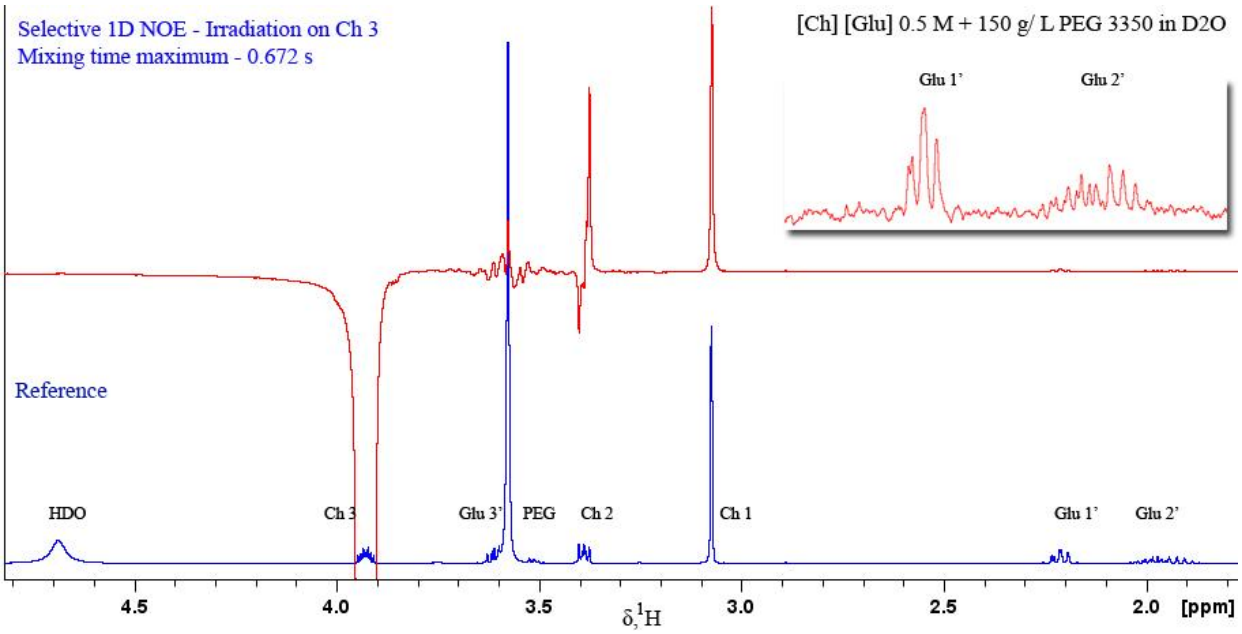

Figure III.2. NOE data for H3-Ch of [Ch][Glu] (1571.14 Hz in D_2O) with 150 g/L PEG 3350 from a selective 1D-^{1}H-NOE with 0.672 s mixing time (top) and reference spectrum with resonance assignments (bottom).

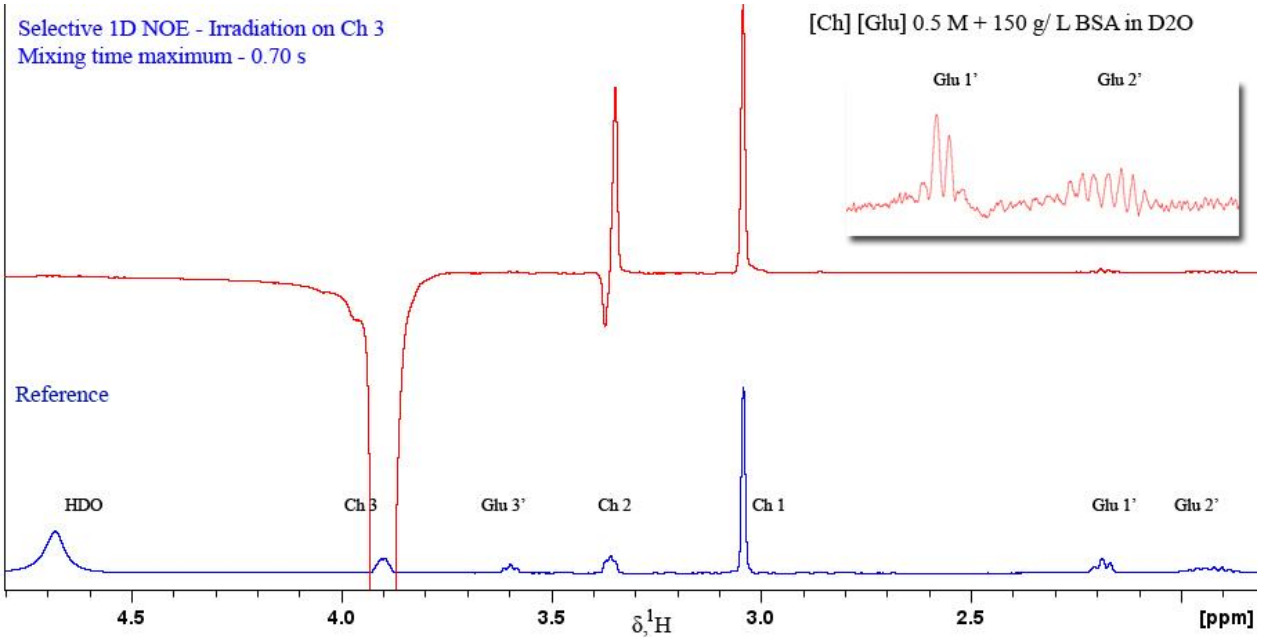

Figure III.3. NOE data for H3-Ch of [Ch][Glu] (1561.41 Hz in D_2O) with 150 g/L BSA from a selective 1D-^{1}H-NOE with 0.70 s mixing time (top) and reference spectrum with resonance assignments (bottom).

Table III.2. 1D-^{1}H-NOE data for H3-Ch in 0.5 M [Ch][Glu] in three different conditions: dilute; crowded with 150 g/L of PEG 3350; and crowded with 150 g/L of BSA; on the range 110 ms/ 134 ms - 2000 ms.

On H3 Ch	Normalized relative NOE intensities (a.u.)									
	Dilute				**150 g/L PEG 3350**				**150 g/L BSA**	
Mixing time (ms)	**H1 Ch**	**H1' Glu**	**H2' Glu**	**Mixing time (ms)**	**H1 Ch**	**H1' Glu**	**H2' Glu**	**Mixing time (ms)**	**H1 Ch**	**H1' Glu**	**H2' Glu**
110	0.080	0.008	0.009	**110**	0.121	0.023	0.034	**134**	0.172	0.029	0.058
160	0.102	0.019	0.020	**134**	0.158	0.034	0.037	**270**	0.334	0.061	0.072
325	0.259	0.047	0.041	**270**	0.289	0.055	0.053	**420**	0.495	0.086	0.087
490	0.418	0.057	0.044	**400**	0.397	0.061	0.057	**540**	0.595	0.097	0.091
650	0.557	0.068	0.056	**540**	0.509	0.073	0.070	**700**	0.715	0.101	0.089
812	0.643	0.084	0.068	**670**	0.596	0.077	0.073	**800**	0.763	0.107	0.091
1000	0.748	-	-	**800**	0.670	0.085	0.074	**1000**	0.876	0.111	0.104
1200	0.827	0.112	0.086	**1000**	0.767	0.089	0.093	**1200**	0.933	0.130	0.106
1500	0.918	0.098	0.072	**1500**	0.921	0.111	0.088	**1500**	1.000	0.148	0.121
2000	1.000	0.095	0.025	**2000**	1.000	0.099	0.074	**2000**	0.998	0.081	0.105

Plotting these intensities versus the mixing time leads to the NOE build-up curves shown in **Fig. III. 4**, **Fig. III. 6** and **Fig. III. 8** for the intermolecular cross correlation, in different conditions, between H3-Ch and H1-Ch, H1'-Glu and H2'-Glu, respectively. The initial build-up rates were fitted as shown in **Fig. III. 5**, **Fig. III. 7** and **Fig. III. 9**.

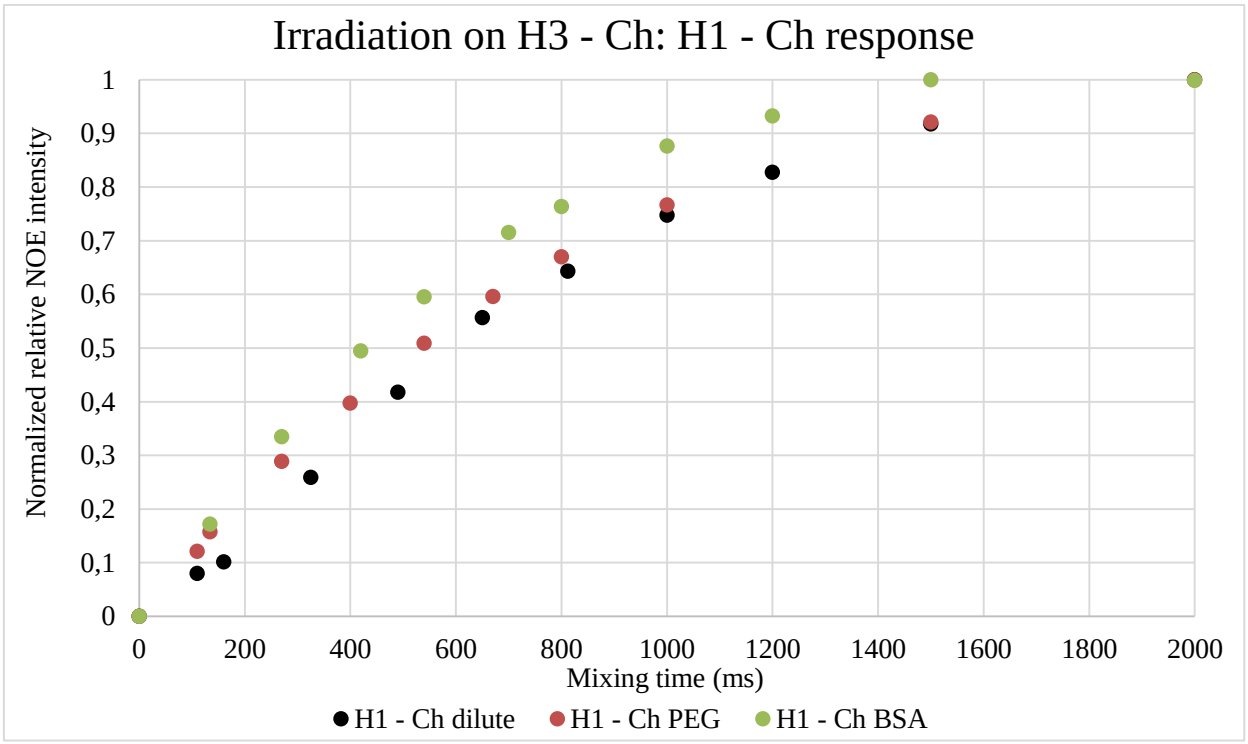

Figure III.4. Calculated normalized relative NOE intensity for the mixing time variation range from 110/134 ms to 2000 ms (1D-NOE build-up curves) for H1-Ch (intramolecular NOE) in different conditions: diluted, crowded with PEG 3350 (150 g/L) and crowded with BSA (150 g/L).

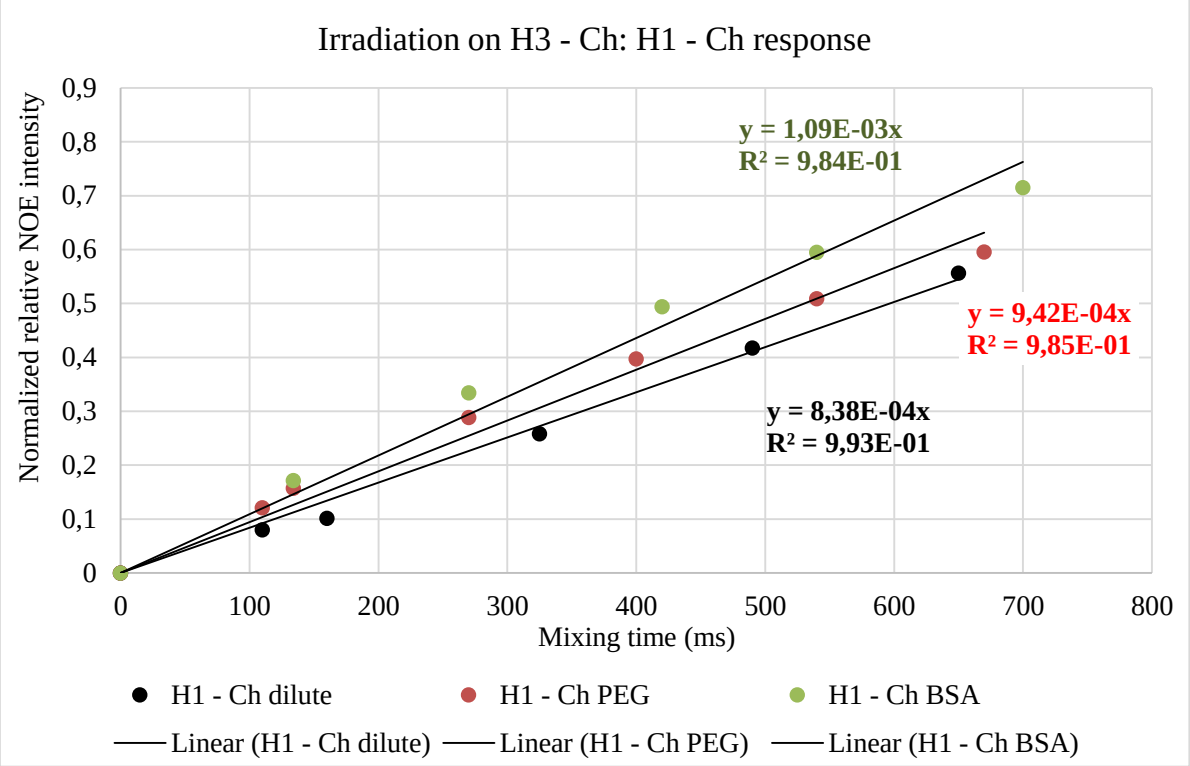

Figure III.5. 1D - NOE Build-up initial stage curves with linear fitting for H1 – Ch for the time range 110/ 134 – 700 ms in different conditions: diluted, crowded with PEG 3350 (150 g/L) and crowded with BSA (150 g/L).

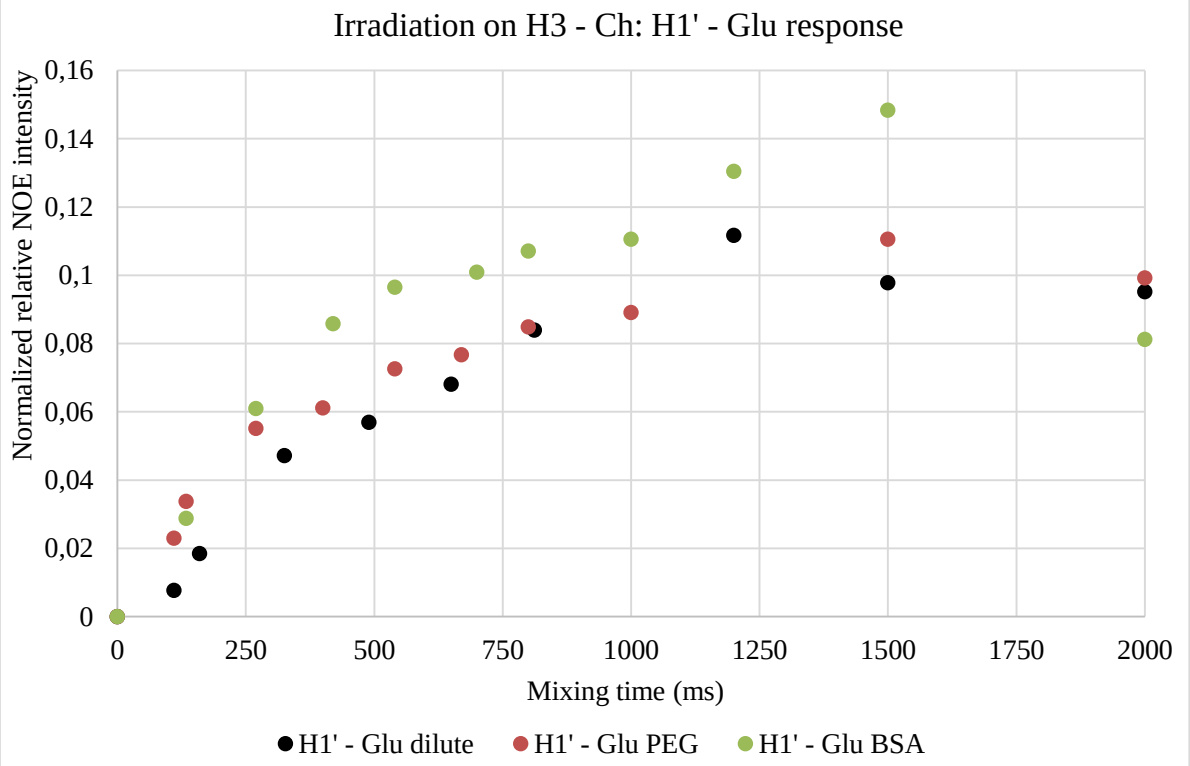

Figure III.6. Calculated normalized relative NOE intensity for the mixing time variation range from 110/134 ms to 2000 ms (1D-NOE build-up curves) for H1'- Glu (intermolecular NOE) in different conditions: diluted, crowded with PEG 3350 (150 g/L) and crowded with BSA (150 g/L).

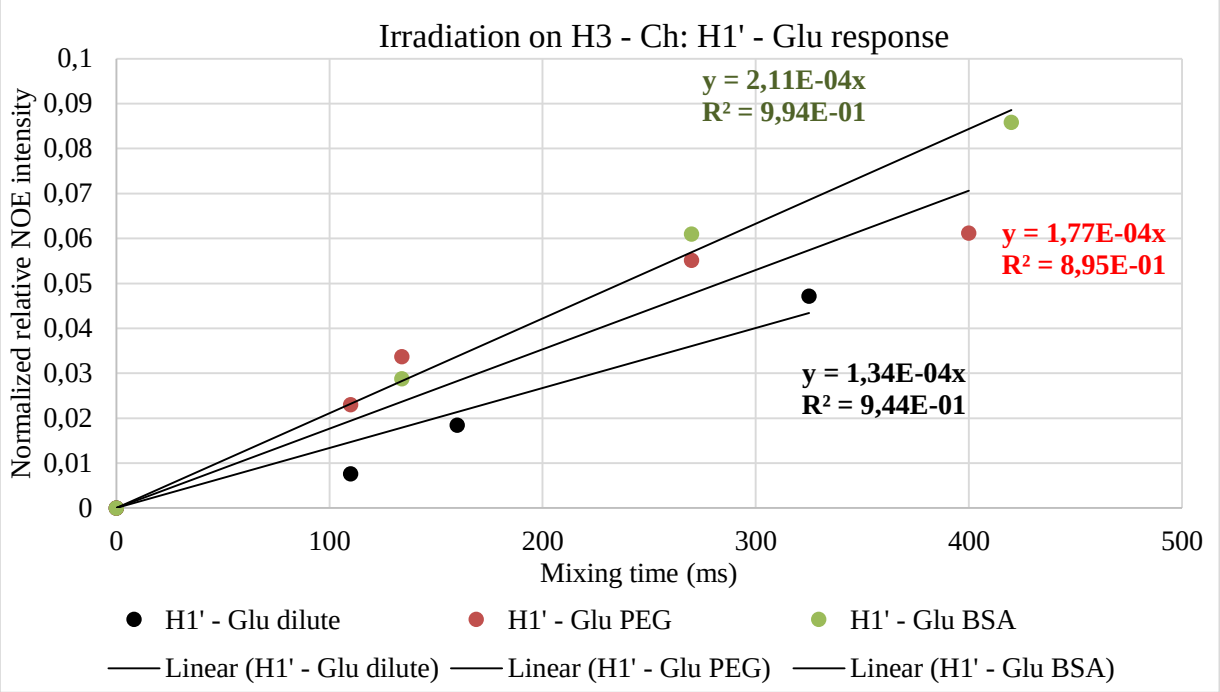

Figure III.7. 1D - NOE Build-up initial stage curves with linear fitting for H1' – Glu for the time range 110/ 134 – 500 ms in different conditions: diluted, crowded with PEG 3350 (150 g/ L) and crowded with BSA (150 g/L).

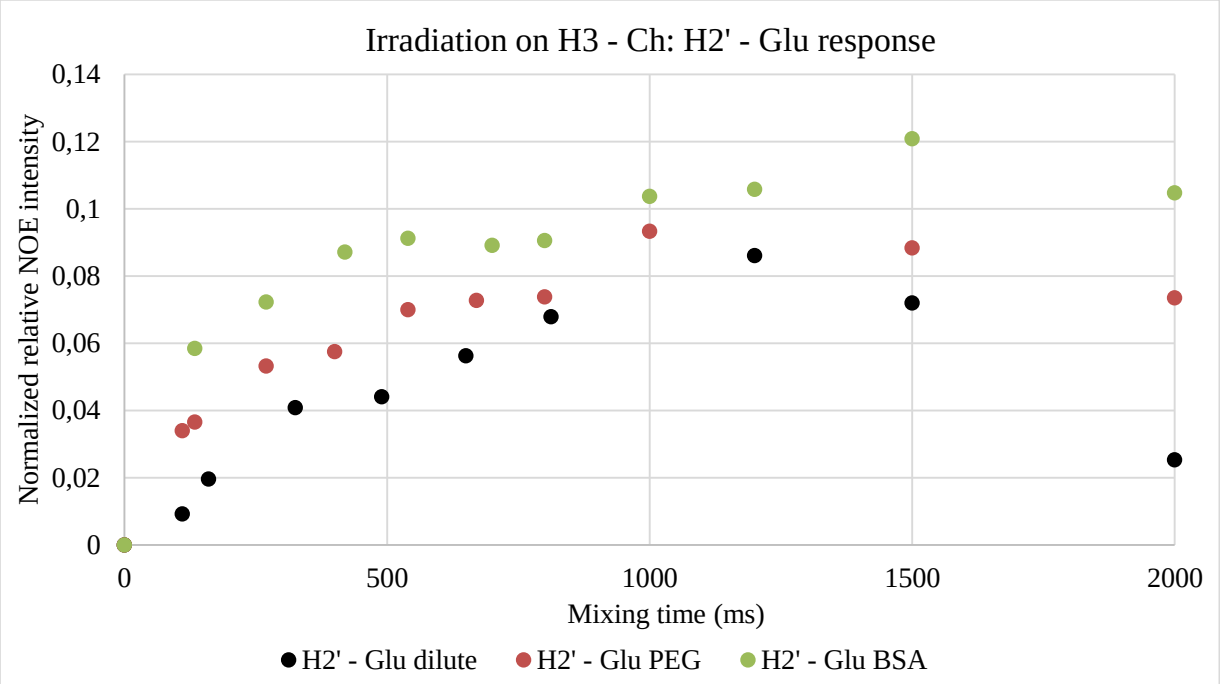

Figure III.8. Calculated normalized relative NOE intensity for the mixing time variation range from 110/ 134 ms to 2000 ms (1D-NOE build-up curves) for H2'- Glu (intermolecular NOE) in different conditions: diluted, crowded with PEG 3350 (150 g/L) and crowded with BSA (150 g/L).

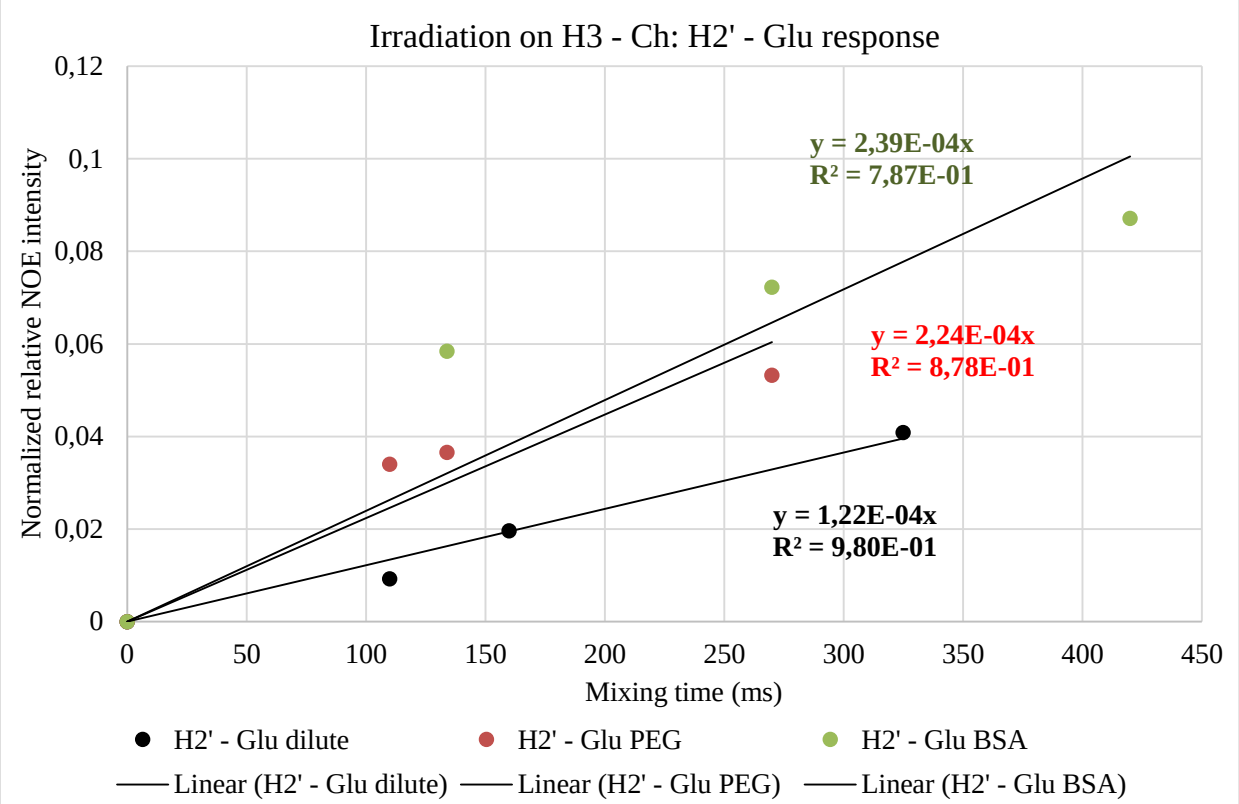

Figure III.9. 1D - NOE Build-up initial stage curves with linear fitting for H 1' – Glu for the time range 110/ 134 – 450 ms in different conditions: diluted, crowded with PEG 3350 (150 g/L) and crowded with BSA (150 g/L).

Notably, the different linear fittings observed in **Figure III.7** and **Figure III.9** would be better if lower mixing time points were collected as 50, 100, 200 and 250 ms.

Using **(Equation II.5**, in the same way as in Chapter II, with the σ_{AB} and σ_{IS} extracted from **Figure III.5, Figure III.7 and Figure III.9,** it was possible to determine the intermolecular average distance (r_{IS}) from H3 - Ch protons to H1' - Glu and H2' - Glu protons in the crowded environments:

$$\frac{\sigma_{IS}}{\sigma_{AB}} = \left(\frac{r_{IS}}{r_{AB}}\right)^{-6} \Leftrightarrow r_{IS} = \frac{r_{AB}}{\left(\sqrt[6]{\frac{\sigma_{IS}}{\sigma_{AB}}}\right)}$$

Table III.3. Intermolecular distances of Ch-Glu under different conditions, determined with calibration distance since H3 - Ch.
The dilute condition data was from Chapter II to comparison use.

Condition	**Dilute**			**Crowded by 150 g/ L PEG 3350**			**Crowded by 150 g/ L BSA**		
Interaction	Intramolecular	Intermolecular		Intramolecular	Intermolecular		Intramolecular	Intermolecular	
Protons	**H1 Ch**	**H1' Glu**	**H2' Glu**	**H1 Ch**	**H1' Glu**	**H2' Glu**	**H1 Ch**	**H1' Glu**	**H2' Glu**
Initial build up NOE rate (10^{-4})	8.380	1.340	1.220	9.420	1.770	2.240	10.900	2.110	2.390
σ_{IS}/σ_{AB}	1.000	0.160	0.146	1.000	0.188	0.238	1.000	0.194	0.219
Average distance, r (Å)	**4.1** [a]	**5.6**	**5.7**	**4.1**	**5.5**	**5.3**	**4.1**	**5.5**	**5.3**
Standard deviation (Å)	**± 0.7** [a]								

[a] The intramolecular distance (r_{AB}) and his standard deviation were determined with the geometry of optimized choline cation, from reference.[211]

Looking now to the spatial distances determined in **Table III.3** by **(Equation II.5)** is possible to verify that exists a small changes from dilute condition to crowded conditions. In PEG and BSA environments (the viscosity was increased but for NOE technique was irrelevant), the strongest NOE was observable for the H2' - Glu protons instead H1' - Glu of dilute, however the relevance is minimal once R^2 factors reflect very poor correlation and standard deviation is around ± 0.7. Anyway, the intermolecular distances slightly decreased and these determinations are reliable. Therefore the choline-glutamate ion-pair remained under macromolecular crowding and their extension may have increased.

Supposedly the crowder agents should reinforces the tight contact cation-anion when they find each other once that crowder take up space and the IL concentration is insignificant compared to the total concentration of macromolecules. Thus, test IL or in other words, cation-cation/ anion-anion/ cation-anion rarely interact with each other, supporting the idea that there ionic pair is because it is persistent enough (ion pair with long life time).[74] The reasons previously presented are valid to the synthetic or natural crowder: the PEG crowder is completely uncharged instead the BSA with overall positive charge that could preferential interact with anion and disrupt the ion pair. However, this not happen and globally was considered that the distance Choline – Glutamate was positively affected by two crowders. The direction of the net effect is the same whether the crowder is larger (PEG) than or very larger (BSA) than the co-solute/ IL.

The macromolecular crowding theme was never studied only with ILs which makes difficult to evaluate the interactions crowders-IL, yet I try to the system studied which contains 0.5 M [Ch][Glu] and 150 g/L of crowder.

The excluded volume generated by crowder is the sum of two parts: steric repulsions and chemical interactions, also called soft interactions or longer-range interactions (include hydrogen bonding, charge-charge interactions, hydrophobic effect, *etc.*), although individually weak, their final effect depends on the sum of individual components. In the IL-crowders system, I considered the ion pair entirely hydrated, concerning the closest water molecules. As one article author puts it, if the biomolecule (IL in my case) is constrained to the smaller volume between crowders, why is it not also constrained to the smaller volume between the waters? The volume between big crowding molecules is also filled with small crowding molecules![193] This statement explains that the steric effect of large crowders reduces the excess chemical potential of a biomolecule in solution relative to pure water.

The ion pair promotion under BSA supports the idea that not exists IL-BSA soft chemical interactions (charge-charge effects). In both crowders, the steric repulsions are the mainly interactions but weak once the ion pair was slightly promoted by 0.4 Å (less hydrated) from dilute condition (more hydrated). For disrupting the ion pair or contrariwise it will be necessary perturb the water molecules surrounding the ion pair by hydrophobic effect.

III. 4. Conclusions

The selective ^{1}H-1D-NOE NMR technique can measure cation-anion pair of [Ch] [Glu] at the sensitive level of 5.3 – 5.7 Å under crowded conditions mimicking the cellular interior. Summary, the excluded volume effects in IL are much smaller than expected, there is a surprisingly weak dependence on crowder size or charge, however the crowding slightly promoting the ion-pair.

The results of this chapter revealed that choline-glutamate ion pair is reinforced under natural or synthetic packed conditions. Their effect on proteins under macromolecular crowding can be studied (as a source for excluded volume effects). Therefore, the effect of ions and ion-pair of [Ch][Glu] on structure and stability of proteins was studied in the next chapter.

IV

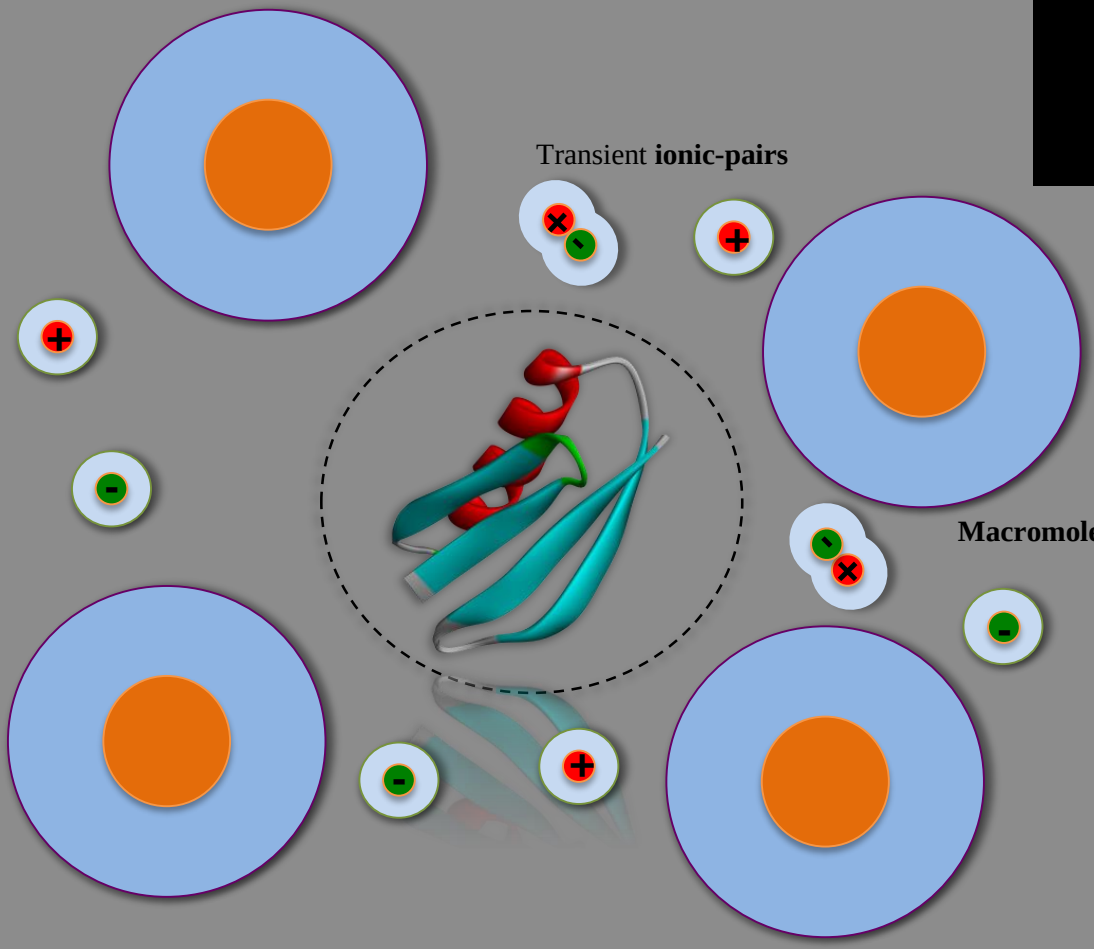

Representation of protein GB1, small organic charged metabolites and transient ionic pairs under macromolecular crowding.

Chapter IV: Bio-IL effect on protein stability and structure under crowding conditions

In this chapter, I have used NMR spectroscopy (protein diffusion, ^{15}N-HSQC experiments, hydrogen-deuterium exchange) and differential scanning calorimetry for IL effect evaluation on proteins (stability and preferential interactions) plus the influence of crowder agents.

Table of contents

IV. Bio-IL effect on protein stability and structure under crowding conditions

IV. 1. Introduction

To expand the level of understanding of protein-ILs interactions and to explore the possibility of protein-ILs interactions being modulated by macromolecular crowding, particularly in terms of protein stability and nature of specific contacts established with the ion pair, I have focused my studies on [Ch][Glu] IL (for which the formation of ion pairs even under crowding conditions has been shown on the previous chapter) with the immunoglobulin-binding domain B1 of *streptococcal* protein G (GB1).[217] GB1 is a small (56 residues, 6.2 kDa and pI 4.8), stable, biologically inert, single domain protein with one long α-helix (on top) and a four-stranded β-sheet comprised of two hairpins. This compact highly globular protein has no disulphide bridges and the topology of secondary structural elements (an extensive hydrogen-bonding network, a tightly packed and buried hydrophobic core) is probably responsible for the extreme thermal stability (reversible melting at 87 ºC).[203] This protein was chosen as a test protein because its small size and high thermal stability make GB1 well appropriate for studies by NMR spectroscopy, and its structure, stability and folding kinetics have been extensively studied in dilute solution,[203,218–224] and recently, *in vitro* crowding,[182,190,225] in prokaryotic cells,[182,225–230] and in eukaryotic cells.[190] Recently, these studies with GB1 were reviewed by Pielak *et al.*[189] and Smith *et al*.[166] In addition, for details and procedure about live cell NMR, see the review by Freedberg and Selenko.[191]

Selenko *et al.*[190] have reported that the positions of the GB1 resonances (^{15}N-enriched) in the HSQC spectra remained the same in dilute condition, in solutions containing 250-300 g/L BSA, and in *Xenopus laevis* oocytes/eukaryotic cellular system (in cell NMR spectra with exceptional high quality), meaning that neither artificial crowding nor the environment in the cell changes the structure of GB1. Different performance was observed for cross-peak intensity (resonances of amides involved in intramolecular hydrogen bonds showed diminished intensity in cells and in BSA compared to dilute solution), suggesting that more dynamic parts of the protein are less affected by the increased viscosity in cells (which is estimated to be up to 8 times as high as in water).

In *E. coli*, more than 70−90% of the most abundant proteins are acidic or neutral, with an average pI of 5.5, which strongly suggests that their surfaces are anionic (negatively charged) at ambient pH of 7.2 in the cell.[231] Since GB1 is also negatively charged at neutral pH (high net charge of -4), this would lead to significant self-repulsion (charge-charge repulsive interactions) that reinforce the hard-core repulsion (steric interactions), thereby compensating short-range attractive forces and leading to an overall stabilisation.[225] Indeed, GB1 displays almost no interactions with *E. coli* macromolecules even at millimolar intracellular concentrations.[227] Contrary to the stabilisation of

GB1 in cells, accordingly with Monteith and Pielak[182], the individual protein crowders (BSA and lysozyme) destabilize the protein compared with buffer alone. Notably, stabilization of GB1 in 100 g/L BSA (pI = 4.7) was expected, compared with buffer, because both GB1 and BSA have anionic surfaces. However, this destabilization supports the hypothesis that nonspecific and attractive backbone interactions can overcome charge–charge effects and hard-core repulsions. Nevertheless, according to Zhou's work[232] above a certain temperature crowding will be stabilizing, based on these authors, for GB1 on BSA crowder, such temperature is above 37 ºC. On other hand, the destabilisation of anionic GB1 in the presence of positively charged lysozyme (pI =11.3) as a crowder can be presumed by the prevalence of weak and attractive interactions, since these interactions with the protein backbone will assist in the exposure of more surface, which leads to unfolding of protein.

In a related work by Sarkar and Pielak[202] already explored in Chapter III, likewise using an anionic protein, CI2 (pI= 6.0), they reported that glycine betaine osmolyte decreases the interactions between CI2 and the protein's crowders (*E. Coli* lysate) suggesting that glycine betaine causes proteins to be "invisible" to one another, a similar effect as that happens in dilute solution (osmolytes stabilize globular proteins because the backbone prefers to interact with water rather than osmolyte).

In this chapter, the [Ch][Glu] IL effect on anionic GB1 was studied under PEG (uncharged), BSA (negatively charged), lysozyme (positively charged) crowders and on *E. coli* lysate (mainly negatively charged), assessed by protein diffusion (DOSY), ^{15}N-HSQC's, amide proton exchange and differential scanning calorimetry (DSC). Therefore, in DOSY experiment, the crowder concentration range selected was from 0 to 300 g/L since the macromolecules can occupy more than 30% of a cell's volume, reaching concentrations exceeding 300 g/L.[156] In the other experiments, the crowder concentration selected was 150 g/L since is the typical concentration used in the most reports and the macromolecular crowding in these conditions is easy to appraise.

IV. 2. Experimental Section

IV. 2. 1. Materials

Lyophilised bovine serum albumin (BSA), lyophilised lysozyme from chicken egg white, poly(ethylene glycol) average M_n 3350 in powder (PEG 3350) and choline chloride [Ch][Cl] were purchased from *Sigma-Aldrich* with a purity of 99%. 1-butyl-3-methylimidazolium chloride [C_4mim][Cl], 1-butyl-3-methylimidazolium dicyanamide [C_4mim][dca] were purchased from *IoliTec* (Denzlingen, Germany). Choline glutamate [Ch][Glu] was synthetized as explained in Experimental Section of Chapter II. The ILs were at least 99% pure and were dried for 24 h under vacuum at 60 ºC. Deuterium oxide (D_2O) 99.90% [D] and D_2O "100% D", >= 99.96% [D] were purchased from *Euriso-Top*. Distilled water and Milli-Q water were obtained from laboratory facility instruments. pH values

are direct meter readings uncorrected for any isotope effect and were measured with *Docu-pH, Startovarius*.

IV. 2. 2. Molecular biology of protein GB1 wild-type

IV. 2. 2. 1. Recombinant protein production

The pET11a plasmid containing the gene encoding T2Q B1 immunoglobulin G binding domain of streptococcal protein G (GB1) with resistance to ampicillin, was kindly provided by Professor Gary Pielak from University of North Carolina at Chapel Hill.

The T2Q mutation prevents N-terminal deamidation, and we refer to this form as wild type (WT) or only "GB1". The amino acid sequence is as follows:

MQYKLILNGKTLKGETTTEAVDAATAEKVFKQYANDNGVDGEWTYDDATKTFTVTE

IV. 2. 2. 2. Protein expression and purification

The isolation and purification of WT GB1 was based on the supporting information of Monteith and Pielak,[182] well as on the protocol of Lindman *et al.*[233]

The plasmid encoding GB1 was transformed into competent BL21 (DE3) *Escherichia Coli* cells (*NZYTech*). For the transformation 1 µL were added to 50 µL of *E. Coli* BL21 competent cells and then incubated 15 min in ice. Then the cells were incubated at 42 ºC during 40 s and transferred to ice where they rested for 15 min. 500 µL of sterile Luria-Bertani (LB) Medium (10 g/L tryptone, 5 g/L yeast extract and 10 g/L NaCl, **see Appendix C, Table C.1** for details) pre-warmed at 37 ºC was added to the cells and incubated at the same temperature for 1h. 100 µL were spread onto luria broth–agar plates containing 100 µg/mL ampicillin (*Sigma*), followed by incubation overnight at 37 °C.

A single colony was used to inoculate a 20 mL (7x) overnight culture in LB medium containing 100 µg/mL ampicillin. This culture was incubated overnight with shaking at 37 °C and 200 rpm (*200D, Optic-Ivymen System)*. The next morning, each 20 mL culture was poured into 1 L of LB Medium (5x). This 5 L culture was grown with shaking at 37 °C and 180 rpm until the optical density at 600 nm reached 0.7 (took 3 hours). Protein expression was then induced with 1 mM isopropyl-β-D-thiogalactopyranidose (IPTG). After 3h induction in the same conditions, the cells were harvested for 12 min at 6000 rpm, 4ºC (*Avanti j-26 XPI, Beckman Coulter, JA-10 rotor*) and frozen at -20ºC overnight.

The cell pellet was resuspended into 150 mL lysis buffer (10 mM Tris-HCl, 1 mM EDTA, pH 7.5) preheated to 80ºC. The sample was stirred and heated until the temperature reached 80 °C for 5 min. The lysed cells were cooled on ice for 10 min and then centrifuged at 15,500 rpm for 30 min at 4ºC (*Avanti j-26 XPI, Beckman Coulter, JA-25.50 rotor*). The supernatant was frozen with 30% Glycerol for a week and after dialyzed against 20 mM Tris-HCl, pH 7.5 overnight (*Snake Skin 3.5 K MWCO, Thermo Cientific)*.

Fractions were assessed by using SDS polyacrylamide gel electrophoresis, 12% Tris-Tricine gels[234] with coomassie brilliant blue staining (see **Appendix C, Table C.2 - C.5** for details in the preparation and running of the samples), shown in **Figure IV.1**.

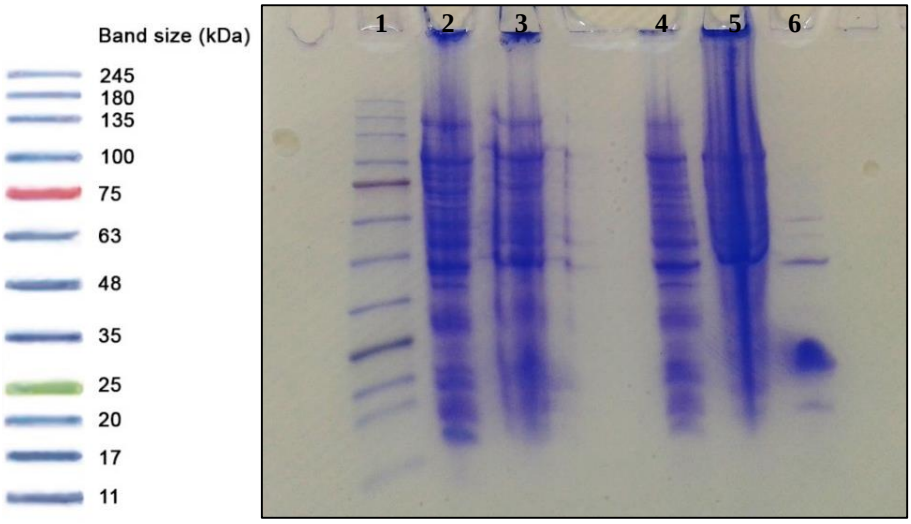

Figure IV.1. SDS-PAGE gel after isolation of GB1 (12% Tris-Tricine).
Lane 1 – NZY Colour Protein Marker II; 2 – Before IPTG induction; 3 – After IPTG induction; 4 – Cellular extract after heating; 5 – Pellet; 6 – Supernatant (GB1).

The supernatant dialysed was purified via anion exchange chromatography with a HiTrap Q HP (*GE Healthcare*) using diethylaminoethyl cellulose resin on an AKTA fast protein liquid chromatograph (*GE Healthcare*). Buffer A (20 mM Tris·HCl, pH 7.5) was used to load the crude lysate onto the column and elute impurities. Buffer B (20 mM Tris·HCl, 1 M NaCl, pH 7.5) was used to produce a linear gradient of 0–400 mM NaCl. The initial flow rate was 5 mL/min and the amount of sample, which was applied to a column, was about 35 mL in each purification the obtained chromatogram is shown in **Figure IV.2** and evaluate by SDS-PAGE gel in **Figure IV.3**.

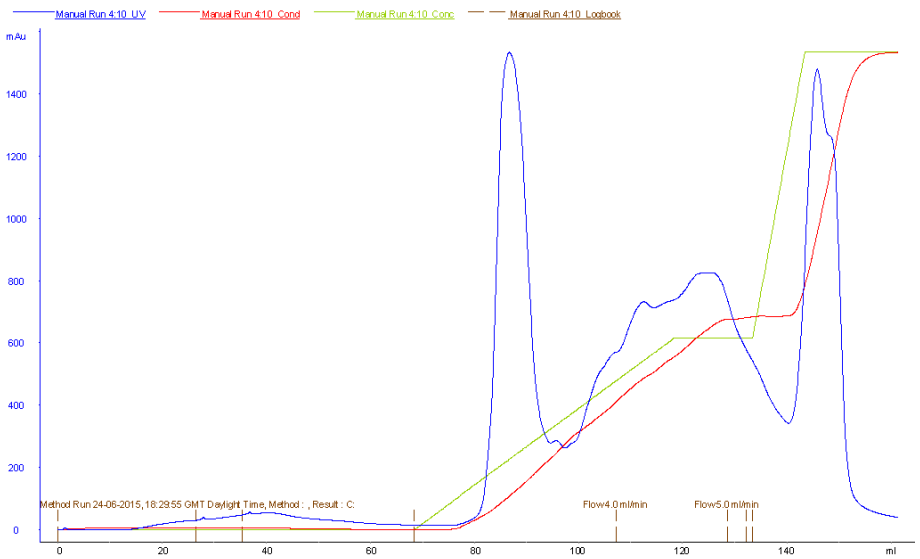

Figure IV.2: One of the purifications by anion exchange chromatography, GB1 found at 180 mM NaCl.

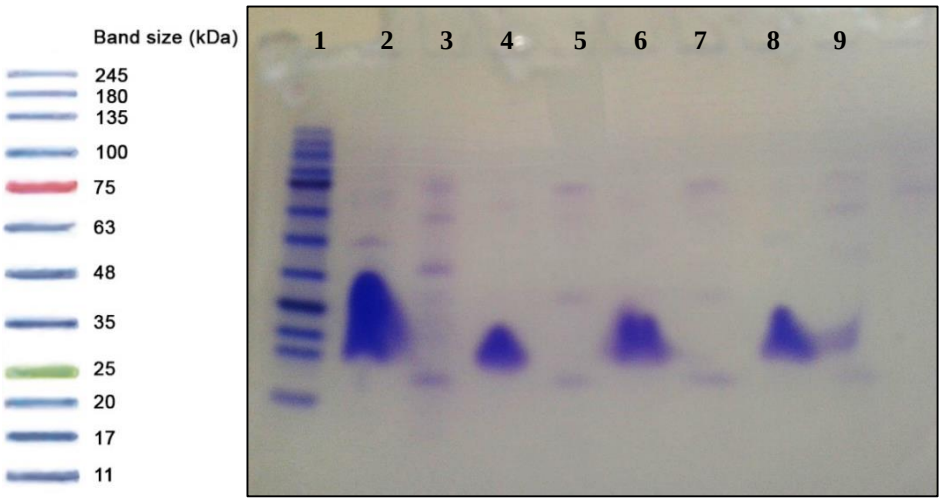

Figure IV.3: Tris-Tricine SDS-PAGE gel after anion exchange purification.
Lane 1 – NZY Colour Protein Marker II; Lanes 2, 4, 6, 8 – purified fractions; Lanes 3, 5, 7, 9 – fractions at 400 mM NaCl.

Fractions containing GB1 were pooled (~5.1 mg/ mL) and concentrated (~10 mg/ mL) with Amicon Centricons with 3-kDa molecular-mass centrifugal membranes (*Amicon Ultra-15 3 K MWCO, Millipore)* by centrifuging at 5000 rpm at 4ºC for further purification by size exclusion chromatography (Superdex 75 10/300 GL, *GE Healthcare*) with a running buffer of 20 mM potassium phosphate, 50 mM NaCl, pH 6.0. The initial flow rate was 0.6 mL/min and the amount of sample which was applied to a column was about 1 mL in each purification. The obtained chromatogram is shown in **Figure IV.4**.

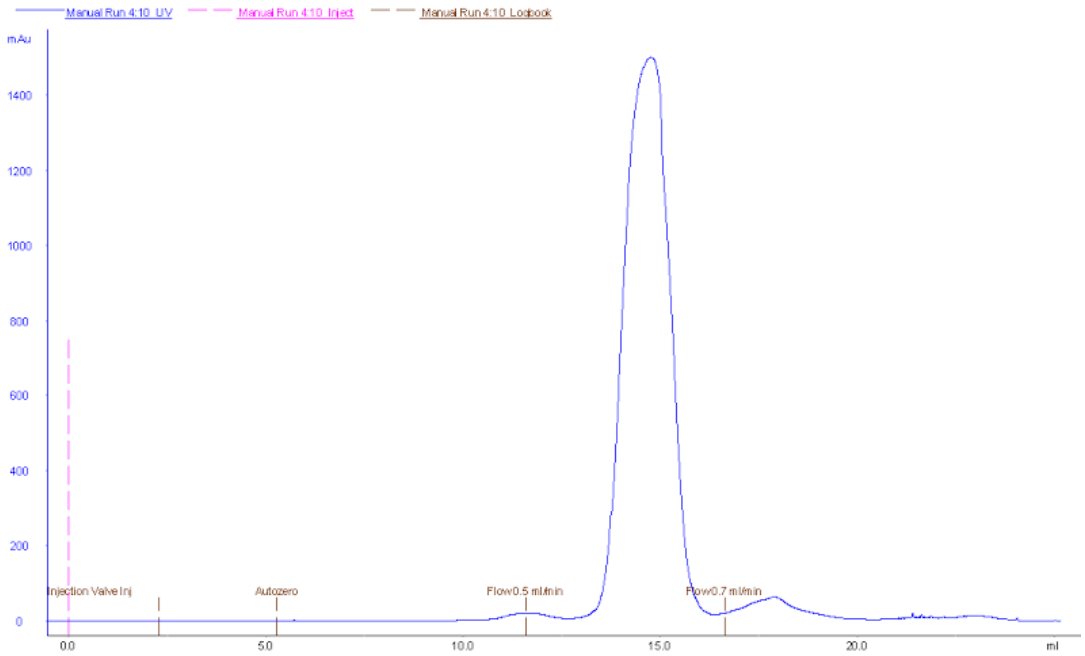

Figure IV.4: One of the purifications by size exclusion chromatography.

The pure fractions will be pooled, dialyzed against water, frozen, and lyophilized (*Edwards Freeze Dryer Modulyo*). The final concentration of the protein was kept around 2 mg/mL and the yields obtained were around 36 mg/L of protein. GB1 with 6.223 kDa the molar extinction coefficient (ε) was estimated at 9970 M^{-1} cm^{-1} by Expasy ProtParam (http://web.expasy.org/protparam/) and reading the absorbance (A) at 280 nm by UV-visible spectroscopy with a NanoDrop (*2000, Thermo Scientific*), the concentration (c) was determined through the Lambert-Beer Law (**A= εcl**, where l is the path length in cm).

IV. 2. 2. 3. ^{15}N Labelled protein expression and purification

To express ^{15}N labelled GB1 in *E. Coli* I have used the same transformation procedure as in no labelled GB1 (in **IV. 2. 2.** 2. Protein expression and purification **section**). A single colony was used to inoculate a 20 mL (5x) overnight culture in LB medium containing 100 μg/mL Ampicillin. This culture was incubated overnight with shaking at 37 °C and 200 rpm.

The next morning, each 20 mL culture was poured into 500 mL of autoclaved M9 minimal medium (50 mM Na_2HPO_4, 20 mM KH_2PO_4, 9 mM NaCl, 2.5 g/L $^{15}NH_4Cl$ as the sole nitrogen source and supplemented with 4 g/L glucose, 2 mM $MgSO_4$, 10 mg/L thiamine HCl, 100 μM $CaCl_2$, 100 μM $FeSO_4$ and 100 μg/mL ampicillin) accompanied with 5 mL of MEM vitamin solution 100x (*Sigma*) (4x). This 2 L culture was grown with shaking at 37 °C and 180 rpm until the optical density at 600 nm reached 0.8 (took 4 hours). Protein expression was then induced with 1 mM IPTG filter sterile. After 3h induction in the same conditions, the cells were harvested for 12 min at 6000 rpm, 4ºC and frozen at -20ºC overnight. The cell pellet was resuspended into 60 mL lysis buffer preheated to 80ºC. From this point on, all the steps are the same as described previously (in **IV. 2. 2. 2. Protein expression and purification**). See **Appendix C, Figure C.1 – C. 5**, for protocol details and results. The final concentration of the ^{15}N labelled GB1 (6.29 kDa of molecular weight) was kept around 1.43 mg/mL and the yields obtained were around 15 mg/L of protein. **Figure IV.5** show the obtained SDS-PAGE gel for the high purity of ^{15}N GB1 and no labelled GB1.

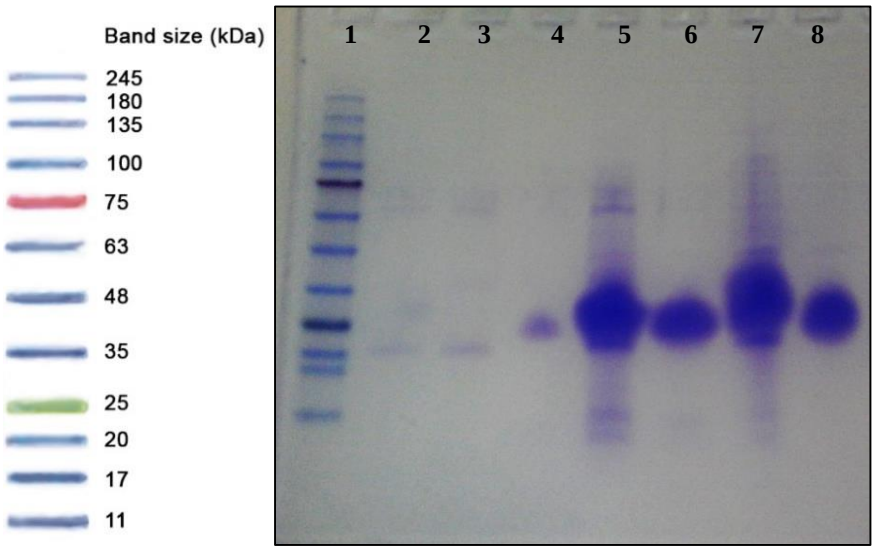

Figure IV.5: Tris-Tricine SDS-PAGE gel before and after exclusion molecular (EM) purification.
Lane 1 – NZY Colour Protein Marker II; 2 – impurities in purification of no labelled GB1; 3, 4 – impurities in purification of ^{15}N labelled GB1; 5 – ^{15}N labelled GB1 before EM; 6 – Purified ^{15}N labelled GB1; 7 – No labelled GB1 before EM; 8 – Purified no labelled GB1.

IV. 2. 3. Deuterated *E. Coli* lysates

The preparation of *Escherichia Coli* cell lysates was based on the protocols of *Wang et al.*[179] and Sarkar *et al.*[181] Cultures of strain BL21 (DE3) (*NZYTech*) containing an pET11a plasmid holding the gene encoding GB1 WT (I used an single colony from the same plate for GB1 WT production but an empty plasmid could be used) were grown at 37 ºC with shaking at 180 rpm (*200D, Optic-Ivymen System)* in 10 mL of deuterated LB medium (10 g/L tryptone, 5g/L yeast extract and 10 g/L NaCl in 99.9% D_2O) and 100 μg/mL ampicillin. The overnight culture was diluted into 100 mL of deuterated LB medium containing 100 μg/mL ampicillin. After 10 h at 37 ºC with shaking at 200 rpm, the cultures were harvested by centrifugation at 3500 rpm (*Avanti j-26 XPI, Beckman Coulter, JA-10 rotor*) for 30 min at 4 ºC. The pellet was stored at -20 ºC overnight. For lysis the pellet was resuspended in 7.5 mL of 99.9% D_2O with protease inhibitor cocktail (one tablet *complete ULTRA Tablets, Mini, EDTA-free, EASYpack Roche*). The cells were lysed by sonication (*UP 100H, Hielscher* equipped with 1/8 inch tip, 50% amplitude) on ice for 10 min with a duty cycle of 1 min on/ 1 min off. The lysate was collected after centrifugation at 8000 rpm (*Avanti j-26 XPI, Beckman Coulter, JA-25.50 rotor*) for 30 min and lyophilized (*Edwards Freeze Dryer Modulyo*). The lysate obtained from this experience was 113 mg of dry weight protein lysate (the yields obtained were around 11.3 g/L of lysate) and is shown in **Figure IV.6** in comparison with purified GB1.

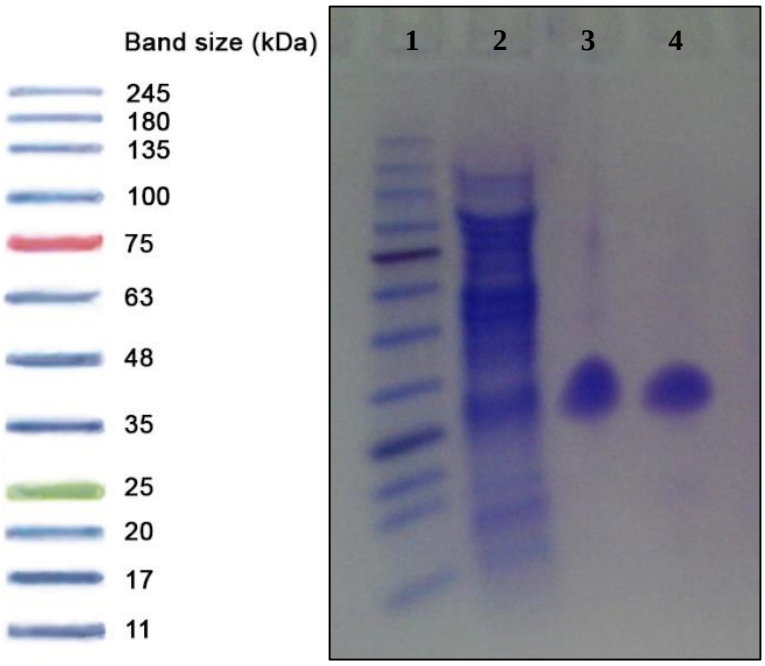

Figure IV.6: Tris-Tricine SDS-PAGE gel of Lysate and purified GB1.

Lane 1 – NZY Colour Protein Marker II; Lane 2 – Deuterated Protein Lysate; Lane 3 – Purified no labelled GB1; Lane 4 – Purified ^{15}N labelled GB1.

IV. 2. 4. NMR Spectroscopy

IV. 2. 4. 1. Data acquisition

All NMR spectra were acquired in one of the two spectrometers:

- 400 MHz Bruker Avance III spectrometer equipped with a 5 mm high-resolution BBO probe.
- 600 MHz Bruker Avance III spectrometer equipped with a 5 mm inverse detection triple-resonance z-gradient cryogenic probehead (CP TCI).

All data was processed using Bruker TopSpin™ 3.5.

IV. 2. 4. 2. Diffusion studies (DOSY)

Diffusion measurements were conducted at 37 ºC at 400 MHz. These experiments were performed according to the protocol described in **II.** 2. Experimental section **of Chapter II.** Using the pulse sequence ledbpgp2s that uses a stimulated echo, a longitudinal eddy current delay (LED), bipolar sine gradient pulses and 2 spoil gradients; the same sequence with water suppression using excitation sculpting with gradients (ledbpgpes2s) was also used when necessary.

Diffusion studies of GB1/PEG 3350 and GB1/lysozyme in the presence and absence of [Ch][Glu].

For each system, a series of five diffusion spectra was recorded in which the concentration of protein was maintained at 1 mM in 99.9% D_2O and the concentration of crowder varied from 0 to 300 g/ L (0, 50, 100, 150, and 300 g/L). Experiments were repeated with addition of 100 mM [Ch][Glu].

Typically, in each experiment 32 spectra with 16 scans of 32 K data points were collected, with a duration of the magnetic field pulsed gradients (δ) of 2.4 - 3.0 ms a diffusion time (Δ) of 100 - 150 ms, and an eddy current delay set to 5 ms. The gradient recovery time was 700 μs. The sine shaped pulsed gradient (g) was incremented from 5 to 95% of the maximum gradient strength in a linear ramp.

In the PEG system an excitation-sculpting module with gradients was employed to suppress the PEG proton signals. Each spectra was recorded with 160 scans repeated 4 times in a matrix with 16 K points in a spectral window of 4 kHz centred at the PEG signals (1519.6 Hz).

In addition, one diffusion spectrum was recorded for *E. coli* lysate condition, in which the concentration of protein was 1 mM (^{15}N labelled) in 100% D_2O and the concentration of crowder was 150 g/L.

Due to high concentrations used for protein crowders, huge overlay exists in ^{1}H-NMR spectrum between GB1 and lysozyme/ lysate, for this reason, the ^{1}H-NMR spectra of GB1 in lysozyme and GB1 in lysate are displayed in **Appendix C, Figure C.27** and **Figure C.28** with indications of the followed signals of GB1 for diffusion.

IV. 2. 4. 3. NMR Chemical shift perturbations (^{1}H-^{15}N HSQC)

NMR experiments were performed at 25 ºC at 600 MHz. Proton chemical shifts were referenced against external DSS while nitrogen chemical shifts were referenced indirectly to DSS using the absolute frequency ratio. GB1 assignments are based on published work[203] and denoted by its PDB identifier 2GB1.

Chemical shift perturbation experiments were followed by ^{1}H-^{15}N-HSQC. Each ^{1}H-^{15}N-HSQC (hsqcetfpf3gpsi2 pulse sequence from Bruker library) spectrum was acquired with 32 scans repeated 8 times on a matrix with 2048 x 128 complex points, in a spectral window of 9615.385 Hz (centered at the water resonance signal) x 2311.077 (centre at 118 ppm), in ^{1}H and ^{15}N sweep's width, respectively.

- **NMR chemical shift perturbation in the presence of ILs**

One ^{1}H-^{15}N HSQC spectrum was acquired for each IL concentration sample:

A 0.24 mM solution of ^{15}N-labelled WT GB1 in H_2O with 10% D_2O was titrated individually with different ILs ([C_4mim][Cl], [C_4mim][dca], [Ch][Cl]) at 100 mM concentration.

A 1 mM solution of ^{15} N-labelled WT GB1 in H_2O with 10% D_2O was titrated individually with [Ch][Glu] at 100 mM and 200 mM.

- **NMR chemical shift perturbation in the presence of ILs and crowders**

One ^{1}H-^{15}N HSQC spectra were recorded for each GB1 samples with [Ch][Glu] in the presence of 150 g/L PEG 3350, 150 g/L BSA and 150 g/L lysozyme:

To a 0.24 mM GB1 solution and to a 0.24 mM GB1/100 mM [Ch][Glu] mixture were added the BSA at 150 g/L.

To a 1 mM GB1 solution and to a 1 mM GB1/100 mM [Ch][Glu] mixture were added the synthetic crowder (PEG 3350) or lysozyme, at 150 g/L.

Also, a blank of lysozyme 150 g/ L was acquired as reference.

IV. 2. 4. 4. Amide proton exchange

Lysozyme, PEG 3350 and [Ch][Glu] were previously exchanged in D_2O. Briefly, 300 mg crowder and 100 mg IL were resuspended each in 5 mL D_2O, the samples were then frozen and lyophilized, and the process repeated twice. The decay of the amide proton signal intensities due to hydrogen exchange with D_2O was followed by a series of ^{1}H-^{15}N HSQC.

Before hydrogen exchange experiments, the spectrometer was first tuned and shimmed with a sample with the same contents without GB1 at 37 ºC. The sample for the exchange experiment was prepared by dissolving 4 mg of lyophilized ^{15}N – labelled WT GB1 in 600 µL of D_2O (>= 99,96% isotopic purity) containing the D_2O exchanged [Ch][Glu] and/or PEG 3350 or lysozyme 150 g/L to a final concentration of 1 mM. Likewise to assess the effect of protein lysate (described in IV. 2. 3.) on GB1 stability, I acquired exchange data in 150 g/L (90 mg of dry weight in 600 µL of 100% D_2O). All D_2O was pre-equilibrated at 37 ºC.

The time required between dissolving the sample and starting the acquisition of the spectrum was 57 s for GB1 + [Ch][Glu]; 1 min and 30 s for GB1 + [Ch][Glu] + PEG 3350; 1 min and 58 s for GB1 + PEG; 1 min and 46 s for GB1 + [Ch][Glu] + Lysozyme; 1 min and 31 s for GB1 + Lysozyme; and 1 min and 44 s for GB1 + Lysate.

For each experiment, a series of 52 - 55 ^{1}H-^{15}N HSQC (hsqcetfpf3gpsi2 pulse sequence) spectra were acquired at 600 MHz, 37 ºC with 2048 x 128 complex points, in a spectral window of 9615.385 Hz (centre at water) x 2311.077 (centre at 118 ppm), in ^{1}H and ^{15}N sweep's width, respectively. Consecutive spectra were collected with the increasing number of scans each t_1 increment - 8 (11 scans to GB1+[Ch][Glu]) with 1 scan (2 min and 46 s); 8 (5 scans to GB1+[Ch][Glu]) with 3 scans (5 min and 13 s); 6 with 4 scans (10 min and 6 s); 16 with 8 scans (19 min and 53 s); 11 with 16 scans (39 min and 27s); 1-4 with 32 scans (1h, 18 min and 34 s) – due to the loss of signal intensity and consequent decrease of the signal/ noise ratio.

Pielak and Monteith[182] have already provided the backbone amide exchange rates (k_{obs}, s^{-1}) data for WT GB1 in buffer (PBS, pH 7.6, 37 ºC) that were used for comparison purposes.

IV. 2. 5. Differential scanning calorimetry

Lysozyme and WT GB1 were used and Differential scanning calorimetry (DSC) data was recorded using a NanoDSC (*TA instruments*). The protein concentrations were previous determined by a NanoDrop (*2000, Thermo Scientific*).

Lysozyme. The freshly prepared lysozyme was dissolved in Milli-Q water in different conditions: 2.01 mg/mL lysozyme sample (final pH 7.28), in buffer (100 mM [Na][HPO_4], pH 7.25) and in buffer + PEG 3350 150 g/L (pH 7.23), 1.98 mg/mL lysozyme/[Ch][Glu] 100 mM sample (final pH 7.37) and 2.03 mg/mL lysozyme/[Ch][Glu] 100 mM/PEG 3350 150 g/L sample (final pH 7.31). A scan rate of 1.0 ºC/min, from 25 to 100 ºC with an equilibration period of 10 min was used with a constant cell pressure of 3 atm and 12 – 15 baselines (consecutive heating scans) were acquired before each experiment.

WT GB1. The freshly prepared WT GB1 was dissolved in Milli-Q water in different conditions: 1.94 mg/mL GB1 sample (pH 7.09), in buffer (100 mM [Na][HPO_4], pH 7.25) and in buffer + PEG 3350 150 g/L (pH 7.23), 1.93 mg/mL GB1/[Ch][Glu] 100 mM sample (final pH 7.23), 1.95 mg/mL GB1/[Ch][Glu] 100 mM/PEG3350 150 g/L sample (final pH 7.17) and protein lysate sample 23 g/L (in this case, the protein was 1.03 mg/mL ^{15}N labelled and pH around 6.8). A scan rate of 1.0 ºC/min, from 25 to 100 ºC with an equilibration period of 10 min was used with a constant cell pressure of 3 atm and 12 – 15 baselines (consecutive heating scans) were acquired before each experiment.

Samples for DSC analysis were degassed prior to any DSC measurement to avoid bubble formation during the temperature scan. Data were analysed using the NanoAnalyze software package with the NanoDSC. Sample scans were baseline corrected against buffer, concentration normalised, corrected with the progress baseline option, and fitted by nonlinear least squares analysis using a two-state scaled model option. The two-state scaled model adds the additional A_w variable, which is a scaling factor to compensate for errors in the assigned concentration. If the assigned concentration is accurate, then A_w will be close to 1 after fitting the model. If A_w is something significantly different than 1, then it can actually be used to empirically determine the "active" concentration of the sample by multiplying the assigned concentration by A_w. Using this new concentration value to reanalyse the data, the new A_w value will then be close to 1 after refitting the model.

IV. 3. Results and discussion

IV. 3. 1. Protein stability

Differential scanning calorimetry (DSC) enable to measure the excess heat capacity of protein unfolding as a function of temperature and directly calculate the calorimetric enthalpy of thermal unfolding in the IL and/or in the presence of a particular macromolecular crowder under study and through the corresponding melting temperatures associated.

The thermodynamics parameters (ΔH, ΔS and ΔG) for protein unfolding were estimated from the heat capacity changes upon protein unfolding. Since the unfolding transitions of proteins used in all solutions consisted of a single peak, it was used a two-state transition model which assumes

completely cooperative unfolding, *i.e.* $\Delta H_{exp}(T_m) \approx \Delta H_{vH}(T_m)$ at the transition temperature (T_m) the population of native and unfolded states is equal.[235,236] This means that Gibbs free energy difference between the native and unfolded states at T_m is equal to zero and $\Delta G(T_m) = \Delta H(T_m) - T_m \times \Delta S(T_m) = 0$. Thus the entropy change upon protein unfolding at the transition temperature, $\Delta S(T_m)$, is equal to:

$$\Delta S(T_m) = \frac{\Delta H(T_m)}{T_m}$$

(Equation IV.1)

A complete thermodynamic description of the system at any other temperature can then be calculated as follows:

$$\Delta G(T) = \Delta H(T_m) - T\frac{\Delta H(T_m)}{T_m} + \int_{T_m}^{T} \Delta C_p \, dT - \int_{T_m}^{T} \Delta C_p \, d \, lnT$$

(Equation IV.2)

Where the heat capacity change upon protein folding, ΔC_p is a function of temperature itself. Nevertheless, if no extrapolations over a wide temperature range are necessary, as a first approximation a temperature-independent ΔC_p is a reasonable assumption.[236]

In addition, based on the work of Monteith and Pielak,[182] if necessary, the free energy of denaturation can be extrapolated to 37 °C using **(Equation IV.3** from the work of Becktel and Schellman[235] and the value of ΔC_p from the work of Alexander *et al.*,[218] which corresponds to 25 kJ/ mol (37 ºC):

$$\Delta G = \Delta H - T\Delta S + \Delta C_p \left[T_m - T - T_m \ln(\frac{T_m}{T})\right]$$

(Equation IV.3)

Where T is any reference temperature (37 ºC) and ΔS and ΔH are the changes in partial molar entropy and enthalpy at that temperature, respectively. However, the protein stability comparisons in this section were based only in melting temperatures (T_m).

For proteins, the thermally induced process detected in calorimetry is the structural melting or unfolding during the transition from the native (folded) to the denatured (unfolded) conformation where the temperature of melting (T_m) is a decent indicator of thermal stability.

Essentially, two proteins lysozyme (cationic) and (WT) GB1 (anionic) with different pI were studied with [Ch][Glu] IL and PEG crowder:.

The first system (**lysozyme** - pI 11.3) with T_m 73.7 ºC at pH 7.20 (*ca.* 1 mg/ mL lysozyme in 0.1 M sodium phosphate buffer) reported by Weaver *et al.*,[118] was repeated and used as a reference. The effect of [Ch][Glu] and the influence of PEG crowder was studied by calorimetry. **Figure IV.7** shows the DSC plots obtained for lysozyme in buffer [Na][HPO_4] 100 mM, buffer with PEG3350 150 g/L, in [Ch][Glu] 100 mM and in [Ch][Glu] 100 mM with PEG3350 150 g/L .

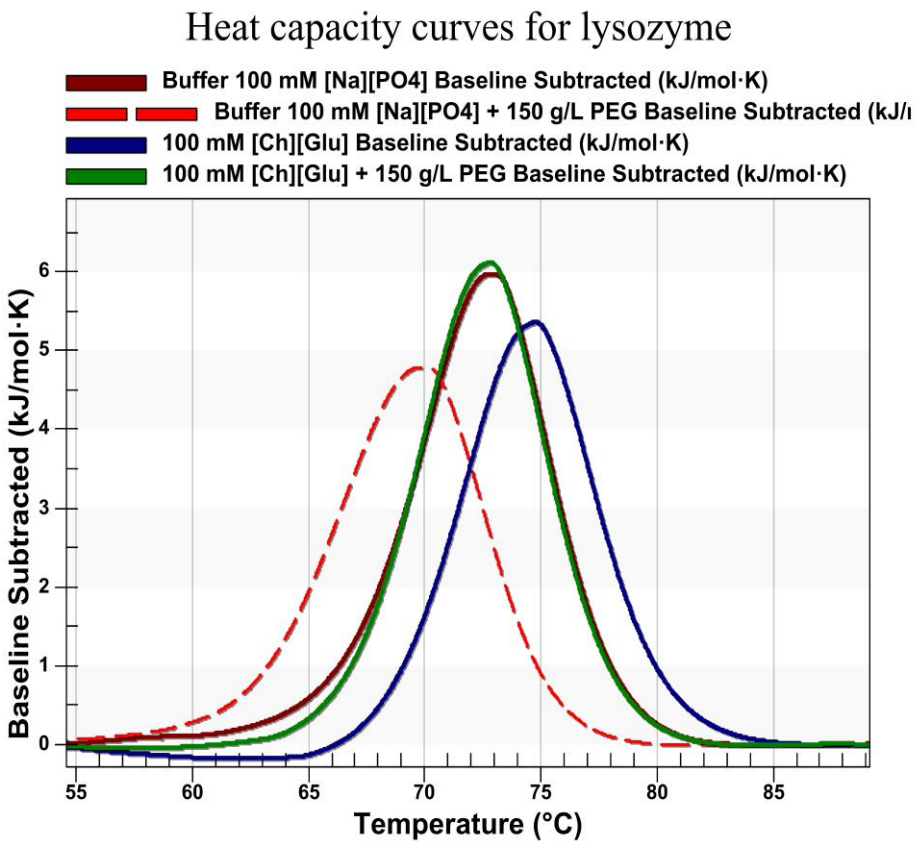

Figure IV.7. Baseline subtracted, heat capacity curves for lysozyme in [Ch][Glu] in dilute condition, IL crowded by PEG, in aqueous buffer and crowded by PEG, observed by DSC.

The best fitting for all data to yield T_m values was fitting to a two-scaled transition model (**Table IV.1**).

Table IV.1. Transition temperature T_m for the thermal denaturation of lysozyme determined by DSC under different conditions.

pH	Lysozyme solution [2.0 mg/ml]	T_m (ºC)
7.37	[Ch][Glu] 100 mM	**74.69 ± 0.04**
7.31	[Ch][Glu] 100 mM + PEG 3350 150 g/L	**72.74 ± 0.03**
7.25	Aqueous buffer ([Na][HPO_4] 100 mM)	**72.78 ± 0.03**
7.23	Aqueous buffer ([Na][HPO_4] 100 mM) + PEG 3350 150 g/L	**69.74 ± 0.03**
7.18	Water	**77.46 ± 0.09**

In **Table IV.1** the denaturing transitions tend to progressively shift towards lower temperatures following the order **water > [Ch][Glu]> aqueous buffer≥ [Ch][Glu] + PEG > aqueous buffer + PEG**. However the T_m value of lysozyme in water might be influenced by changes in the pH during the measurement. Blumlein and McManus[237] showed a decrease in lysozyme T_m as pH was

increased from pH 5 to pH 9, with constant ionic strength. According to Light[238] a temperature dependence of pure water pH exists and on so a pH water value of 7.18 at 25ºC can correspond to a pH of 6.5 at 77 ºC.

Therefore we have disregarded the T_m of lysozyme in water due the likely lower pH leading to increased protein stability and all values were compared to the buffer.

The highly positively charged lysozyme was slightly stabilised by 100 mM [Ch][Glu] (T_m increased 1.91 ºC) however in the presence of uncharged PEG 3350 a minimal destabilisation is observed (decreased 0.04 ºC). Therefore, the stabilising effect is certainly a consequence of the [Ch][Glu] and salt effects on the stability of lysozyme has been reported before. Blumlein and McManus[237] have reported the stability of lysozyme changes with increasing ionic strength from 0 to 1M [Na][HPO_4]. They observed at low salt concentrations (0-100 mM) the phosphate anions bind to the positive side chains and neutralize the charge, thus reducing repulsion. When the electrostatic binding has reached saturation point (> 500 mM), the polarizability of the anion determines its degree of interaction with hydrophobic binding sites. The melt transition temperature is expected to decrease initially as the phosphate anions are accumulated at the protein surface relative to the bulk water (decrease in T_m). As the positive charges on the lysozyme become neutralized, the phosphate anions accumulate preferentially in the bulk. Thus, the salting-out process becomes favoured with an accompanying increase in T_m. Likewise, based on lysozyme stability in [Ch][dhp] study by Weaver *et al.*,[118] they report the maximum effect for lysozyme thermal stability (increase in T_m by 15.1 ºC) was observed ~2 M [Ch][dhp] at pH 7.2, and considered as intermediate between [Ch][Cl] and [Na][H_2PO_4] at the same concentration and at similar pH conditions ($[Ch]^+$ was slightly destabilizing cation and [dhp] was highly stabilizing anion). In addition, they report that at low concentrations, [Ch][dhp] should be considered as an osmolyte similar in effect as other water-soluble compounds known to protect against protein denaturation, including sugars and salts and other naturally occurring osmolytes.[126,239] Despite the high concentrations, Kar *et al.*,[240] have demonstrated that 2.0 M hydroxyproline osmolyte at pH 4.5 can act as a stabilizer of lysozyme by increasing the transition temperature approximately 26.4 ºC. Also, trehalose osmolyte at the same concentration level has been reported to increase the T_m of lysozyme by over 10.6 ºC at pH 4.0.[241,242] Similar levels of thermal stabilization have been observed for lysozyme in the presences of carboxylic acid salts,[243] protic ILs[98] ethylammonium formate IL[122] among others.[92,101,141] Likewise said in Chapter I, these authors explained the protein stability increase results from the formation of a layer of water around the protein in which osmolyte is excluded.

Thus, the stability order of lysozyme in the different conditions (**Table IV.1**), **[Ch][Glu]> aqueous buffer≥ [Ch][Glu] + PEG > aqueous buffer + PEG** suggest that the electrostatics interactions of solvated [Ch][Glu] with the lysozyme, in the absence of PEG, are so weak that the overall T_m reflect a non-interacting tendency of choline and glutamate ions with protein residues.

Conversely, as observed in chapter III, the ion pairing observed in the IL is slightly promoted by the presence of PEG in which the protein is destabilised by 1.95 ºC when compared to the IL per se. Synthetic polymers tend to act as inert spheres and to stabilize proteins by hard-core interactions, however this effects seems abolished by weak protein-IL interactions. In addition, the lysozyme destabilisation observation in crowding condition without IL (by 3 ºC) reveals unspecific destabilising interactions by PEG and reinforces the idea of IL stabilising effect. Since the ion pair association is mediated by electrostatic and hydrogen-bonding interactions, the ion pair is more hydrophobic and less hydrated than the solvated ions in the absence of PEG. In uncharged PEG crowded environment, the higher level of ion pairing compared with dilute condition can be relevant to induce modifications of local hydrophobic interactions. The ion pair can establish more hydrophobic interactions with lysozyme disrupting the hydration layer with subsequent destabilisation and conformational alteration.

The second system studied was **GB1** (anionic at physiological pH, pI 4.8) in order to understand the influence of global charge surface of proteins. Gronenborg *et al.*[203] and Alexander *et al.*[218] reported the highest thermal stability of GB1, T_m 87 ºC at pH 5.4 in 50 mM sodium acetate. At physiological pH, Monteith and Pielak[182] reported a T_m of 79.0 ºC at pH 7.6 (8.5 mM Na_2HPO_4, 1.8 mM NaH_2PO_4, 150 mM NaCl).

As before, the stability of GB1 was evaluated by DSC (**Figure IV.8**) under the same experiental conditions reported for lysozyme, *i.e.*: in water, in aqueous buffer, crowded by PEG, in the presence of [Ch][Glu] and with [Ch][Glu]/PEG.

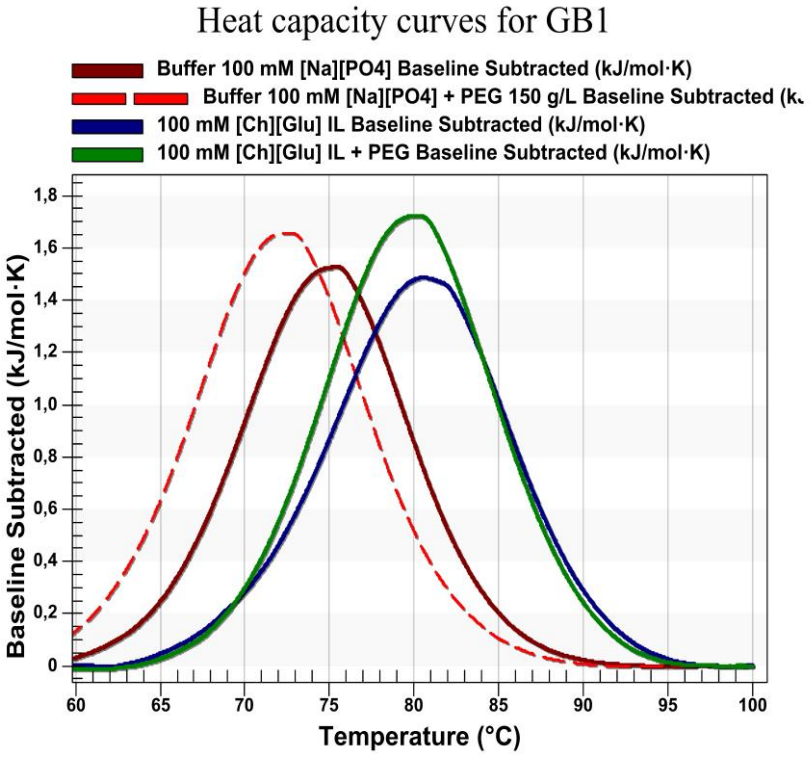

Figure IV.8. Baseline subtracted, heat capacity curves for WT GB1 in [Ch][Glu] in dilute condition, IL crowded by PEG, in aqueous buffer crowded by PEG, observed by DSC.

Due to the high thermal stability of GB1 protein it is difficult to acquire adequate baselines for rigorous fitting. Nevertheless, the two state scaled transition model was applied as in lysozyme leading to a higher uncertainty on T_m values as seen on **Table IV.2**.

The stability of GB1 was also determined in the presence of *E. coli* lysate (23 g/L) as shown in **Figure IV.9**.

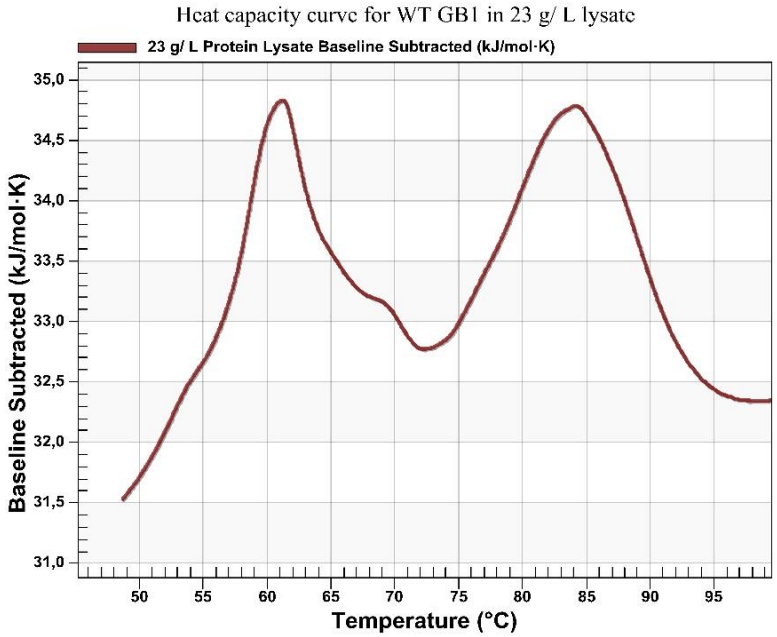

Figure IV.9. Baseline subtracted, heat capacity curves for WT GB1 in *E. coli* lysate condition observed by DSC.

As seen on **Figure IV.9** the DSC profile in the *E. coli* lysate shows two thermodynamics transitions: one around 61 ºC and another around 84 ºC. An explanation for these two transitions may be due to the intracellular *E. coli* environment. Interestingly, in terms of charged proteins, GB1 is similar to that of the majority of *E. coli* proteins at intracellular pH of 7.2[189] (anionic proteins with average pI of 5.5) as exposed in **Figure IV.10**, found in lysate.[231]

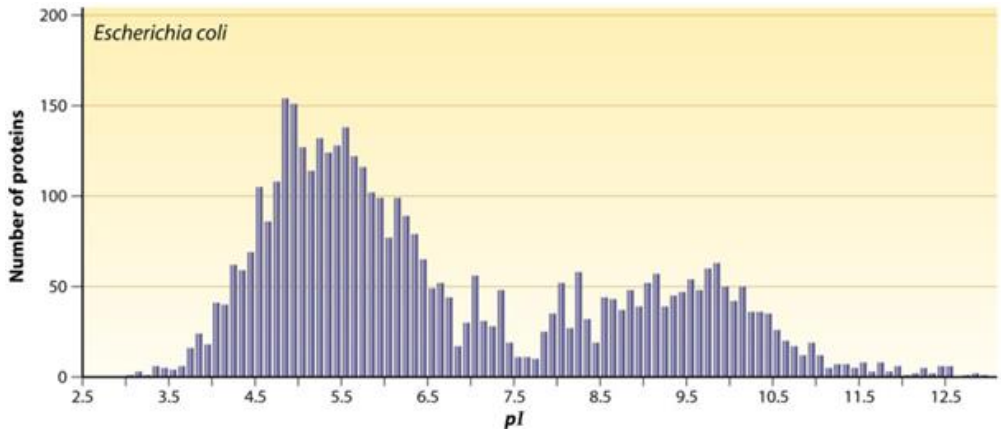

Figure IV.10. Distribution of protein abundance in Escherichia coli as a function of the predicted isoelectric point (pI).
Adapted from Spitzer and Poolman.[231]

Therefore, in the DSC experiment the transition on 61 ºC probably reflects the presence of other proteins. Thus, the two state scaled model transition was applied only in the second transition (**Table IV.2**).

Table IV.2. Transition temperature T_m for the thermal denaturation of WT GB1 determined by DSC under different conditions.

pH	GB1 solution [1.9 mg/mL]	T_m (ºC)
7.23	[Ch][Glu] 100 mM	**80.7 ± 0.2**
7.17	[Ch][Glu] 100 mM + PEG 3350 150 g/L	**80.0 ± 0.1**
7.25	Aqueous buffer ([Na][HPO_4] 100 mM)	**75.1 ± 0.2**
7.23	Aqueous buffer ([Na][HPO_4] 100 mM) + PEG 3350 150 g/L	**72.4 ± 0.1**
6.80	*E. coli* lysate 23 g/L [a]	**84.4 ± 0.2**
7.09	Water	**87.2 ± 0.4**

[a] The protein concentration in lysate case was 1.0 mg/mL GB1 ^{15}N-labelled.

As seen in **Table IV.2**, the denaturing transitions shift towards lower temperatures following the order: **water > *E. Coli* lysate > [Ch][Glu] > [Ch][Glu] + PEG > aqueous buffer > aqueous buffer + PEG**. As explained before for lysozyme pH differences due to temperature effects may affect the T_m values of GB1 in water - in reality the water pH can be 6.33 at 87 ºC.[238] On the other hand, in the *E. coli* lysate T_m may be overestimated once the solution pH was around 6.80.

Relevant to the interpretation of the DSC data are the observations of Lindman *et al.* [233] that have monitored the GB1 protein folding equilibrium as a function of temperature at pH values ranging from 1.5 to 11 at three different NaCl salt concentrations: no-salt, 0.15 M (considered as physiological), and 2 M. At no-salt and physiological salt GB1 is most stable at pH 4.5 close to isoelectric point 4.8, while at high salt the stability is less sensitive to pH variations around the pI. In detail GB1 at low pH and high salt concentration is stabilized and no effect is seen at physiological salt concentration. Therefore the T_m values obtained for the lysate and in water might be affected by the differences between the measured and the real (lower) pH value.

According to the T_m values, **Table IV.2**, the addition of [Ch][Glu] stabilised the negatively charged GB1 by 5.6 ºC when compared to buffer. On the other hand, the subsequent addition of PEG leads to a slight destabilisation (T_m decreased 0.7 ºC), however GB1 remains more stable than in buffer (T_m is still 4.9 ºC above). In spite of the opposite global charge of the protein, the results are similar to the ones obtained for lysozyme. The same explanation used for the lysozyme system, concerning the non-interacting tendency of the [Ch][Glu] ions in the aqueous sample, with the protein surface, and the higher occurrence of ion/pairing in the presence of PEG can be used to justify this trend. The fact

that lysozyme is more destabilized by the ion pair than GB1 suggests that there are more hydrophobic interactions in lysozyme than in GB1. Overall, the combined data suggests that the global charged surface of proteins is of little relevance in IL-protein interactions (under crowding). Once again, the crowding condition caused by PEG destabilises GB1 by 2.7 ºC, probably due to unspecific interactions and seems abolished by [Ch][Glu] IL.

Concerning the data obtained for the *E. coli* lysate, due to the existence of a large number of proteins with similar charge to GB1 charge–charge repulsions will occur as it happens in cells.[182,190] These repulsions allow GB1 to tumble freely in the cell and are responsible for the high quality in-cell ^{15}N–^{1}H HSQC spectra.[189,225] These repulsive interactions enhance the volume excluded by hard-core interactions in our lysate, thus favouring the compact native state and resulting in the observed stabilization by 9.3 ºC (compared to aqueous buffer). Nonetheless, care should be taken, since the lysate used was 23 g/L instead of the usual 150 g/L, and an increase in concentration might produce other type of interactions. Accordingly, weak, transient, and nonspecific attractive interactions with GB1 and the cell lysate will lead to destabilisation. This was reported by Sarkar *et al.*[181] with protein chymotrypsin inhibitor 2 (CI2), with similar pI to GB1, where the anionic protein lysate was nearly as destabilizing as the total protein lysate. In spite of the intuitive fact that anionic proteins will repulse negatively charged CI2, favouring the compact native state over the ensemble of larger unfolded states, increasing stability, even anionic proteins, which have the same net charge as CI2, can interact strongly enough with the backbone by nonspecific attractive interactions overcoming both charge - charge and steric repulsions and leading to an overall destabilization.

IV. 3. 2. Protein structural studies

The degree of structural perturbation of GB1 by [Ch][Glu], [Ch][Cl], [C_4mim][Cl], [C_4mim][dca] and different crowders (PEG, BSA and lysozyme) was studied by ^{1}H-^{15}N HSQC chemical shift perturbation experiments.

The ^{1}H-^{15}N HSQC spectrum of native GB1 in water is well-dispersed, as seen in **Figure IV.11** (the same experiment was done at 25 ºC and 37 ºC, the comparison data is available as **Appendix C, Fig. C. 5**). The assignments displayed in **Figure IV.11** are from Gronenborn *et al.*[203] and provide an easy way to follow structural perturbations.

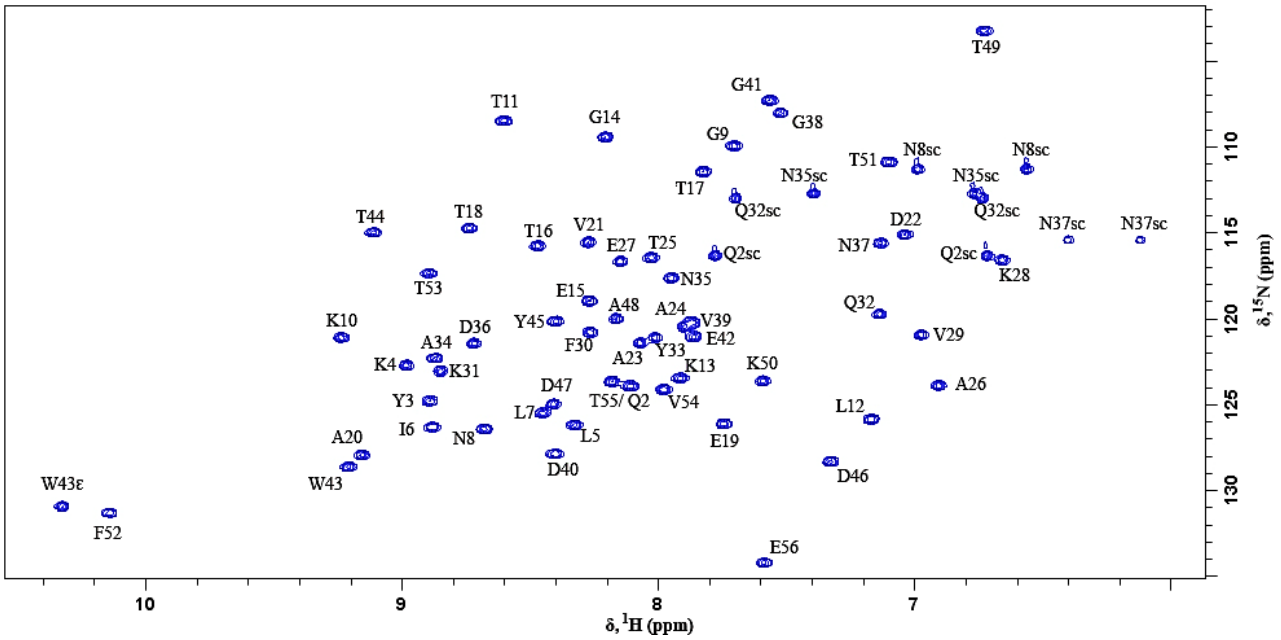

Figure IV.11. ^{1}H-^{15}N spectrum of GB1 in 90% H_2O/ 10% $^{2}H_2O$ (pH 7.13) at 5 ºC. Assignments are based on published work.[203]

Figure IV.12, **Figure IV.13**, **Figure IV.14** and **Figure IV.15** show representative spectra of the titrations. The complete set of ^{1}H-^{15}N HSQC spectra and some significant overlays are available as **Appendix C, Figure C.16 – Figure C.19**, and the total summary of perturbed residues are presented in **Table IV.3**.

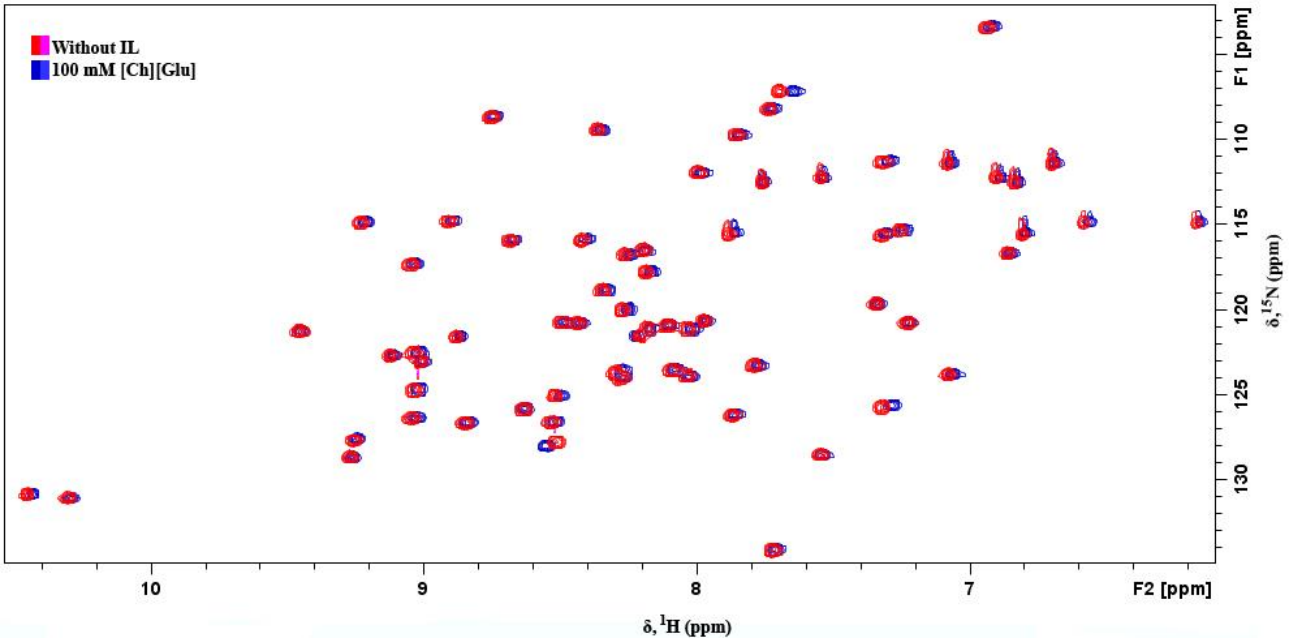

Figure IV.12. Superposition of the ^{1}H-^{15}N-HSQC spectra of 1 mM GB1 without IL (red) and GB1 with 100 mM [Ch][Glu] (blue), both in 90% H_2O/ 10% $^{2}H_2O$ at 25 ºC.

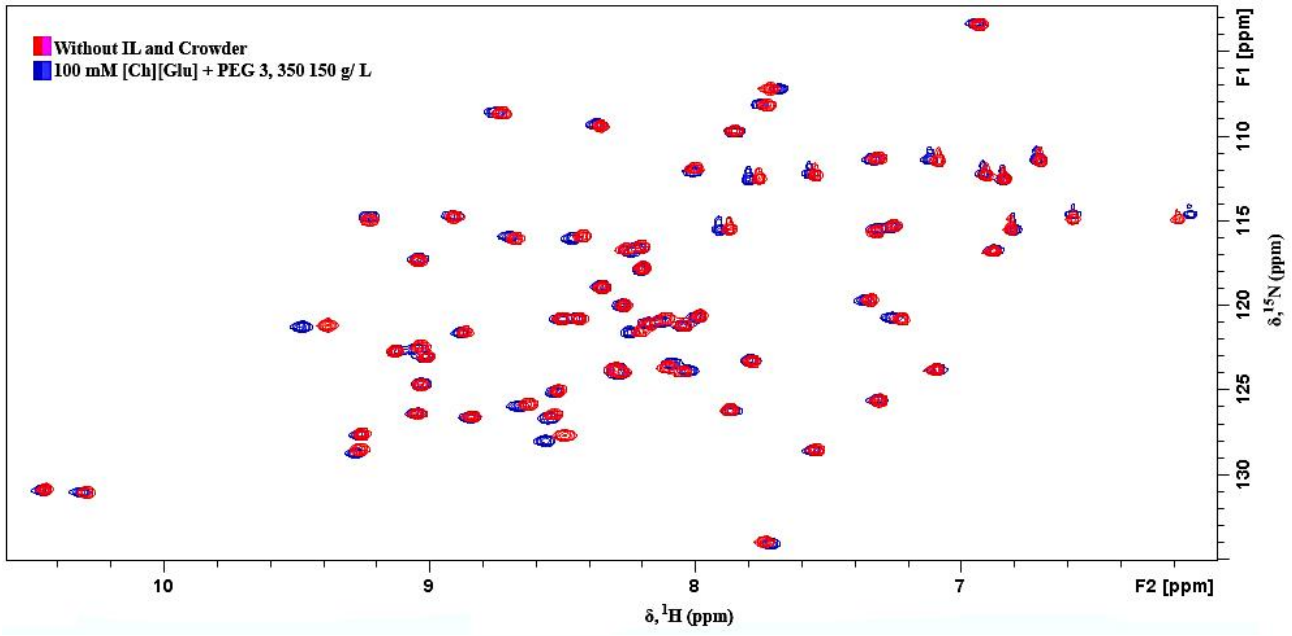

Figure IV.13. Superposition of the ^{1}H-^{15}N-HSQC spectra of 1 mM GB1 without IL and crowder (red) and GB1 with 100 mM [Ch][Glu] + 150 g/L PEG 3350 (blue), both in 90% H_2O/ 10% $^{2}H_2O$ at 25 ºC.

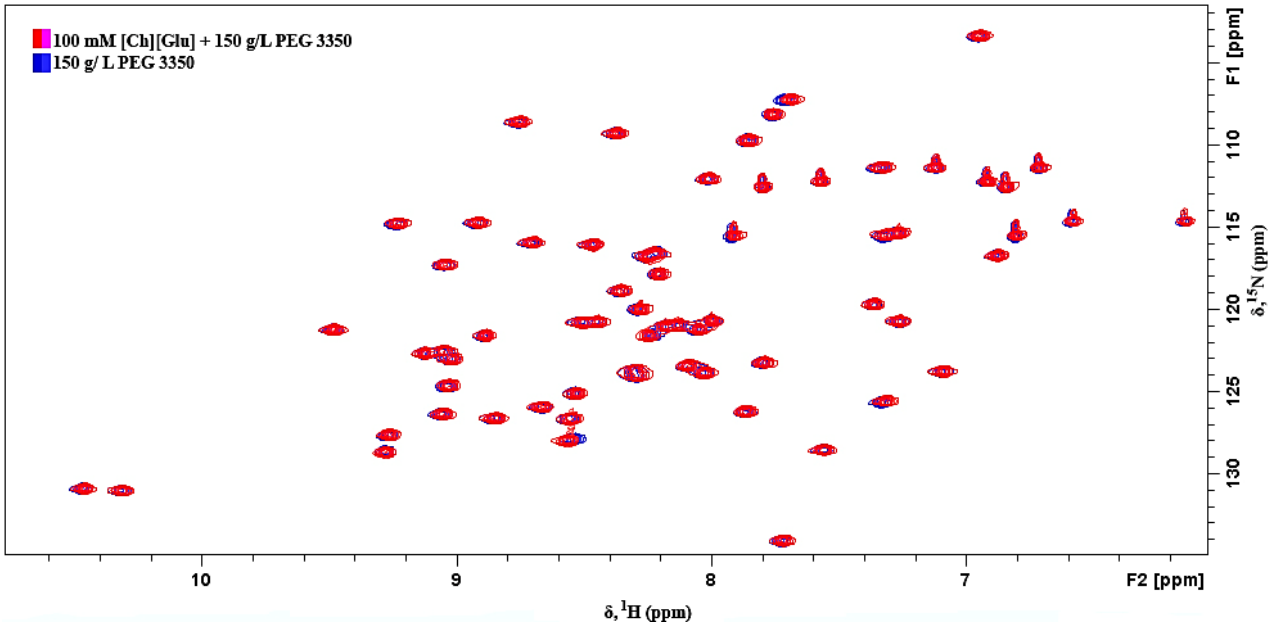

Figure IV.14. Superposition of the ^{1}H-^{15}N-HSQC spectra of 1 mM GB1 with 100 mM [Ch][Glu] + 150 g/L PEG 3350 (red) and GB1 with crowder (blue), both in 90% H_2O/ 10% $^{2}H_2O$ at 25 ºC.

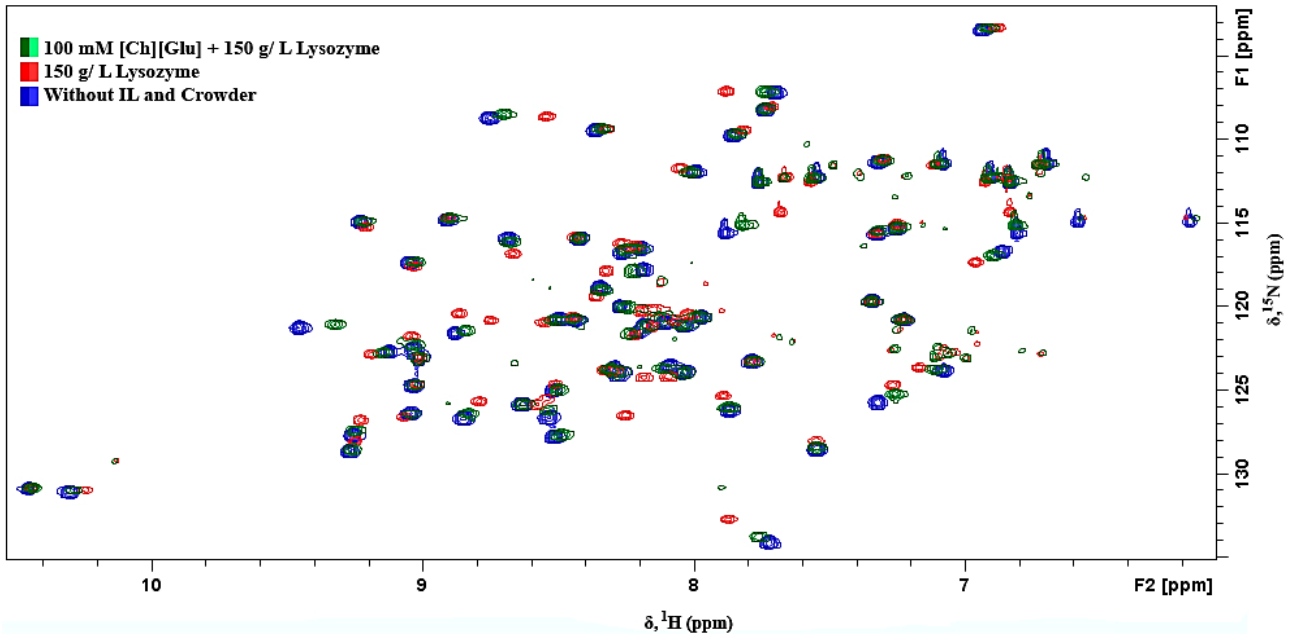

Figure IV.15. Superposition of the ^{1}H-^{15}N-HSQC spectra of 1 mM GB1 with 100 mM [Ch][Glu] + 150 g/L lysozyme (green), GB1 with crowder (red) and GB1 without crowder and IL (blue), all in 90% H_2O/ 10% $^{2}H_2O$ at 25 ºC.

The background noise (weak signals represented as green and red) belongs only the lysozyme due the high concentration used (150 g/L). The blank experiment was performed and is available as **Appendix C, Figure C.20**.

Table IV.3. Perturbed residues observed for GB1 for the different solutions studied.

GB1 solution	**More perturbed residues**	**Charged residues number** [a,b]	**Hydrophobic residues number** [e]	**Polar residues number** [c]
100 mM [Ch][Cl]	L12[e], D40[b], G41[d],	1	1	NA[f]
100 mM [C_4mim][Cl]	L5[e], L7[e], T16[c], T25[c], E27[b], V29[e], Q32[c], N35[c], N37sc[c], D40[b]	2	3	4
100 mM [C_4mim][dca]	(increase chemical shift perturbation) L5[e], L7[e], T16[c], T17[c], T25[c], E27[b], V29[e], Q32[c], N35[c], N37sc[c], D40[b]	2	3	5
100 mM [Ch][Glu]	L12[e], D40b, G41d	1	1	NA
150 g/L PEG 3350	Q2sc[c], K10[a], V21[e], V29[e], Q32[c], Q32sc[c], N37sc[c], D40[b]	2	2	1
100 mM [Ch][Glu] + 150 g/L PEG 3350	Q2sc[c], K10[a], L12[e], V21[e], A23[e], V29[e], Q32[c], Q32sc[c], N37sc[c], D40[b], G41[d] (L12[e], D40[b], G41[d], compared with 150 g/L PEG)	2 (1)	3 (1)	1 (NA)
200 mM [Ch][Glu] + 150 g/L PEG 3350	L12[e], A23[e] (compared with 100 mM IL+PEG)	(NA)	(2)	ND

150 g/L BSA	D40[b], G41[d]	1	NA	NA
100 mM [Ch][Glu] + 150 g/L BSA	Q2sc[c], L12[e], D40[b], G41[d]	1	1	NA
150 g/ L Lysozyme	High chemical shift perturbations in almost all residues. L5[e], K10[a], T11[c], D40[b], G41[d], E56[b]	3	1	1
100 mM [Ch][Glu] + 150 g/L lysozyme	Chemical shift of almost all residues return to no-added solution. Q2sc[c], K8[a], K10[a], T11[c], L12[e], A26[e], N35[c], G41[d]	2	2	2

[a] Amino acids (AA) with positively charged side chain (acidic); [b] AA with negatively charged side chain (basic); [c] AA with polar uncharged side chain; [d] Special cases; [e] AA with hydrophobic side chains (non-polar). [f] NA: not applicable. The NH of side chain was counted as perturbed residue but not for number quantification.

In terms of electrostatic interactions is important to understand which residues are charged in GB1. Based on reports of Khare *et al.*[244] and Tomlinson *et al.*,[245]in physiological pH, the five Glutamates (E) and the five Aspartates (D) are all deprotonated with a pK_a range from 2.70 to 4.56, where the Glu27 and Glu42 have a pK_a of about 4.5, while the c-terminus carboxylate and Glu15 also have pK_a values near 4.5, and the other six Glu/Asp have pK_a values ranging from 4 down to 2.7. The six (K) lysines are all protonated with a pK_a range from 10.5 to 11.5. Yet Tomlinson *et al.*[245] admits salt bridges between E15-K4, E37-K31 and D47-K50.

Based on **Table IV.3**, the imidazolium-based ILs ([C_4mim][Cl] and [C_4mim][dca]) revealed that the number of perturbed residues is low: only 9-10 residues are found to be perturbed and none of them are positively charged, however Asp40 e Glu27 will be negatively charged at pH 7 and likely provide an electrostatic contribution to the cation binding. The 4-5 polar uncharged residues suffer perturbations probably by the combination of polarity and solvent accessibility and the 3 hydrophobic residues (Val29, Leu5 and Leu7) by interactions with the alkyl chain of the cation. Significantly, the hydrophobic residues are more affected in [C_4mim][dca] than in [C_4mim][Cl] (see **Appendix C, Figure C.7 and Figure C.8**) in accordance with the existence of a stronger hydrophobic ion-pair in [C_4mim][dca]. These results are consistent with the anionic proteins-ILs interactions in our previous studies.[107,108]

The choline-based ILs ([Ch][Cl] and [Ch][Glu]) shown only 3 perturbed residues: Gly41, Asp40 (negatively charged) and Leu12 (hydrophobic). Leu12 is more perturbed by [Ch][Glu] (**Figure IV.12**) probably due to the prevalence of ion pairs in [Ch][Glu] when compared to [Ch][Cl].

The presence of the synthetic crowder PEG3350 is expected to induce steric repulsions that stabilise the GB1, however destabilising effect was observed by DSC, probably due to unspecific interactions. The ^{1}H-^{15}N HSQC spectra revealed that almost all residues suffer a slight perturbation. The most perturbed residues are 2 charged (Lys10 and Asp40), 2 hydrophobic (Val21 and Val29) and

1 polar uncharged (Gln) which indicate that interactions are mediated by the solvent accessibility via steric repulsions since PEG is uncharged. However, when [Ch][Glu] is added (**Figure IV.13**, **Figure IV.14**), only Asp40, Gly41 and Leu12 are perturbed as observed in the absence of crowder. As before the occurrence of ion pairing in crowding conditions should be responsible by hydrophobic interactions. This is confirmed by increasing [Ch][Glu] concentration under crowded environment with reflection in Leu12 and Ala23 perturbation (**see Appendix C, Figure C.13**), both hydrophobic. Accordingly with the DSC results, these hydrophobic interactions with the ion-pair suggest the disrupting of the protein hydration layer, leading to destabilisation. Nonetheless, the crowder alone seems more destabilising than when adding IL.

BSA as crowder does not perturb the GB1 residues with the exception of Asp40 and the structurally adjacent, Gly41. The Asp40 is exceptionally sensible to the microenvironment changes.

When 100 mM [Ch][Glu] is added, a few residues display a small chemical shift perturbation (**Appendix C, Figure C.16**). The most affected residues are: Leu12, Asp40, Gly41 and Q2-side chain, practically the same residues which are affected in other experiments as dilute condition and PEG crowding. Since I know *a priori* that the ion pair in the presence of BSA crowding is more dominant than in dilute condition, the hydrophobic ion pair - GB1 interaction can be reinforced by soft interactions with crowder, disrupting the hydration layer with greater strength (in comparison with PEG crowding).

In the presence of the cationic protein crowder lysozyme, almost all residues have a high chemical shift perturbation (**Figure IV.15**). Lys10, Thr11, Asp40, Gly41 and Glu56 are the most affected residues. Unpredictably, the [Ch][Glu] in this crowding environment cancels the lysozyme effects in GB1 and the chemical shift return to be as they were in dilute condition. This suggests that the ion pair mitigates the crowder effect.

NMR chemical shifts are highly sensitive, empirical indicators of the chemical environment of the nucleus being studied. Therefore, changes in this environment induced by binding or alteration in protein structure can result in significant chemical shift changes and even crosspeak disappearance due to severe line-broadening. In addition, NMR-detected amide $^{1}H/^{2}H$ exchange is the only technique that provides equilibrium stability data for proteins on a per-residue basis under crowded conditions. When coupled with *in vitro* experiments using macromolecular crowding agents, valuable information about the combination of excluded volume effects and nonspecific interactions can be obtained.

Thus, for a complete report, NMR-detected amide $^{1}H/^{2}H$ exchange experiments were done in order to obtain quantitative information about solvent accessibility and to access how ion and/ or crowders interact with polypeptide backbone affecting protein stability. However, the data are still being treated. Only the ^{1}H-^{15}N HSQC spectra at different times are displayed as **Appendix C, Figure C.21 – Figure C.26.**

IV. 3. 3. Protein diffusion

As discussed in Chapter II, the self-diffusion coefficients and the structural properties of a molecule are connected by the dependence of the self-diffusion coefficients on molecular size and shape. Despite increased attention, little is known about how the crowded intracellular environment affects basic phenomena like protein diffusion.[246,247] The theory relating crowding to NMR studies of protein diffusion has been reviewed by Bernado *et al*.[248]

The size of the crowding molecule is important. Li *et al.*[249] reported that the same weight concentration of synthetic 40 kDa polyvinyl pyrrolidone (PVP) slows rotational and translational types of diffusion more than 10 kDa PVP. The data for the 1:1 mixture of 10 and 40 kDa PVP show that the larger polymer dominates the negative deviation than is expected by the Stokes-Einstein law ($\boldsymbol{D=k_BT/(6\pi\eta r_H)}$), where *D* is diffusion, η is viscosity, k is the Boltzmann constant, T is temperature, and r_H is the protein's radius). These observations agree with results from studies using synthetic polymers with fluorescence detection[247,250] showing that NMR is a useful tool. In addition, Wang *et al.*[179] demonstrated that the effects of macromolecular crowding on collisional frequency are harder to rationalize because synthetic polymers and globular proteins have opposite effects on translational diffusion. Whereas synthetic polymers slow diffusion less than is expected by the Stokes-Einstein law, globular proteins can have a larger than expected effect.

Here, I use the DOSY technique to quantify translational diffusion of a 6.22 kDa globular protein, GB1, as a function of crowder concentration in the presence of [Ch][Glu] IL. The crowders studied were PEG 3350, lysozyme and *E. coli* lysate. Some relevant data concerning the size of the mixture components is displayed in **Table IV.4**.

Table IV.4. Properties of GB1 and crowders.

Molecule	MW, kDa	pI	Charge at pH 7.20
GB1	6.22 (6.29 ^{15}N labelled)	4.80	Anionic
PEG 3350	3.35	NA[a]	Neutral
Lysozyme	14.31	11.35	Cationic

[a] NA: not applicable

- **Diffusion of GB1 in the presence of crowders**

The DOSY spectra obtained for GB1 in different environments are displayed in **Figure IV.16** and the calculated diffusion coefficients are presented in **Table IV.5.**

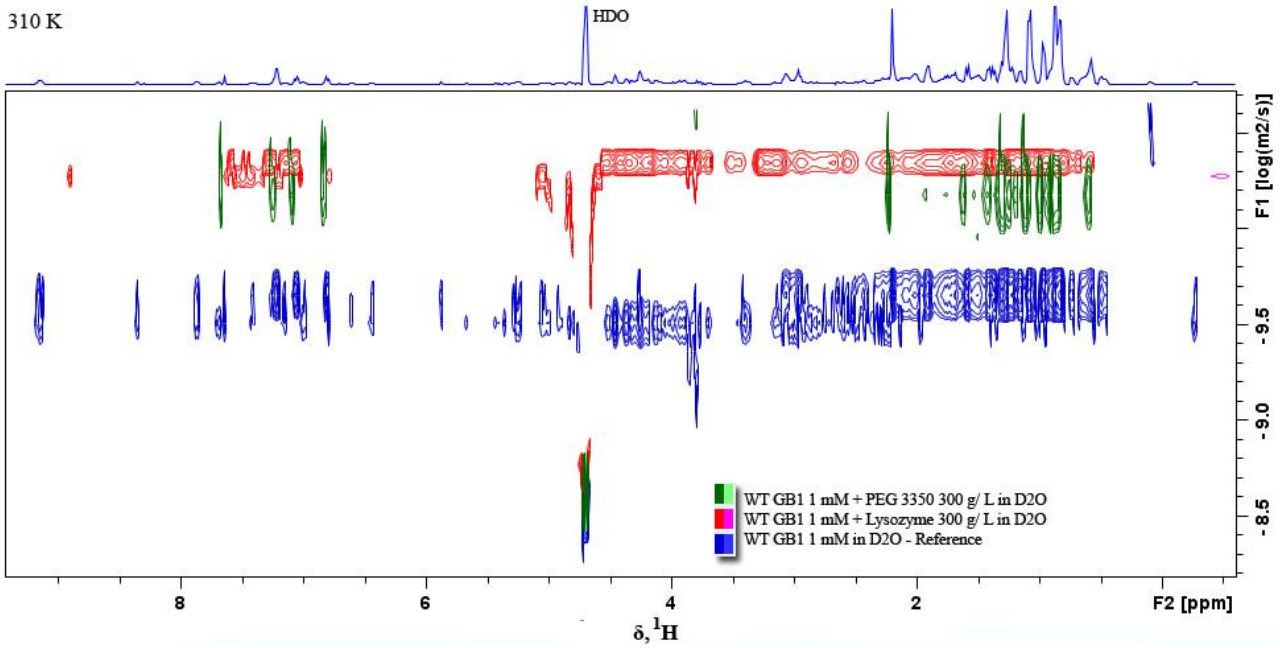

Figure IV.16. Superposition of ^{1}H-DOSY plots of 1 mM GB1 with 300 g/L PEG 3350 (green), 1 mM GB1 with 300 g/L lysozyme (red) and 1 mM GB1 in dilute condition (blue), all in 99.9% $^{2}H_2O$ at 37 ºC.

A quantitative description of the apparent modifications in the protein hydrodynamic radius can then be made through the use of the Stokes–Einstein equation, and changes in hydrodynamic radii can be determined. From this equation, it follows that the ratio of the diffusion of a reference compound (D_{ref}) and particular protein (D) can be related to the inverse ratio of the corresponding hydrodynamic radii (r_H/r_{Href}).[251] Using the diffusion coefficient of HDO as internal diffusion reference, the corrected diffusion value, D_{HDO}/D was determined, corresponding to the ratio of the hydrodynamic radii, r_H/r_{HDO}. In this way, and taking into consideration a static water hydrodynamic radius (r_{HDO}), any changes in this ratio may be attributed to the modifications in the hydrodynamic radius of the protein in study. The direct comparison of values among solutions after the addition of a co-solute (IL) (D'_{HDO}/D'_H=, $r'_H/'r_{HDO}$) is then possible by $\mathbf{Rr_H=r'_H/r_H}$.

The ratios of hydrodynamic radius (Rr_H) for GB1 in different environments are presented in **Table IV.5** and **Table IV.6** (for E. coli lysate), and plotted in function of crowder in **Figure IV.17.**

The ^{1}H-DOSY plot for protein lysate and significant superposition of spectra are displayed in **Appendix C, Figure C.29 and Figure C.30.**

Table IV.5. Diffusion coefficients and hydrodynamic radius of 1 mM GB1 in different environments in 99.9% $^{2}H_2O$ at 37 ºC as extracted from ^{1}H- DOSY plots.

	PEG 3350 (3.35 kDa, uncharged)			**Lysozyme (14.31 kDa, cationic)**		
Crowder (g/L)	Diffusion Coefficients (D) (10^{-10} m^2 s^{-1})		Hydrodynamic radius ratio ($D_{HDO}/D_{protein}$)	Diffusion Coefficients (D) (10^{-10} m^2 s^{-1})		Hydrodynamic radius ratio ($D_{HDO}/D_{protein}$)
	GB1	**HDO**	**GB1**	**GB1**	**HDO**	**GB1**
0	1.78 ± 0.02 [a]	24.1 ± 0.5	13.6	1.73 ± 0.02	23.7 ± 0.5	13.7
50	1.19 ± 0.01	21.2 ± 0.4	17.8	1.14 ± 0.01	22.4 ± 0.4	19.6
100	0.850 ± 0.009	18.8 ± 0.4	22.1	1.00 ± 0.01	21.2 ± 0.4	21.1
150	0.680 ± 0.008	17.3 ± 0.3	25.5	0.85 ± 0.01	20.1 ± 0.4	23.7
300	0.302 ± 0.004	13.6 ± 0.3	45.1	0.426 ± 0.005	16.8 ± 0.3	39.3

[a] The standard deviation was obtained by fitting.

Table IV.6. Diffusion coefficients and hydrodynamic radius ratio of 1 mM GB1 in protein lysate (150 g/L) in 99.9% $^{2}H_2O$ at 37 ºC K as extracted from ^{1}H- DOSY plots.

	***E. coli* lysate (mainly anionic proteins)**		
Crowder (g/L)	Diffusion Coefficients (D) (10^{-10} m^2 s^{-1})		Hydrodynamic radius ratio ($D_{HDO}/D_{protein}$)
	GB1	**HDO**	**GB1**
150	1.16 ± 0.01 [a]	18.2 ± 0.4	15.7

[a] The standard deviation was obtained by fitting.

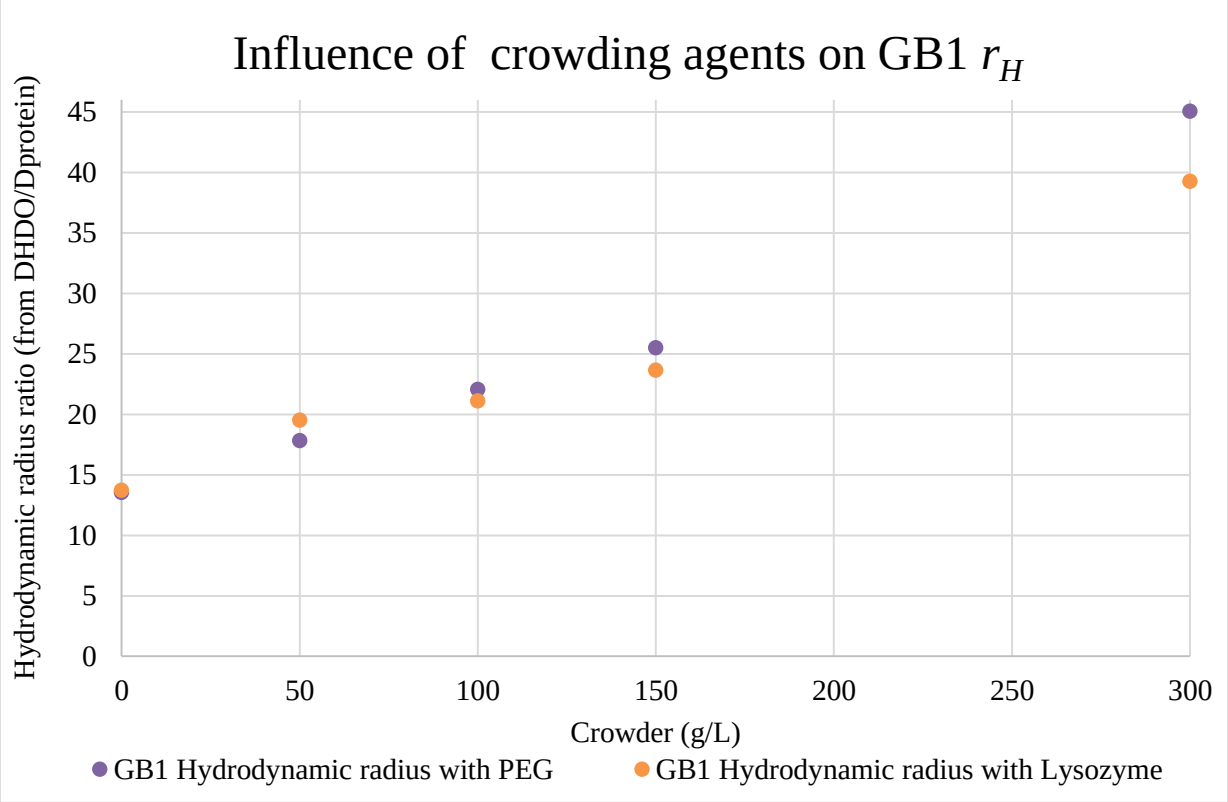

Figure IV.17. Ratio of hydrodynamic radius of GB1 in function of crowder concentration.

As expected due to the increase in the solution viscosity the translational diffusion of GB1 in the presence of the crowders PEG and Lysozyme was significantly slowed down by increasing concentrations of the crowder molecules when compared to its diffusion in dilute buffer (**Table IV.5**). However, the data may be further interpreted after the correction for the viscosity introduced by calculating the ratio $D_{HDO}/D_{protein}$ (**Figure IV.17**). As can be seen in **Figure IV.17** until 50 g/L of crowder, GB1 has a smaller hydrodynamic radius in PEG than in lysozyme, nonetheless from 100 to 300 g/L it is the opposite, GB1 has a larger apparent hydrodynamic radius in PEG.

The fact that until 50 g/L of crowder GB1 is acting as a smaller protein in PEG than in lysozyme solution is not unexpected due to weak, favourable and attractive interactions between anionic GB1 and cationic lysozyme, therefore the higher size in lysozyme suggests that GB1 interacts with lysozyme proteins at 50 g/L of crowder.

At ≥ 100 g/L of PEG, these polymers can overlap to form a mesh.[252] Furthermore, several reports point to attractive interaction between PEG and nonpolar or hydrophobic sidechains on proteins surface.[253] Thus the repulsive excluded volume contribution to PEG-protein interaction can be partially compensated to an unknown extent by an attractive interaction leading to an apparent higher hydrodynamic radius in high concentrated PEG solutions. On the other hand in 150 and 200 g/L lysozyme solution, the charge surface of lysozyme becomes irrelevant and this might justify the different behaviour when compared with PEG.

When considering the *E. coli* lysate (**Table IV.6**) it can be seen that GB1 behaves even as a smaller protein than in all the other studied crowded solutions. Probably, the proteins of lysate interact less strongly with GB1 (repulsive interactions).

For the same concentration of crowder, 150 g/L, the apparent molecular weights in PEG, lysozyme and *E. coli* lysate are 1.88, 1.72 and 1.16 times, respectively, higher than those calculated from GB1's amino acid sequence. These values show that diffusion in cell lysates is different from the crowded solutions.

Wang *et al.*[179] reported for CI2 in 200 g/L crowder solutions (BSA and lysozyme) that the apparent molecular weights are more than 7 times those calculated from C12. This indicates that in spite of having similar charge and size GB1 interacts less than C12 in lysozyme crowded environments. Interestingly, these authors also reported than CI2 protein acts like a smaller protein (2 times smaller) in solutions of PVP and Ficoll polymers (200 g/L). This fact is contrary to our results with PEG that shows an increase in size of GB1 compared to dilute solution. However, the PVP and Ficoll used have 40 and 70 kDa of Mw, respectively, while PEG used in this work has 3.35 kDa. The difference of size of the artificial crowder seems to be clearly relevant, the smallest can interact with proteins by soft interactions while bigger crowders should mediate only hard interactions.

The possible formation of dimers of GB1 to explain the values obtained experimentally for high crowder concentration is excluded because only at low pH[254] or by mutant variants of GB1,[255–257] the dimerization can occurs.

- **Diffusion of GB1 in the presence of crowders and [Ch][Glu]**

The ^{1}H-DOSY plots obtained for GB1 in the presence of [Ch][Glu] are displayed in **Figure IV.18** and **Figure IV.19**. The corresponding ratio of hydrodynamic radius for GB1 are presented in **Table IV.7**, and observed in function of crowder concentration in **Figure IV.20.** The influence of [Ch][Glu] IL in comparison with no-added IL is presented in **Figure IV.21** and **Figure IV.22.** Important ^{1}H-DOSY overlay is available in **Appendix C, Figure C.31.**

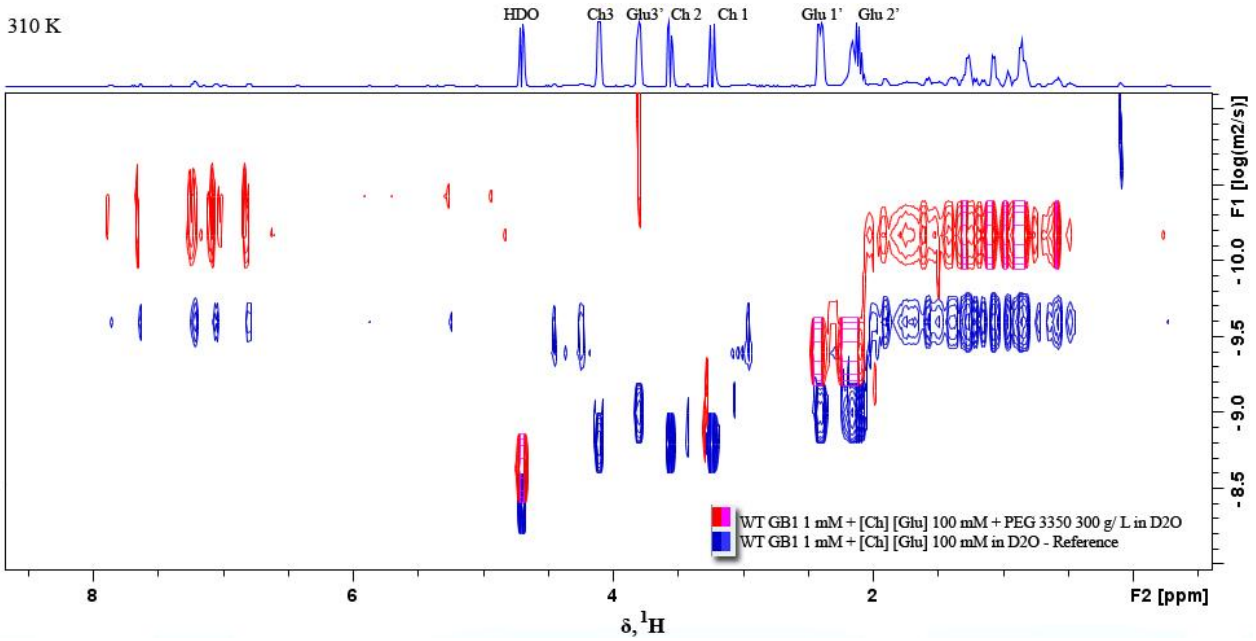

Figure IV.18. Superposition of ^{1}H-DOSY plots of 1 mM GB1 with 100 mM [Ch][Glu] crowded by 300 g/L PEG 3350 (red) and 1 mM GB1 with 100 mM [Ch][Glu] in dilute condition (blue), both in 99.9% $^{2}H_2O$ at 37 ^{o}C.

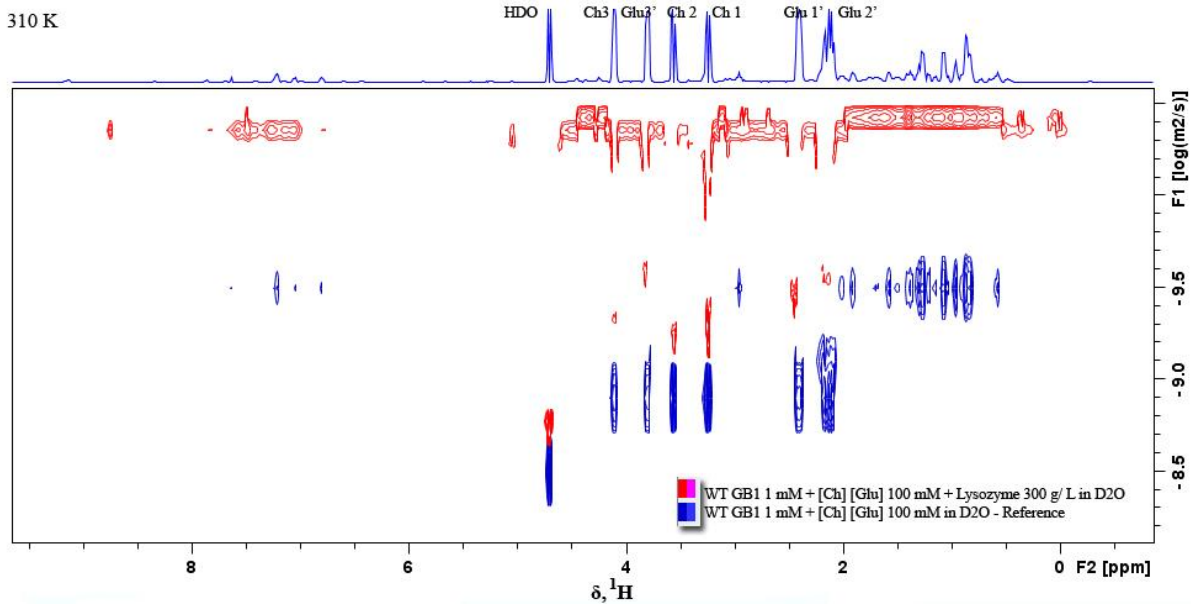

Figure IV.19. Superposition of ^{1}H-DOSY plots of 1 mM GB1 with 100 mM [Ch][Glu] crowded by 300 g/L Lysozyme (red) and 1 mM GB1 with 100 mM [Ch][Glu] in dilute condition (blue), both in 99.9% $^{2}H_2O$ at 37 ^{o}C.

Table IV.7. Diffusion coefficients and hydrodynamic radius of 1 mM GB1 with 100 mM [Ch][Glu] in different environments in 99.9% $^{2}H_2O$ at 37 ºC as extracted from ^{1}H- DOSY plots.

100 mM [Ch][Glu] IL

Crowder (g/ L)	PEG 3350 (3.35 kDa, uncharged)				Lysozyme (14.31 kDa, cationic)			
	Diffusion Coefficients (D) (10^{-10} m^2 s^{-1})		Hydrodynamic radius ratio ($D_{HDO}/D_{protein}$)	Rr_H	Diffusion Coefficients (D) (10^{-10} m^2 s^{-1})		Hydrodynamic radius ratio ($D_{HDO}/D_{protein}$)	Rr_H
	GB1	**HDO**	**GB1**	**GB1**	**GB1**	**HDO**	**GB1**	**GB1**
0	1.68 ± 0.03 [a]	22.8 ± 0.5	13.6	1.003	1.73 ± 0.02	22.9 ± 0.6	13.2	0.964
50	1.07 ± 0.02	19.8 ± 0.4	18.6	1.040	1.13 ± 0.02	21.4 ± 0.6	18.9	0.976
100	0.78 ± 0.01	18.2 ± 0.4	23.3	1.053	0.90 ± 0.01	20.3 ± 0.5	22.4	1.060
150	0.598 ± 0.009	16.8 ± 0.3	28.1	1.101	0.81 ± 0.01	19.1 ± 0.5	23.6	1.008
300	0.269 ± 0.004	12.8 ± 0.3	47.6	1.056	0.420 ± 0.006	15.8 ± 0.4	37.6	0.967

[a] The standard deviation was obtained by fitting.

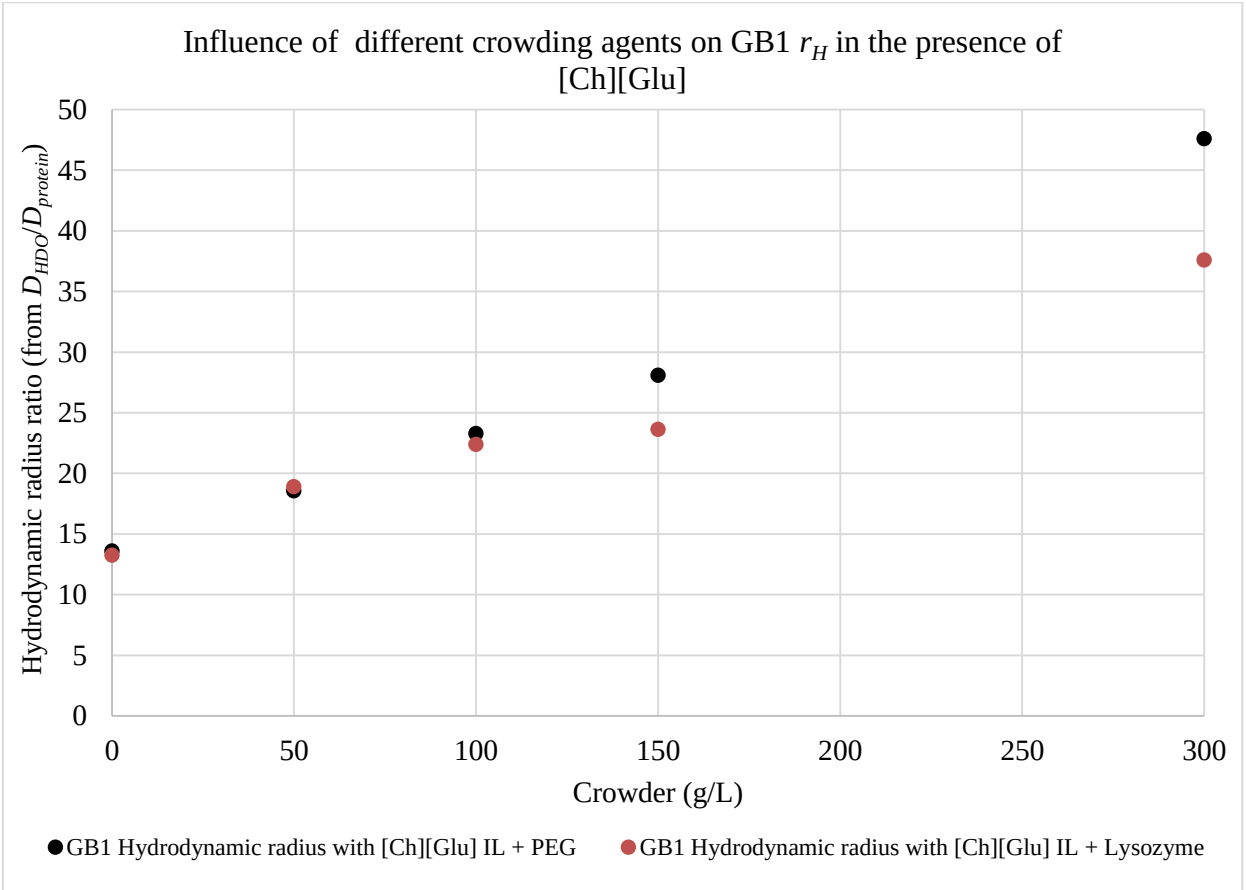

Figure IV.20. Ratio of hydrodynamic radius of GB1 as a function of crowder concentration in the presence of [Ch][Glu].

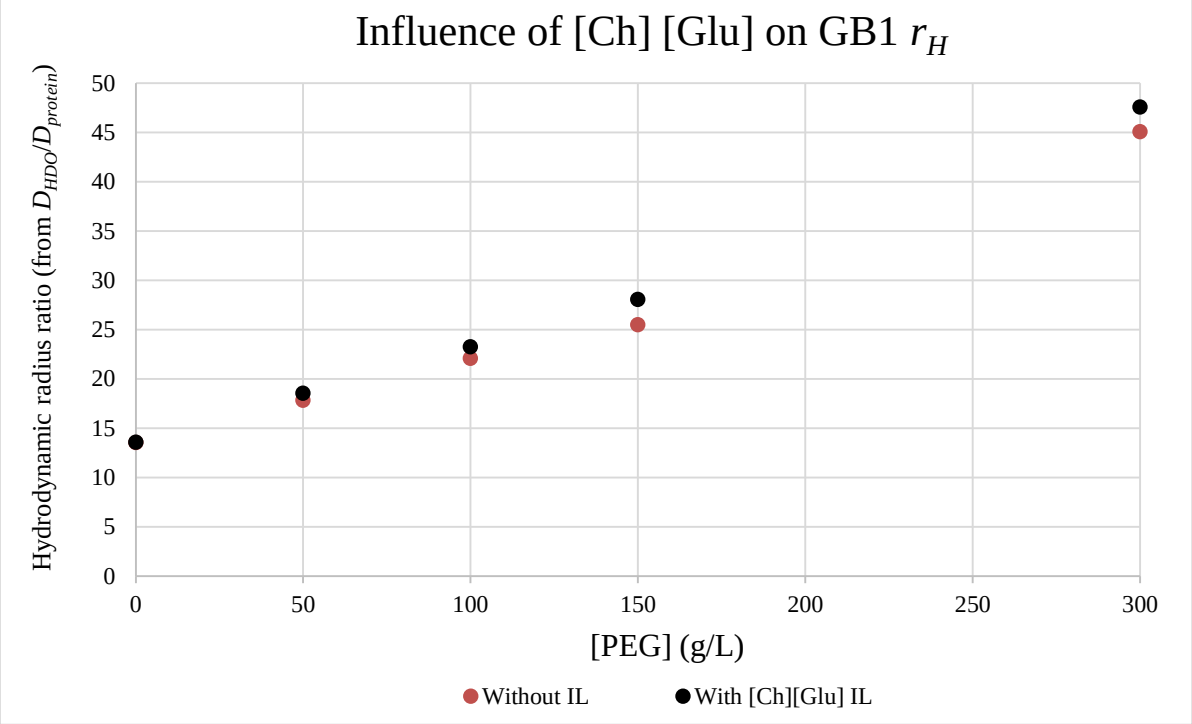

Figure IV.21. Ratio of hydrodynamic radius of GB1 as a function of PEG concentration in the presence of [Ch][Glu].

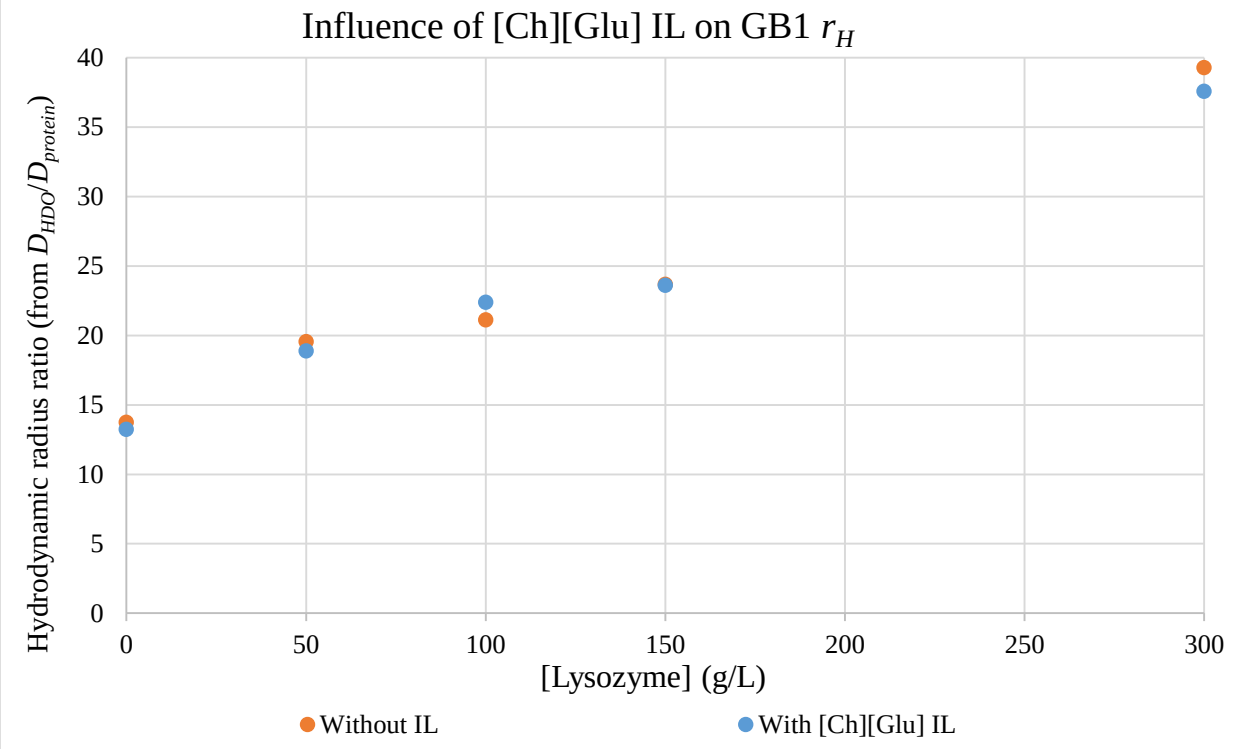

Figure IV.22. Ratio of hydrodynamic radius of GB1 as a function of lysozyme concentration in the presence of [Ch][Glu]..

In a similar way to the previous experiences without IL the translational diffusion of GB1 in PEG and lysozyme in the presence of [Ch][Glu] was significantly slowed down by increasing concentrations of the crowder when compared to its diffusion in dilute buffer, Table IV.7 and Figure

IV.20. However, the results concerning the hydrodynamic radius suggest a major effect of IL on GB1 under PEG crowding (Figure IV.21) than under lysozyme crowding (**Figure IV.22**), since GB1 had a significantly increase of size across the range of PEG studied.

On PEG crowding, the increase of GB1 size suggests a layer of [Ch][Glu], since the ion-pair in these conditions can disrupt the hydration layer formed contributing to an increase on the hydrophobic protein surface area that interacts preferentially with PEG at higher concentrations. Since it was already shown that PEG favours the formation of ion-pairs the two effects reinforce for higher crowder concentration.

On lysozyme crowding, the decrease of GB1 size at high concentrations of crowder reflects the solvation of protein by ions of [Ch][Glu] and ion-pairs that neutralize the overall protein charge and act as a screen for interactions with lysozyme. This is also in accordance with the ^{1}H-^{15}N HSQC data showing that the addition of [Ch][Glu] breaks the interaction with lysozyme. Probably [Ch][Glu] is acting as protectant osmolyte by directly interacting with the protein surface mitigating the interaction with other proteins.

In addition, the diffusion coefficients of the ions of [Ch][Glu] were measured and their hydrodynamic radius compared as presented in **Table IV.8**.

Table IV.8. Diffusion coefficients and hydrodynamic radius of the ions of 100 mM [Ch][Glu] in different environments with 1 mM GB1, in 99.9% $^{2}H_2O$ at 37 ºC as extracted from ^{1}H- DOSY plots.

100 mM [Ch][Glu] IL

	PEG 3350					Lysozyme				
Crowder (g/L)	Diffusion Coefficients (D) (10^{-10} m^2 s^{-1})		Hydrodynamic radius ratio (D_{HDO}/D_{ion})		Rr_H	Diffusion Coefficients (D) (10^{-10} m^2 s^{-1})		Hydrodynamic radius ratio (D_{HDO}/D_{ion})		Rr_H
	Ch^+	**Glu^-**	**Ch^+**	**Glu^-**	**Glu^-/Ch^+**	**Ch^+**	**Glu^-**	**Ch^+**	**Glu^-**	**Glu/Ch**
0	9.2 ± 0.3 [a]	6.9 ± 0.1	2.5	3.3	1.3	9.58 ±0.09	6.92 ±0.09	2.4	3.3	1.4
50	7.7 ± 0.2	5.57 ± 0.09	2.6	3.6	1.4	8.3 ±0.4	5.7 ±0.3	2.6	3.8	1.5
100	7.2 ± 0.2	4.82 ± 0.08	2.5	3.8	1.5	7.4 ±0.5	4.6 ±0.5	2.7	4.5	1.6
150	6.3 ± 0.2	4.22 ± 0.07	2.7	4.00	1.5	6.6 ±0.7	4.0 ±0.4	3.00	4.9	1.7
300	4.4 ± 0.1	2.79 ± 0.04	2.9	4.6	1.6	5.2 ±0.3	2.9 ±0.3	3.1	5.6	1.8

[a] The standard deviation in Ch^+ in PEG was obtained by fitting and in the other ions by average of different signals.

The **Table IV.8** show the ratio of hydrodynamic radius in the same conditions as performed in the preceding experiments about protein diffusion. The translational diffusion of choline cation and glutamate in PEG and lysozyme was slowed down with an increasing cation-anion difference with increasing concentrations of crowder compared to dilute buffer. Also, both the ions size and cation/anion hydrodynamic radius ratio are generally higher in lysozyme, probably due to extra weak interactions with crowder.

IV. 4. Conclusions

Using the temperature of melting (T_m) as an indicator of thermal stability, the [Ch][Glu] displays ability for protein stabilisation, however under macromolecular crowding (by ion-pair influence), the ions replace the water molecules from the hydration layer destabilising the protein (indifferently the crowder under study). However, mitigates the unspecific destabilising interactions by crowder.

Chemical shift perturbation experiments revealed that interactions with crowder and [Ch][Glu] are non-specific and weak and do not depend on the size or charge of crowder, however the IL ion-pair can mitigate the attractive effect of lysozyme on GB1.

The strong attenuation of translational diffusion observed in the presence of the studied crowders does not depend on their differences of size and/or charge. The dramatically different effects of synthetic polymers and proteins arise essentially from nonspecific, noncovalent chemical interactions between the crowders and GB1. The protein diffusion with [Ch][Glu] is consistent with an interference of the IL on the mechanism of crowder/GB1 interaction, the reinforcement of hydrophobic interactions with the crowder seems to be most relevant factor to influence GB1 diffusion.

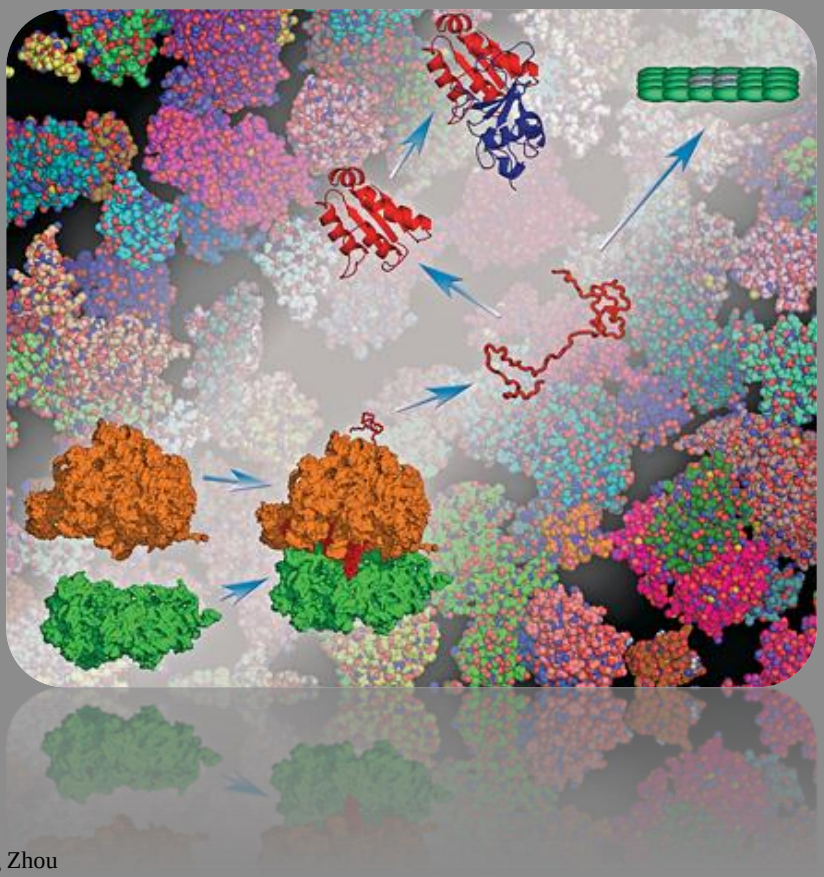

Huan-Xiang Zhou
TIGHTLY PACKED
Biological processes such as protein synthesis, folding, binding, and aggregation are affected by the crowded conditions in cells.

Chapter V: Final conclusions and future perspectives

V. Final conclusions and future perspectives

The general aim of this thesis was to contribute to the understanding of the possible role of *transient ion-pairs* (hydrated ionic liquids) under macromolecular crowding and its effects on protein structure and stability, using advanced NMR techniques and calorimetric techniques.

The main conclusion of this work is that transient ion pairs, namely [Ch][Glu] ion – pair can be relevant to protein stabilisation under biological conditions. Their ability for protein dehydration must be considered with repercussions for protein-crowder interactions.

In particular in this work, the biocompatible [Ch][Glu] IL, that can be potentially formed by natural organic ions found in cell milieu, was synthetized and characterized. The ion-pair was detected (5.7 Å of intermolecular interaction) in dilute conditions by the sensitive and selective ^{1}H – 1D – NOE NMR technique. Also, the method used for the synthesis of the choline-based ILs revealed to be an efficient method for organic anion exchange in order to prepare new bio-inspired combinations with relevant organic cations.

Using the selective ^{1}H – 1D – NOE NMR technique it was possible to detect an ion-pair promotion through crowding conditions mimicking the cellular interior derived by PEG and BSA. Essentially, the cation-anion distance decreased in both crowders, likewise revealed that ion-pair promotion does not depend on their differences of size and/or charge but mainly of steric repulsions.

Concerning protein stability, the temperature of melting (T_m) was used as an indicator of thermal stability and demonstrated the stabilisation by [Ch][Glu] on different charged proteins (GB1 and lysozyme). Therefore, when the ion pair extent increase, under macromolecular crowding, it is assumed that the hydration layer is disrupted due the surface protein – ion/pair hydrophobic interactions (small protein destabilisation) giving rise to a new layer composed by ions. This schematic hypothesis is shown in **Scheme V.1** where the opposing osmolyte effect of [Ch][Glu] in different conditions (dilute vs. macromolecular crowding) on the GB1 protein stability is presented.

Chemical shift perturbation experiments revealed that interactions with crowder and [Ch][Glu] are non-specific and weak and do not depend on the size or charge of crowder. However the IL ion-pair act as protectant osmolyte by directly interacting with the protein surface mitigating the attractive effect of lysozyme on GB1.

Furthermore, the strong attenuation of translational diffusion observed for GB1 in the presence of the studied crowders confirmed the weak dependence on their differences of size and/or charge. The dramatically different effects of synthetic polymers and proteins arise essentially from nonspecific, non-covalent chemical interactions between the crowders and GB1.

The protein diffusion with [Ch][Glu] is consistent with an interference of the IL on the mechanism of crowder/GB1 interaction, the reinforcement of hydrophobic interactions via ion-pair with the crowder seems to be most relevant factor to influence GB1 diffusion.

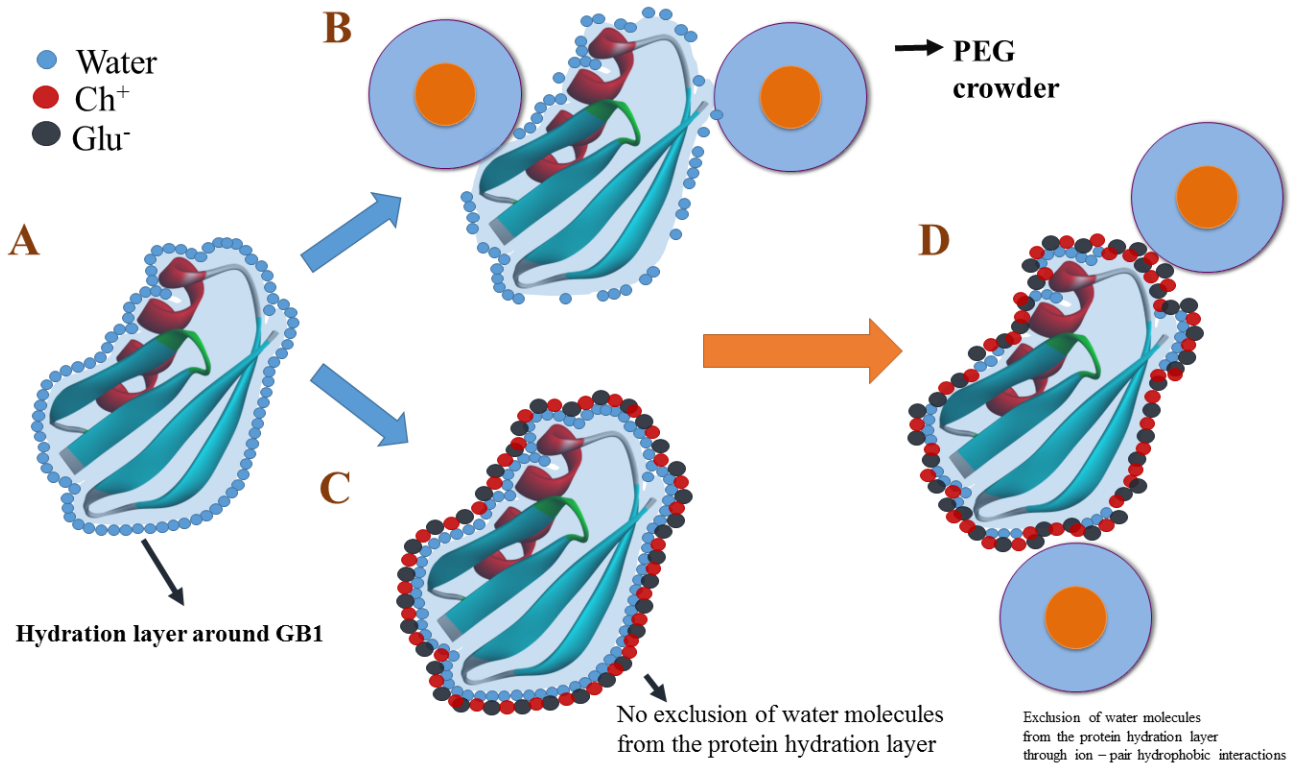

Scheme V.1. Hypothesis for the osmolyte effect of [Ch][Glu] IL and their ion-pair on GB1 protein showing unfavorable (C) and favorable interactions (B and D). **A:** GB1 in dilute condition, **B:** GB1 under macromolecular crowding through synthetic PEG. , **C:** GB1 with [Ch][Glu] in dilute condition, **D:** GB1 with [Ch][Glu] under macromolecular crowding.

As concluding remarks, independently of size and charge of test protein or crowder:

- Under dilute condition, is possible to assert that the [Ch][Glu] act as a protectant/ compatible osmolyte since their ions are located in the second shell that induced a preferential hydration which leads to a significant stabilisation.
- On the other hand, under crowding environment, the [Ch][Glu] ion pair is promoted and act as an non-compatible osmolyte, destabilizing the protein by favourable interaction with the interior of protein leading to solvent-accessible surface area of protein hydrophobic patches leading to protein unfolding. However, the IL mitigates the unspecific and destabilising effect of crowder.

As future work it is logical to propose the extension of these studies to other Bio-ILs and crowders. Also, the protein diffusion with IL should be studied with a negatively charged crowder.

Despite a few studies with protein-osmolytes under crowding, this work represents the first time that bio-ILs and crowding are shared *in vitro*. Hence an extensive *in cell* investigation should be employed in order to understanding if *transient ion-pairs* occur in cell and the "genuine" [Ch][Glu] effect on proteins.

Overall, more water-biocompatible ILs should be used in the next related studies, bio-ILs that allow inclusion of water in the protein surface stimulating the hydrogen-bond strength of interfacial water acting as an bio-compatible osmolyte. Their ion-pair should be detected in nanoseconds time range but with less hydrophobic character and promoting hydrogen-bond with the surface protein. In this way, the charged metabolites found in cell can be understood as key for protein stabilisation and the protein conservation/ storage industry revolutionized.

Bibliography

[1] T. Welton, *Chem. Rev.* **1999**, *99*, 2071–2084.

[2] P. Wasserscheid, W. Keim, *Angew. Chemie* **2000**, *39*, 3772–3789.

[3] P. Walden, *Bull. Acad. Imper. Sci. (St. Petersburg)* **1914**, *8*, 405–422.

[4] S. Sugden, H. Wilkins, *J. Chem. Soc.* **1929**, 1291–1298.

[5] F. H. Hurley, T. P. Wier, Jr., *J. Electrochem. Soc.* **1951**, *98*, 207.

[6] H. L. Chum, V. R. Koch, L. L. Miller, R. A. Osteryoung, *J. Am. Chem. Soc.* **1975**, *97*, 3264–3265.

[7] N. V Plechkova, K. R. Seddon, *Chem. Soc. Rev.* **2008**, *37*, 123–150.

[8] C. G. Swain, A. Ohno, D. K. Roe, R. Brown, T. Maugh, *J. Am. Chem. Soc.* **1967**, *89*, 2648–2649.

[9] D. Appleby, C. L. Hussey, K. R. Seddon, J. E. Turp, *Nature* **1986**, *323*, 614–616.

[10] J. S. Wilkes, C. L. Hussey, *Selection of Cations for Ambient Temperature Chloroaluminate Molten Salts Using MNDO Molecular Orbital Calculations*, **1982**, FJSRL-TR-82-0002.

[11] J. S. Wilkes, M. J. Zaworotko, *J. Chem. Soc. Chem. Commun.* **1992**, 965.

[12] E. I. Cooper, E. J. M. O' Sullivan, in *Eight Int. Molten Salts Symp.* (Eds.: R.J. Gale, G. Blomgren, H. Kojima), The Electrochemical Society, Inc., Pennington, New Jersey, **1992**, pp. 386–396.

[13] P. Bonhôte, A.-P. Dias, N. Papageorgiou, K. Kalyanasundaram, M. Grätzel, *Inorg. Chem.* **1996**, *35*, 1168–1178.

[14] M. Grätzel, *J. Photochem. Photobiol. C Photochem. Rev.* **2003**, *4*, 145–153.

[15] J. D. Holbrey, K. R. Seddon, *Clean Prod. Process.* **1999**, *1*, 223–236.

[16] R. A. Mantz, P. C. Trulove, R. T. Carlin, R. A. Osteryoung, *Inorg. Chem.* **1995**, *34*, 3846–3847.

[17] J. P. Hallett, T. Welton, *Chem. Rev.* **2011**, *111*, 3508–3576.

[18] H. Weingärtner, *Angew. Chemie Int. Ed.* **2008**, *47*, 654–670.

[19] A. D. Sawant, D. G. Raut, N. B. Darvatkar, M. M. Salunkhe, *Green Chem. Lett. Rev.* **2011**, *4*, 41–54.

[20] G. S. Fonseca, A. P. Umpierre, P. F. P. Fichtner, S. R. Teixeira, J. Dupont, *Chem. - A Eur. J.* **2003**, *9*, 3263–3269.

[21] H. Weingärtner, *Curr. Opin. Colloid Interface Sci.* **2013**, *18*, 183–189.

[22] L. Crowhurst, P. R. Mawdsley, J. M. Perez-Arlandis, P. A. Salter, T. Welton, *Phys. Chem. Chem. Phys.* **2003**, *5*, 2790–2794.

[23] H. Ohno, M. Yoshizawa, T. Mizumo, in *Electrochem. Asp. Ion. Liq.* (Ed.: H. Ohno), John Wiley & Sons, Inc., Hoboken, NJ, USA, **2005**, pp. 75–81.

[24] H. Li, M. Ibrahim, I. Agberemi, M. N. Kobrak, *J. Chem. Phys.* **2008**, *129*, 124507.

[25] M. Freemantle, *Chem. Eng. News Arch.* **1998**, *76*, 32–37.

[26] T. L. Greaves, C. J. Drummond, *Chem. Rev.* **2008**, *108*, 206–237.

[27] S. Z. El Abedin, F. Endres, *Acc. Chem. Res.* **2007**, *40*, 1106–1113.

[28] Y. Dai, J. van Spronsen, G. J. Witkamp, R. Verpoorte, Y. H. Choi, *Anal. Chim. Acta* **2013**, *766*, 61–68.

[29] S. Zhang, N. Sun, X. He, X. Lu, X. Zhang, *J. Phys. Chem. Ref. Data* **2006**, *35*, 1475–1517.

[30] F. van Rantwijk, R. Madeira Lau, R. A. Sheldon, *Trends Biotechnol.* **2003**, *21*, 131–8.

[31] F. van Rantwijk, R. A. Sheldon, *Chem. Rev.* **2007**, *107*, 2757–2785.

[32] M. C. Corvo, J. Sardinha, S. C. Menezes, S. Einloft, M. Seferin, J. Dupont, T. Casimiro, E. J. Cabrita, *Angew. Chemie Int. Ed.* **2013**, *52*, 13024–13027.

[33] T. L. Greaves, C. J. Drummond, *Chem. Soc. Rev.* **2008**, *37*, 1709–1726.

[34] K. M. Docherty, C. F. Kulpa, Jr., *Green Chem.* **2005**, *7*, 185.

[35] Q. Liu, X. Hou, N. Li, M. Zong, *Green Chem.* **2012**, *14*, 304–307.

[36] X. Hou, Q. Liu, T. J. Smith, N. Li, M. Zong, *PLoS One* **2013**, *8*, e59145.

[37] D. Tao, Z. Cheng, F.-F. Chen, Z. Li, N. Hu, X. Chen, *J. Chem. Eng. Data* **2013**, *58*, 1542–1548.

[38] P. Moriel, E. J. García-Suárez, M. Martínez, A. B. García, M. A. Montes-Morán, V. Calvino-Casilda, M. A. Bañares, *Tetrahedron Lett.* **2010**, *51*, 4877–4881.

[39] E. Alcalde, I. Dinarès, A. Ibáñez, N. Mesquida, *Molecules* **2012**, *17*, 4007–4027.

[40] K. Fukumoto, M. Yoshizawa, H. Ohno, *J. Am. Chem. Soc.* **2005**, *127*, 2398–2399.

[41] G. Tao, L. He, N. Sun, Y. Kou, *Chem. Commun.* **2005**, 3562.

[42] K. Fukumoto, H. Ohno, *Chem. Commun.* **2006**, 3081.

[43] J. Kagimoto, K. Fukumoto, H. Ohno, *Chem. Commun.* **2006**, 2254–2256.

[44] J. K. Blusztajn, *Science* **1998**, *281*, 794–795.

[45] S. H. Zeisel, K. A. Da Costa, P. D. Franklin, E. A. Alexander, J. T. Lamont, N. F. Sheard, A. Beiser, *FASEB J.* **1991**, *5*, 2093–2098.

[46] J. Pernak, *Eur. J. Med. Chem.* **2001**, *36*, 313–320.

[47] J. Arning, S. Stolte, A. Böschen, F. Stock, W.-R. Pitner, U. Welz-Biermann, B. Jastorff, J. Ranke, *Green Chem.* **2008**, *10*, 47–58.

[48] A. Romero, A. Santos, J. Tojo, A. Rodríguez, *J. Hazard. Mater.* **2008**, *151*, 268–273.

[49] R. S. Boethling, E. Sommer, D. DiFiore, *Chem. Rev.* **2007**, *107*, 2207–2227.

[50] Y. Deng, P. Besse-Hoggan, M. Sancelme, A.-M. Delort, P. Husson, M. F. Costa Gomes, *J. Hazard. Mater.* **2011**, *198*, 165–174.

[51] P. Nockemann, B. Thijs, K. Driesen, C. R. Janssen, K. Van Hecke, L. Van Meervelt, S. Kossmann, B. Kirchner, K. Binnemans, *J. Phys. Chem. B* **2007**, *111*, 5254–5263.

[52] K. D. Weaver, H. J. Kim, J. Sun, D. R. MacFarlane, G. D. Elliott, *Green Chem.* **2010**, *12*, 507.

[53] M. Petkovic, J. L. Ferguson, H. Q. N. Gunaratne, R. Ferreira, M. C. Leitão, K. R. Seddon, L. P. N. Rebelo, C. S. Pereira, *Green Chem.* **2010**, *12*, 643.

[54] D. Coleman, N. Gathergood, *Chem. Soc. Rev.* **2010**, *39*, 600.

[55] N. S. Isaacs, *Physical Organic Chemistry*, Longman Scientific & Technical, New York, NY, **1987**.

[56] J. D. Tubbs, M. M. Hoffmann, *J. Solution Chem.* **2004**, *33*, 381–394.

[57] T. Köddermann, C. Wertz, A. Heintz, R. Ludwig, *ChemPhysChem* **2006**, *7*, 1944–1949.

[58] P. A. Hunt, B. Kirchner, T. Welton, *Chem. – A Eur. J.* **2006**, *12*, 6762–75.

[59] P. A. Hunt, I. R. Gould, B. Kirchner, *Aust. J. Chem.* **2007**, *60*, 9–14.

[60] A. G. Avent, P. A. Chaloner, M. P. Day, K. R. Seddon, T. Welton, *J. Chem. Soc. Dalt. Trans.* **1994**, 3405–3413.

[61] M. G. Del Pópolo, G. a. Voth, *J. Phys. Chem. B* **2004**, *108*, 1744–1752.

[62] W. Zhao, F. Leroy, B. Heggen, S. Zahn, B. Kirchner, S. Balasubramanian, F. Müller-Plathe, *J. Am. Chem. Soc.* **2009**, *131*, 15825–15833.

[63] K. Dong, S. Zhang, D. Wang, X. Yao, *J. Phys. Chem. A* **2006**, *110*, 9775–9782.

[64] L. Cammarata, S. G. Kazarian, P. a. Salter, T. Welton, *Phys. Chem. Chem. Phys.* **2001**, *3*, 5192–5200.

[65] A. Pádua, M. Gomes, J. N. A. C. Lopes, *Acc. Chem. Res.* **2007**, *40*, 1087–1096.

[66] T. Cremer, C. Kolbeck, K. R. J. Lovelock, N. Paape, R. Wölfel, P. S. Schulz, P. Wasserscheid, H. Weber, J. Thar, B. Kirchner, et al., *Chem. - A Eur. J.* **2010**, *16*, 8929–8929.

[67] K. J. Fraser, E. I. Izgorodina, M. Forsyth, J. L. Scott, D. R. MacFarlane, *Chem. Commun.* **2007**, 3817–3819.

[68] H. Tokuda, K. Hayamizu, K. Ishii, M. A. B. H. Susan, M. Watanabe, *J. Phys. Chem. B* **2004**, *108*,

16593–16600.

[69] H. Tokuda, K. Hayamizu, K. Ishii, M. A. B. H. Susan, M. Watanabe, *J. Phys. Chem. B* **2005**, *109*, 6103–6110.

[70] H. Tokuda, K. Ishii, M. A. B. H. Susan, S. Tsuzuki, K. Hayamizu, M. Watanabe, *J. Phys. Chem. B* **2006**, *110*, 2833–2839.

[71] C. Daguenet, P. J. Dyson, I. Krossing, A. Oleinikova, J. Slattery, C. Wakai, H. Weingärtner, *J. Phys. Chem. B* **2006**, *110*, 12682–12688.

[72] P. S. Pregosin, *Pure Appl. Chem.* **2009**, *81*, 615–633.

[73] T. Brand, E. J. Cabrita, S. Berger, *Prog. Nucl. Magn. Reson. Spectrosc.* **2005**, *46*, 159–196.

[74] S. Gabl, O. Steinhauser, H. Weingärtner, *Angew. Chemie Int. Ed.* **2013**, *52*, 9242–9246.

[75] D. Neuhaus, M. P. Williamson, *The Nuclear Overhauser Effect in Structural and Conformational Analysis*, Wiley-VCH Verlag GmbH, New York, **2000**.

[76] T. C. Pochapsky, P. M. Stone, *J. Am. Chem. Soc.* **1990**, *112*, 6714–6715.

[77] A. Mele, G. Romanò, M. Giannone, E. Ragg, G. Fronza, G. Raos, V. Marcon, *Angew. Chem. Int. Ed.* **2006**, *45*, 1123–1126.

[78] D. Nama, P. G. A. Kumar, P. S. Pregosin, T. J. Geldbach, P. J. Dyson, *Inorganica Chim. Acta* **2006**, *359*, 1907–1911.

[79] J. Dupont, P. A. Z. Suarez, R. F. De Souza, R. A. Burrow, J.-P. Kintzinger, *Chem. - A Eur. J.* **2000**, *6*, 2377–2381.

[80] Y. Lingscheid, S. Arenz, R. Giernoth, *ChemPhysChem* **2012**, *13*, 261–266.

[81] J. T. Gerig, *J. Org. Chem.* **2003**, *68*, 5244–5248.

[82] K. Modig, E. Liepinsh, G. Otting, B. Halle, *J. Am. Chem. Soc.* **2004**, *126*, 102–114.

[83] A. Sirjoosingh, S. Alavi, T. K. Woo, *J. Phys. Chem. B* **2009**, *113*, 8103–8113.

[84] D. H. Dagade, K. R. Madkar, S. P. Shinde, S. S. Barge, *J. Phys. Chem. B* **2013**, *117*, 1031–1043.

[85] D. K. Magnuson, J. W. Bodley, D. F. Evans, *J. Solution Chem.* **1984**, *13*, 583–587.

[86] L. Gianfreda, M. Scarfi, *Mol. Cell. Biochem.* **1991**, *100*, 97–128.

[87] A. Illanes, *Electron. J. Biotechnol.* **1999**, *2*, 1–9.

[88] M. M. Santoro, Y. Liu, S. M. Khan, L. X. Hou, D. W. Bolen, *Biochemistry* **1992**, *31*, 5278–83.

[89] R. M. Vrikkis, K. J. Fraser, K. Fujita, D. R. MacFarlane, G. D. Elliott, *J. Biomech. Eng.* **2009**, *131*, 074514–4.

[90] K. Fujita, D. R. MacFarlane, M. Forsyth, *Chem. Commun.* **2005**, *70*, 4804.

[91] H. Noritomi, K. Minamisawa, R. Kamiya, S. Kato, *J. Biomed. Sci. Eng.* **2011**, *04*, 94–99.

[92] H. Weingärtner, C. Cabrele, C. Herrmann, *Phys. Chem. Chem. Phys.* **2012**, *14*, 415–26.

[93] D. Constantinescu, H. Weingärtner, C. Herrmann, *Angew. Chem. Int. Ed.* **2007**, *46*, 8887–8889.

[94] T. A. Page, N. D. Kraut, P. M. Page, G. A. Baker, F. V. Bright, *J. Phys. Chem. B* **2009**, *113*, 12825–12830.

[95] C. Lange, G. Patil, R. Rudolph, *Protein Sci.* **2005**, *14*, 2693–2701.

[96] R. Buchfink, A. Tischer, G. Patil, R. Rudolph, C. Lange, *J. Biotechnol.* **2010**, *150*, 64–72.

[97] C. A. Summers, R. A. Flowers, *Protein Sci.* **2000**, *9*, 2001–2008.

[98] N. Byrne, C. A. Angell, *J. Mol. Biol.* **2008**, *378*, 707–714.

[99] S. Mangialardo, L. Gontrani, L. Francesca, R. Caminiti, P. Postorino, *RSC Adv.* **2012**, *2*, 12329–12336.

[100] N. Byrne, L.-M. Wang, J.-P. Belieres, C. A. Angell, *Chem. Commun.* **2007**, 2714–2716.

[101] D. Constantinescu, C. Herrmann, H. Weingärtner, *Phys. Chem. Chem. Phys.* **2010**, *12*, 1756–1763.

[102] A. Kumar, P. Venkatesu, *Int. J. Biol. Macromol.* **2014**, *63*, 244–53.

[103] R. Patel, M. Kumari, A. B. Khan, *Appl. Biochem. Biotechnol.* **2014**, *172*, 3701–3720.

[104] P. Bharmoria, A. Kumar, *Biochim. Biophys. Acta* **2015**, DOI 10.1016/j.bbagen.2015.08.022.

[105] I. Jha, P. Venkatesu, *Phys. Chem. Chem. Phys.* **2015**, *17*, 20466–20484.

[106] K. Fujita, D. R. MacFarlane, M. Forsyth, M. Yoshizawa-Fujita, K. Murata, N. Nakamura, H. Ohno, *Biomacromolecules* **2007**, *8*, 2080–2086.

[107] A. M. Figueiredo, J. Sardinha, G. R. Moore, E. J. Cabrita, *Phys. Chem. Chem. Phys.* **2013**, *15*, 19632–19643.

[108] M. Silva, A. M. Figueiredo, E. Cabrita, *Phys. Chem. Chem. Phys.* **2014**, *16*, 23394–23403.

[109] X. Chen, T. Yang, S. Kataoka, P. S. Cremer, *J. Am. Chem. Soc.* **2007**, *129*, 12272–12279.

[110] H. Zhao, O. Olubajo, Z. Song, A. L. Sims, T. E. Person, R. a Lawal, L. a Holley, *Bioorg. Chem.* **2006**, *34*, 15–25.

[111] Z. Yang, *J. Biotechnol.* **2009**, *144*, 12–22.

[112] F. Hofmeister, *Arch. Exp. Pathol. Pharmakol* **1888**, *24*, 247–260.

[113] R. L. Baldwin, *Biophys. J.* **1996**, *71*, 2056–2063.

[114] E. A. Algaer, N. F. A. van der Vegt, *J. Phys. Chem. B* **2011**, *115*, 13781–13787.

[115] P. E. Mason, G. W. Neilson, C. E. Dempsey, a C. Barnes, J. M. Cruickshank, *Proc. Natl. Acad. Sci.* **2003**, *100*, 4557–4561.

[116] N. Galamba, *J. Phys. Chem. B* **2012**, *116*, 5242–5250.

[117] Y. Shu, M. Liu, S. Chen, X. Chen, J. Wang, *J. Phys. Chem. B* **2011**, *115*, 12306–12314.

[118] K. D. Weaver, R. M. Vrikkis, M. P. Van Vorst, J. Trullinger, R. Vijayaraghavan, D. M. Foureau, I. H. McKillop, D. R. MacFarlane, J. K. Krueger, G. D. Elliott, *Phys. Chem. Chem. Phys.* **2012**, *14*, 790.

[119] J.-Q. Lai, Z. Li, Y.-H. Lü, Z. Yang, *Green Chem.* **2011**, *13*, 1860.

[120] E. Sedlák, L. Stagg, P. Wittung-Stafshede, *Arch. Biochem. Biophys.* **2008**, *479*, 69–73.

[121] N. Kaftzik, P. Wasserscheid, U. Kragl, *Org. Process Res. Dev.* **2002**, *6*, 553–557.

[122] J. P. Mann, A. McCluskey, R. Atkin, *Green Chem.* **2009**, *11*, 785.

[123] Y. Akdogan, M. J. N. Junk, D. Hinderberger, *Biomacromolecules* **2011**, *12*, 1072–1079.

[124] Z. Wang, H. Xiao, Y. Han, P. Jiang, Z. Zhou, *J. Chem. Eng. Data* **2011**, *56*, 1700–1703.

[125] G. A. Baker, W. T. Heller, *Chem. Eng. J.* **2009**, *147*, 6–12.

[126] D. W. Bolen, in *Protein Struct. Stability, Fold.*, Humana Press, New Jersey, **2001**, pp. 017–036.

[127] Z. Ignatova, L. M. Gierasch, in *Methods Enzymol.*, Elsevier Masson SAS, **2007**, pp. 355–372.

[128] P. I. Larsen, L. K. Sydnes, B. Landfald, A. R. Strøm, *Arch. Microbiol.* **1987**, *147*, 1–7.

[129] P. H. Yancey, *J. Exp. Biol.* **2005**, *208*, 2819–2830.

[130] S. Cayley, M. T. Record, *Biochemistry* **2003**, *42*, 12596–12609.

[131] T. O. Street, D. W. Bolen, G. D. Rose, *Proc. Natl. Acad. Sci.* **2006**, *103*, 13997–14002.

[132] B. J. Bennion, V. Daggett, *Proc. Natl. Acad. Sci.* **2004**, *101*, 6433–6438.

[133] Y. Zhang, P. S. Cremer, *Annu. Rev. Phys. Chem.* **2010**, *61*, 63–83.

[134] P. Attri, P. Venkatesu, M.-J. Lee, *J. Phys. Chem. B* **2010**, *114*, 1471–1478.

[135] P. Venkatesu, M.-J. Lee, H. Lin, *Arch. Biochem. Biophys.* **2007**, *466*, 106–115.

[136] S. Ortiz-Costa, M. M. Sorenson, M. Sola-Penna, *FEBS J.* **2008**, *275*, 3388–3396.

[137] P. Attri, P. Venkatesu, A. Kumar, *Phys. Chem. Chem. Phys.* **2011**, *13*, 2788–2796.

[138] P. Attri, P. Venkatesu, *Phys. Chem. Chem. Phys.* **2011**, *13*, 6566.

[139] K. Sankaranarayanan, G. Sathyaraj, B. U. Nair, a. Dhathathreyan, *J. Phys. Chem. B* **2012**, *116*, 4175–4180.

[140] D. K. Sasmal, T. Mondal, S. Sen Mojumdar, A. Choudhury, R. Banerjee, K. Bhattacharyya, *J. Phys. Chem. B* **2011**, *115*, 13075–13083.

[141] T. Takekiyo, K. Yamazaki, E. Yamaguchi, H. Abe, Y. Yoshimura, *J. Phys. Chem. B* **2012**, *116*, 11092–11097.

[142] S. N. Timasheff, *Annu. Rev. Biophys. Biomol. Struct.* **1993**, *22*, 67–97.

[143] G. Chevrot, E. E. Fileti, V. V. Chaban, *J. Comput. Chem.* **2015**, 1–8.

[144] J. Smiatek, *J. Phys. Chem. B* **2014**, *118*, 771–782.

[145] V. Lesch, A. Heuer, V. a. Tatsis, C. Holm, J. Smiatek, *Phys. Chem. Chem. Phys.* **2015**, DOI 10.1039/C5CP03838C.

[146] B. D. Bennett, E. H. Kimball, M. Gao, R. Osterhout, S. J. Van Dien, J. D. Rabinowitz, *Nat. Chem. Biol.* **2009**, *5*, 593–599.

[147] D. S. Wishart, T. Jewison, A. C. Guo, M. Wilson, C. Knox, Y. Liu, Y. Djoumbou, R. Mandal, F. Aziat, E. Dong, et al., *Nucleic Acids Res.* **2013**, *41*, D801–D807.

[148] F.-X. Theillet, A. Binolfi, T. Frembgen-Kesner, K. Hingorani, M. Sarkar, C. Kyne, C. Li, P. B. Crowley, L. Gierasch, G. J. Pielak, et al., *Chem. Rev.* **2014**, *114*, 6661–6714.

[149] S. Sundararaj, A. Guo, B. Habibi-Nazhad, M. Rouani, P. Stothard, M. Ellision, D. S. Wishart, *Nucleic Acids Res.* **2004**, *32*, 293D–295.

[150] A. E. Pegg, P. P. McCann, *Am. J. Physiol.* **1982**, *243*, C212–221.

[151] N. Minois, D. Carmona-Gutierrez, F. Madeo, *Aging (Albany. NY).* **2011**, *3*, 716–732.

[152] S. I. Watanabe, K. Kusama-Eguchi, H. Kobayashi, K. Igarashi, *J. Biol. Chem.* **1991**, *266*, 20803–20809.

[153] E. T. M. Leermakers, E. M. Moreira, J. C. Kiefte-de Jong, S. K. L. Darweesh, T. Visser, T. Voortman, P. K. Bautista, R. Chowdhury, D. Gorman, W. M. Bramer, et al., *Nutr. Rev.* **2015**, *73*, 500–522.

[154] K. R. Pugh, S. J. Frost, D. L. Rothman, F. Hoeft, S. N. Del Tufo, G. F. Mason, P. J. Molfese, W. E. Mencl, E. L. Grigorenko, N. Landi, et al., *J. Neurosci.* **2014**, *34*, 4082–9.

[155] L. Chen, G. E. Mullen, M. Le Roch, C. G. Cassity, N. Gouault, H. Y. Fadamiro, R. E. Barletta, R. a O'Brien, R. E. Sykora, A. C. Stenson, et al., *Angew. Chemie Int. Ed.* **2014**, *53*, 11762–11765.

[156] S. B. Zimmerman, S. O. Trach, *J. Mol. Biol.* **1991**, *222*, 599–620.

[157] R. J. Ellis, *Trends Biochem. Sci.* **2001**, *26*, 597–604.

[158] K. Luby-Phelps, *Mol. Biol. Cell* **2013**, *24*, 2593–2596.

[159] S. R. McGuffee, A. H. Elcock, *PLoS Comput. Biol.* **2010**, *6*, e1000694.

[160] A. P. Minton, J. Wilf, *Biochemistry* **1981**, *20*, 4821–4826.

[161] D. Homouz, M. Perham, A. Samiotakis, M. S. Cheung, P. Wittung-Stafshede, *Proc. Natl. Acad. Sci.* **2008**, *105*, 11754–11759.

[162] A. H. Elcock, *Curr. Opin. Struct. Biol.* **2010**, *20*, 196–206.

[163] A. C. Miklos, C. Li, N. G. Sharaf, G. J. Pielak, *Biochemistry* **2010**, *49*, 6984–6991.

[164] Y. Wang, M. Sarkar, A. E. Smith, A. S. Krois, G. J. Pielak, *J. Am. Chem. Soc.* **2012**, *134*, 16614–16618.

[165] M. Sarkar, C. Li, G. J. Pielak, *Biophys. Rev.* **2013**, *5*, 187–194.

[166] A. E. Smith, Z. Zhang, G. J. Pielak, C. Li, *Curr. Opin. Struct. Biol.* **2015**, *30*, 7–16.

[167] G. J. Pielak, A. C. Miklos, *Proc. Natl. Acad. Sci. U. S. A.* **2010**, *107*, 17457–17458.

[168] A. Dhar, A. Samiotakis, S. Ebbinghaus, L. Nienhaus, D. Homouz, M. Gruebele, M. S. Cheung, *Proc. Natl. Acad. Sci.* **2010**, *107*, 17586–17591.

[169] A. P. Minton, *Biophys. J.* **2005**, *88*, 971–985.

[170] A. P. Minton, *J. Cell Sci.* **2006**, *119*, 2863–2869.

[171] H.-X. Zhou, G. Rivas, A. P. Minton, *Annu. Rev. Biophys.* **2008**, *37*, 375–397.

[172] L. A. Munishkina, E. M. Cooper, V. N. Uversky, A. L. Fink, *J. Mol. Recognit.* **2004**, *17*, 456–64.

[173] L. M. Charlton, C. O. Barnes, C. Li, J. Orans, G. B. Young, G. J. Pielak, *J. Am. Chem. Soc.* **2008**, *130*, 6826–6830.

[174] L. A. Benton, A. E. Smith, G. B. Young, G. J. Pielak, *Biochemistry* **2012**, *51*, 9773–9775.

[175] A. Soranno, I. Koenig, M. B. Borgia, H. Hofmann, F. Zosel, D. Nettels, B. Schuler, *Proc. Natl. Acad. Sci.* **2014**, *111*, 4874–4879.

[176] D. Gnutt, M. Gao, O. Brylski, M. Heyden, S. Ebbinghaus, *Angew. Chemie Int. Ed.* **2015**, *54*, 2548–2551.

[177] P. Molyneux, *Water-Soluble Synthetic Polymers: Properties and Behavior*, CRC Press, Boca Raton, FL, **1983**.

[178] W. H. Fissell, S. Manley, A. Dubnisheva, J. Glass, J. Magistrelli, A. N. Eldridge, A. J. Fleischman, A. L. Zydney, S. Roy, *AJP Ren. Physiol.* **2007**, *293*, F1209–F1213.

[179] Y. Wang, C. Li, G. J. Pielak, *J. Am. Chem. Soc.* **2010**, *132*, 9392–9397.

[180] M. Feig, Y. Sugita, *J. Phys. Chem. B* **2012**, *116*, 599–605.

[181] M. Sarkar, J. Lu, G. J. Pielak, *Biochemistry* **2014**, *53*, 1601–1606.

[182] W. B. Monteith, G. J. Pielak, *Proc. Natl. Acad. Sci.* **2014**, *111*, 11335–11340.

[183] F. Roosen-Runge, M. Hennig, F. Zhang, R. M. J. Jacobs, M. Sztucki, H. Schober, T. Seydel, F. Schreiber, *Proc. Natl. Acad. Sci.* **2011**, *108*, 11815–11820.

[184] T. Knubovets, J. J. Osterhout, P. J. Connolly, A. M. Klibanov, *Proc. Natl. Acad. Sci.* **1999**, *96*, 1262–1267.

[185] Y. C. Kim, J. Mittal, *Phys. Rev. Lett.* **2013**, *110*, 208102.

[186] A. P. Minton, *Biopolymers* **2013**, *99*, 239–244.

[187] A. C. Miklos, M. Sarkar, Y. Wang, G. J. Pielak, *J. Am. Chem. Soc.* **2011**, *133*, 7116–7120.

[188] A. C. Miklos, C. Li, G. J. Pielak, in *Methods Enzymol.*, Elsevier Inc., **2009**, pp. 1–18.

[189] G. J. Pielak, C. Li, A. C. Miklos, A. P. Schlesinger, K. M. Slade, G.-F. Wang, I. G. Zigoneanu, *Biochemistry* **2009**, *48*, 226–234.

[190] P. Selenko, Z. Serber, B. Gadea, J. Ruderman, G. Wagner, *Proc. Natl. Acad. Sci. U. S. A.* **2006**, *103*, 11904–11909.

[191] D. I. Freedberg, P. Selenko, *Annu. Rev. Biophys.* **2014**, *43*, 171–192.

[192] M. B. Elowitz, M. G. Surette, P. E. Wolf, J. B. Stock, S. Leibler, *J. Bacteriol.* **1999**, *181*, 197–203.

[193] K. A. Sharp, *Proc. Natl. Acad. Sci.* **2015**, *112*, 7990–7995.

[194] R. Politi, D. Harries, *Chem. Commun.* **2010**, *46*, 6449.

[195] M. Senske, L. Törk, B. Born, M. Havenith, C. Herrmann, S. Ebbinghaus, *J. Am. Chem. Soc.* **2014**, *136*, 9036–9041.

[196] L. Sapir, D. Harries, *Curr. Opin. Colloid Interface Sci.* **2015**, *20*, 3–10.

[197] I. Kuznetsova, B. Zaslavsky, L. Breydo, K. Turoverov, V. Uversky, *Molecules* **2015**, *20*, 1377–1409.

[198] R. D. Cohen, A. J. Guseman, G. J. Pielak, *Protein Sci.* **2015**, *In press*, n/a–n/a.

[199] D. Gnutt, S. Ebbinghaus, *Biol. Chem.* **2015**, *In press*, DOI 10.1515/hsz-2015-0161.

[200] D. J. Felitsky, J. G. Cannon, M. W. Capp, J. Hong, A. W. Van Wynsberghe, C. F. Anderson, M. T. Record, *Biochemistry* **2004**, *43*, 14732–14743.

[201] K. D. Collins, *Methods* **2004**, *34*, 300–311.

[202] M. Sarkar, G. J. Pielak, *Protein Sci.* **2014**, *23*, 1161–1164.

[203] A. Gronenborn, D. Filpula, N. Essig, A. Achari, M. Whitlow, P. Wingfield, G. Clore, *Science* **1991**, *253*, 657–661.

[204] R. Ferraz, L. C. Branco, I. M. Marrucho, J. M. M. Araújo, L. P. N. Rebelo, M. N. da Ponte, C. Prudêncio, J. P. Noronha, Ž. Petrovski, *Medchemcomm* **2012**, *3*, 494.

[205] D. H. Wu, A. D. Chen, C. S. Johnson, *J. Magn. Reson. Ser. A* **1995**, *115*, 260–264.

[206] E. O. Stejskal, J. E. Tanner, *J. Chem. Phys.* **1965**, *42*, 288.

[207] M. J. Thrippleton, J. Keeler, *Angew. Chemie Int. Ed.* **2003**, *42*, 3938–3941.

[208] H. Ohno, K. Fukumoto, *Acc. Chem. Res.* **2007**, *40*, 1122–1129.

[209] N. Muhammad, Z. B. Man, M. A. Bustam, M. I. A. Mutalib, C. D. Wilfred, S. Rafiq, *J. Chem. Eng. Data* **2011**, *56*, 3157–3162.

[210] C. R. Allen, P. L. Richard, A. J. Ward, L. G. A. van de Water, A. F. Masters, T. Maschmeyer, *Tetrahedron Lett.* **2006**, *47*, 7367–7370.

[211] C. Alcorn, M. Cuperlovic-Culf, K. Ghandi, *J. Phys. Conf. Ser.* **2012**, *341*, 012013.

[212] K. Devanand, J. C. Selser, *Macromolecules* **1991**, *24*, 5943–5947.

[213] R. Haag, F. Kratz, *Angew. Chemie Int. Ed.* **2006**, *45*, 1198–1215.

[214] J. M. Harris, *Poly(Ethylene Glycol) Chemistry*, Springer US, Boston, MA, **1992**.

[215] M. M. Cecchini, C. Charnay, F. De Angelis, F. Lamaty, J. Martinez, E. Colacino, *ChemSusChem* **2014**, *7*, 45–65.

[216] Z. E. Reinert, E. D. Musselman, A. H. Elcock, W. S. Horne, *ChemBioChem* **2012**, *13*, 1107–1111.

[217] S. R. Fahnestock, P. Alexander, J. Nagle, D. Filpula, *J. Bacteriol.* **1986**, *167*, 870–880.

[218] P. Alexander, S. Fahnestock, T. Lee, J. Orban, P. Bryan, *Biochemistry* **1992**, *31*, 3597–3603.

[219] P. Alexander, J. Orban, P. Bryan, *Biochemistry* **1992**, *31*, 7243–7248.

[220] T. Gallagher, P. Alexander, P. Bryan, G. L. Gilliland, *Biochemistry* **1994**, *33*, 4721–4729.

[221] J. Orban, P. Alexander, P. Bryan, D. Khare, *Biochemistry* **1995**, *34*, 15291–15300.

[222] K. Ding, J. M. Louis, A. M. Gronenborn, *J. Mol. Biol.* **2004**, *335*, 1299–1307.

[223] J. J. Barchi, B. Grasberger, A. M. Gronenborn, G. M. Clore, *Protein Sci.* **2008**, *3*, 15–21.

[224] A. Morrone, R. Giri, R. D. Toofanny, C. Travaglini-Allocatelli, M. Brunori, V. Daggett, S. Gianni, *Biophys. J.* **2011**, *101*, 2053–2060.

[225] Q. Wang, A. Zhuravleva, L. M. Gierasch, *Biochemistry* **2011**, *50*, 9225–9236.

[226] P. N. Reardon, L. D. Spicer, *J. Am. Chem. Soc.* **2005**, *127*, 10848–10849.

[227] P. B. Crowley, E. Chow, T. Papkovskaia, *ChemBioChem* **2011**, *12*, 1043–1048.

[228] Y. Ye, X. Liu, Z. Zhang, Q. Wu, B. Jiang, L. Jiang, X. Zhang, M. Liu, G. J. Pielak, C. Li, *Chem. - A Eur. J.* **2013**, *19*, 12705–12710.

[229] J. Hamatsu, D. O'Donovan, T. Tanaka, T. Shirai, Y. Hourai, T. Mikawa, T. Ikeya, M. Mishima, W. Boucher, B. O. Smith, et al., *J. Am. Chem. Soc.* **2013**, *135*, 1688–1691.

[230] W. B. Monteith, R. D. Cohen, A. E. Smith, E. Guzman-Cisneros, G. J. Pielak, *Proc. Natl. Acad. Sci.* **2015**, *112*, 1739–1742.

[231] J. Spitzer, B. Poolman, *Microbiol. Mol. Biol. Rev.* **2009**, *73*, 371–388.

[232] H.-X. Zhou, *FEBS Lett.* **2013**, *587*, 1053–1061.

[233] S. Lindman, W.-F. Xue, O. Szczepankiewicz, M. C. Bauer, H. Nilsson, S. Linse, *Biophys. J.* **2006**, *90*, 2911–2921.

[234] H. Schägger, *Nat. Protoc.* **2006**, *1*, 16–22.

[235] W. J. Becktel, J. A. Schellman, *Biopolymers* **1987**, *26*, 1859–1877.

[236] G. I. Makhatadze, in *Curr. Protoc. Protein Sci.*, John Wiley & Sons, Inc., Hoboken, NJ, USA, **2001**, p. Unit 7.9.

[237] A. Blumlein, J. J. McManus, *Biochim. Biophys. Acta - Proteins Proteomics* **2013**, *1834*, 2064–2070.

[238] T. S. Light, *Anal. Chem.* **1984**, *56*, 1138–1142.

[239] C. Avanti, V. Saluja, E. L. P. van Streun, H. W. Frijlink, W. L. J. Hinrichs, *PLoS One* **2014**, *9*, e86244.

[240] K. Kar, N. Kishore, *Biopolymers* **2007**, *87*, 339–351.

[241] J. K. Kaushik, R. Bhat, *J. Biol. Chem.* **2003**, *278*, 26458–26465.

[242] S. James, J. J. McManus, *J. Phys. Chem. B* **2012**, *116*, 10182–10188.

[243] J. K. Kaushik, R. Bhat, *Protein Sci.* **1999**, *8*, 222–233.

[244] D. Khare, P. Alexander, J. Antosiewicz, P. Bryan, M. Gilson, J. Orban, *Biochemistry* **1997**, *36*, 3580–

3589.

[245] J. H. Tomlinson, S. Ullah, P. E. Hansen, M. P. Williamson, *J. Am. Chem. Soc.* **2009**, *131*, 4674–4684.

[246] N. Muramatsu, A. P. Minton, *Proc. Natl. Acad. Sci.* **1988**, *85*, 2984–2988.

[247] S. Zorrilla, M. a. Hink, A. J. W. G. Visser, M. P. Lillo, *Biophys. Chem.* **2007**, *125*, 298–305.

[248] P. Bernadó, J. G. de la Torre, M. Pons, *J. Mol. Recognit.* **2004**, *17*, 397–407.

[249] C. Li, Y. Wang, G. J. Pielak, *J. Phys. Chem. B* **2009**, *113*, 13390–13392.

[250] A. B. Goins, H. Sanabria, M. N. Waxham, *Biophys. J.* **2008**, *95*, 5362–5373.

[251] C. Johnson, *In Encyclopedia of Nuclear Magnetic Resonance*, John Wiley & Sons: Chichester, **1996**.

[252] M. Rubinstein, R. H. Colby, *Polymer Physics*, Oxford University Press, New York, NY, **2003**.

[253] R. Bhat, S. N. Timasheff, *Protein Sci.* **1992**, *1*, 1133–1143.

[254] J. H. Tomlinson, C. J. Craven, M. P. Williamson, M. J. Pandya, *Proteins Struct. Funct. Bioinforma.* **2010**, *78*, 1642–1661.

[255] I.-J. L. Byeon, J. M. Louis, A. M. Gronenborn, *J. Mol. Biol.* **2003**, *333*, 141–152.

[256] I.-J. L. Byeon, J. M. Louis, A. M. Gronenborn, *J. Mol. Biol.* **2004**, *340*, 615–625.

[257] J. M. Louis, I.-J. L. Byeon, U. Baxa, A. M. Gronenborn, *J. Mol. Biol.* **2005**, *348*, 687–698.

Appendix
A, B and C

List of Figures in Appendix A, B and C

List of Tables in Appendix A, B and C

A. Appendix

A. 1. Characterization by NMR

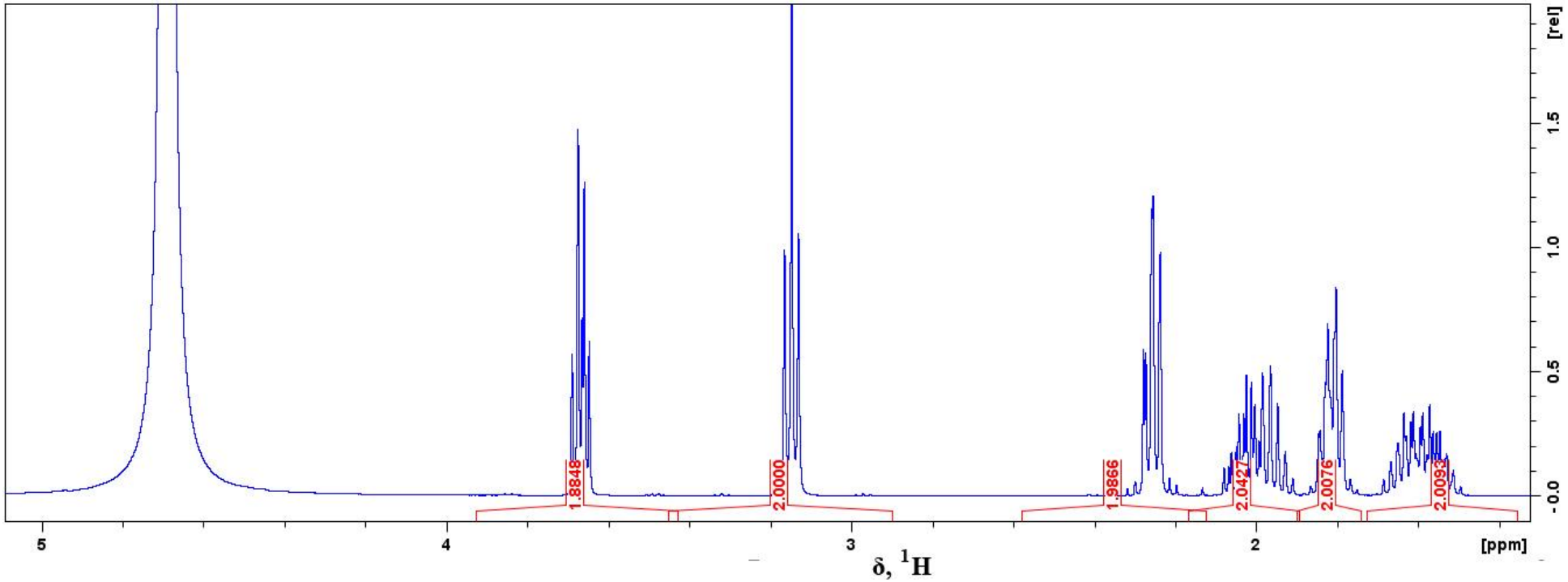

Figure A.1. ^{1}H NMR Spectrum of 100 mM [Arg][Glu] in D_2O.

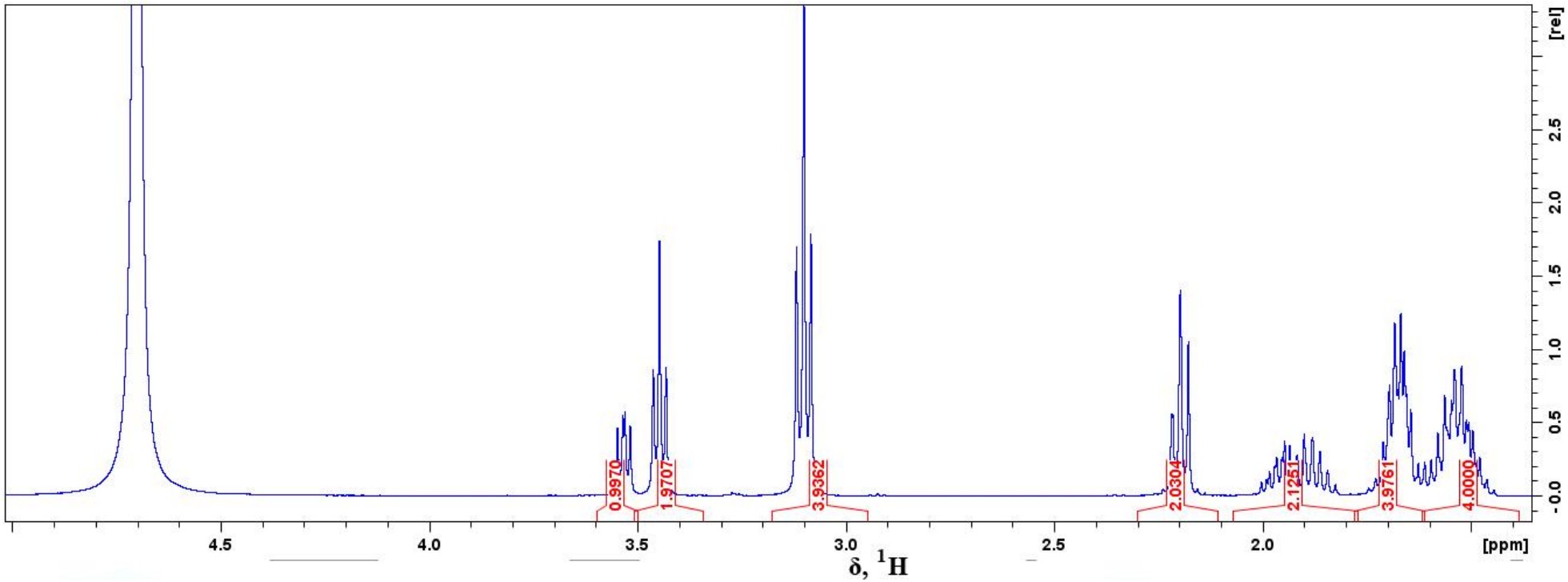

Figure A.2. ^{1}H NMR Spectrum of 100 mM [Arg_2][Glu] in D_2O.

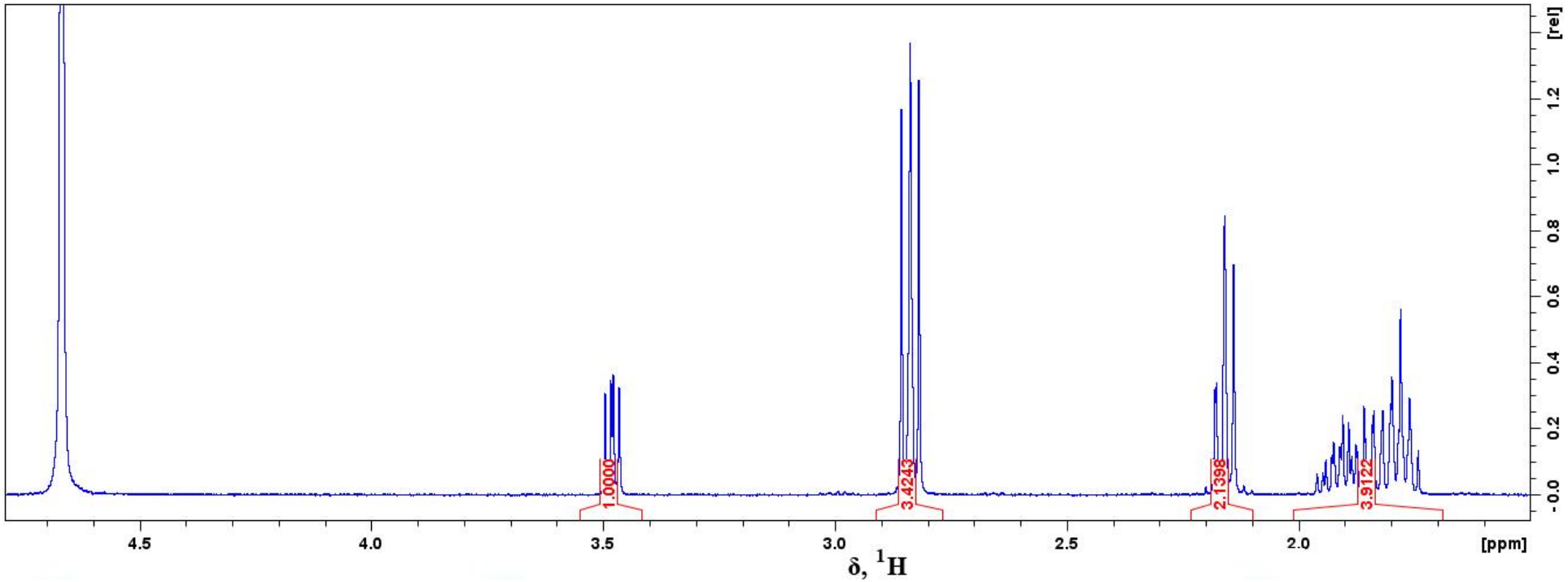

Figure A.3. ^{1}H NMR Spectrum of 100 mM [1,3-Diaminopropane][Glu] in D_2O.

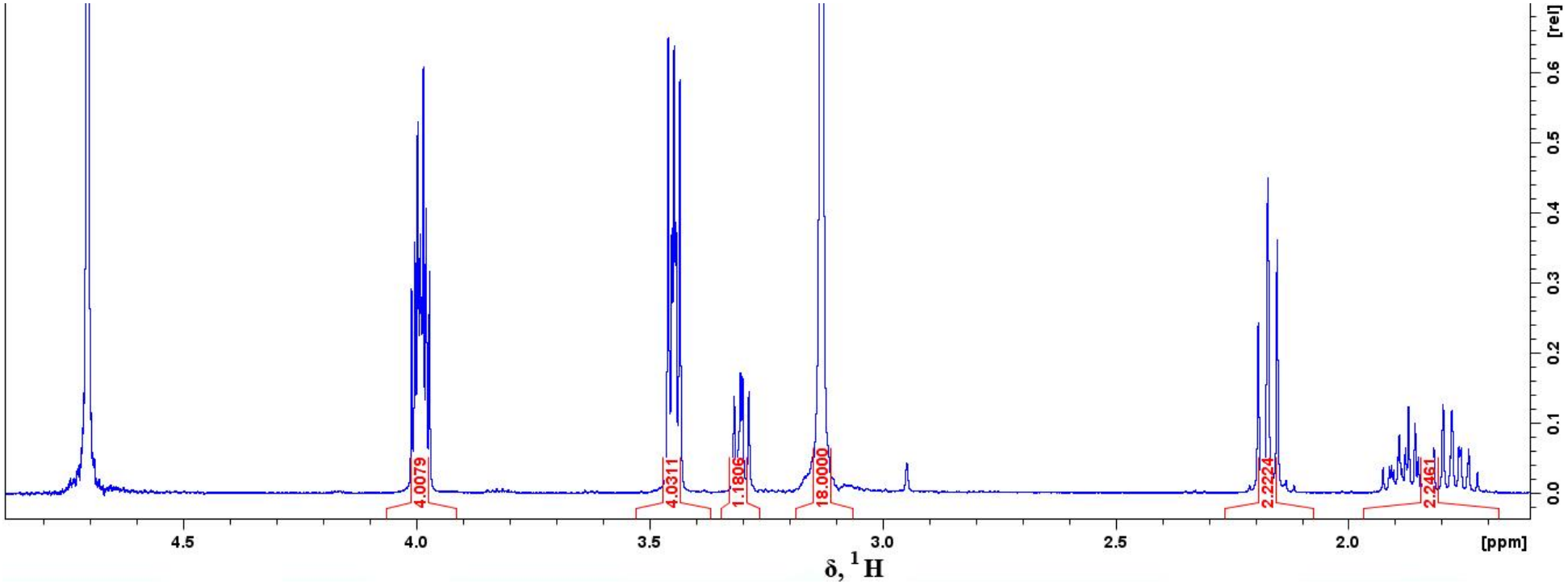

Figure A.4. ^{1}H NMR Spectrum of 100 mM [Ch_2][Glu] in D_2O.

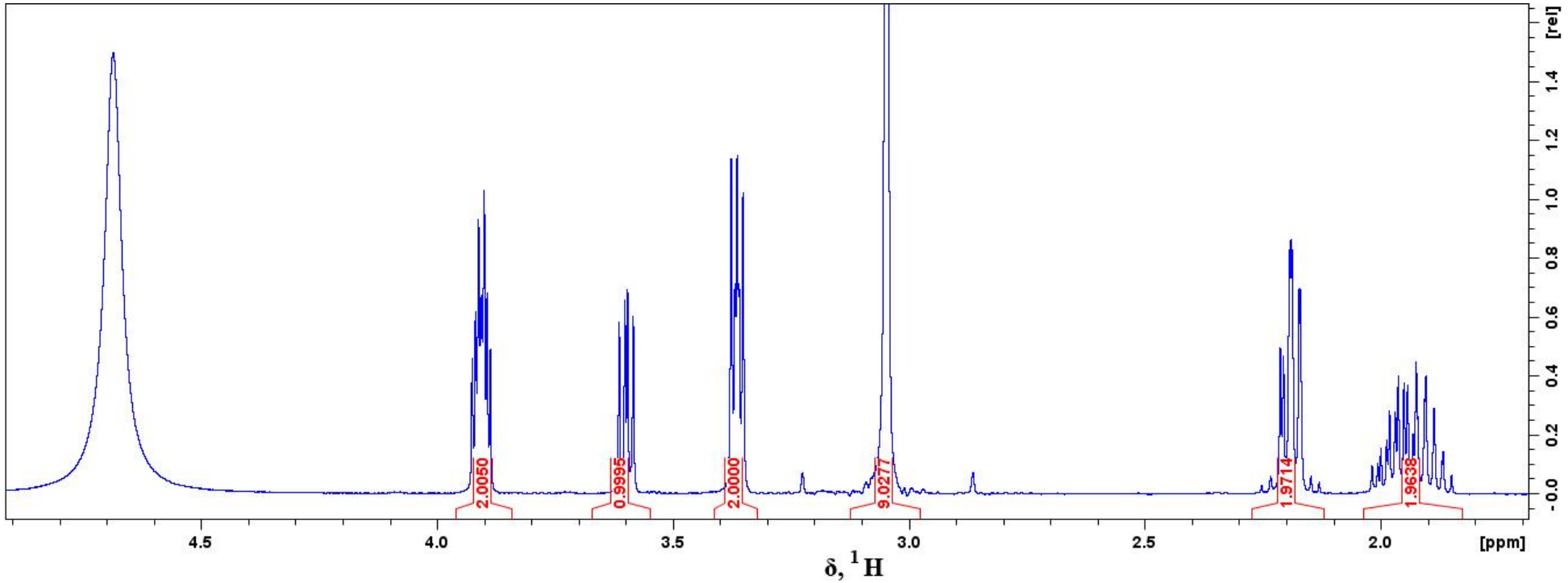

Figure A.5. ^{1}H NMR Spectrum of 500 mM [Ch][Glu] in D_2O.

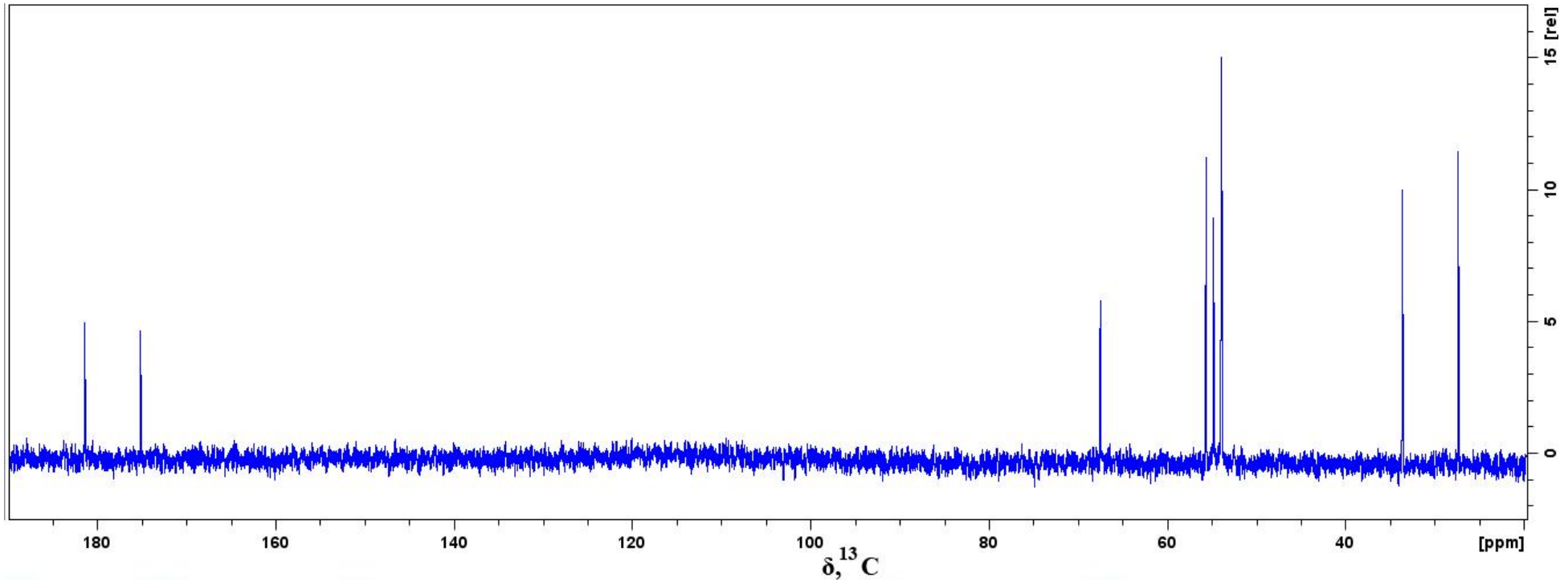

Figure A.6. ^{13}C NMR Spectrum of 100 mM [Ch][Glu] in D_2O.

A. 2. Selective NOE

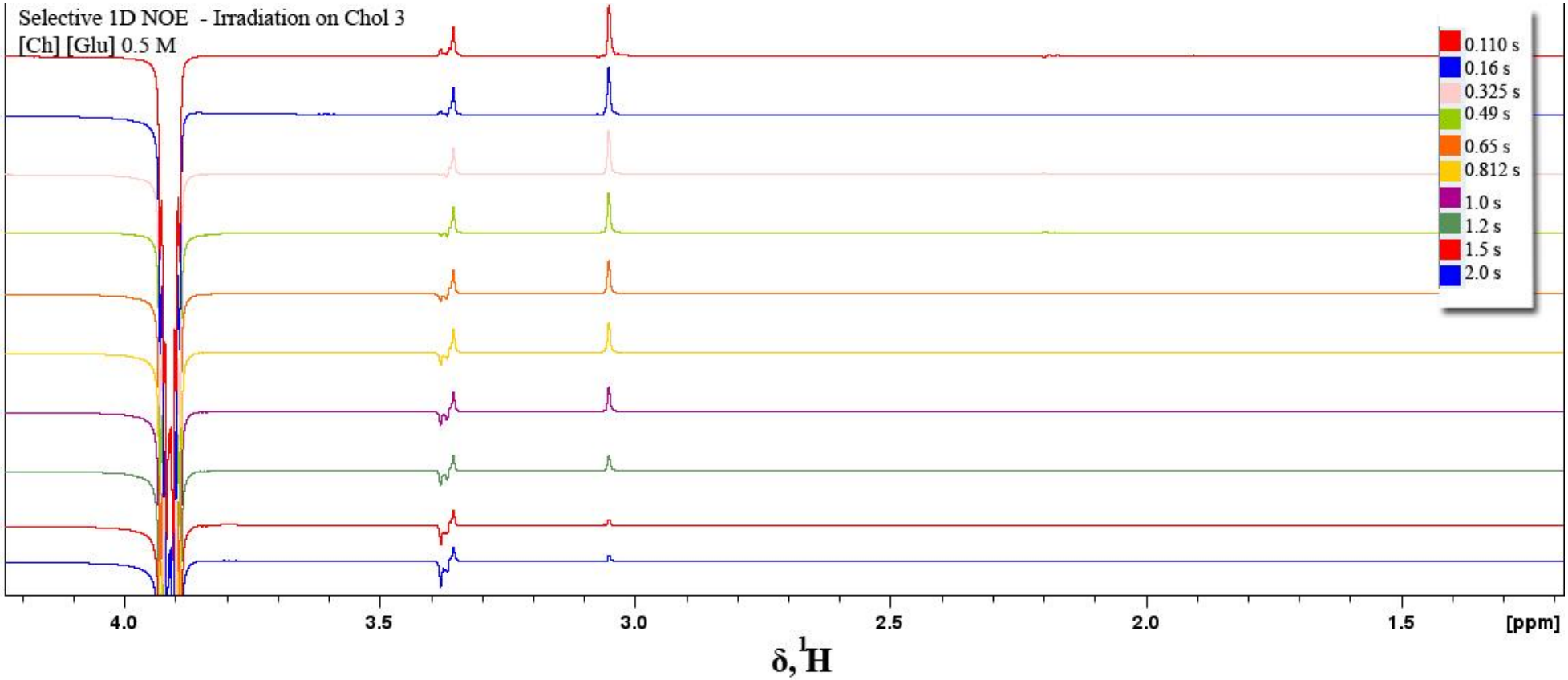

Figure A.7. NOE data for Ch 3 of [Ch][Glu] (1564.15 Hz in D_2O) from a selective 1D-NOESY with the range from 0.110 s to 2.0 s.

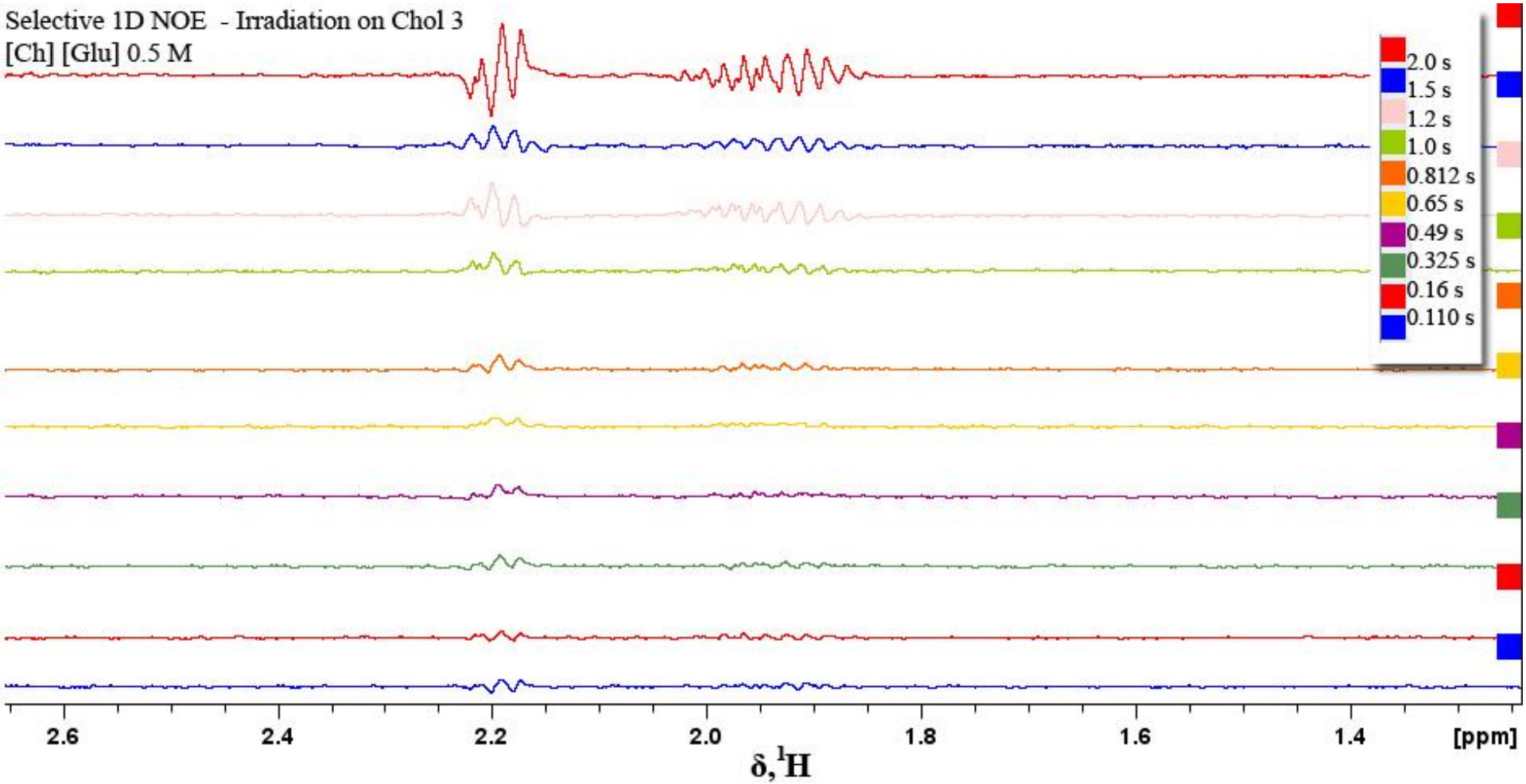

Figure A.8. Zoom of NOE data for Ch 3 of [Ch][Glu] (1564.15 Hz in D_2O) from a selective 1D-NOESY with the range from 0.110 s to 2.0 s.

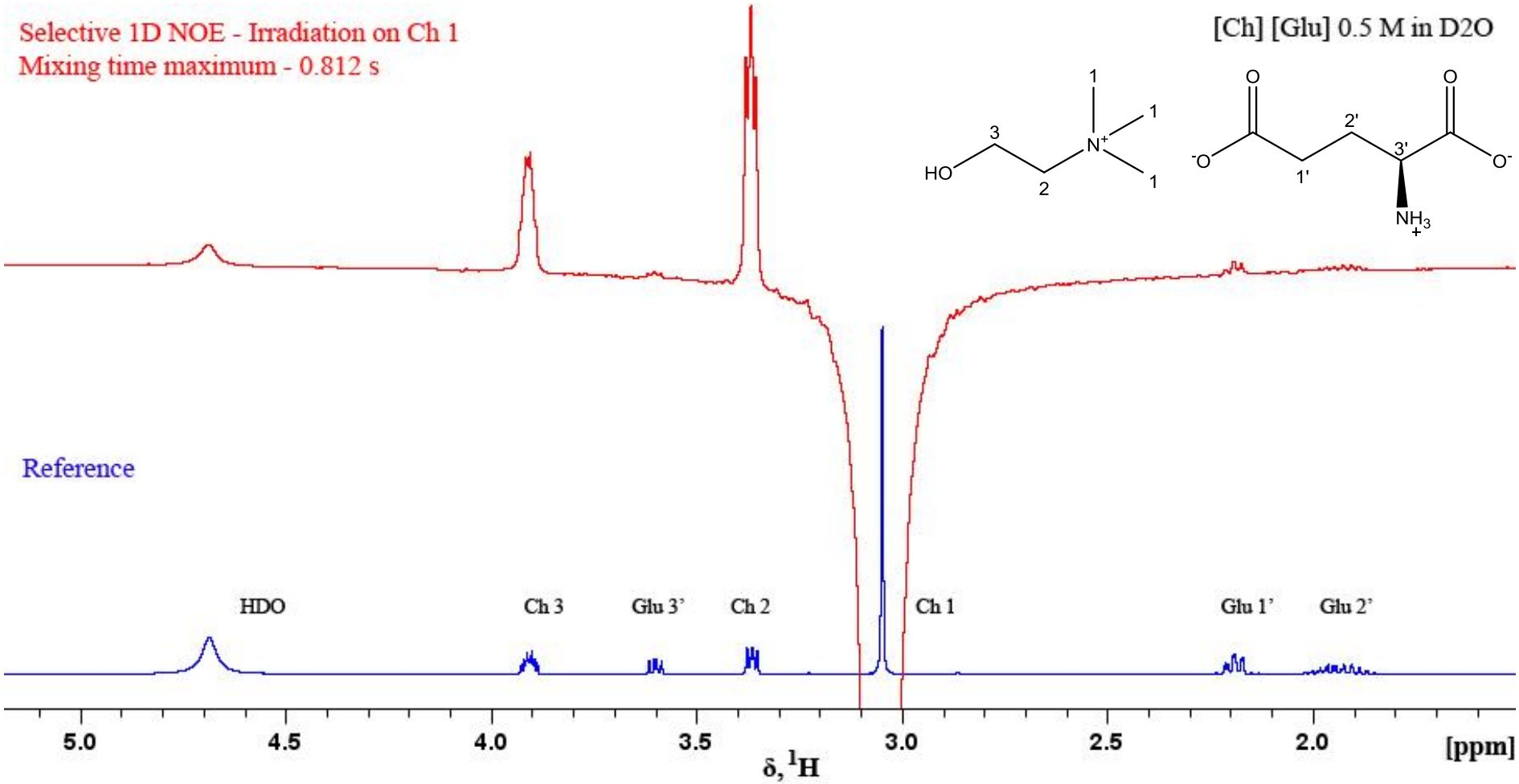

Figure A.9. NOE data for Ch 1 of [Ch][Glu] (1219.13 Hz in D_2O) from a selective 1D-NOESY with 0.812 s mixing time (Top) and reference spectrum with resonance assignments (bottom).

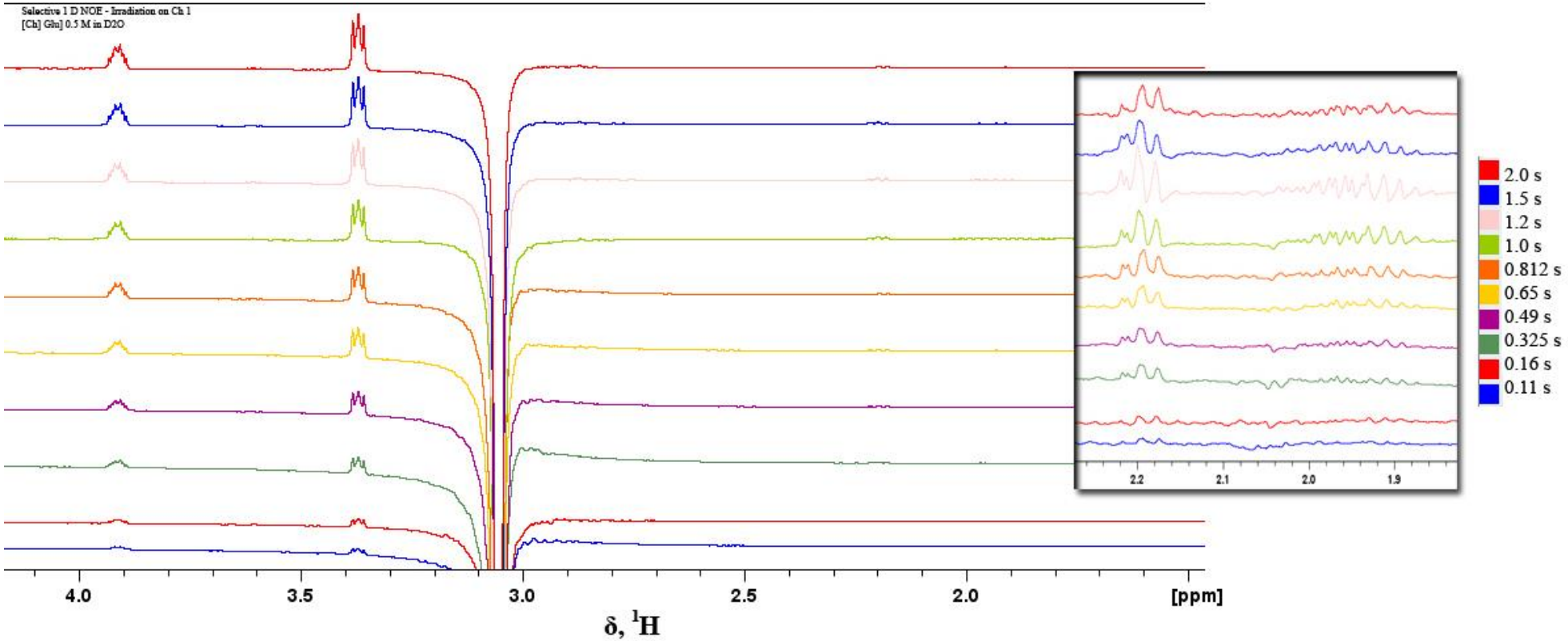

Figure A.10. NOE data for Ch 1 of [Ch][Glu] (1219.13 Hz in D_2O) from a selective 1D-NOESY with the range from 0.110 s to 2.0 s.

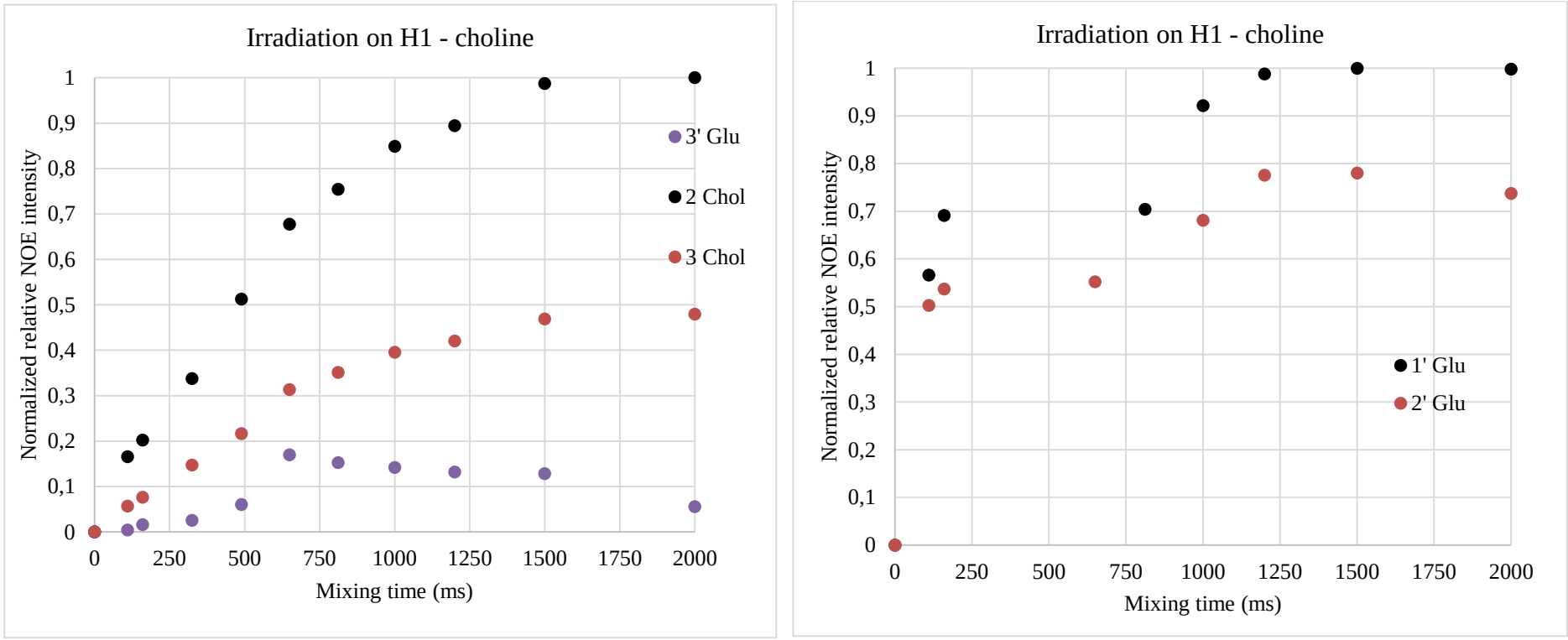

Figure A.11. Left: Calculated normalized relative NOE intensity (1D-NOE Build-up curves) for H 2-Ch and H 3-Ch (intramolecular NOE), H 3'-Glu (intermolecular NOE); Right: Calculated normalized relative NOE intensity for H 1'-Glu and H 2'-Glu (right); For the time range 110 – 2000 ms.

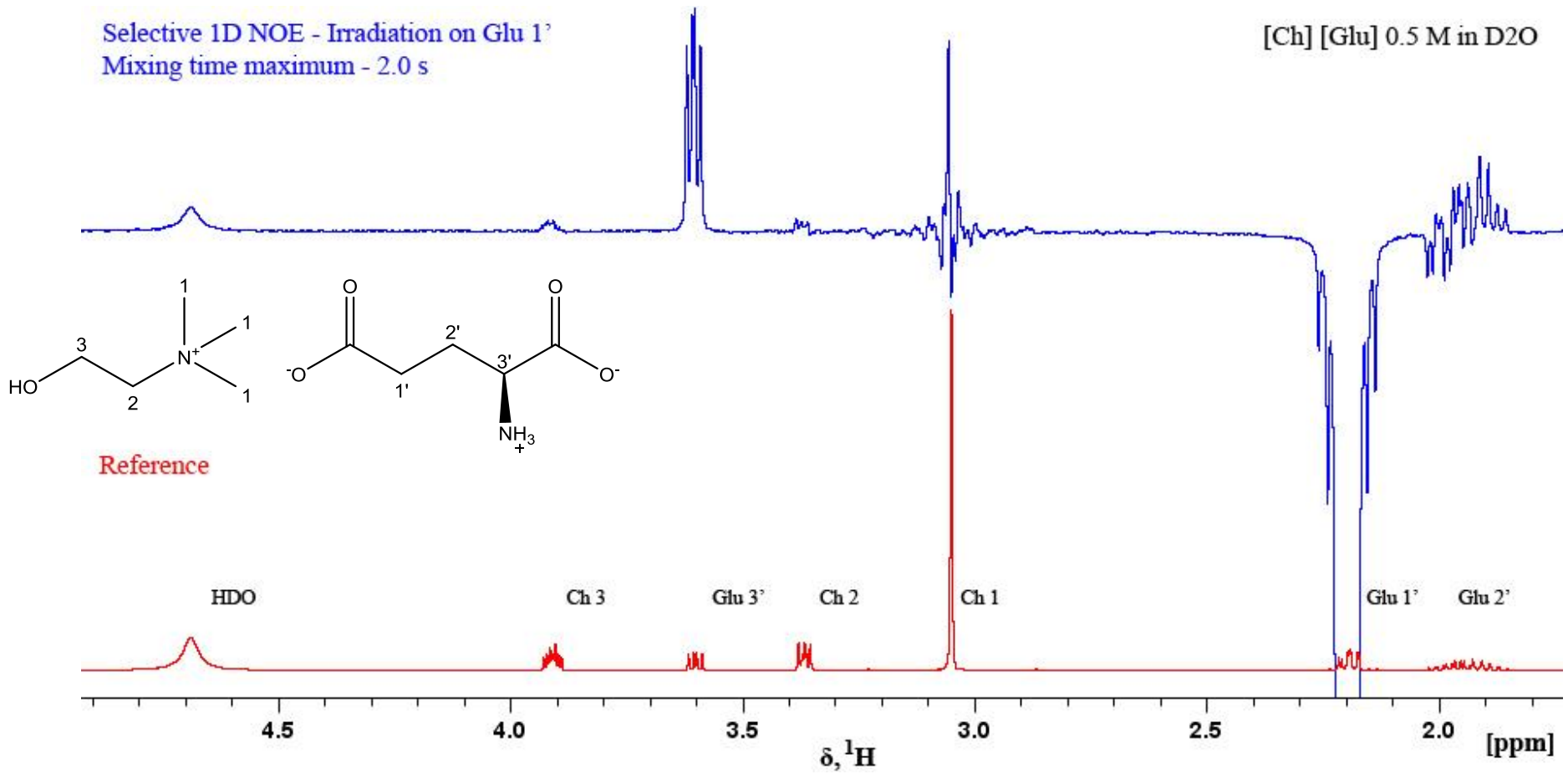

Figure A.12. NOE data for Glu 1' of [Ch][Glu] (876.20 Hz in D_2O) from a selective 1D-NOESY with 2.0 s mixing time (Top) and reference spectrum with resonance assignments (bottom).

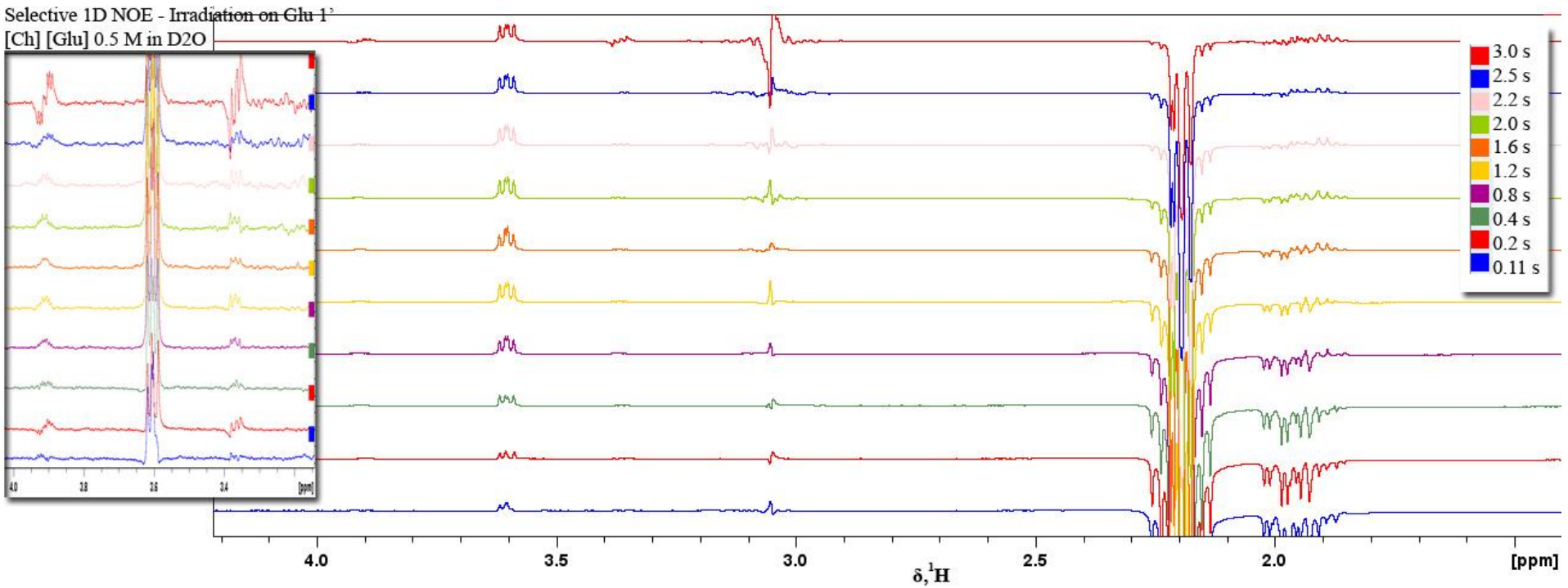

Figure A.13. NOE data for Glu 1' of [Ch][Glu] (876.20 Hz in D_2O) from a selective 1D-NOESY with the range from 0.110 s to 3.0 s.

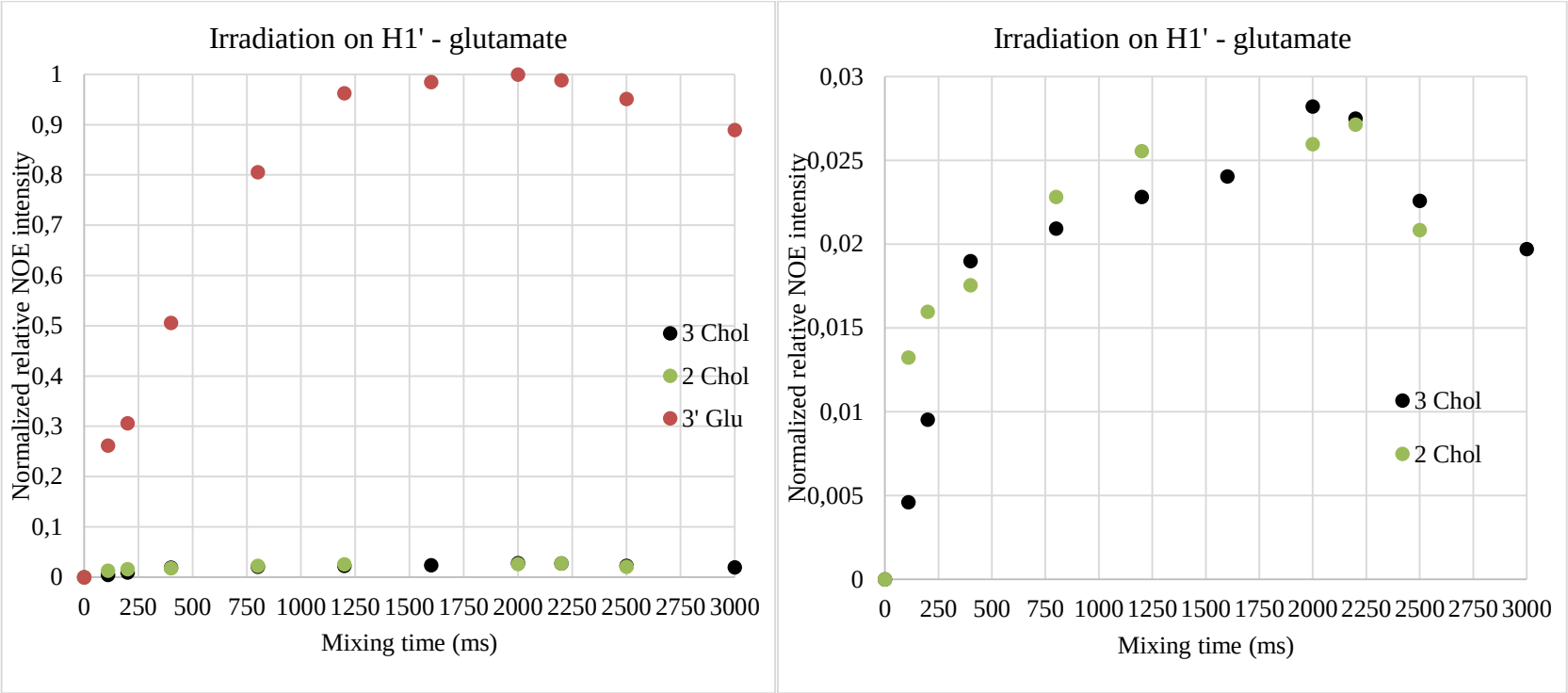

Figure A.14. Left: Calculated normalized relative NOE intensity (1D-NOE Build-up curves) for H 2-Ch and H 3-Ch (intermolecular NOE), H 3'-Glu (intramolecular NOE); Right: Calculated normalized relative NOE intensity for H 3-Ch and H 2-Ch (right); For the time range 110 – 3000 ms.

B. Appendix

B. 1. Selective 1D NOE of Choline-Glutamate IL under crowding conditions

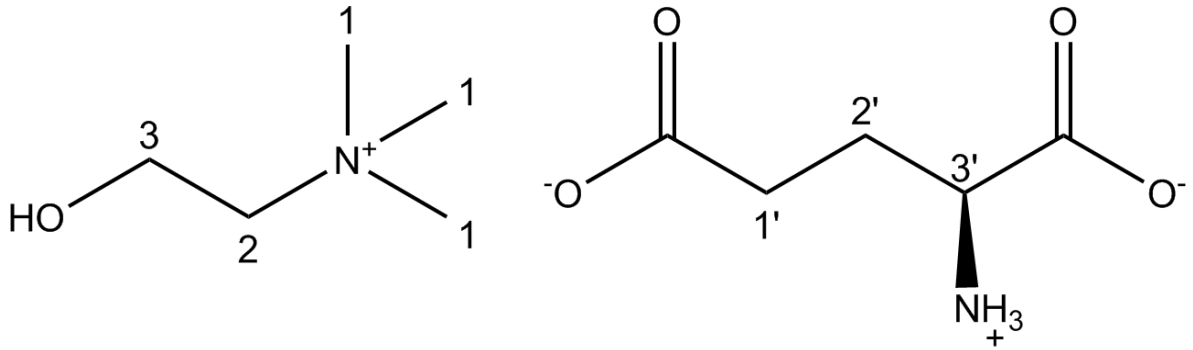

Figure B.1. Structure assignment of [Ch] [Glu] IL.

In aqueous solution (dilute), the distance H3 – Ch/ H2' – Glu, H3' - Glu was around 5.7 Å, discovered by Selective 1D NOE with selectively irradiation on Ch 3 (Chapter II).

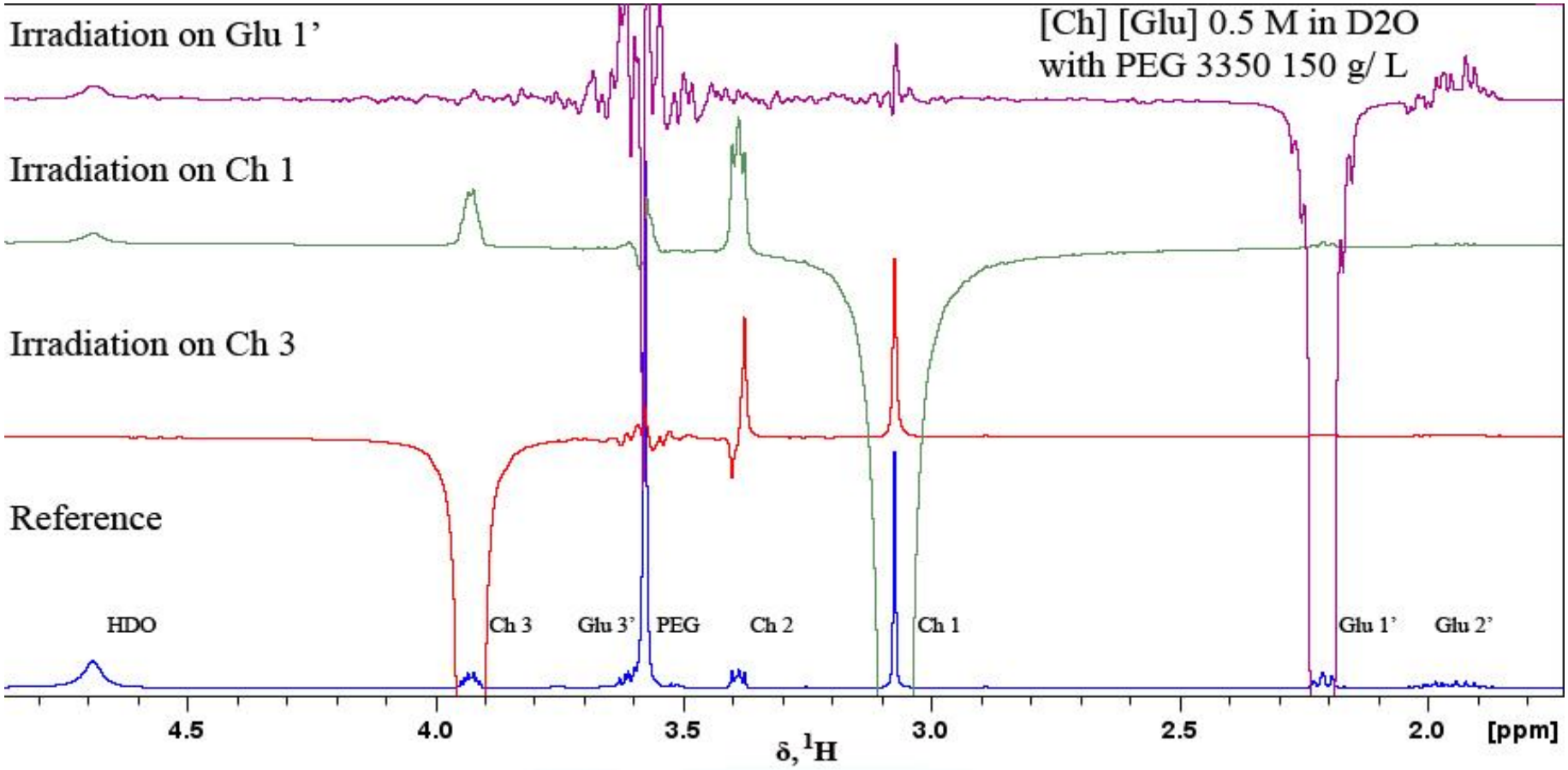

Figure B.2. NOE data for Ch 3; Ch1 and Glu 1' (1571.14 Hz; 1229.67 Hz and 884.96 Hz respectively in D_2O) of 0.5 M [Ch] [Glu] with 150 g/ L PEG 3350, from a selective 1D-NOESY with 0.672 s mixing time and reference spectrum with resonance assignments (bottom).

Due to overlap of PEG on Glu 3' from Figure B. 2. It was not possible the NOE build-up curve for Glu 3' neither the selective 1D NOE for Glu 1' due to the need for an intramolecular interaction for calibration.

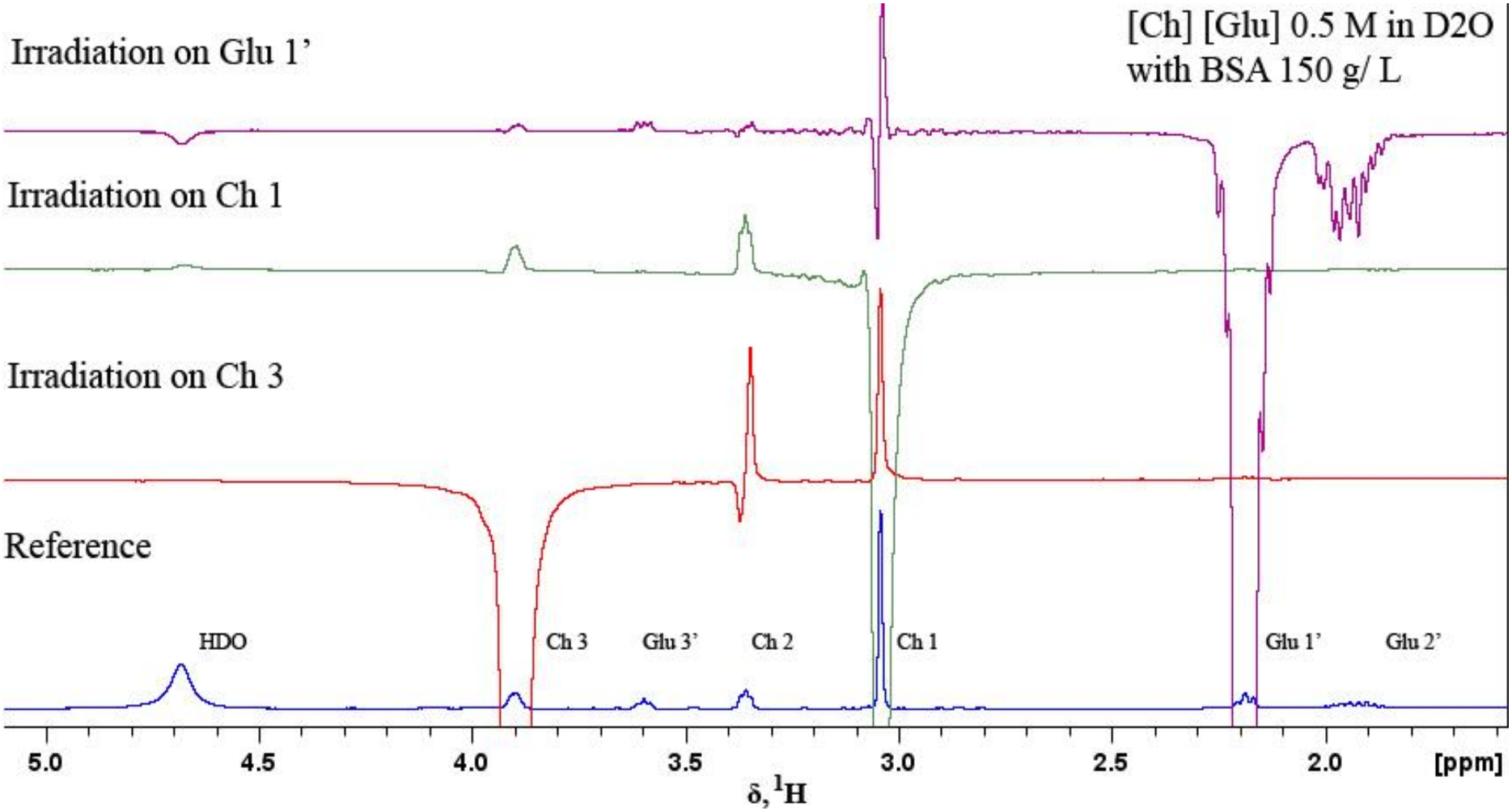

Figure B.3. NOE data for Ch 3; Ch 1 and Glu 1' (1561.41 Hz; 1217.91 Hz and 875.69 Hz respectively in D_2O) of 0.5 M [Ch] [Glu] with 150 g/ L BSA, from a selective 1D-NOESY with 0.70 s mixing time and reference spectrum with resonance assignments (bottom).

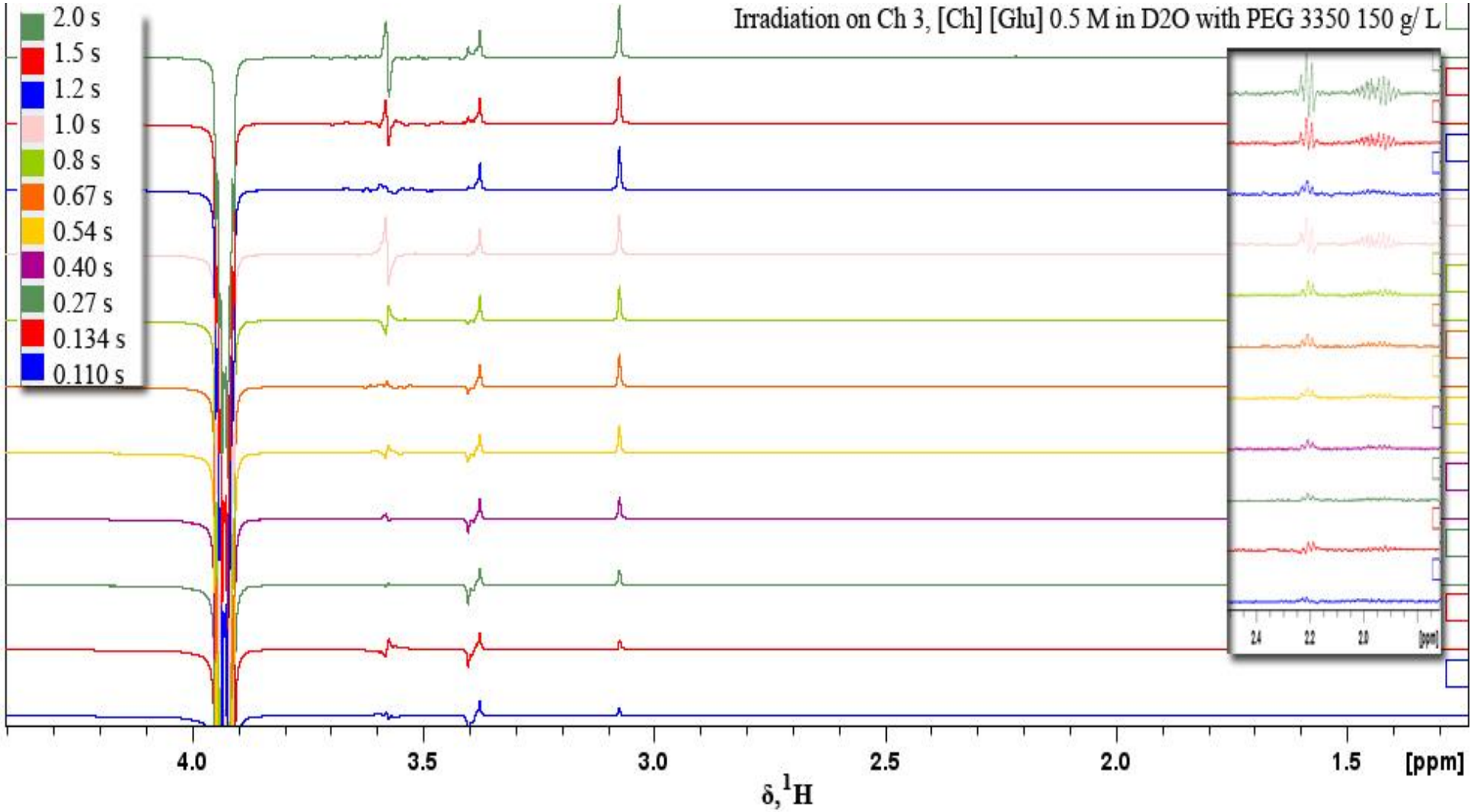

Figure B.4. NOE data for Ch 3 of 0.5 M [Ch] [Glu] with 150 g/L PEG 3350 (1571.13 Hz in D_2O) from a selective 1D-NOESY with the range from 0.110 s to 2.0 s.

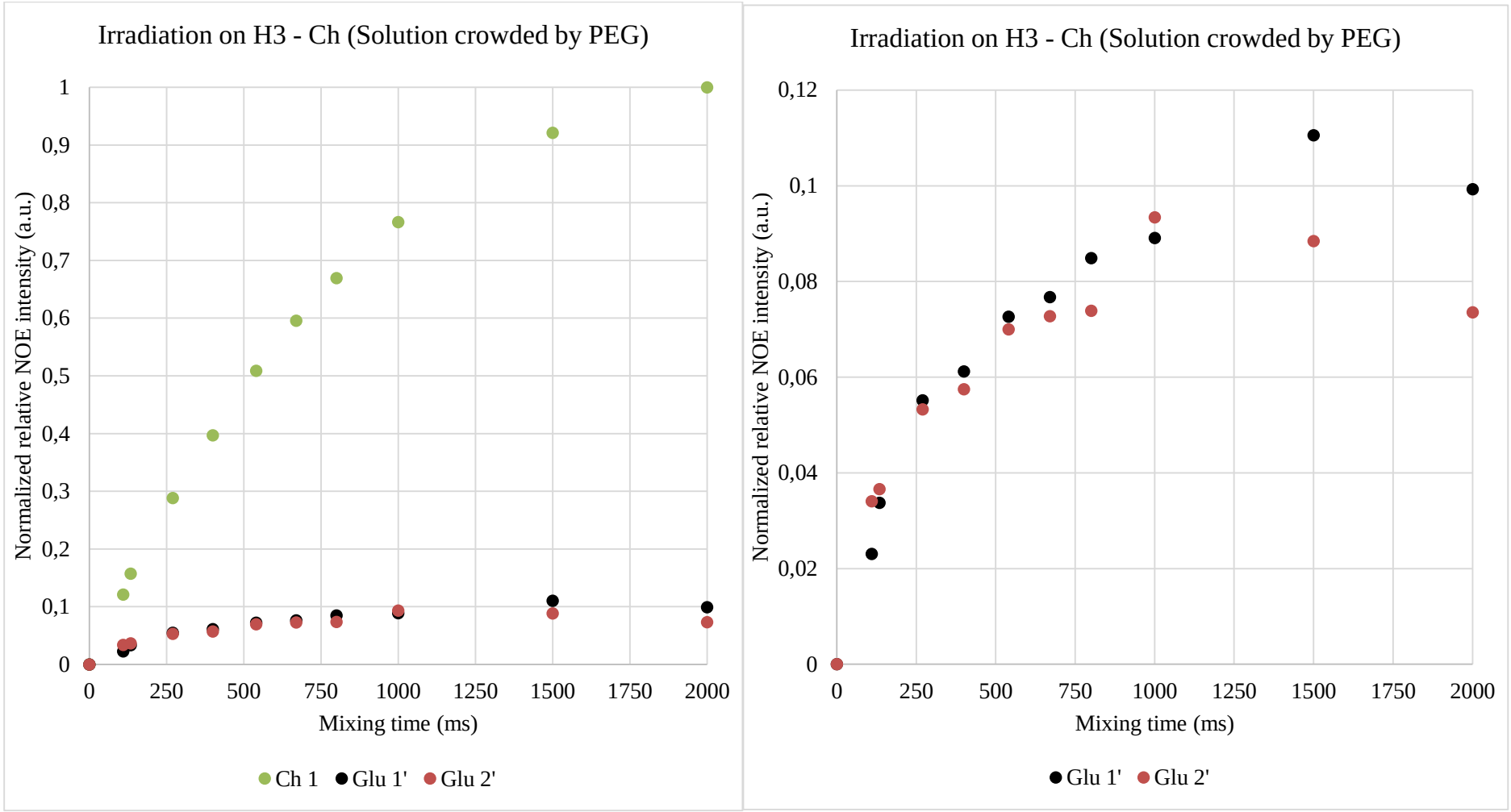

Figure B.5. Left: Calculated normalized relative NOE intensity (1D-NOE Build-up curves) for H 1-Ch (intramolecular NOE), H 1'-Glu and H 2'-Glu (intermolecular NOE); Right: Zoom for H 1'-Glu and H 2'-Glu build-up curves. For the time range 110 – 2000 ms.

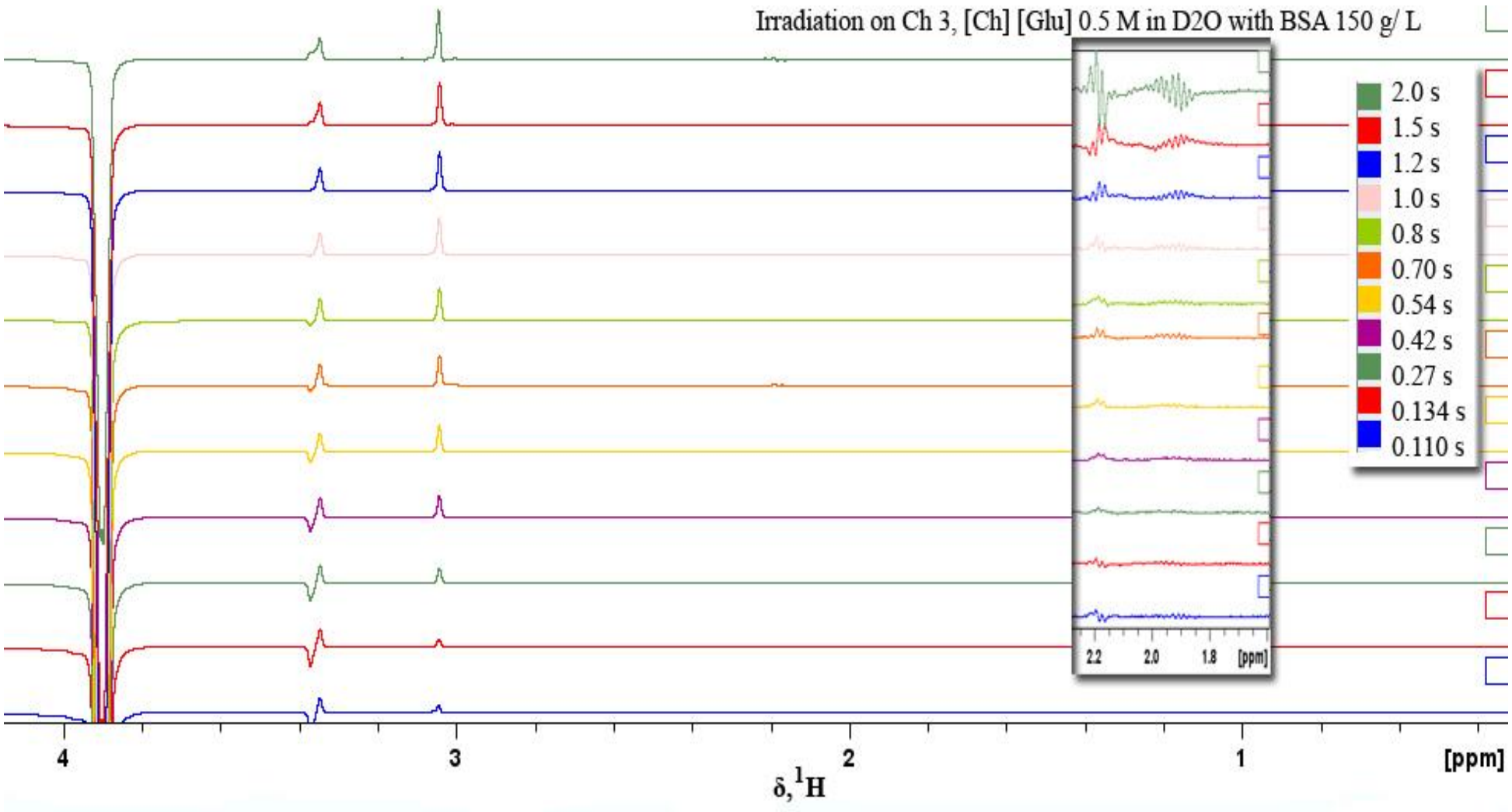

Figure B.6. NOE data for Ch 3 of 0.5 M [Ch] [Glu] with 150 g/ L BSA (1561.41 Hz in D_2O) from a selective 1D-NOESY with the range from 0.110 to 2.0 s.

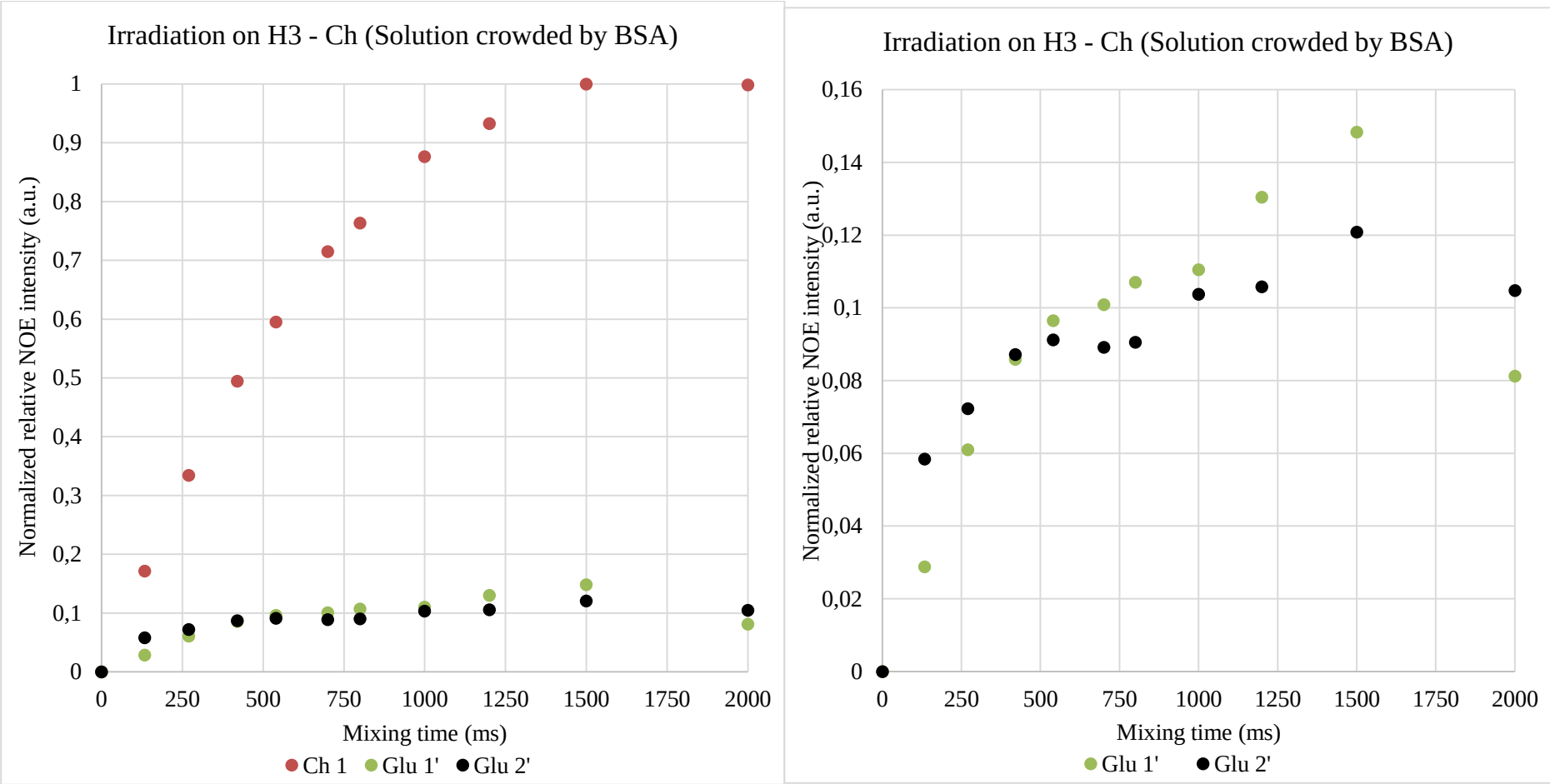

Figure B.7. Left: Calculated normalized relative NOE intensity (1D-NOE Build-up curves) for H 1-Ch (intramolecular NOE), H 1'-Glu and H 2'-Glu (intermolecular NOE); Right: Zoom for H 1'-Glu and H 2'-Glu (intermolecular) build-up curves. For the time range 134 – 2000 ms.

Table B.1. 1D - NOE data for Ch 1 on 0.5 M [Ch] [Glu] with 150 g/ L of PEG 3350 or BSA, on the range 110 ms - 2000 ms. [a]Not possible to integrate.

On Ch 1	Normalized relative NOE intensities (a.u.)								
150 g/ L PEG 3350					150 g/ L BSA				
Mixing time (ms)	**Ch 3**	**Ch 2**	**Glu 1'**	**Glu 2'**	**Mixing time (ms)**	**Ch 3**	**Ch 2**	**Glu 1'**	**Glu 2'**
110	0.053	0.104	0.194	0.240	**110**	- [a]	-	0.43501	0
160	0.066	0.125	0.295	0.200	**134**	0.067	0.219	-	-
325	0.141	0.287	0.442	0.379	**270**	0.149	0.404	-	-
490	0.202	0.425	0.579	0.434	**420**	0.221	0.553	-	-
650	0.262	0.551	0.674	0.594	**540**	0.272	0.643	0.755	0.681
812	0.308	0.651	0.791	0.608	**700**	0.324	0.745	-	-
1000	0.350	0.724	0.852	0.714	**800**	0.354	0.817	-	-
1200	0.395	0.826	1.000	0.715	**1000**	0.401	0.904	0.933	0.845
1500	0.441	0.913	0.910	0.729	**1200**	0.434	0.961	0.967	0.903
2000	0.480	1.000	0.904	0.676	**1500**	0.458	1.000	1.000	0.894
					2000	0.466	0.993	0.880	0.614

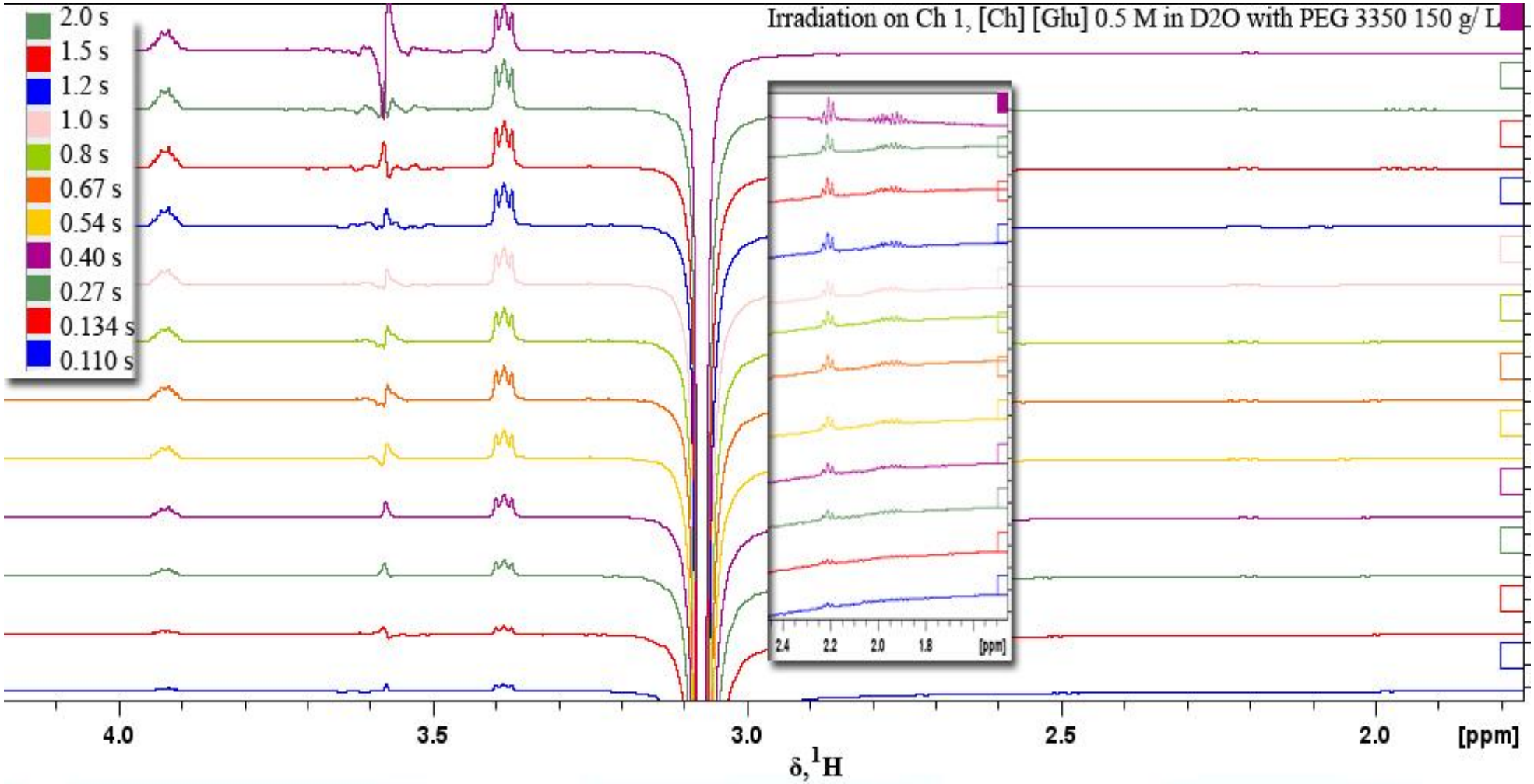

Figure B.8. NOE data for Ch 1 of 0.5 M [Ch] [Glu] with 150 g/ L PEG 3350 (1229.67 Hz in D_2O) from a selective 1D-NOESY with the range from 0.110 s to 2.0 s.

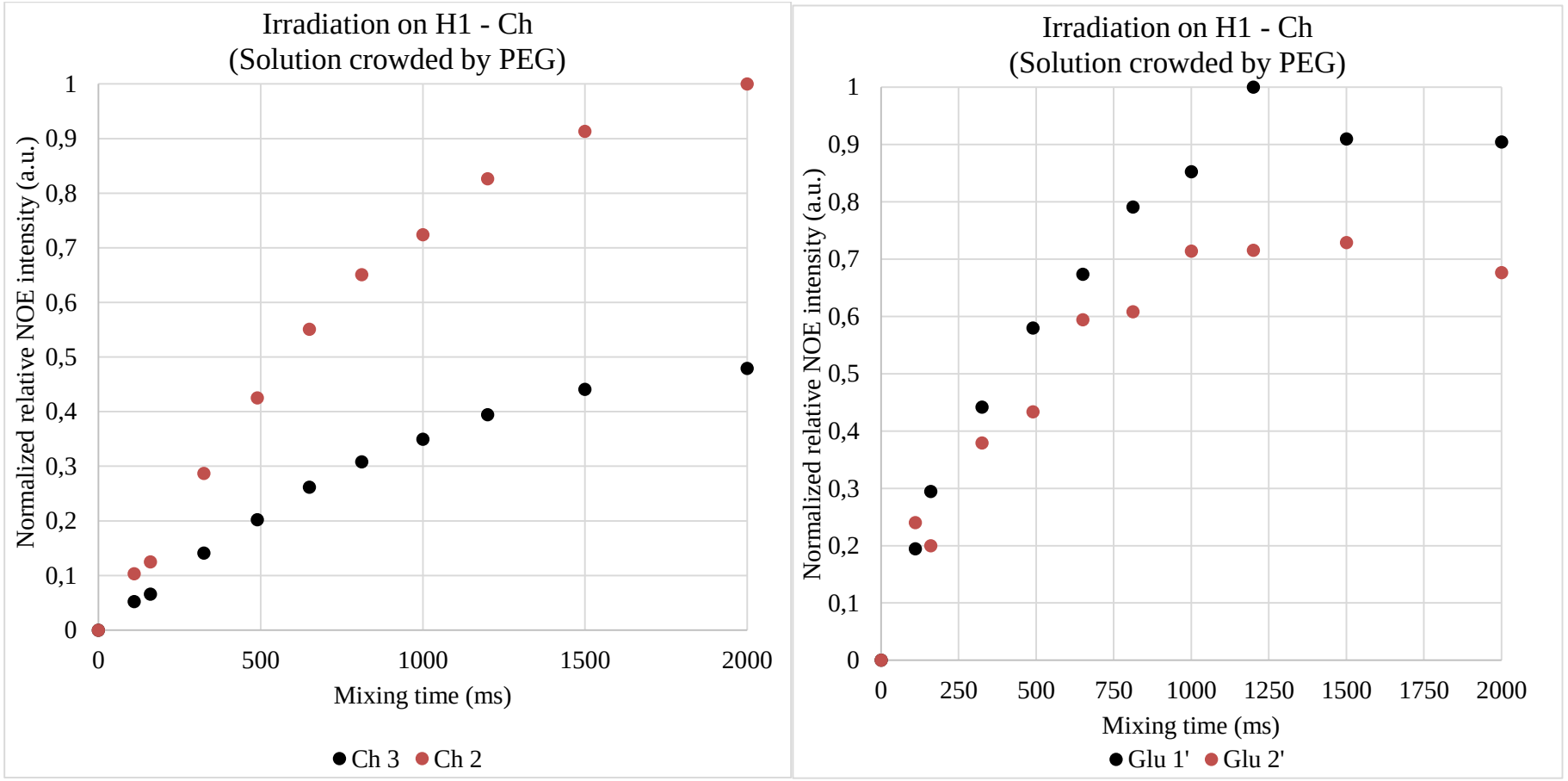

Figure B.9. Top: Calculated normalized relative NOE intensity (1D-NOE Build-up curves) for H 3-Ch and H 2-Ch (intramolecular NOE); Right: Calculated normalized relative NOE intensity for H 1'-Glu and H 2'-Glu (intermolecular) build-up curves. For the time range 110 – 2000 ms.

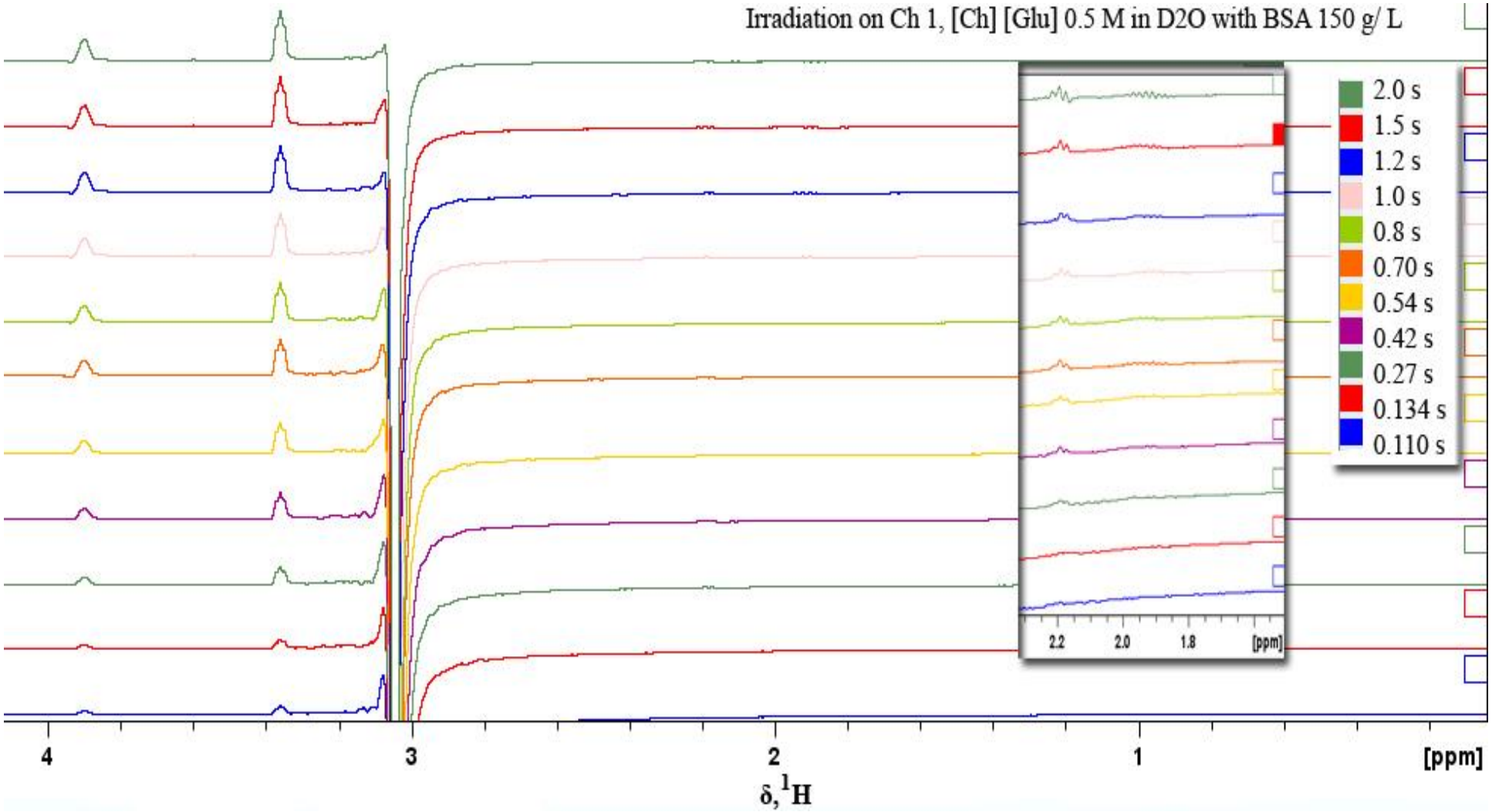

Figure B.10. NOE data for Ch 1 of 0.5 M [Ch] [Glu] with 150 g/ L BSA (1217.91 Hz in D_2O) from a selective 1D-NOESY with the range from 0.110 s to 2.0 s.

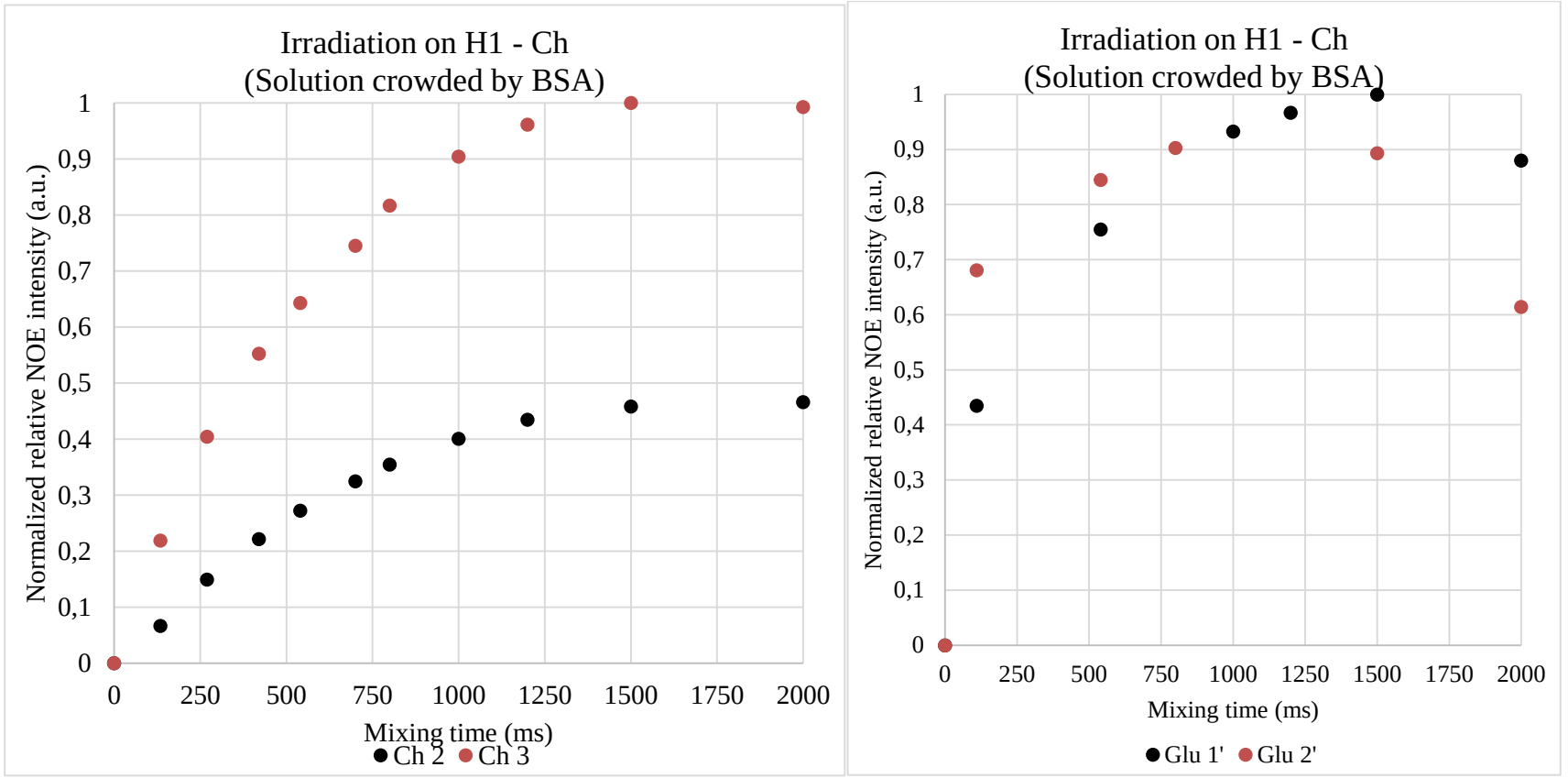

Figure B.11. Left: Calculated normalized relative NOE intensity (1D-NOE Build-up curves) for H 3-Ch and H 2-Ch (intramolecular NOE); Right: Calculated normalized relative NOE intensity for H 1'-Glu and H 2'-Glu (intermolecular) build-up curves. For the time range 110 – 2000 ms.

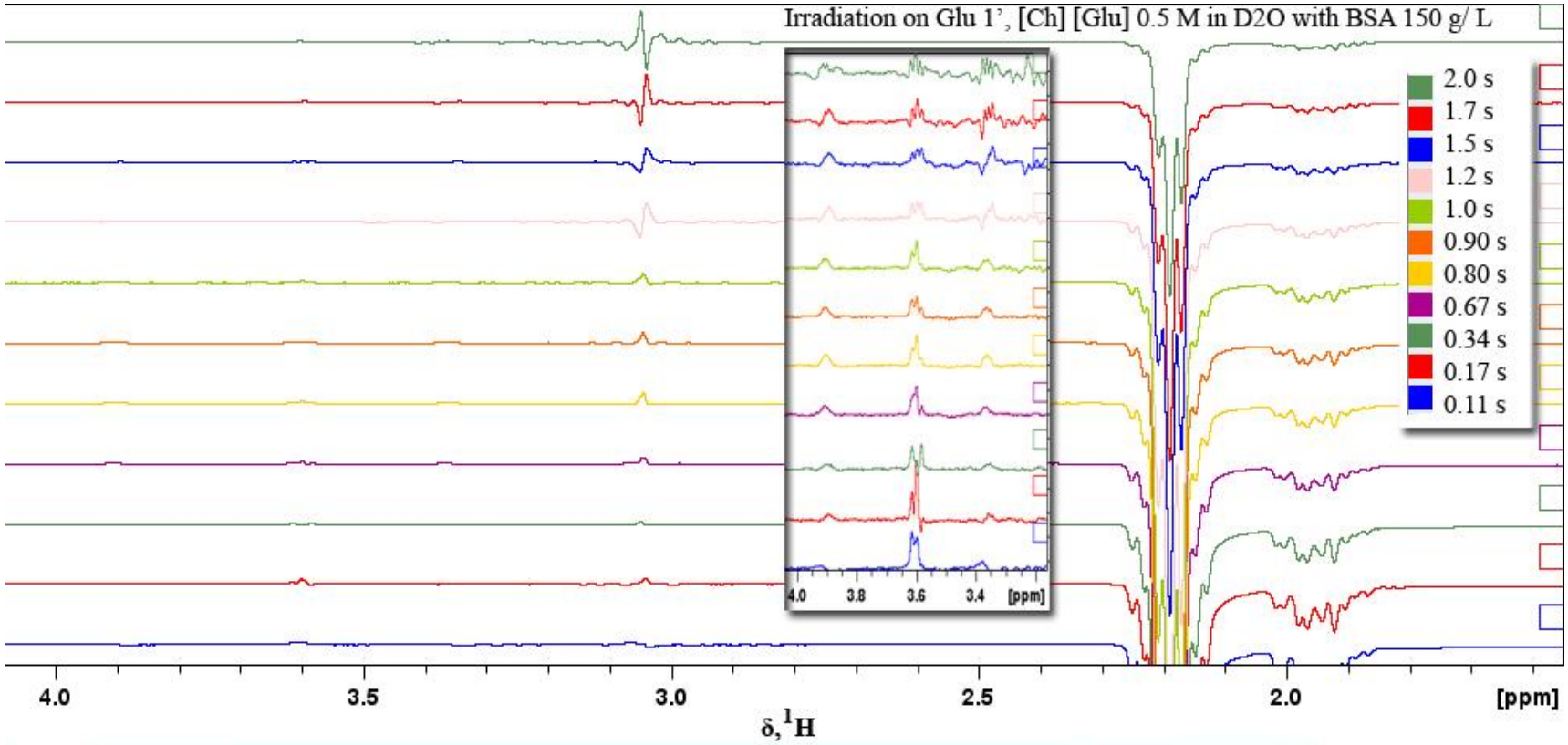

Figure B.12. NOE data for Glu 1' of 0.5 M [Ch] [Glu] with 150 g/ L BSA (1217.91 Hz in D_2O) from a selective 1D-NOESY with the range from 0.110 s to 2.0 s.

Due to weak intensities from Figure B. 12. It was not possible plotting these intensities against the mixing time leads to the NOE build-up curves.

C. Appendix

C. 1. Molecular Biology Reagents

Table C.1. Preparation of the Luria-Bertani (LB) Medium.

1 L H_2O *	LB Medium	**Tryptone**	10 g/L
		Yeast extract	5 g/L
		NaCl	10 g/L

*D2O (oxide deuterium) 99.9% D (*Euriso-Top*) in the deuterated protein lysate case.

Table C.2. Preparation of the M9 minimal medium composition.

500 mL	**10 x M9 Salts * pH= 7.5 (50 mL)**	**$Na_2HPO_4.7H2O$**	**128 g**/L
		KH_2PO_4	30 g/L
		NaCl	5 g/L
	M9 Medium	**$MgSO_4$**	2 mM
		$CaCl_2$	100 µM
		Glucose	4 g/L
		Thiamine-HCl	10 mg/ L
		$FeSO_4$	100 µM
		Ampicillin	100 µg/ mL
		$^{15}NH_4Cl$ (15N 99% *Cambridge Isotope Laboratories*)	2.5 g/L

*Autoclave for 15 min at 121°C. Let cool down to room temperature.

SDS-PAGE (Gel Electrophoresis): The preparation of Tris-Tricine SDS-PAGE was based on the protocol of Schägger.[234]

Table C.3. Compositions of the Tris-Tricine SDS-PAGE stacking and running gels.

Number of gels	**Stock Solution**	**Stacking gel**	**Running gel**	
2		**4%**	**10%**	**12%**
	3M Tris-HCl/SDS pH=8.45	1550 µL	5000 µL	5000 µL
	Acrylamide (30%)	800	5000	6000
	H2O	3900	3500	2500
	Glycerol	-	1500	1500
	APS 30%	14	14	14
	TEMED	14	14	14

Running of the samples:
Loading 15-20 µL into the gel.
Sample: 5µL Sample Buffer (6x) + 15 µL Sample (Boiled for 5 min if necessary).
Marker: 3 µL Marker, 5 µL Sample Buffer + 12 µL H_2O.
Electrophoresis: 45 min, 200 mV, 200 mA.

Table C.4. Composition of the stock solutions for Tris-Tricine SDS-PAGE.

	Anode Buffer (10x)	**Cathode Buffer (10x)**	**Gel buffer (3x)**
Tris (M)	1.0	1.0	3.0
Tricine (M)	-	1.0	-
HCl (M)	0.225	-	1.0
SDS (%)	-	1.0	0.3
pH	8.9	8.25	8.45

Keep solutions at room temperature (20–25 °C).
Do not correct the pH of the cathode buffer, which ideally should be close to 8.25.

Table C.5. Composition of Sample Buffer, Coomassie brilliant blue and destaining solution.

SDS-PAGE 6x Sample Buffer		**Coomassie brilliant blue**		**Destaining Solution**	
Tris-HCl/SDS, pH=6.8	7mL	Coomassie brilliant blue	1g	Acetic Acid	75 mL
Glycerol (30%)	3 mL	Acetic Acid	15 mL	Methanol	450 mL
SDS (10%)	1g	Methanol	90 mL	H_2O	Up to 1L
DTT (0.6M) or β-Mercaptoethanol	0.93g	H_2O	Up to 200 mL		
Bromophenol Blue	1.2 mg				
H_2O (if necessary)	Up to 20 mL				

C. 2. Results of ^{15}N Labeled WT GB1 expression and purification

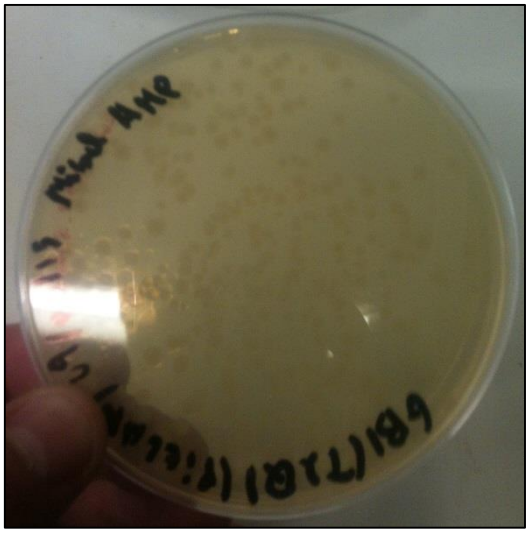

Figure C.1. Plate with colony of WT GB1.

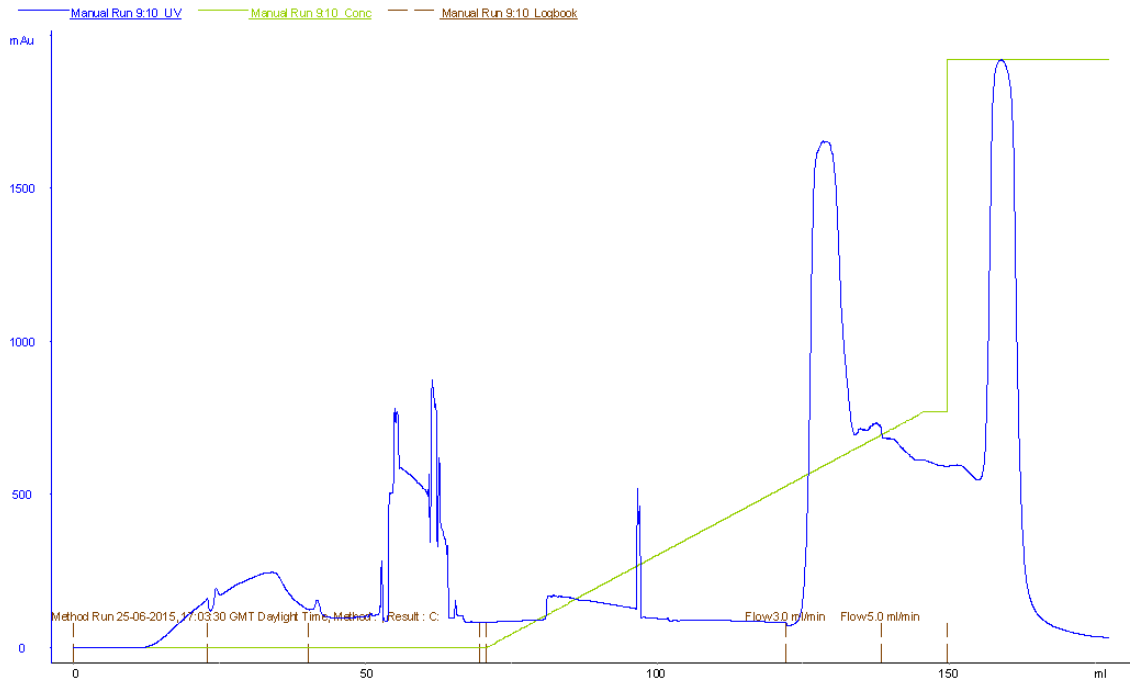

Figure C.2. One of the ^{15}N labeled GB1 purifications by anion exchange chromatography, GB1 found at 350-400 mM NaCl.

Fractions were assessed by using SDS 12% Tris-Tricine gels with Coomassie Brilliant Blue staining.

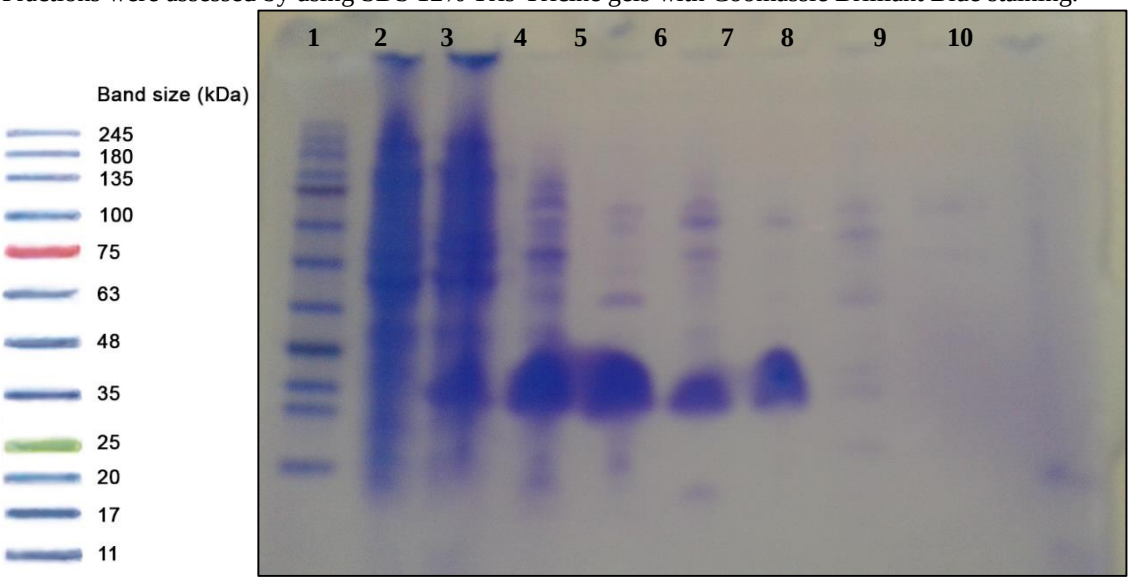

Figure C.3. 12% Tris-Tricine SDS gel of fractions after anion exchange.

Lane 1- NZY Colour Protein Marker II; 2 – Before IPTG induction; 3 – After IPTG induction; 4 – Supernatant dialysed; 5 – (1 purif.) Fraction at 350 mM NaCl (peak, GB1) ; 6 – (1 purif.) Wash with start buffer; 7 – (2 purif.) Fraction at 300 mM NaCl (peak, GB1); 8 – (2 purif.) Fraction at 350 mM NaCl; 9 – (2 purif.) Fraction at 1M NaCl; 10 – GB1 with Tag purified.

In this purification, the GB1 not be linked fully to column, minimal amount leaving in last Wash (without NaCl). Fractions containing GB1 were pooled and concentrated for further purification by size exclusion chromatography:

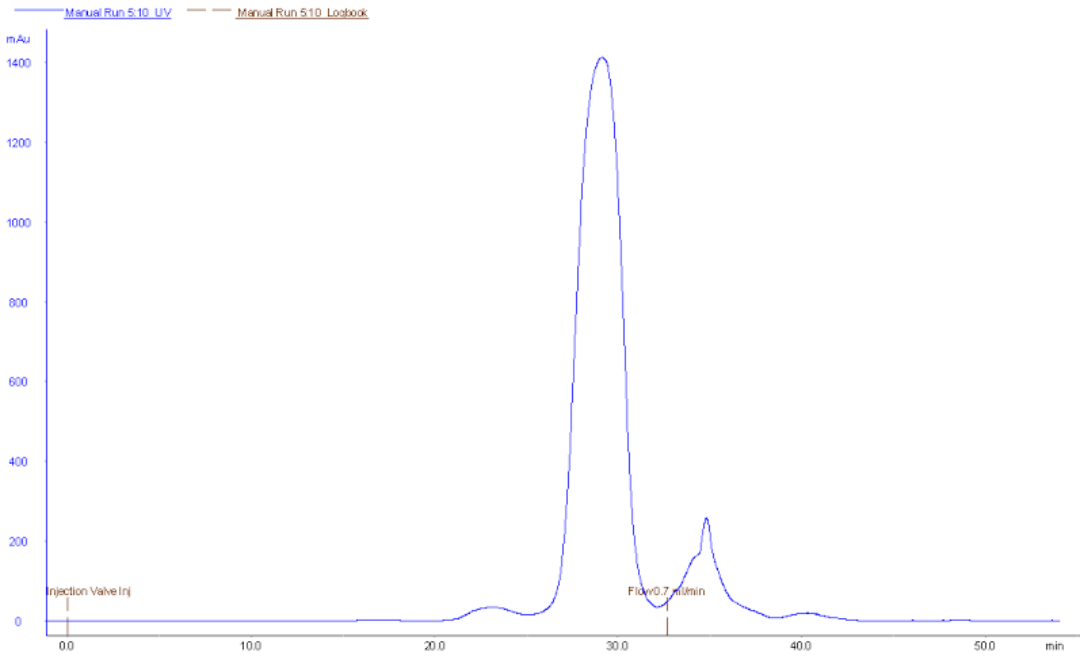

Figure C.4. One of the ^{15}N labeled GB1 purifications by exclusion molecular chromatography.

C. 3. ^{1}H-^{15}N HSQC data

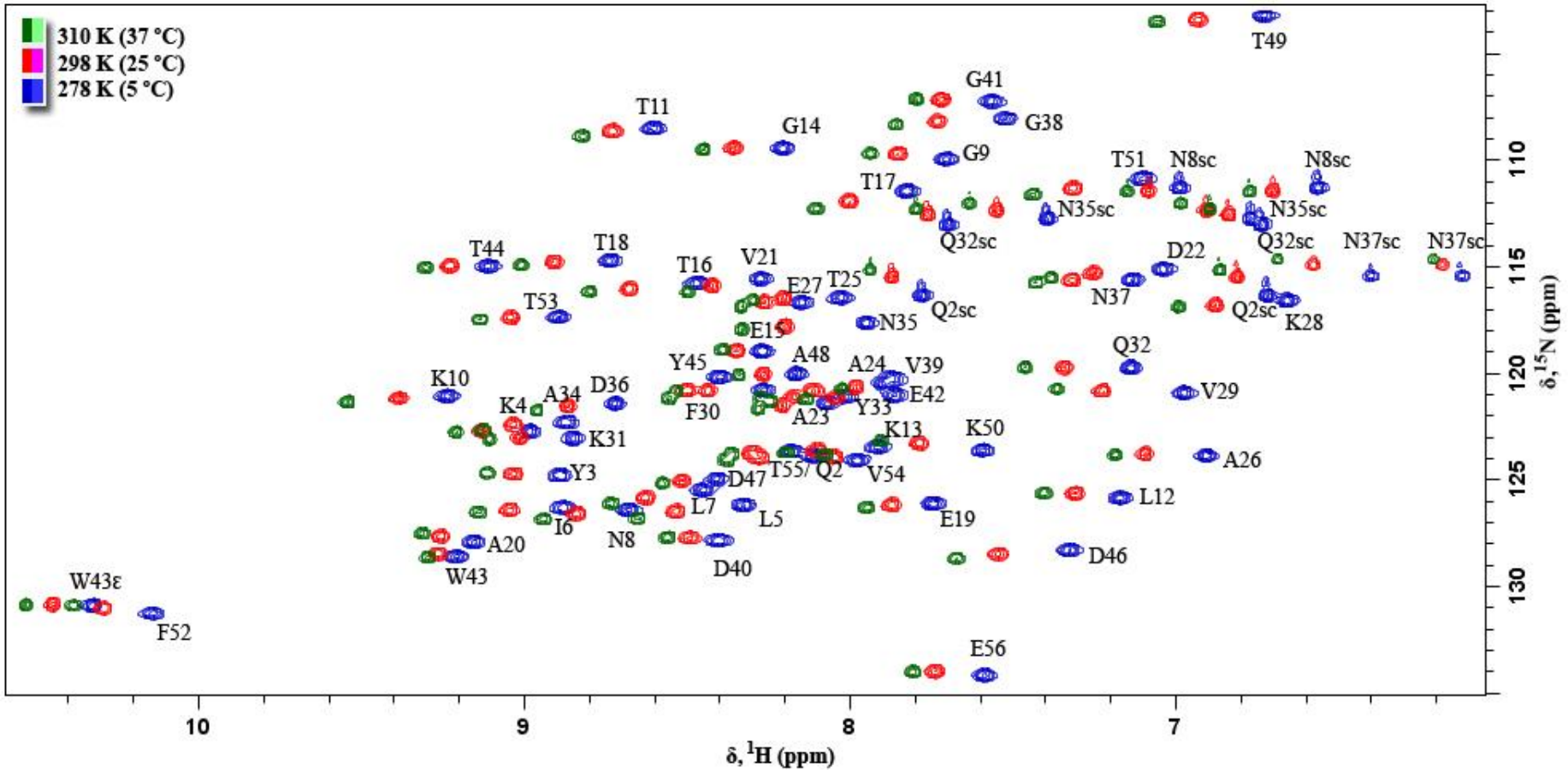

Figure C.5. Superposition of ^{1}H-^{15}N-HSQC spectra of 0.24 mM GB1 in 90% H_2O/ 10% $^{2}H_2O$ (pH 7.13) at 278.15 K (blue), 298.15 (red) and 310.15 K (green). Assignments are based on published work.[203]

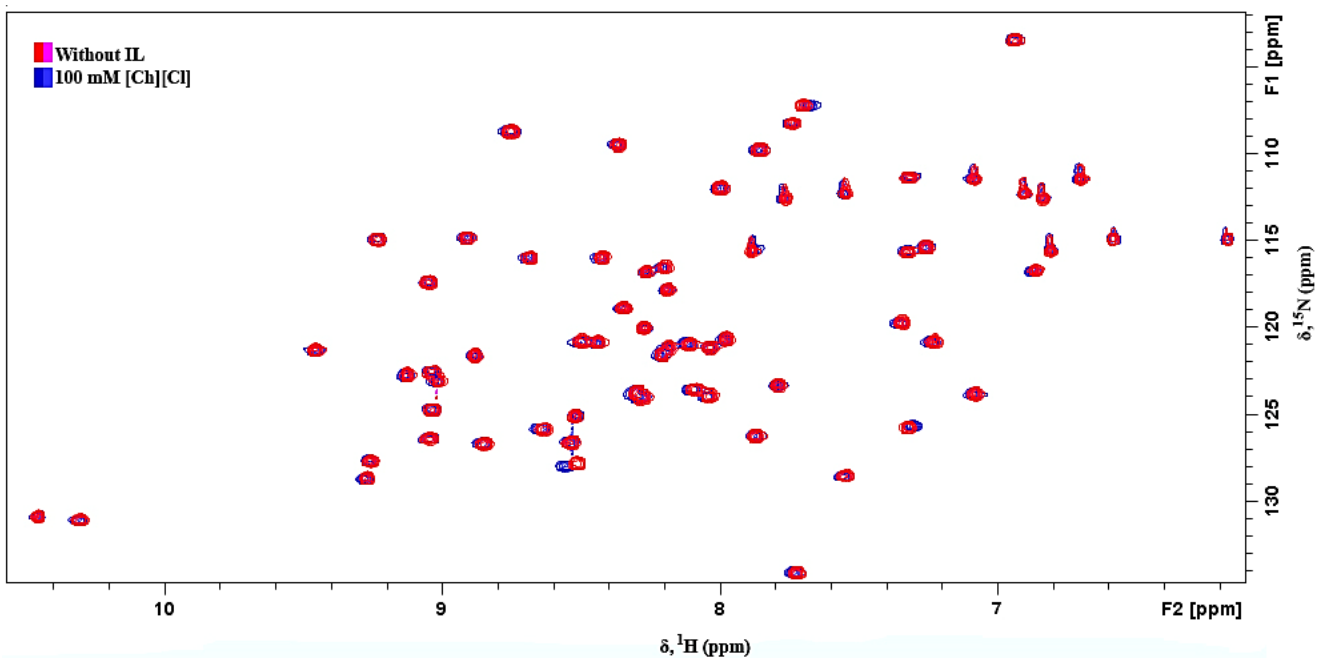

Figure C.6. Superposition of ^{1}H-^{15}N-HSQC spectra of 0.24 mM GB1 without IL (red) and GB1 with 100 mM [Ch][Cl] (blue), in 90% H_2O/ 10% $^{2}H_2O$ at 298.15 K.

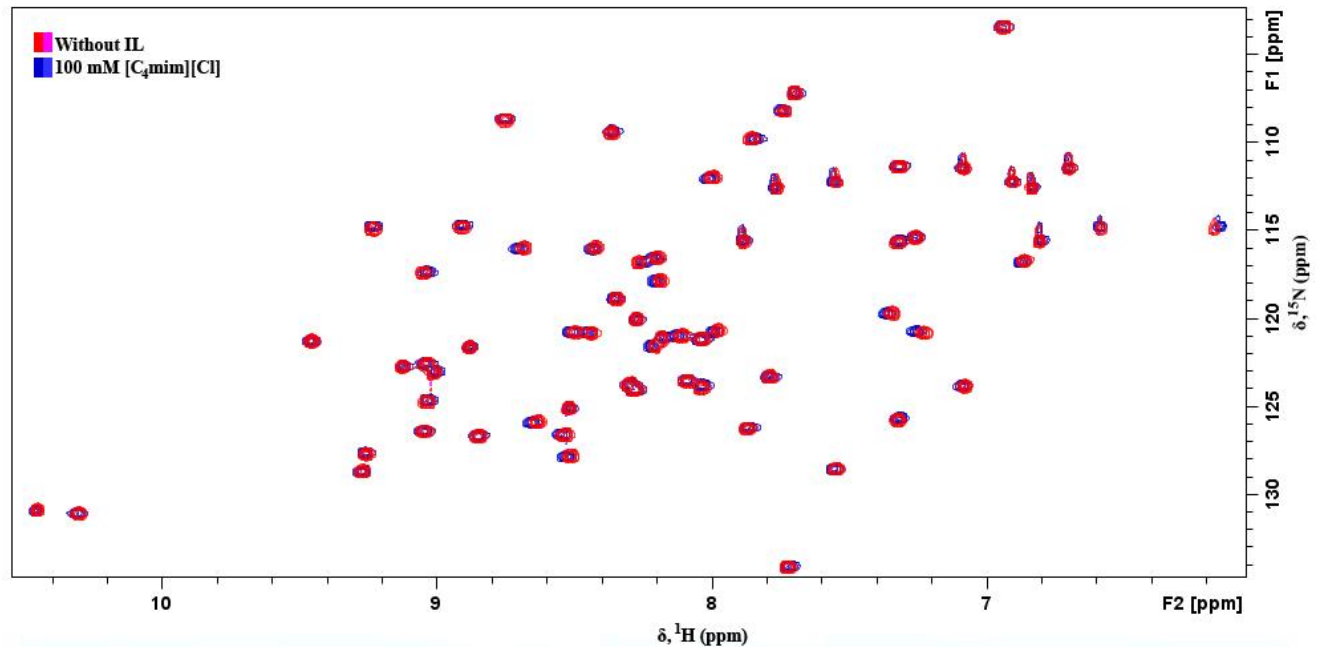

Figure C.7. Superposition of ^{1}H-^{15}N-HSQC spectra of 0.24 mM GB1 without IL (red) and GB1 with 100 mM [C_4mim][Cl] (blue), in 90% H_2O/ 10% $^{2}H_2O$ at 298.15 K.

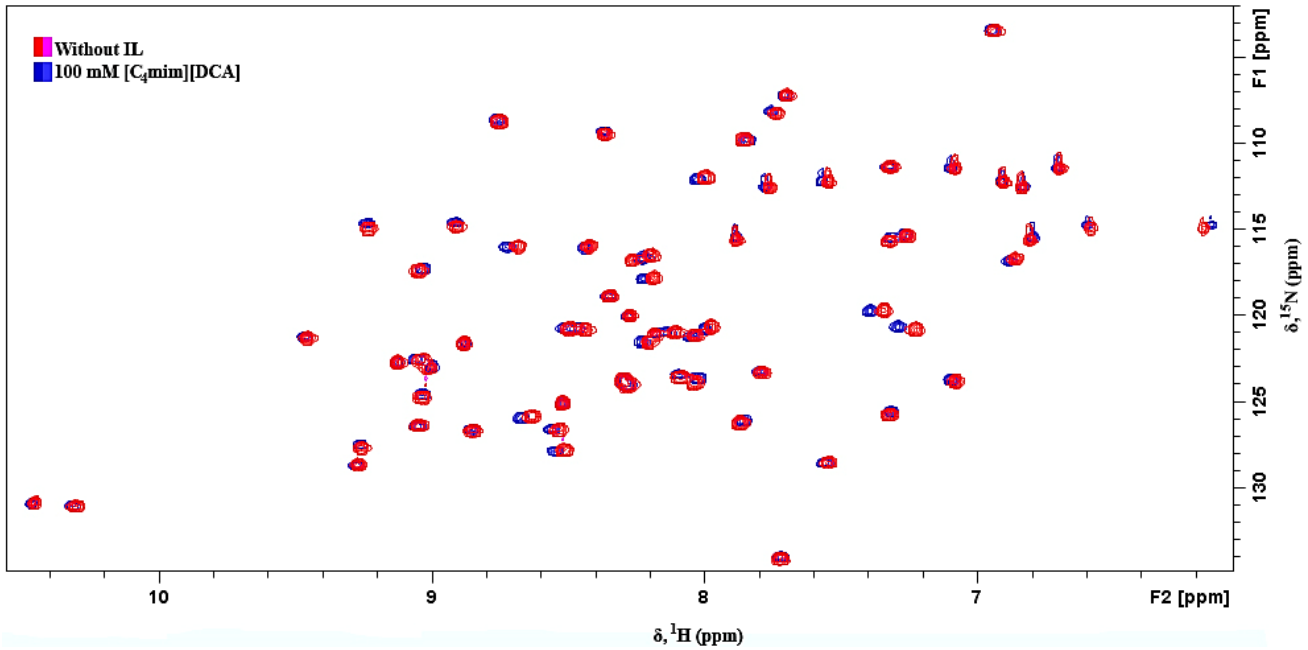

Figure C.8. Superposition of ^{1}H-^{15}N-HSQC spectra of 0.24 mM GB1 without IL (red) and GB1 with 100 mM [C_4mim][dca] (blue), in 90% H_2O/ 10% $^{2}H_2O$ at 298.15 K.

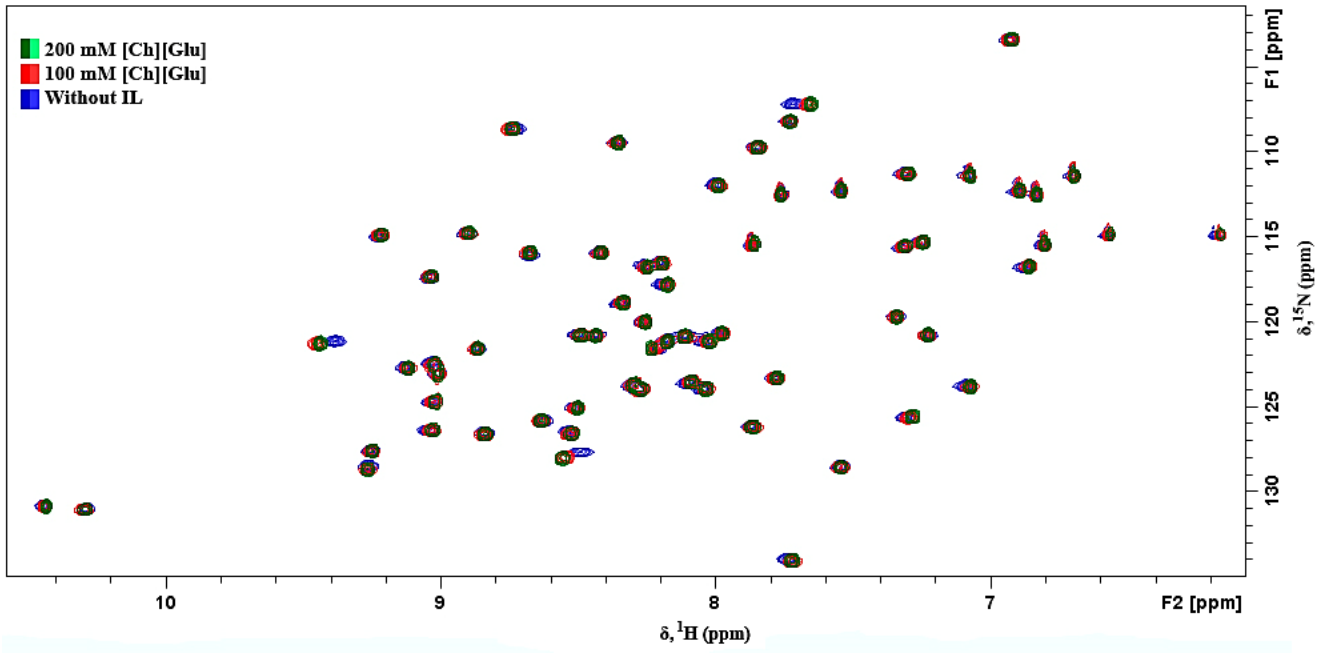

Figure C.9. Superposition of ^{1}H-^{15}N-HSQC spectra of 1 mM GB1 with 200 mM [Ch][Glu] (green), GB1 with 100 mM [Ch][Glu] (red), and GB1 without IL, all in 90% H_2O/ 10% $^{2}H_2O$ at 298.15 K.

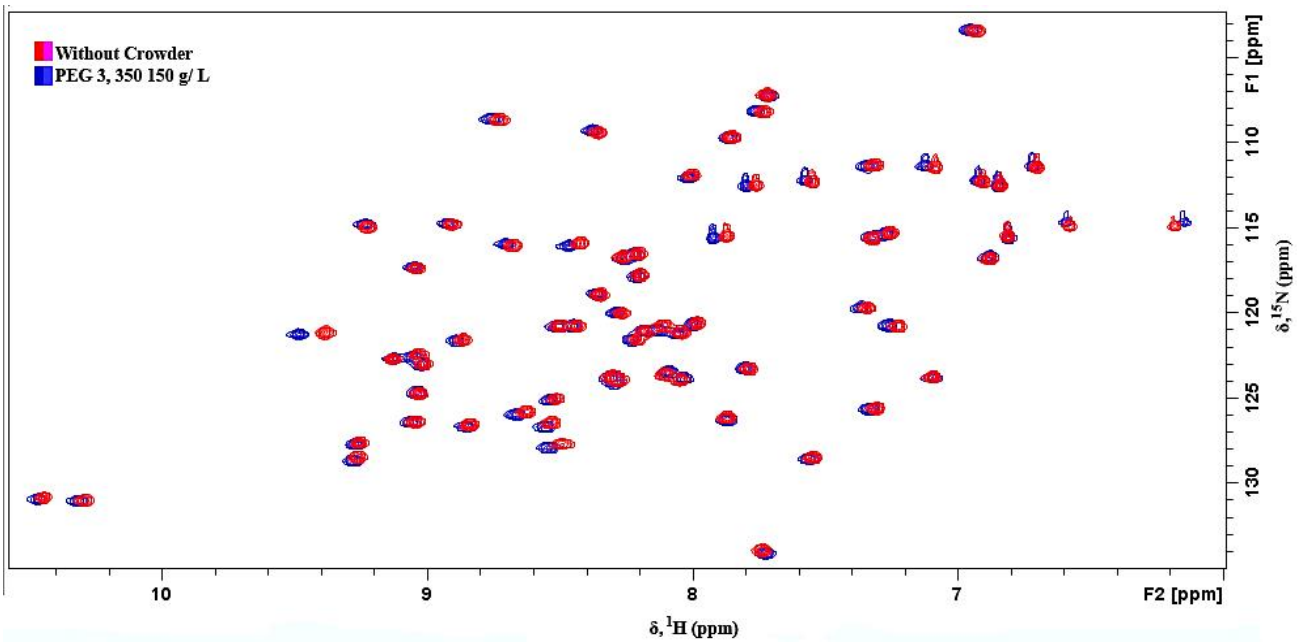

Figure C.10. Superposition of ^{1}H-^{15}N-HSQC spectra of 1 mM GB1 without crowder (red) and GB1 with 150 g/ L PEG 3350 (blue), both in 90% H_2O/ 10% $^{2}H_2O$ at 298.15 K.

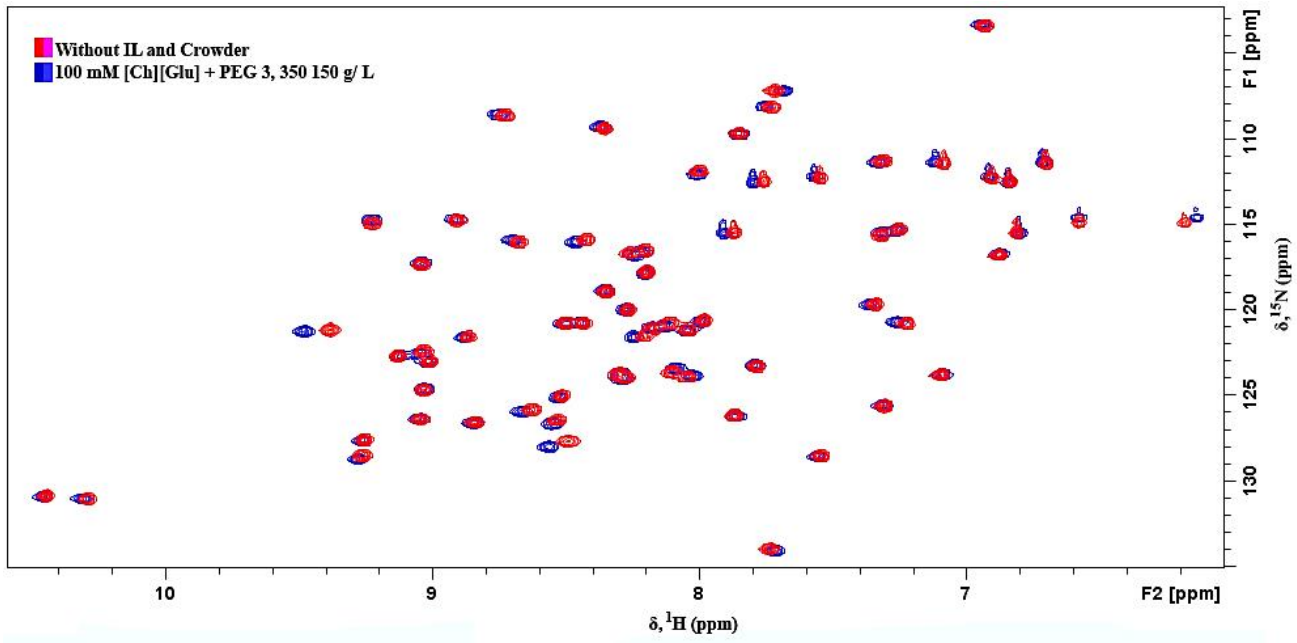

Figure C.11. Superposition of ^{1}H-^{15}N-HSQC spectra of 1 mM GB1 without IL and crowder (red) and GB1 with 100 mM [Ch][Glu] + 150 g/ L PEG 3350 (blue), both in 90% H_2O/ 10% $^{2}H_2O$ at 298.15 K.

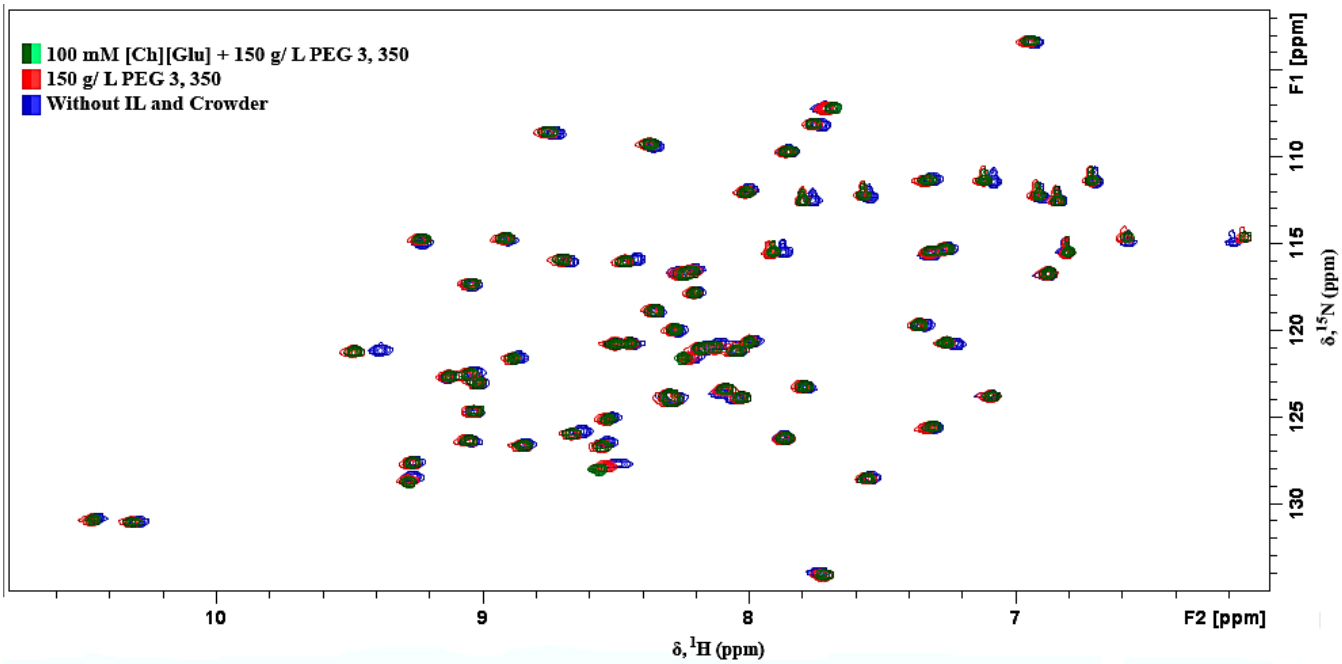

Figure C.12. Superposition of ^{1}H-^{15}N-HSQC spectra of 1 mM GB1 with 100 mM [Ch][Glu] + 150 g/ L PEG 3350 (green), GB1 with 150 g/ L PEG 3350 (red), and GB1 without IL and crowder, all in 90% H_2O/ 10% $^{2}H_2O$ at 298.15 K.

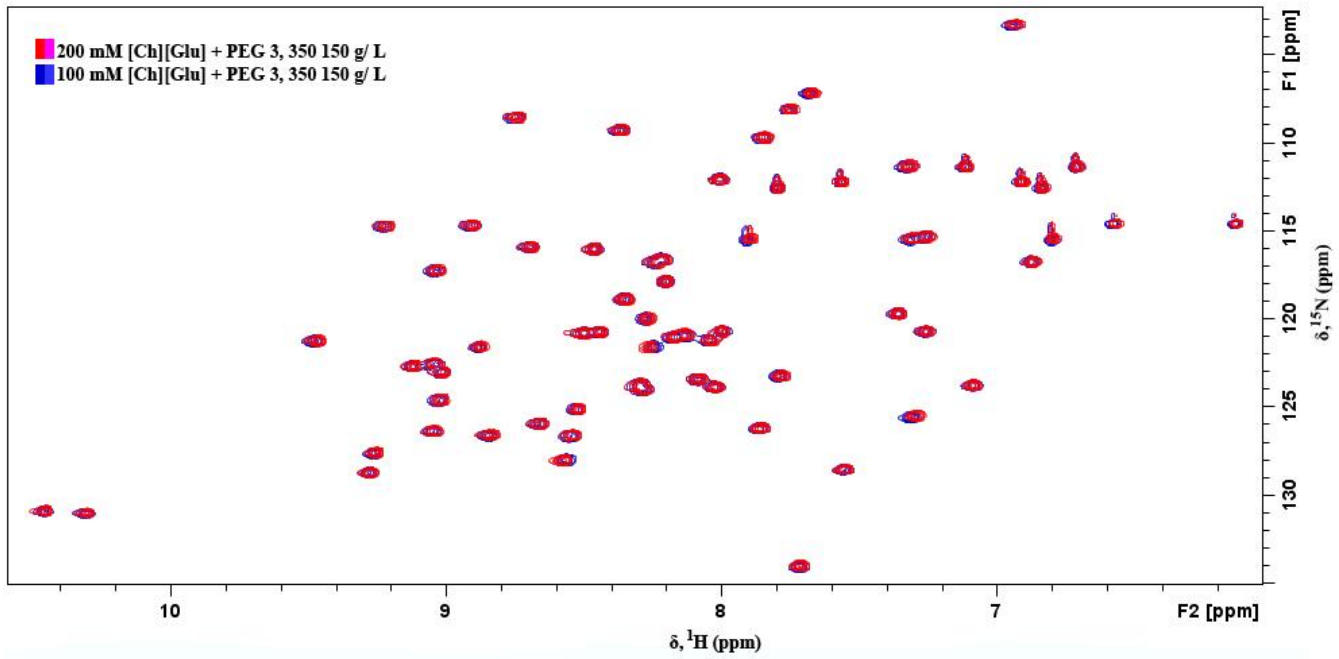

Figure C.13. Superposition of ^{1}H-^{15}N-HSQC spectra of 1 mM GB1 with 200 mM [Ch][Glu] (red) and GB1 with 100 mM [Ch][Glu] (blue), both in 90% H_2O/ 10% $^{2}H_2O$ at 298.15 K.

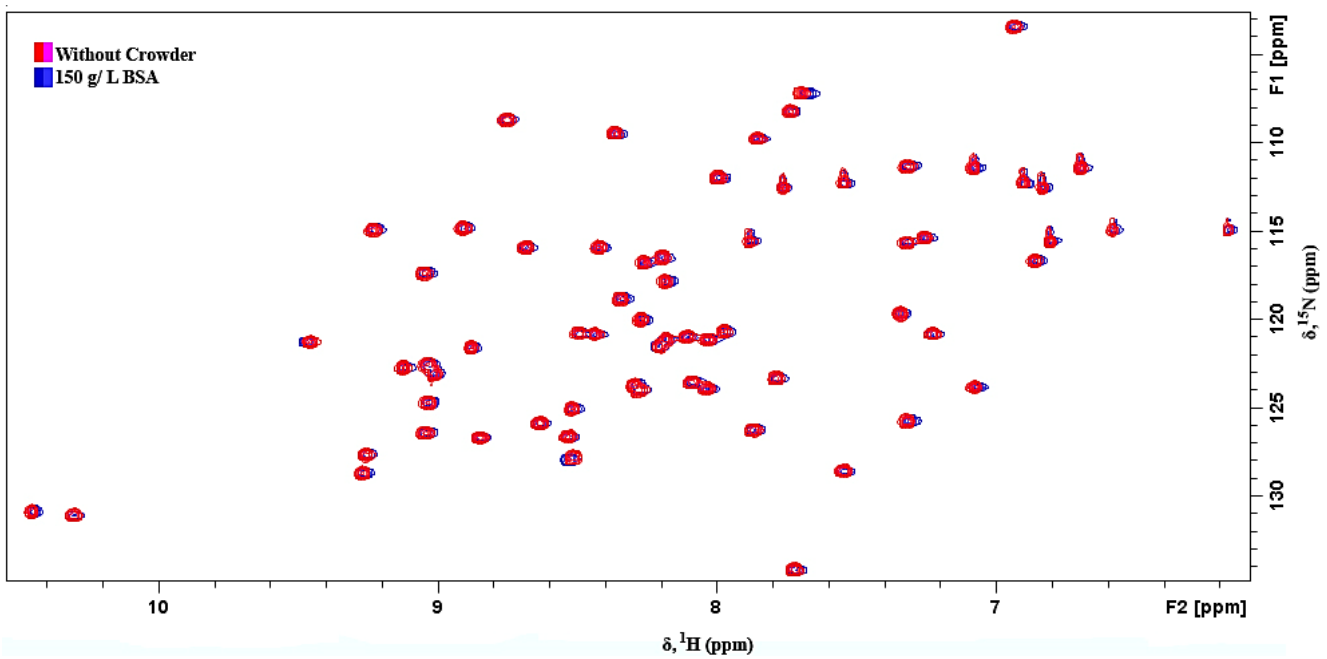

Figure C.14. Superposition of ^{1}H-^{15}N-HSQC spectra of 0.24 mM GB1 without crowder (red) and GB1 with 150 g/ L BSA (blue), both in 90% H_2O/ 10% $^{2}H_2O$ at 298.15 K.

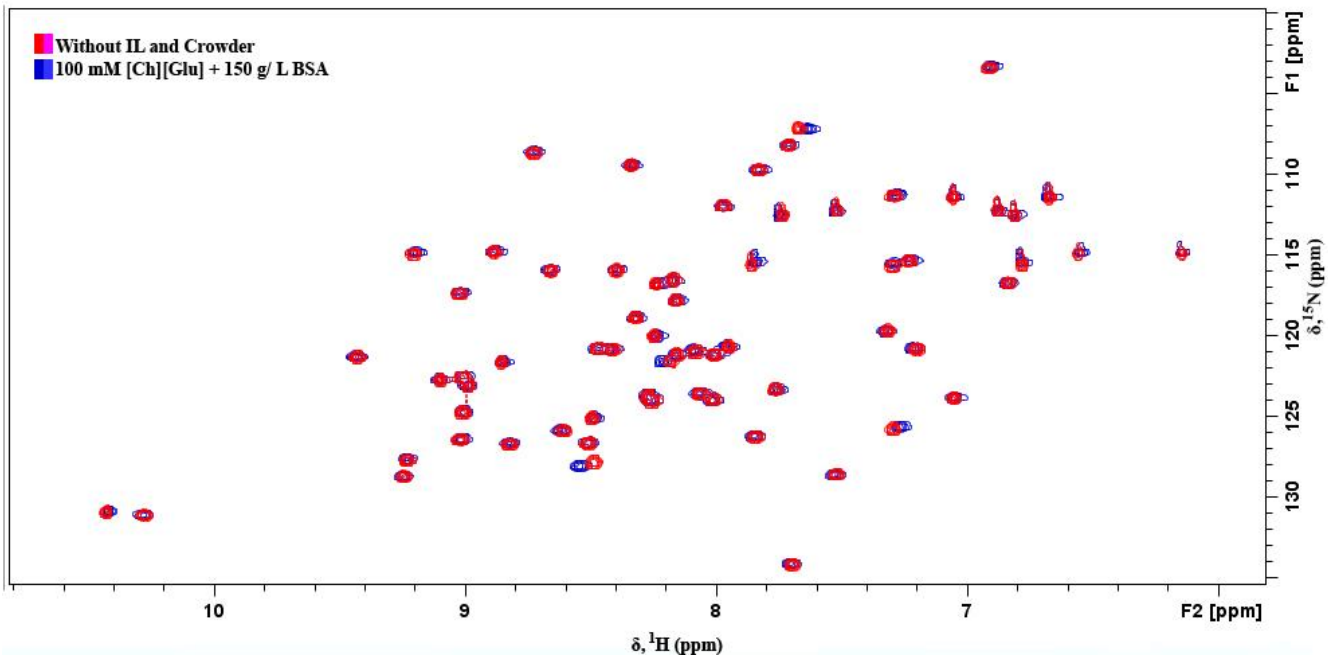

Figure C.15. Superposition of ^{1}H-^{15}N-HSQC spectra of 0.24 mM GB1 without IL and crowder (red) and GB1 with 100 mM [Ch][Glu] + 150 g/ L BSA (blue), both in 90% H_2O/ 10% $^{2}H_2O$ at 298.15 K.

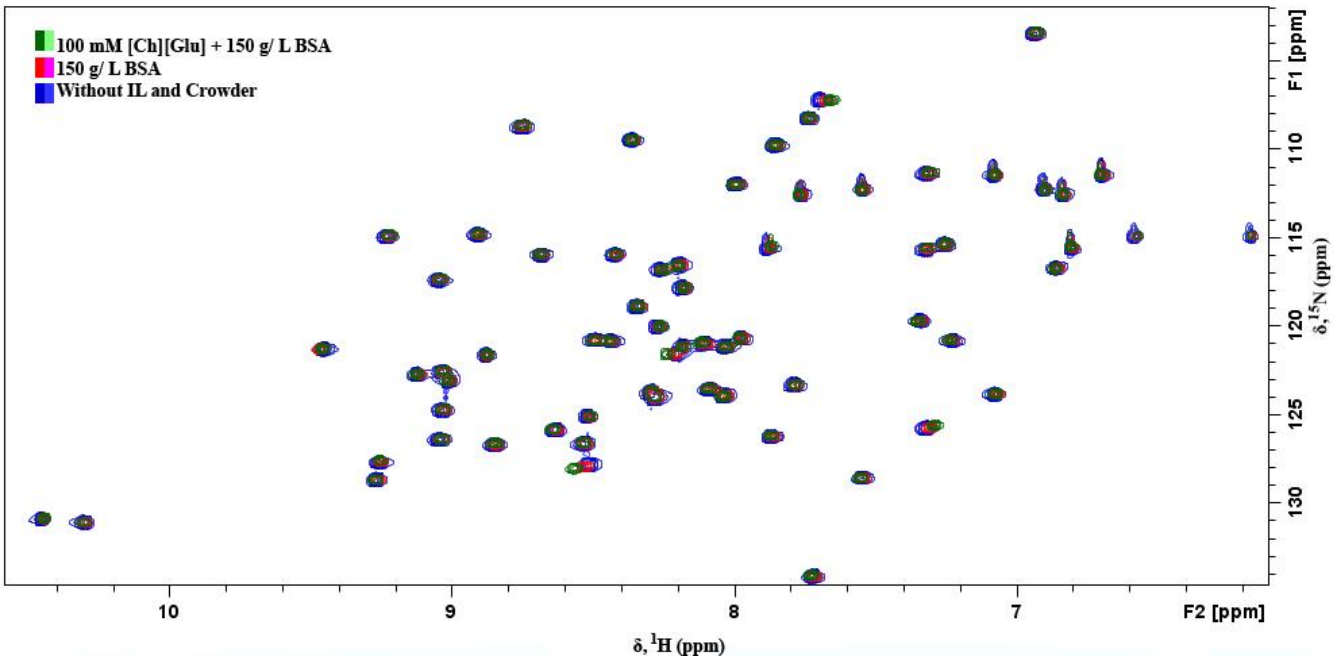

Figure C.16. Superposition of ^{1}H-^{15}N-HSQC spectra of 0.24 mM GB1 with 100 mM [Ch][Glu] + 150 g/ L BSA (green), GB1 with 150 g/ L BSA (red), and GB1 without IL and crowder, all in 90% H_2O/ 10% $^{2}H_2O$ at 298.15 K.

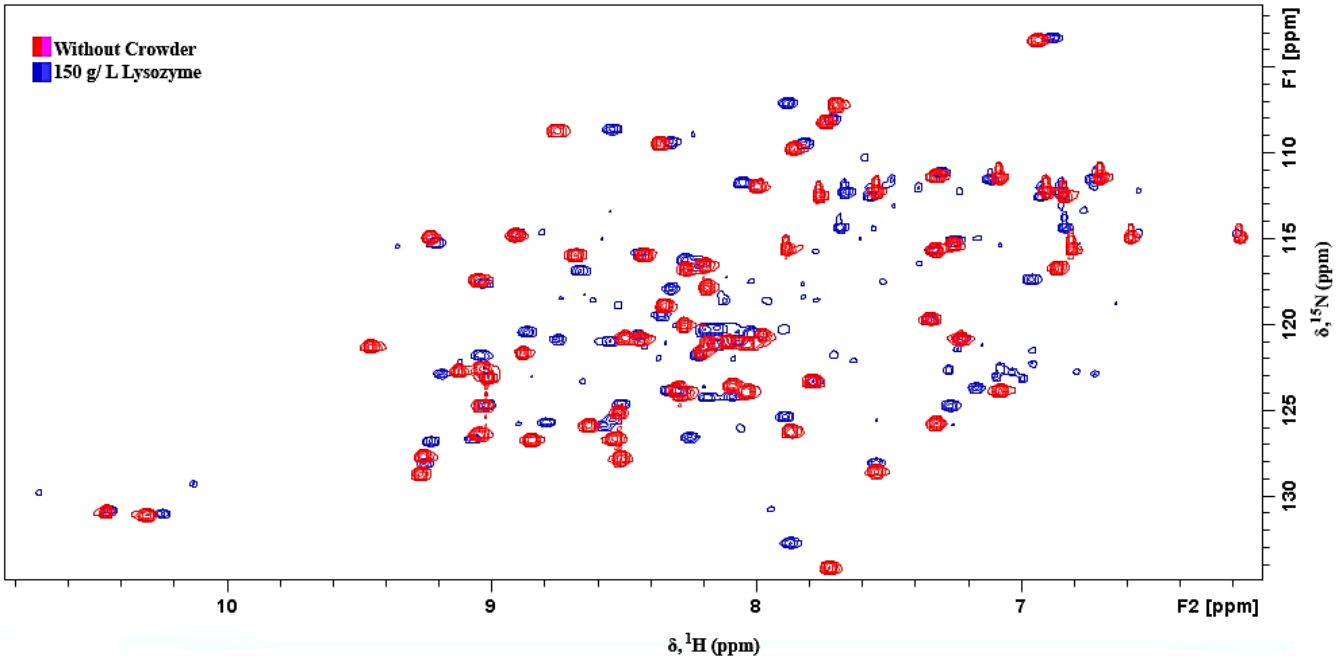

Figure C.17. Superposition of ^{1}H-^{15}N-HSQC spectra of 1 mM GB1 without crowder (red) and GB1 with 150 g/ L Lysozyme (blue), both in 90% H_2O/ 10% $^{2}H_2O$ at 298.15 K.

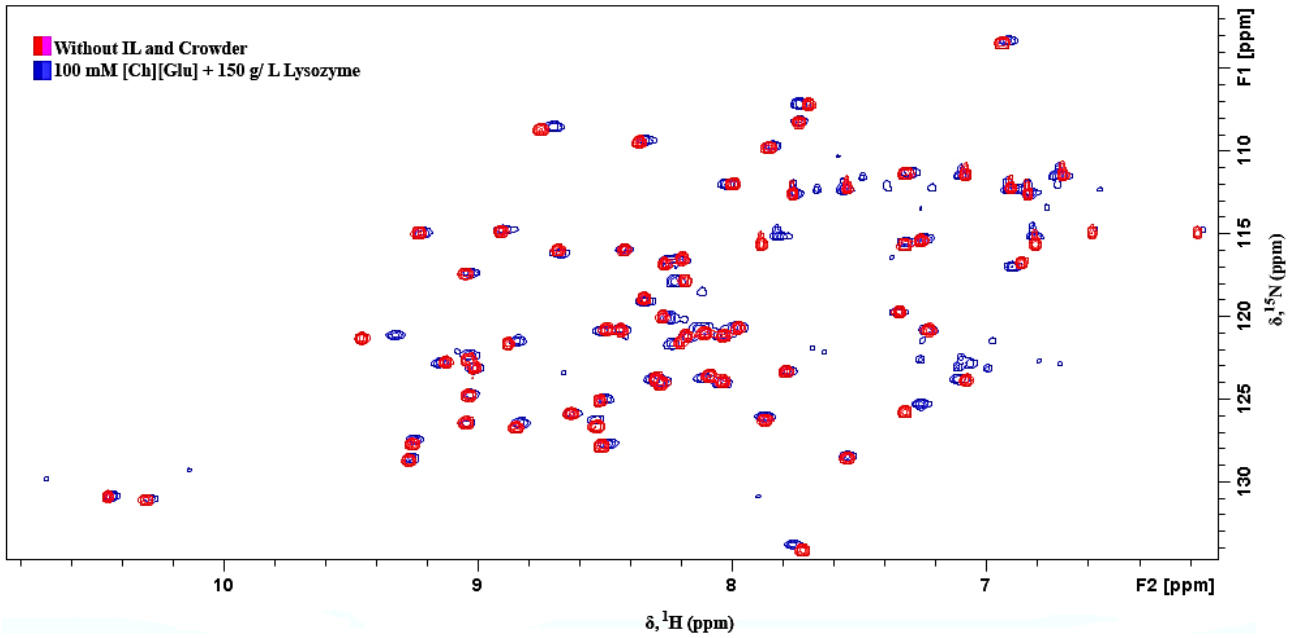

Figure C.18. Superposition of ^{1}H-^{15}N-HSQC spectra of 1 mM GB1 without IL and crowder (red) and GB1 with 100 mM [Ch][Glu] + 150 g/ L Lysozyme (blue), both in 90% H_2O/ 10% $^{2}H_2O$ at 298.15 K.

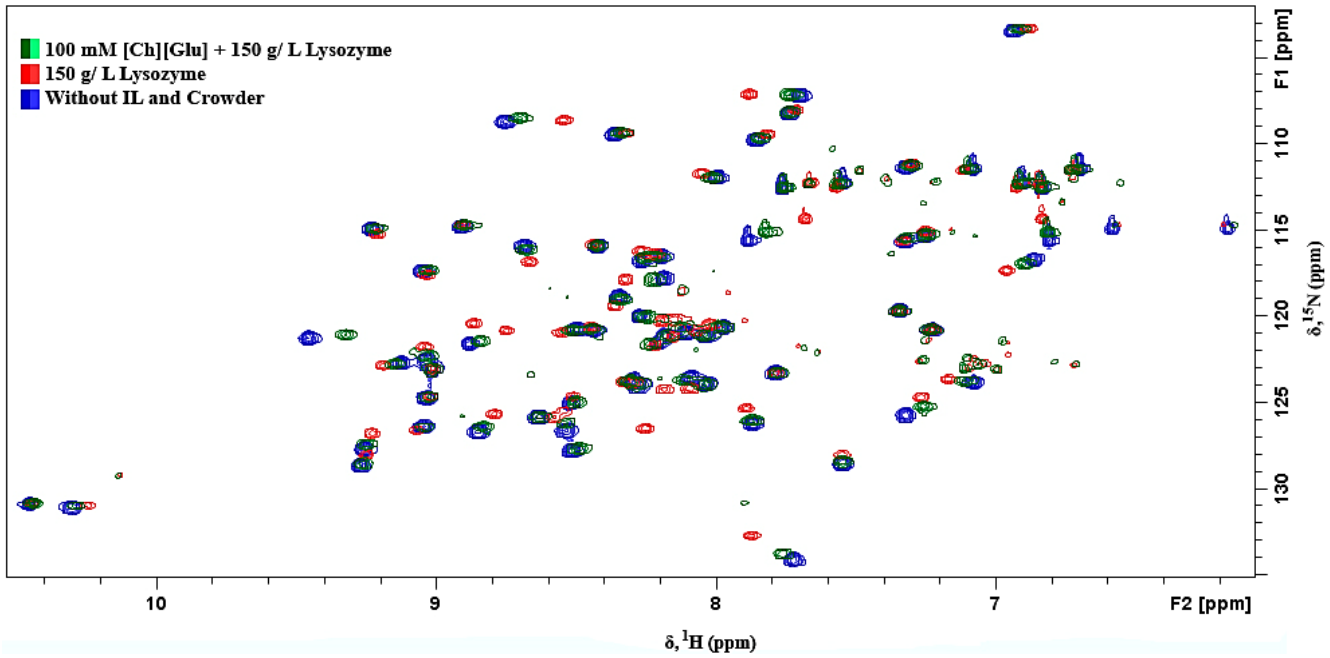

Figure C.19. Superposition of ^{1}H-^{15}N-HSQC spectra of 1 mM GB1 with 100 mM [Ch][Glu] + 150 g/ L Lysozyme (green), GB1 with 150 g/ L Lysozyme (red), and GB1 without IL and crowder, all in 90% H_2O/ 10% $^{2}H_2O$ at 298.15 K.

- **Blank experiment for Lysozyme at 150 g/ L**

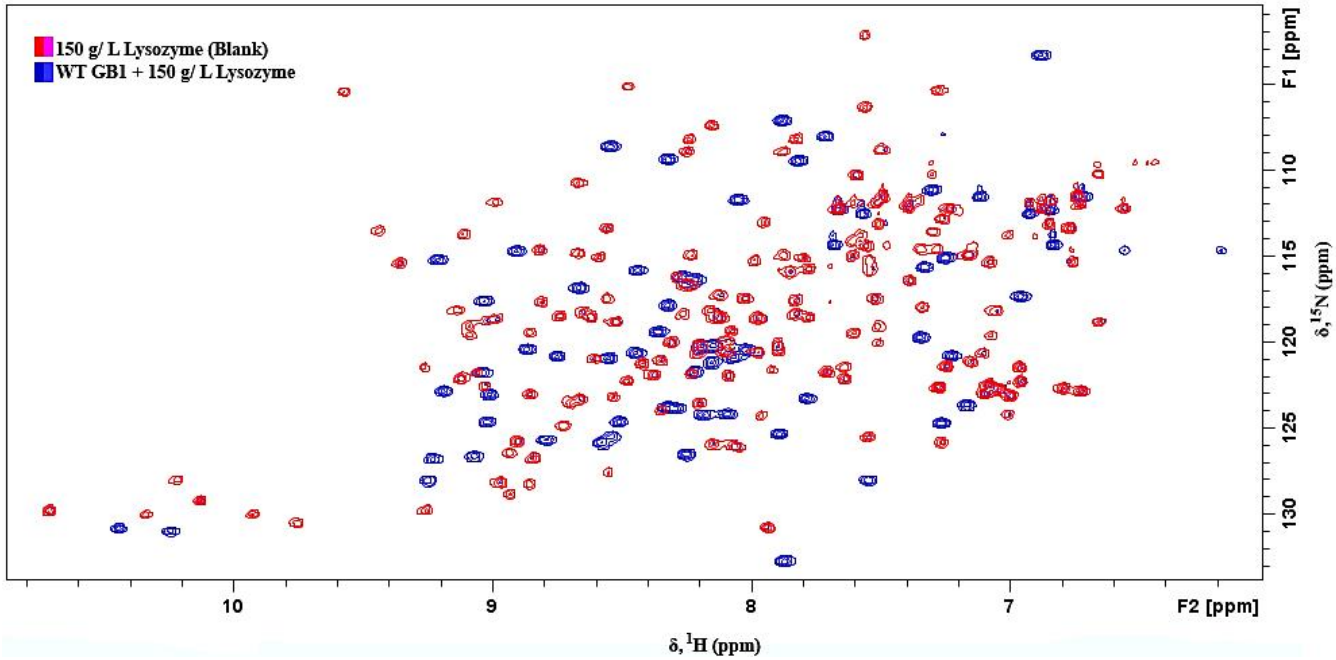

Figure C.20. Superposition of ^{1}H-^{15}N-HSQC spectra of 150 g/ L Lysozyme (red) and GB1 with 150 g/ L Lysozyme (blue), both in 90% H_2O/ 10% $^{2}H_2O$ at 298.15 K.

C. 4. Amide proton exchange data

- **100 mM [Ch][Glu] at 310 K**

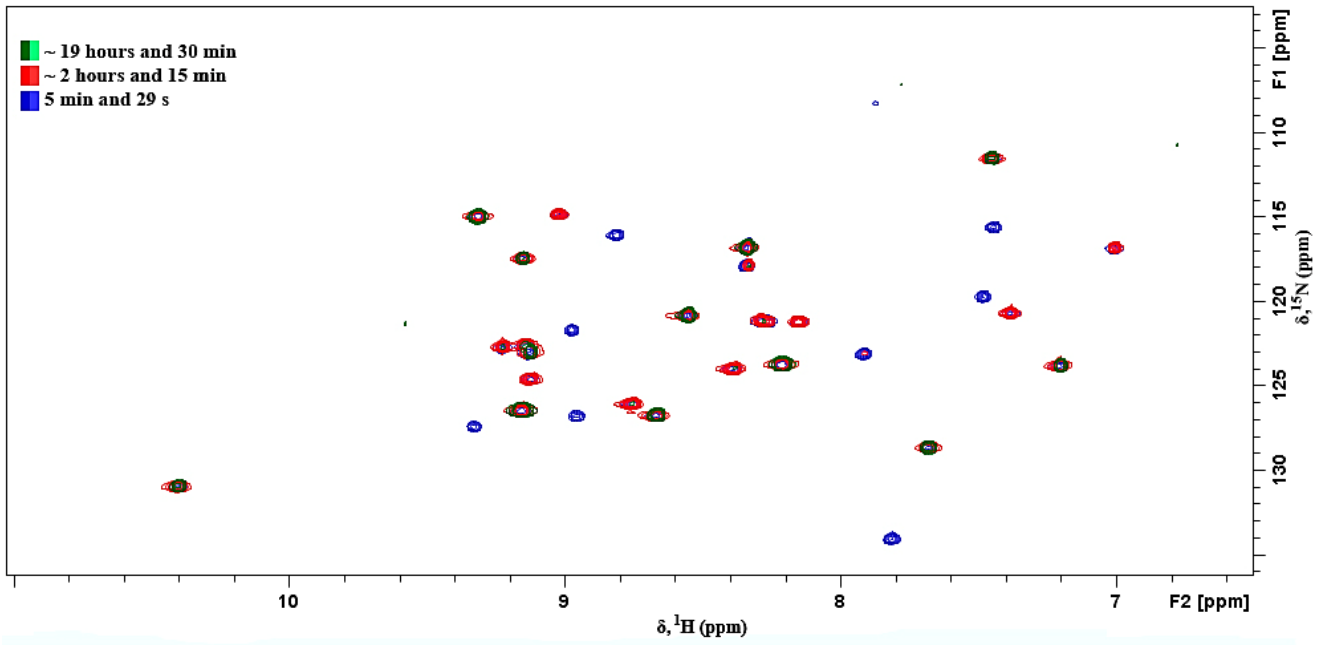

Figure C.21. Superposition of ^{1}H-^{15}N-HSQC spectra of 1 mM GB1 with 100 mM [Ch][Glu] at different times, all in 100% $^{2}H_2O$ at 310.15 K.

- **100 mM CholGlu + 150 g/ L PEG 3350 at 310 K**

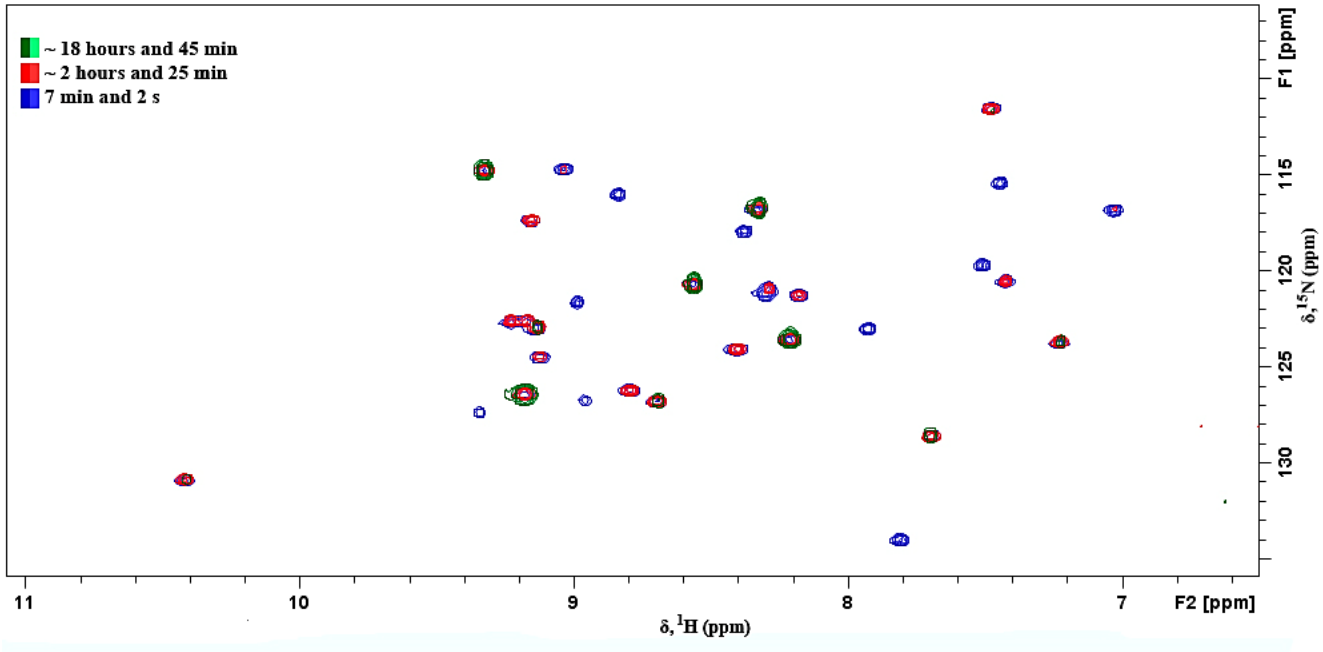

Figure C.22. Superposition of ^{1}H-^{15}N-HSQC spectra of 1 mM GB1 with 100 mM [Ch][Glu] + 150 g/ L PEG 3350 at different times, all in 100% $^{2}H_2O$ at 310.15 K.

- **150 g/ L PEG 3350 at 310 K**

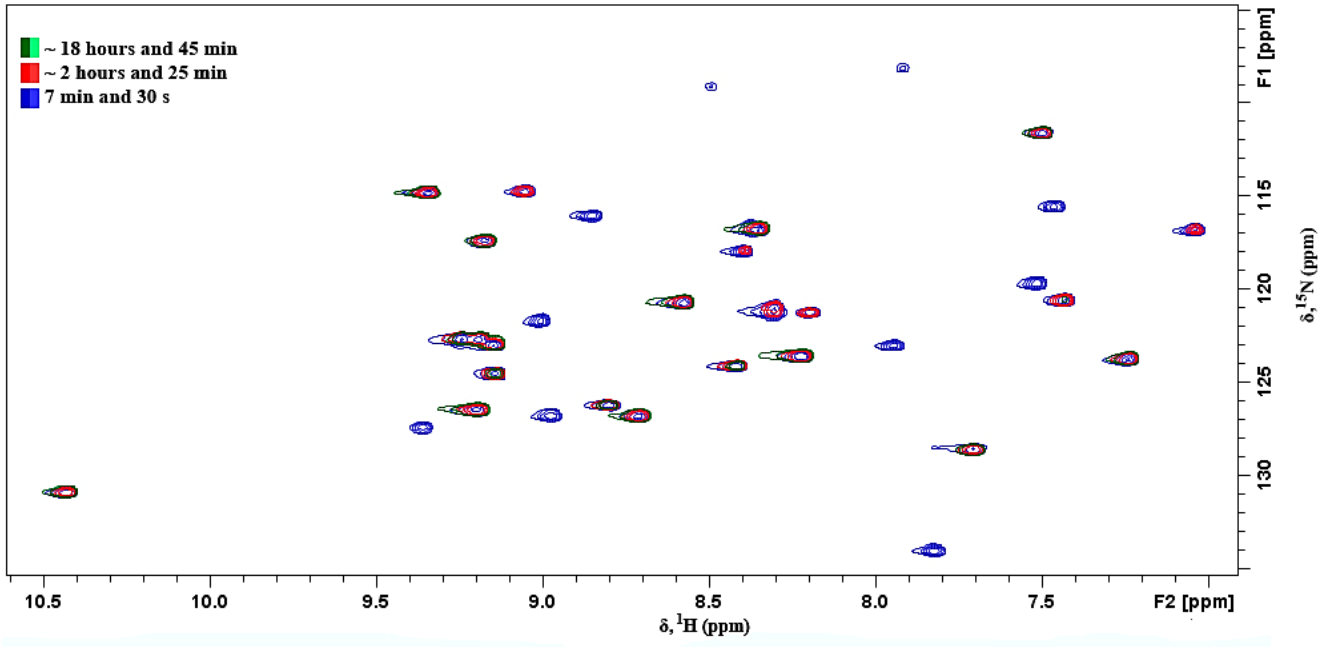

Figure C.23. Superposition of ^{1}H-^{15}N-HSQC spectra of 1 mM GB1 with 150 g/ L PEG 3350 at different times, all in 100% $^{2}H_2O$ at 310.15 K.

- **100 mM [Ch][Glu] + 150 g/ L Lysozyme at 310 K**

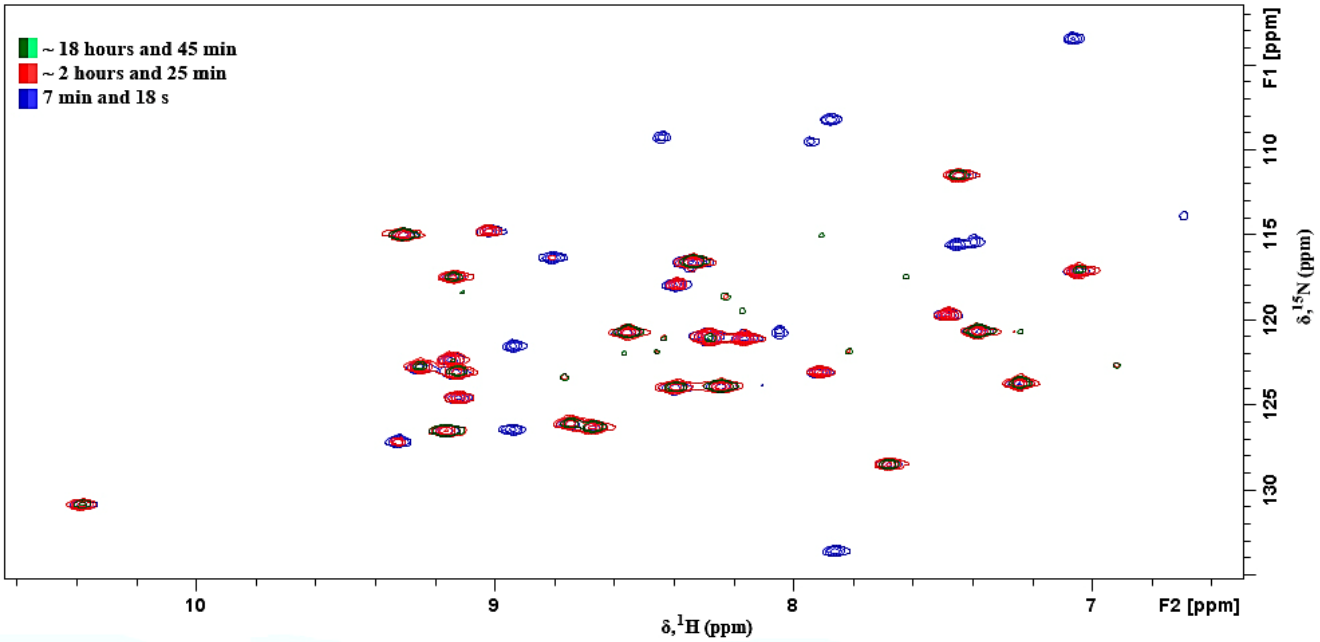

Figure C.24. Superposition of ^{1}H-^{15}N-HSQC spectra of 1 mM GB1 with 100 mM [Ch][Glu] + 150 g/ L Lysozyme at different times, all in 100% $^{2}H_2O$ at 310.15 K.

- **150 g/ L Lysozyme at 310 K**

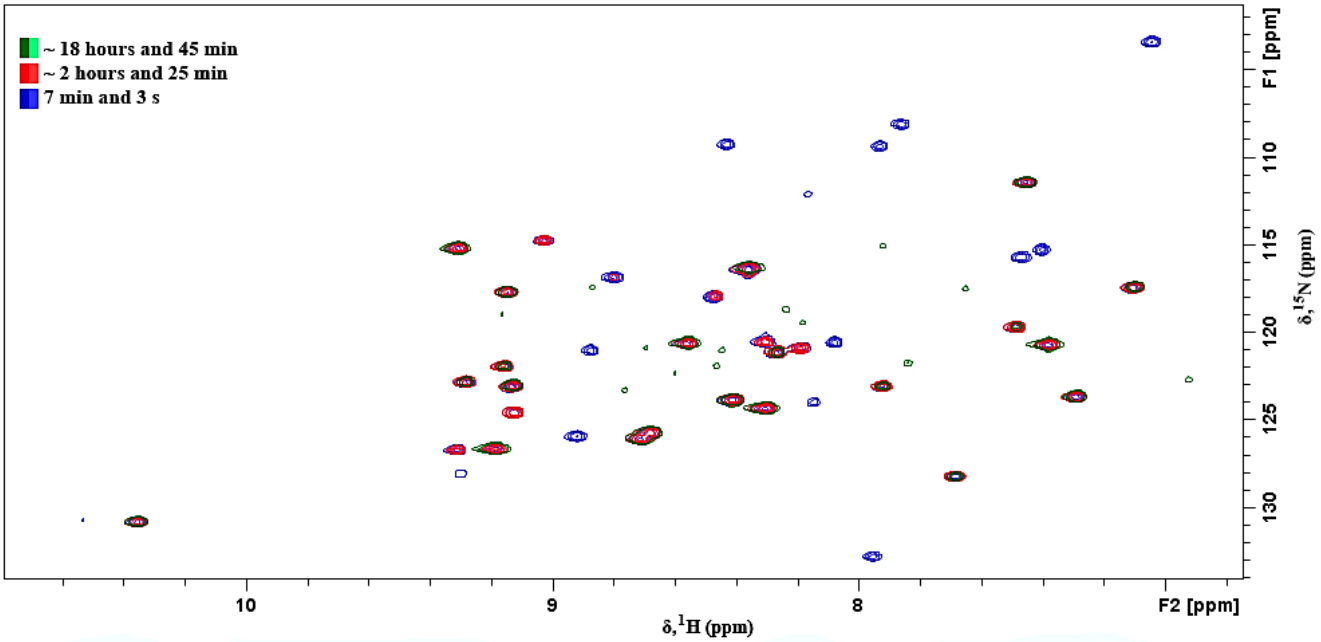

Figure C.25. Superposition of ^{1}H-^{15}N-HSQC spectra of 1 mM GB1 with 150 g/ L Lysozyme at different times, all in 100% $^{2}H_2O$ at 310.15 K.

- **150 g/ L *E. coli* protein Lysate**

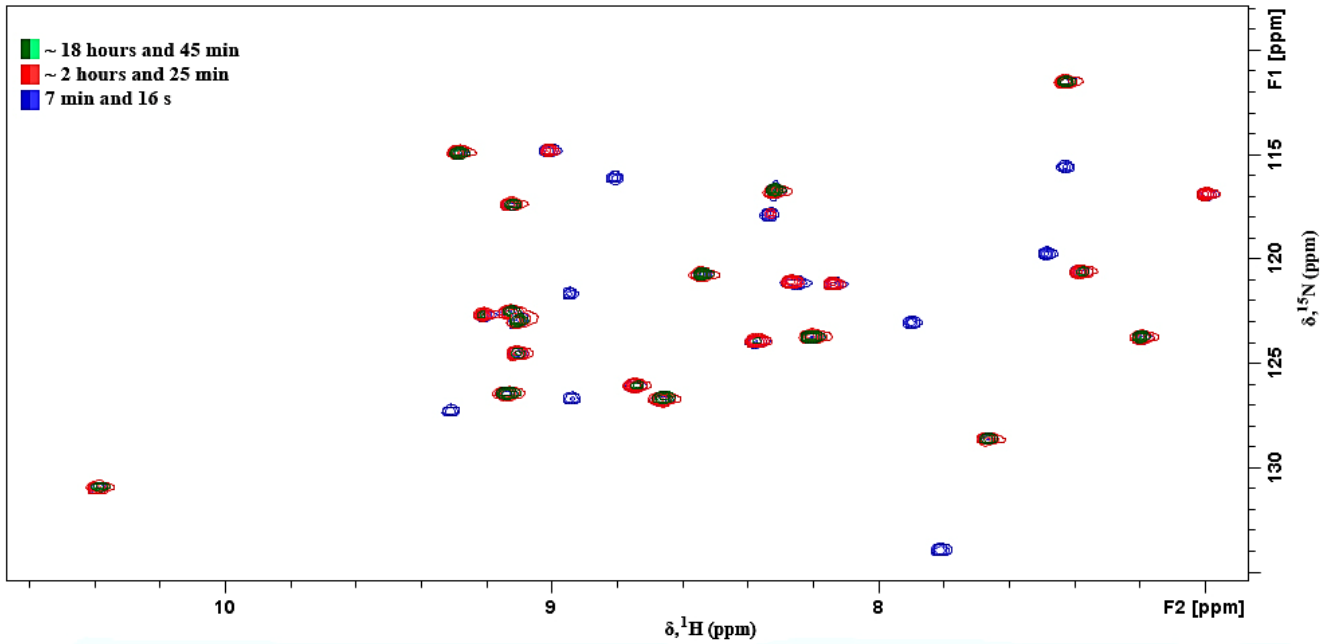

Figure C.26. Superposition of ^{1}H-^{15}N-HSQC spectra of 1 mM GB1 with 150 g/ L Lysozyme at different times, all in 100% $^{2}H_2O$ at 310.15 K.

C. 5. Diffusion data

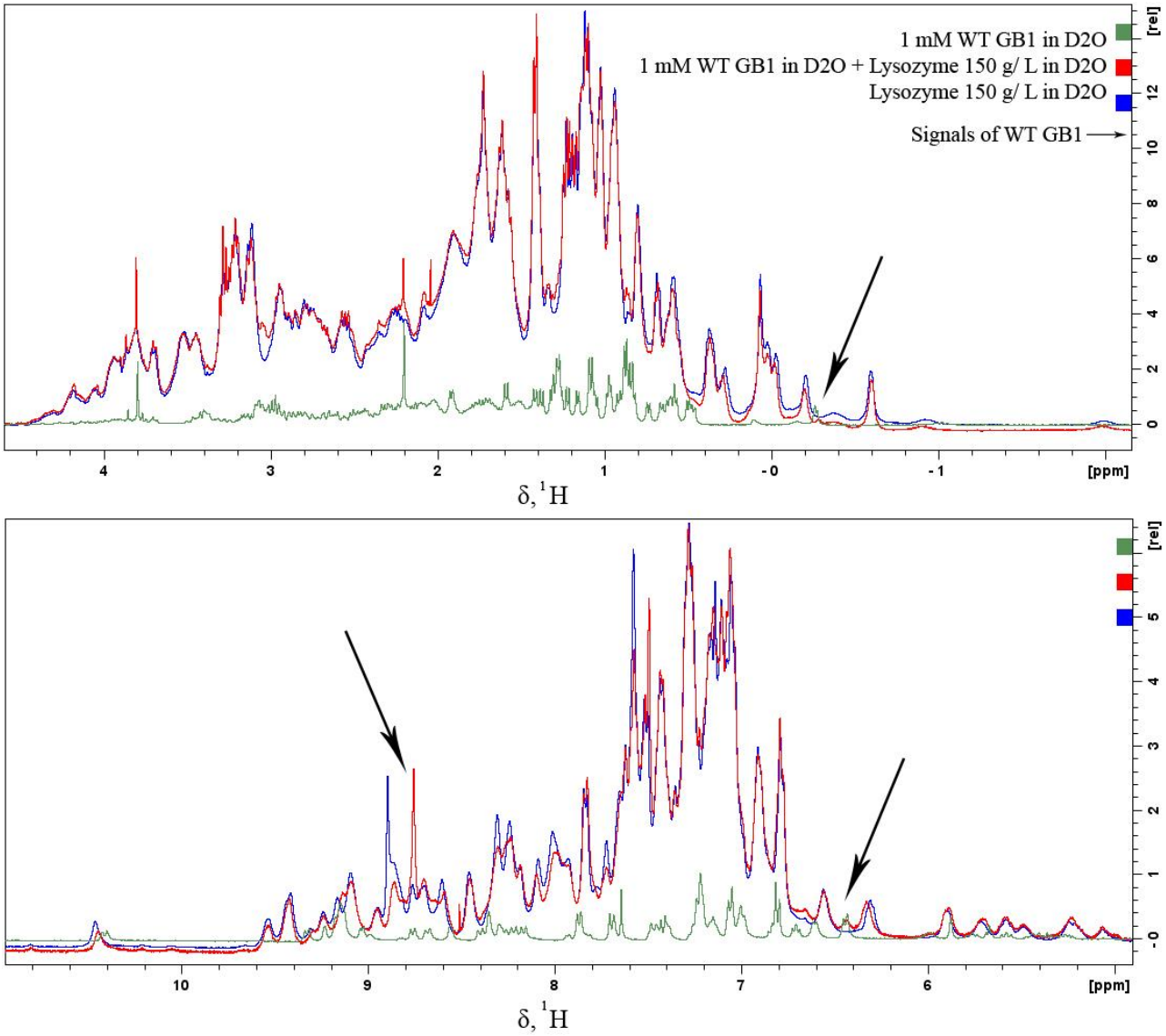

Figure C.27. Superposition of ^{1}H-NMR spectra of 1 mM GB1 in dilute condition (green), GB1 crowded by 150 g/L Lysozyme (red) and Lysozyme at 150 g/L, all in 99.9% $^{2}H_2O$ at 310.15 K.

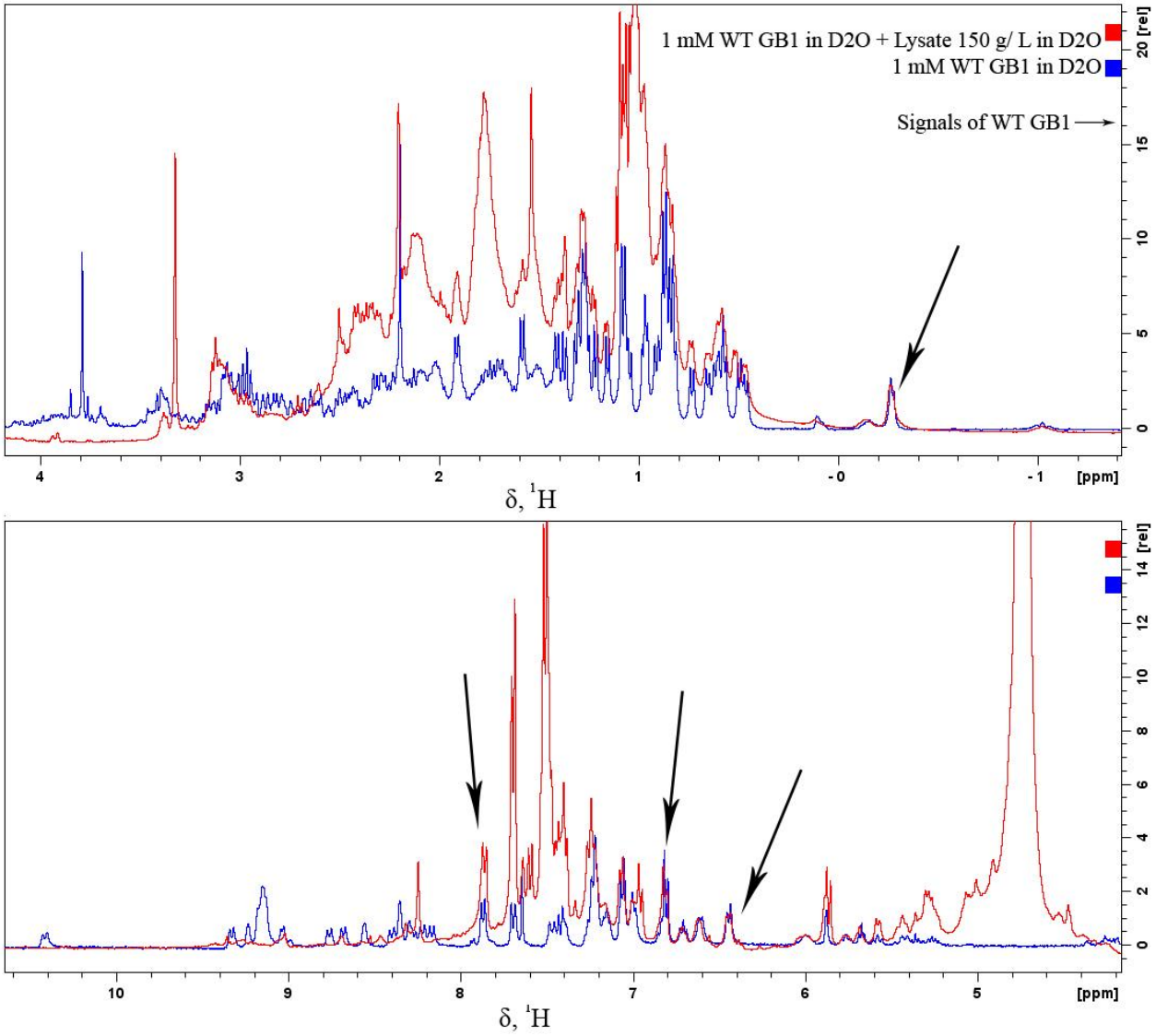

Figure C.28. Superposition of ^{1}H-NMR spectra of 1 mM GB1 in 150 g/L E. coli Lysate (red) and 1 mM GB1 in dilute condition, both in 99.9% $^{2}H_2O$ at 310.15 K.

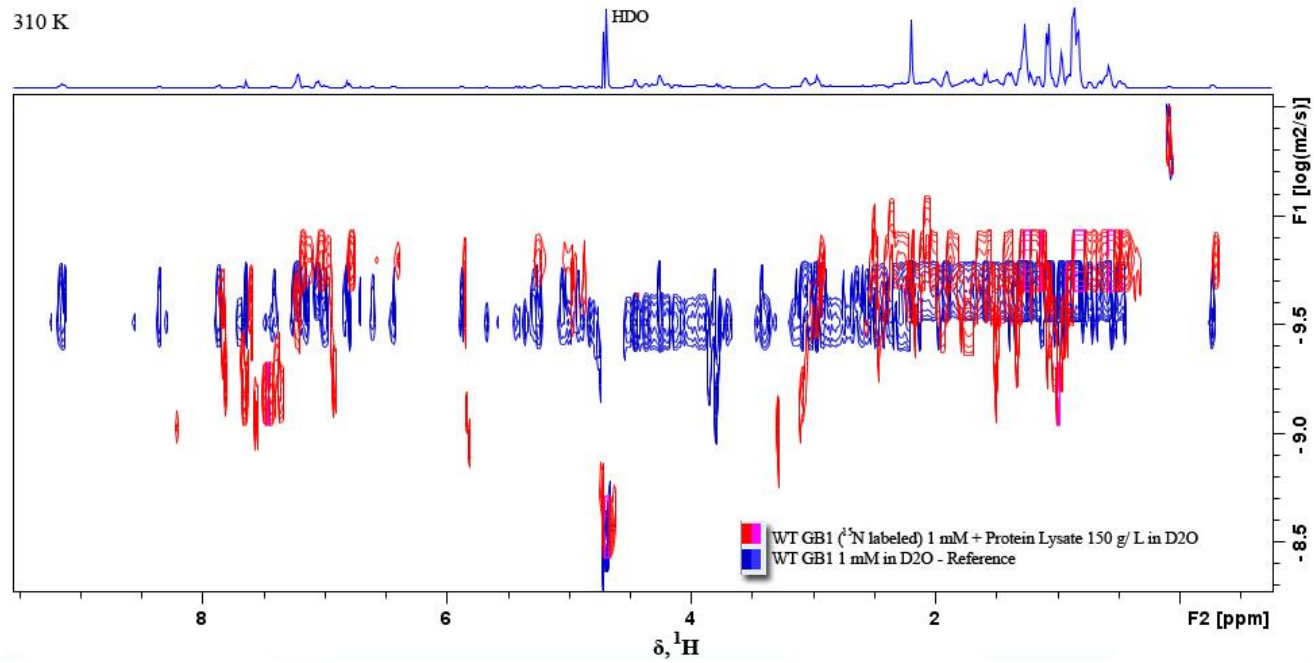

Figure C.29. Superposition of ^{1}H-DOSY plots of 1 mM GB1 in 150 g/L E. coli Lysate (red) and 1 mM GB1 in dilute condition (blue), both in 99.9% $^{2}H_2O$ at 310.15 K.

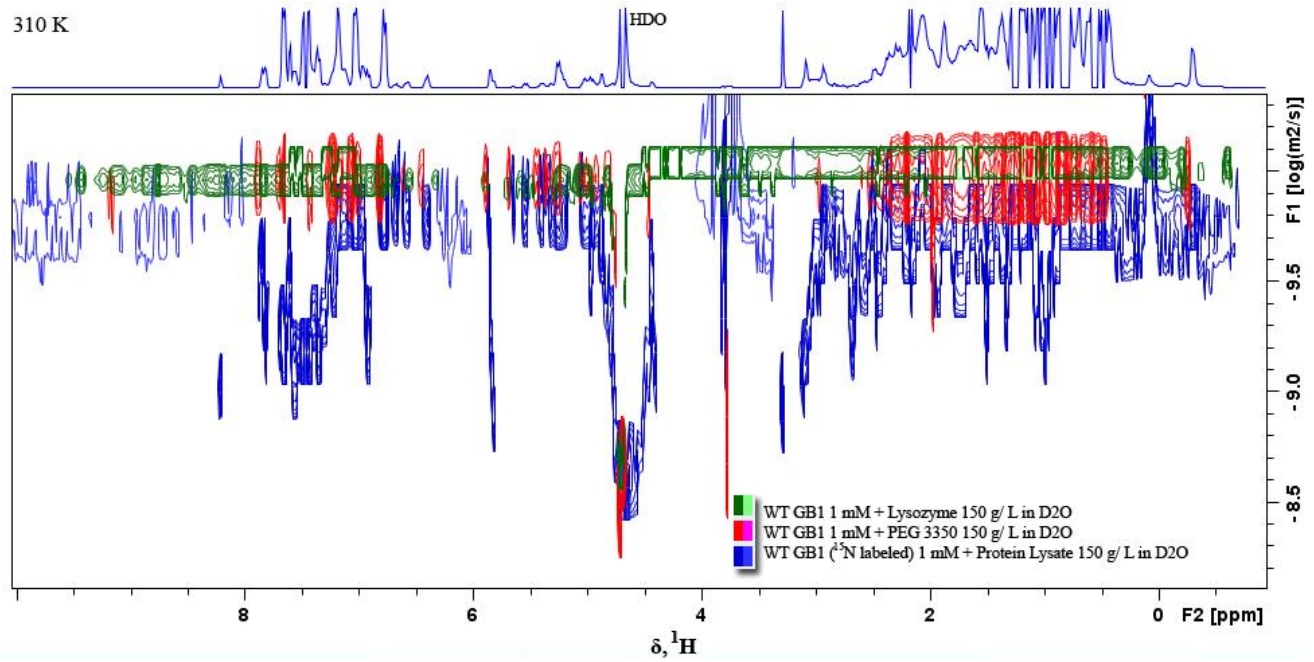

Figure C.30. Superposition of ^{1}H-DOSY plots of 1 mM GB1 crowded by 150 g/L Lysozyme (green), GB1 crowded by 150 g/L PEG 3350 (red) and GB1 crowded by 150 g/L Lysate (blue), all in 99.9% $^{2}H_2O$ at 310.15 K.

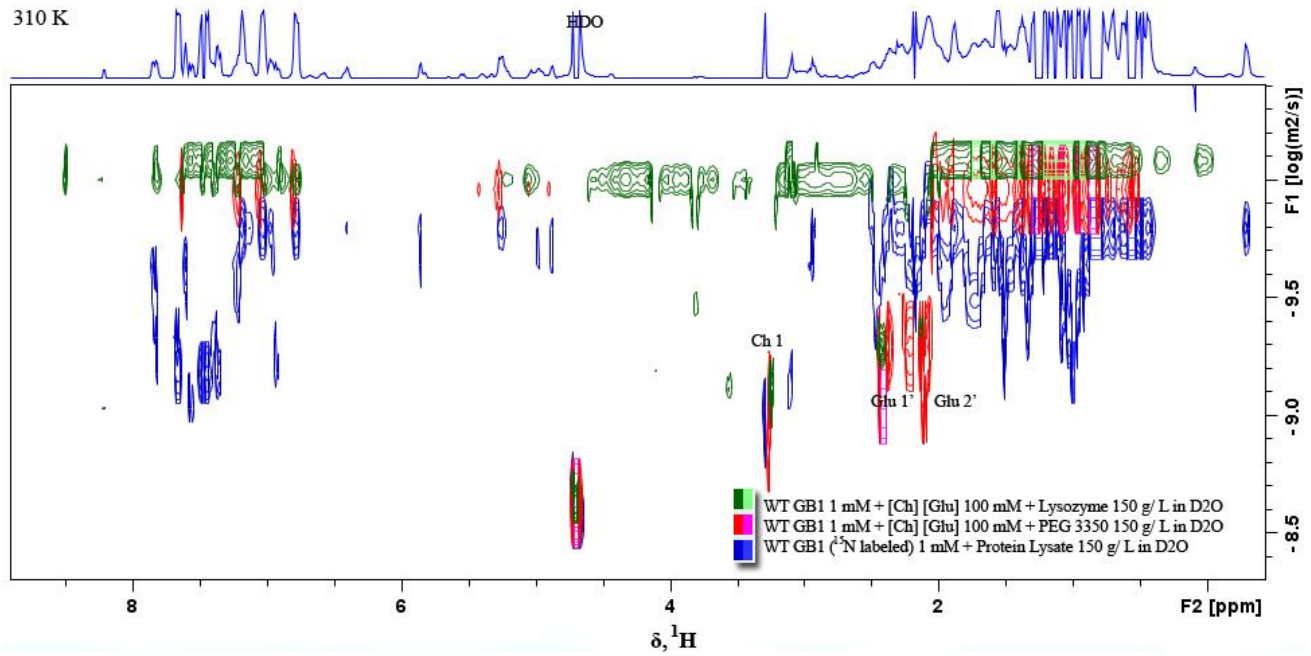

Figure C.31. Superposition of ^{1}H-DOSY plots of 1 mM GB1 with 100 mM [Ch][Glu] IL crowded by 150 g/L Lysozyme (green), GB1 with 100 mM [Ch][Glu] IL crowded by 150 g/L PEG 3350 (red) and GB1 crowded by 150 g/L Lysate (blue), all in 99.9% $^{2}H_2O$ at 310.15 K.